Dynamic Rating based Design and Operation of Offshore Windfarm Export Systems.

Kazmi, Syed Hamza Hasan

Publication date:
2021

Document Version
Publisher's PDF, also known as Version of record

Ørsted

DTU

Dynamic Rating based Design and Operation of Offshore Windfarm Export Systems

Syed Hamza Hasan Kazmi

PhD Dissertation

January 2021, Copenhagen, Denmark

DTU | Center for Electric Power & Energy
Department of Electrical Engineering

DANMARKS TEKNISKE UNIVERSITET
Center for Electric Power and Energy (CEE)
DTU Electrical Engineering

Dynamic Rating based Design and Operation of Offshore Windfarm Export Systems

PhD Dissertation, by Syed Hamza Hasan Kazmi

Supervisors:
Professor Joachim Holbøll, Technical University of Denmark
Lead Engineer Thomas Herskind Olesen, Ørsted
Sr. Chief Specialist (Ph.D.) Troels Stybe Sørensen, Ørsted

DTU - Technical University of Denmark, Kgs. Lyngby - January 2021

Dynamic Rating based Design and Operation of Offshore Windfarm Export Systems

This thesis was prepared by:
Syed Hamza Hasan Kazmi

Supervisors:
Professor Joachim Holbøll, Technical University of Denmark
Lead Engineer Thomas Herskind Olesen, Ørsted
Sr. Chief Specialist (Ph.D.) Troels Stybe Sørensen, Ørsted

Center for Electric Power and Energy (CEE)
DTU Electrical Engineering
Elektrovej, Building 325
DK-2800 Kgs. Lyngby
Denmark

Tel: (+45) 4525 3500
Fax: (+45) 4588 6111
E-mail: cee@elektro.dtu.dk

Release date: 31 Jan 2021

Edition: 1.0

Class: Public

Field: Electrical Engineering

Remarks: The dissertation is presented to the Department of Electrical Engineering of the Technical University of Denmark in partial fulfillment of the requirements for the degree of Doctor of Philosophy.

Baba's Zoey
بابا کی زوئی

Preface

This thesis is prepared at the Department of Electrical Engineering of the Technical University of Denmark (DTU) in partial fulfillment of the requirements for acquiring the degree of Doctor of Philosophy in Engineering. This work was carried out under the Industrial PhD program of Innovation Fund Denmark, which provided partial funding.

During this project, I was employed at Ørsted Offshore Wind A/S from 01 January 2018 until 31 December 2020, while the project was run under the umbrella of the OPTIMUM framework as a cooperation between Energinet.dk, DTU and Ørsted.

This dissertation is written as a monograph, yet parts of the research work carried out in the Industrial PhD project have been published in a number of conference and journal articles. Some of the relevant publications are attached in the appendix. The thesis has been divided into five parts and a total of 10 chapters.

Syed Hamza Hasan Kazmi
31 Jan 2021

Acknowledgements

First and foremost, to my supervisors Joachim, Thomas and Troels for their unparalleled support throughout the project. I could not have asked for a better set of professionals to guide me through this journey. To the OPTIMUM project team from Energinet, Ørsted and DTU, Rasmus, Anders, Mie, Sebastian and Jakob Glårbo, without whom the PhD project would not have aspired to achieve so much. I am highly grateful to the people mentioned above for the candid critical feedback and the valuable insights through out the course of this project, with special mentions to Nicola, Lukasz, Søren and my manager Jacob.

To my colleagues at Ørsted, who welcomed the idea of an industrial research project in a fast-paced work environment, who motivated me and understood my need to drive initiatives beyond the original scope of this thesis. Credits to Stavroula, Nikolaj, Behzad, Shihab, Majid, Mads, Rogvi, Ali, Max, Ivan, my dear friends Zeeshan, Naveed and everyone else who spent their lunch and coffee breaks hearing about the abstract world of dynamic rating and future grids. I thank you for your attention.

To my associates at DTU, KTH Stockholm and Imperial College London, who continuously inspired me and provided a safe work environment to readily bounce my ideas off of: Prof. Bikas Pal, Prof. Vassilios, Guangya, Kateryna, Nenad, Tonny, Jiawei, Alessandro and Anne Due. My students Konstantinos, Benjamin, Ambika, Guillermo, Sandeep, Kaijia and Sharayu, who tolerated my controlling nature and uncausally flourished in their MSc projects. Finally, to a colleague-turned-friend, Tor from Hitachi ABB, who gladly discussed transformer thermodynamics, sushi condiments and everything in between. I am indebted to all of you.

To my friends Qasim, Wasim, Mudassar, Basit, Jawdat, Kamran, Fazeel, their families and everyone else who helped make Denmark my second home. My old confidante in Pakistan, whom I rarely engage with, but hold the selfsame respect nevertheless. I consider you all integral to my success.

Last but not the least, the most important people in my life: My parents, my sisters and my family in-law. I could not have made it so far without the inspiration and pride of my father, without the prayers and never-ending care of my mother, without the love and tease of my sisters. My pagal, you are always there as I relive my memories...

... my one true love, my wife, *my Naan*.

Syed Hamza Hasan Kazmi

Copenhagen, Denmark, 2021

Table of Contents

Abstract

Offshore Windfarms (OWFs) will dominate the energy generation across the globe by 2050. The ten-fold increase in offshore wind over the last decade has primarily been driven by two factors: Firstly, the decrease in its Levelized Cost of Energy (LCOE) from 180 to less than 40 $\frac{€}{MWh}$ in this period, due to optimization of the entire value chain; secondly, the development of large-scale OWFs farther from the shore. In order to keep up with the targets of 2050, further reduction in LCOE is needed. This can be done by making use of the intermittent nature and low capacity factors of the wind to optimally design and utilize the OWF transmission system. In this thesis, novel methodologies and investment decision tools are developed for operation and planning of the OWF export system and its HV components on the basis of Dynamic Thermal Rating (DTR) concept.

Debottlenecking of the OWF export system has revealed that there are inherent thermal pinch-points that need to be resolved for methodical DTR-based design and operation. For this purpose efficient thermal estimation of critical HV components in real-time is possible using empirically derived, differential equations based Thermo-Electric Equivalent (TEE) models. In this thesis, state-of-the-art TEE models (particularly for cables and transformers) are investigated and modified for linear optimization. This is complemented by evaluation of their performance under actual operating conditions from test case OWFs around the globe. Further analysis has revealed that the time-variant physical attributes of the HV components, along with the respective environmental conditions dictate their thermodynamic behavior. Therefore, data analytics and Machine Learning (ML) have been used to develop, test and benchmark statistical tools for thermal estimation and dynamic condition monitoring of these components. The proposed ML-based methods, ranging between semi-physical grey-box and non-physical black-box models, offer unique advantages due to their self-learning nature, which includes identification of information not readily visible to operators due to abundance of data. Furthermore, these models are found to improve the performance of the conventional TEE models and can potentially be used for real-time condition monitoring in the offshore environment.

DTR-based optimal utilization of OWF transformers is given keen attention in this thesis. The analysis of ten test case OWF transformers has revealed that the potential for their optimal utilization is considerable and state-of-the-art thermo-chemical ageing models can be used for this purpose. Therefore, an enhanced DTR methodology for transformer utilization has been developed for a novel optimization problem that facilitates large-scale integration of offshore windfarms by minimizing the energy dispatch cost in the day-ahead market. By testing the methodology on actual generation and load patterns of West-Denmark, the dynamic lifetime based utilization of transformer is found to delay the grid reinforcement costs by facilitating the integration of large-scale OWFs in wind-dominated power systems. The proposed framework accounts for common risk-aversion standards without compromising on system reliability demands.

Finally, cost-effective DTR-based design optimization of HV components in the OWF export system during the planning phase is addressed in the last part of the thesis. The unique uncertainty challenges due to stochastic nature of wind speed profile, wind turbine availability and contingency of components over the entire OWF lifetime are addressed by probabilistic weighing of operational scenarios. Novel investment decision support tools, (one iterative and one two-stage stochastic optimization model developed over the course of this project), account for variation in energy losses and possibility of curtailment, while ensuring reliable system operation. By validating the developed methodologies for a test case OWF off the east coast of UK, the potential for improvement in business case, while balancing the threat of poor transmission efficiency, is successfully demonstrated. All in all, the analysis presented in this thesis shows that DTR can have significant positive impacts on the design and operation of OWF export systems.

Resumé på Dansk

Offshore vindmølleparker (OWFs) er på vej til at være den førende energiproduktion over hele kloden inden 2050. Tidoblingen i antal parker i løbet af det sidste årti har primært været drevet af to faktorer: For det første et fald i energiomkostningerne (levelized cost of energy - LCOE) i denne periode fra 180 til mindre end 40 €/MWh på grund af optimering af hele værdikæden og for det andet udvikling af store vindmølleparker længere væk fra kysten. For at opfylde målene for 2050 er der behov for yderligere reduktion i LCOE. Dette kan gøres ved at udnytte vindens intermitterende natur og lave kapacitetsfaktorer til optimalt at designe og udnytte offshore-transmissionssystemet. I denne afhandling udvikles nye metoder og værktøjer til at understøtte investeringsbeslutninger til drift og planlægning af eksportsystemet og dets højspændingskomponenter på basis af Dynamic Thermal Rating (DTR) konceptet.

En undersøgelse af eksportsystemet har afsløret termiske flaskehalse, der skal fjernes for systematisk at kunne anvende DTR-baseret design og drift. Til dette formål er effektiv termisk estimering af kritiske højspændingskomponenter i realtid en mulighed, som foretages ved hjælp af empirisk afledte differentialligninger baseret på termoelektriske (TEE) modeller. I denne afhandling undersøges moderne TEE-modeller for især kabler og transformere, som modificeres til lineær optimering. Dette suppleres med evaluering af deres ydeevne under faktiske driftsforhold fra vindmølleparker over hele kloden. Yderligere analyser har afsløret, at tidsvariationen af højspændingskomponenternes fysiske egenskaber sammen med de respektive ydre forhold er afgørende for deres termodynamiske opførsel. Derfor er dataanalyse og maskinlæring (ML) blevet brugt til at udvikle, teste og benchmarke statistiske værktøjer til termisk estimering og dynamisk tilstandsovervågning af disse komponenter. De foreslåede ML-baserede metoder spænder fra semi-fysiske grey-box til ikke-fysiske black-box modeller. Modellerne tilbyder unikke fordele på grund af deres selvlærende natur, som inkluderer identifikation af information, der ikke er så synlig for operatører på grund af dataoverflod. Desuden har disse modeller vist sig at forbedre ydeevnen for de konventionelle TEE-modeller og kan potentielt bruges til realtidsovervågning i offshore-installationer.

DTR-baseret optimal udnyttelse af offshore-transformere spiller en vigtig rolle i denne afhandling. Analysen af ti testtransformere har afsløret, at potentialet for deres optimale udnyttelse er betydeligt, og at avancerede termokemiske ældningsmodeller kan bruges til dette formål. Derfor er der blevet udviklet en forbedret DTR-metode til transformatorudnyttelse i forbindelse med en ny optimeringsopgave, som letter storskala-integration af OWFs ved at minimere dispatch-omkostningerne på det daglige energimarked. Ved at teste metoden på faktiske produktions- og belastningsmønstre i Vestdanmark viser det sig, at den dynamiske levetidsbaserede udnyttelse af transformere forsinker omkostninger til netforstærkning ved integration af store vindmølleparker i vinddominerede elsystemer. Den foreslåede metode tager højde for almindelige standarder for risikoaversion uden at gå på kompromis med kravene til systemets pålidelighed.

I den sidste del af afhandlingen behandles omkostningseffektiv DTR-baseret designoptimering af OWF HV-komponenter i planlægningsfasen. De unikke usikkerhedsudfordringer på grund af vindhastighedsprofilens stokastiske karakter, tilgængelighed af vindmøller og komponenter i hele vindmølleparkens levetid løses ved probabilistisk vægtning af driftsscenarier. Nye værktøjer til at understøtte investeringsbeslutninger (en iterativ og en to-trins stokastisk optimeringsmodel udviklet i løbet af dette projekt) tager højde for variation i energitab og mulighed for dets begrænsning, samtidig med at der sikres pålidelig systemdrift. Ved at validere de udviklede metoder på en test case, en vindmøllepark ud for Storbritanniens østkyst, demonstreres potentialet for forbedring af forretningsmodellen, samtidigt med at der sikres balance med risikoen for ringe transmissionseffektivitet. Alt i alt viser analysen præsenteret i denne afhandling, at DTR kan have en signifikant positiv indvirkning på design og drift af vindmølleparkers eksportsystemer.

Nomenclature

Note: The main notation used in this dissertation is stated below. Additional symbols are defined where needed.

Acronyms:

ACF	Auto Correlation Function
ANN	Artificial Neural Network
ARIMA	Auto-Regressive Integrated Moving Avg.
ARX	Auto-Regressive eXogenous
BB2	Burbo Bank 2 Offshore Windfarm
BKR	Borkrum Riffgrund Offshore Windfarm
CAPEX	Capital Expenditures
CCF	Common Cause Failures
CDF	Cumulative Density Function
CfD	Contract for Difference
CIGRE	Int. Council on Large Electric Systems
DCOPF	Direct Current Optimal Power Flow
DOB	Depth of Burrial
DP	Degree of Polymerization, no unit
DTMC	Discrete Time Markov Chain
DTR	Dynamic Thermal Rating
DTR^+	Enhanced Dynamic Thermal Rating
DTS	Distributed Temperature Sensing
DTU	Technical University of Denmark
EL	Expected Lifetime
FAT	Factory Acceptance Test
FiT	Feed-in Tariffs
GLM	Generalized Linear Model
GOW	Gode Wind Offshore Windfarm
HDD	Horizontal Directional Drilling
HST	Hot Spot Temperature
HVAC	High Voltage Alternating Current
HVDC	High Voltage Direct Current
IEC	International Electrotechnical Commission
IEEE	Institute of Electrical & Electronic Engr.
iid	Independent and identically distributed
LCOE	Levelised Cost of Energy
LL	Loss of Life
MILP	Mixed Integer Linear Program
MIQCP	Mixed Integer Quadratically Constrained Program
ML	Machine Learning
MTTF	Mean Time To Failure
MTTR	Mean Time To Repair
NCCF	No Common Cause Failures
NMSE	Normalized Mean Square Error
NPV	Net Present Value [€]
ODAF	Directed Oil Forced Air Forced
ODE	Ordinary Differential Equation
OFAF	Non directed Oil Forced Air Forced
ONAF	Oil Natural Air Forced
ONAN	Oil Natural Air Natural
OnSS	Onshore Substation
OPEX	Operational Expenditures
OSS	Offshore Substation
OWF	Offshore Windfarm
PACF	Partial Auto Correlation Function
PCA	Principal Component Analysis
PCC	Point of Common Coupling
PDF	Probability Density Function
PTDF	Power Transfer Distribution Matrix
RBD	Reliability Block Diagram
RCS	Reactive Compensation Station
ReLU	Rectified Linear Unit
ROW	Race Bank Offshore Windfarm
SCETM	Single Core Equivalent Thermal (TEE) Model
SS	State Space

SSE	Sum of Squared Errors
STR	Static Thermal Rating
TEE	Thermoelectric Equivalent
TOT	Top Oil Temperature
TSO	Transmission System Operator
TUP	Thermally Upgraded Paper
WOW	Walney Offshore Windfarm
WT	Wind Turbine
WTG	Wind Turbine Generator
XLPE	Cross-Linked Poly-Ethylene

Parameters (Constants and Inputs):

$\boldsymbol{B}$	Admittance matrix
$\boldsymbol{M}$	PTDF matrix
Δt	Operational time step, [hour]
$\Delta\vartheta^{\text{hst}}_{rated}$	Rated HST rise over ϑ_{tot}, [°C]
$\Delta\vartheta^{\text{tot}}_{rated}$	Rated TOT rise over ϑ_{amb}, [°C]
F	Power flow through branch, [pu]
γ	Power purchase agreement price, [€/MWh]
κ	Forecast function (local trend)
Λ, Υ	Failure & repair rates for components, [hr^{-1}]
λ^{c}_s	Loss factors for cable screen & armour, [pu]
λ_{rated}	Rated trafo loss of life, [hr]
$\mu_{A^{\text{W}}_{av}}$	Avg. windfarm availability, [pu]
ν, μ	Empirically derived cooling coefficients for oil and winding, [pu]
$\overline{\overline{\vartheta}}$	Emergency temperature limit, [°C]
$\overline{\vartheta}$	Cyclic temperature limit, [°C]
Π^{WF}	Design lifetime of windfarm, [years]
π_s	Probability of each scenario, [pu]
ψ	Function for WTG availability, [pu]
ρ_{soil}	Thermal soil resistivity, [m°C/W]
σ	Standard deviation
τ_{w}	WTG availability duration, [$hour$]
τ_0	Thermal time constant - oil, [$hour$]
τ_h	Thermal time constant - wdg, [$hour$]
ε_t	White noise signal
ϖ_{soil}	Soil specific heat, [m°C/W]
ϑ^{amb}_t	Ambient temperatures, [°C]
ϑ^{sea}_t	Seabed temperatures, [°C]
A	Pre-exponential factor, [1/hour]
A^{SF}_t	Scaling factor for export system [pu]
A^{W}_t A^{c}_t	OWF & transmission circuit availability
a_k, b_k	Thermal coefficients for cables and trafos
c	Cost of components & relevant energy dispatch, [€/unit, €/km, €/tonne, €/MWh]
C_{soil}	Thermal capacitance for soil, [J/m°C]
C_{th}	Thermal capacitance of trafo, [Wh/°C]
C_x	Thermal capacitance for cable, [J/m°C]
e	Empirical coefficients for trafo scaling
E_{curt}	Total curtailed energy, [MWh]
E_{del}	Total energy delivered, [MWh/yr]
E_{loss}	Total energy loss in export system, [MWh]
E_a	Min. activation energy for reaction, [kJ/mol]
g	Cost coefficients for cables
i	Discount rate for NPV calculation, [pu]
$I^{\text{c}}_{Q\,k}$	Reactive component of cable current, [A]
L^{c}	Length of subsea export cable, [m]
m	Mass of relevant components, [tonne]
n	Number of components
n^H	Number of hidden layers (ANN)
n^{test}	Number of test observations
n^{train}	Number of training observations
P^{load}_t	Hourly demand in test system, [pu]
P^{w}_t	OWF power generation, [pu]
$p_{j,l}$ $q_{j,l}$	Slope and intercepts for linear approx.
r	Resistance of components at temp. limits, [Ω]
R_g	Ideal gas constant, [J/(mol.K)]
S	Component rating, [MVA, MW, MVAr]
T_{soil}	Thermal resistance for soil, [m°C/W]
T_x	Thermal resistance for cable, [m°C/W]
u_t, U_t	Input signal (train & test)

$V^{oil\,pu}$	Actual oil viscosity w.r.t. rated TOT, [pu]
V_{ll}	Line to line voltage of export system, [kV]
$W_{rated}^{\text{trf,cu,e}}$	Ratio of transformer rated load losses to no-load losses, [pu]
W_{rated}^{trf}	Transformer total rated losses, [W]
W_d	Dielectric losses in cables, [W]
W_{nl}	No load loss in transformers, [W]
y_t, Y_t	Measured signal for training
Z^{trf}	Representative trafo parameter in Table 8.1
$\mathbf{P}$	State transition matrix

Decision Variables and Outputs:

$\boldsymbol{w}, \boldsymbol{w'}$	Weighing parameters (ARX & ANN)
χ	Forgetting factor for ML models
$\Delta\lambda_t$	Trafo ageing acceleration factor, [hr]
λ_y	Transformer loss of life - yearly (LL), [hr]
τ_p	Estimated time constant (ODE), [$hour$]
$\vartheta_t^{\text{cond}}$	Cable conductor temp. rise over ϑ^{sea} [°C]
ϑ_t^{dts}	Cable DTS meas. or estimation, [°C]
ϑ_t^{hdd}	Cable HDD temperature, [°C]
$\vartheta^{\text{hst}_\text{W}}$	Weighted average HST, [°C]
ϑ_t^{hst}	Transformer hot spot temperature, [°C]
$\vartheta_t^{\text{serv}}$	Cable serving temp. rise over ϑ^{sea}, [°C]
ϑ_t^{tot}	Transformer top oil temperature, [°C]
$\widehat{y_t}$	Estimated signal by ML model
C_0	Investment costs $= f\left(n^{\text{tur}}, C^{\text{fix}}, C_k^{\text{exp}}\right)$, [M€]
$I_{P\,t}$	Component load current (active), [A]
I_t	Component load current, [A]
K_p	Estimated gain (ODE)
n^{tur}	Number of wind turbines
P_t^{conv}	Hourly conv. gen in test system, [pu]
P_t^{cut}	Hourly power curtailed from OWF, [MW]
P_t^{gen}	Hourly power generated by the OWF, [MW]
P_t^{inj}	Hourly power injected to the grid, [MW]
P_t^{OSS}	Hourly OSS input power, [pu]
P_t^{sh}	Hourly load shed in test system, [pu]
P_t^{w}	Hourly wind gen in test system, [pu]
R	Total revenue over OWF lifetime, [M€]
W_t^{exp}	Export system losses, [W]
W_t^{a}, W_t^{s}	Cable losses (armour, screen), [W/m]
W_t^{cond}	Cable conductor losses, [W/m]
$W_{t,\vartheta^{\text{hst}}}^{\text{trf}}$	Temperature dependent transformer load losses, [pu]
W_t	Losses in components, [W]

Superscripts (Components & Test Cases):

pu	Per-unit representation
c	Cables and circuits
conv	Conventional generators
SR	Shunt Reactors
trf	Transformers
tur	Wind Turbines

Subscripts (Sets & Indices):

$\alpha \in \mathcal{A}$	Set of branches
$\beta \in \mathcal{B}$	Set of buses
$g \in \mathcal{G}$	Set of conventional generators
$j \in \mathcal{J}$	Set of tangent lines for losses approximation
$k \in \mathcal{K}$	Set of candidate design cases (Opt. case: k_{opt})
$l \in \mathcal{L}$	Set of tangent lines for ageing approximation
$s \in \mathcal{S}$	Set of scenarios
$t \in \mathcal{T}$	Set of hours in each year
$w \in \mathcal{W}$	Set of windfarms
$y \in \mathcal{Y}$	Set of years in windfarm lifetime Π^{WF} [yr]
base	Base design cases
opt	Optimal design cases

PART I - PRELIMINARIES

CHAPTER 1

Introduction

1.1 Motivation

Over the last decade, the cumulative installed capacity of offshore wind energy has increased ten-fold across the globe as the overall capacity crossed the 23 GW mark in 2019 [1], as shown in Fig. 1.1. This growth is expected to accelerate even further as per the recently announced plans of governments and energy ministries in UK [2], Japan [3], US [4] and the ambitious 450 GW offshore windfarm target in 2050 by the EU [5].

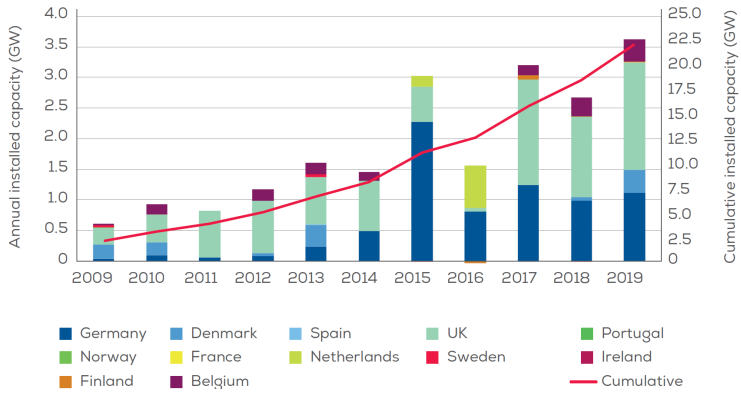

Figure 1.1: Annual installed capacity and cumulative installation capacity of offshore wind energy across the globe between 2009 and 2019 [1].

Until now, the development of major Offshore Windfarm (OWF) projects has primarily been facilitated by energy price support set by the auctioned Contract for Difference (CfD) allowing the energy produced by OWFs to be sold at the strike price of the project which is usually higher than the spot-market price. Alternatively, fixed government subsidies in the form of Feed-in Tariffs (FiT), which allow premium payments for capped annual energy production have further eased the development of OWFs. Some of the relevant projects, along with their subsidies and CfD strike prices, are provided in Fig. 1.2. The process for energy price stimulation allowed OWF projects to become attractive investment opportunities for developers. However, the strike prices have been driven down significantly from 195 $\frac{€}{\text{MWh}}$ for the 402 MW Dudgeon windfarm which was commissioned in 2017 to 45 $\frac{€}{\text{MWh}}$ for the 1200 MW Doggerbank Creyke Beck A to be completed in 2025 [6]. The plummet in strike price and the exponential growth of OWF integration has been expedited by the decrease in Levelized Cost Of Energy (LCOE) from 180 to less than $40\frac{€}{\text{MWh}}$ over the last decade [1]. As a result, intense price competition has flourished in the markets which has prompted both the manufacturers and developers to optimize the entire value chain [7]. Nevertheless, there is need to drive down the LCOE for offshore wind further in order to keep it competitive to alternative/conventional energy sources and to meet the large scale integration goals set by countries around the world.

One source of economic optimization for OWFs that remained relatively unexplored prior to this project is the utilization of intermittent nature of the wind to design and operate the electrical components of the OWF transmission network. As a result of intermittent generation, the annual capacity factor for offshore wind ranges between 38-46 %, which is also demonstrated by the load duration curves for a number of OWF projects in UK in Fig. 1.3. On average, all the OWFs in UK produced more than 90% of their rated capacities

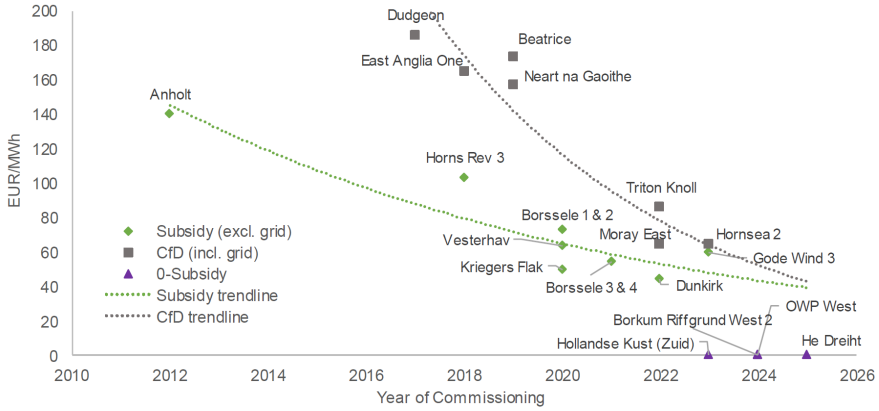

Figure 1.2: Trend for change in energy price support for offshore windfarms considering subsidy (FiT) excluding grid connection costs and auctioned CfD including grid connection costs. Zero subsidy projects to be built in the near future are also mentioned. Source: [6]

only 5% or less of the time since their respective commissioning dates. This number includes the influence of availability of wind turbines which are prone to mechanical failures and frequent maintenance activities [8, 9].

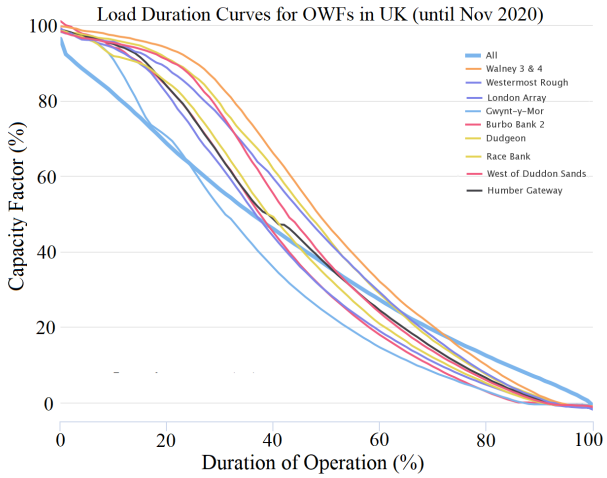

Figure 1.3: Load duration curves for offshore windfarms in UK. The data has been used since the full-commissioning dates of the respective OWF or from January 2009 onward (whichever is more recent). For the cumulative curve representing all windfarms, last 5 year data has been used. Data obtained from [10]

Conventionally, the HV components in OWFs are designed conservatively such that the overall transmission capacity of the OWF is larger than or exactly equal to its production capacity. This is because Static Thermal Rating (STR) principles are predominantly used for the HV electrical equipment which prevents these components from being operated beyond their nameplate capacities at any given time. The alternative operating mechanism of Dynamic Thermal Rating (DTR) can be used to utilize the cyclic operational limits by pushing more power through these components under favorable ambient conditions and by tracking the historic load and thermal profiles of the components. DTR-based operation and design depends significantly on the thermodynamic performance of the HV equipment, which is usually slower to respond to load variation. As an example, the thermal time constants for 3-core XLPE insulated HV cables range up to few days, which means that steady-state operation at the rated load would be needed continuously for weeks to reach the thermal limits of these cables. Therefore, if STR-based loading mechanism is used for the cables installed in OWFs, the respective thermal limits will ideally never be reached. The influence of high thermal

time constants is demonstrated in Fig. 1.4, where simple moving average calculations are made for long-term wind speed and power production profiles for a test case OWF. The moving average curve for cable load does not touch the 100% mark even once during the 15-year observation period, which indicates the need for improvement in component design and operational practices. Moreover, the HV electrical equipment are known to last $\geq$40 years, while the OWFs are designed for an operational lifetime of 25-30 years. As a result, these components are bound to have $\geq$10 years of useful residual life at the time of OWF decommissioning. Hence, by considering all of these factors, the utilization and design of major HV components of the OWF transmission system can be improved significantly.

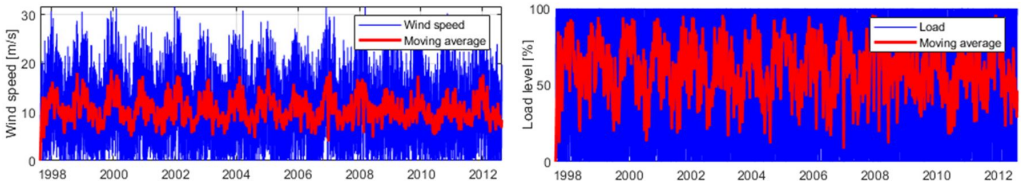

Figure 1.4: Assessment of influence of thermal time constants on load variation due to intermittent nature of wind production in offshore windfarms for a test case OWF in UK. Left: 7-day moving average window is used for 15-year wind speed profile of the test site. Right: Same moving average window is used on the hourly production to assess the thermal development in OWF cables.

The HV transmission system is known to contribute extensively to the overall Capital Expenditures (CAPEX) of the OWF projects as it accounts for up to 43 % of the overall investment [11] and has similar financial impact as the overall wind turbine package (incl. foundation costs). As more and more large-scale OWFs are built further from the shore, the potential to utilize the variable nature of wind for optimum sizing and operation of the transmission components to further decrease the LCOE escalates as well [12]. However, DTR-based design and operation can negatively influence the system losses and availability which can truncate the profitability over the OWF lifetime in the process [13–15]. Therefore, a balance needs to be maintained to identify the optimal solution that maximizes the Net Present Value (NPV) of the project. Besides the need for DTR-based design and operation of HV equipment in the transmission network, OWF projects offer unique challenges because of difficulty in accessibility and logistical support in the offshore environment. Therefore, smart condition monitoring of the critical components using the data available from commonly installed thermal monitoring equipment is critical for sustainable employment of DTR methodologies.
All of the attributes mentioned above serve as the motivation for this PhD project, with focus on the optimization of electrical transmission network for large-scale OWF projects.

1.2 Scope and Background of the Industrial PhD Project

The Industrial PhD project has been focused on the HV export system of the OWF, which is responsible for transmitting the collected wind energy from the offshore substation in the sea to the onshore substation on land and then to the connected grid. The layout of the HVAC-based transmission system along with the scope of the PhD project are highlighted in Fig. 1.5. This layout is further elaborated in detail in Chapter 2.

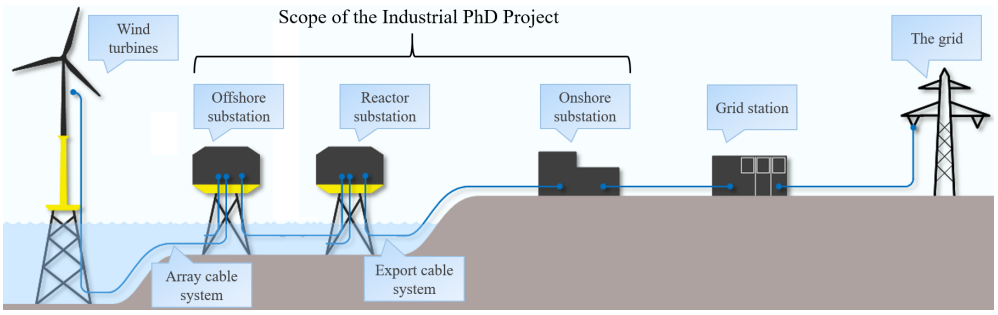

Figure 1.5: HVAC-based transmission system layout for offshore windfarms and scope of the PhD project.

The transmission technology that the PhD project focuses on is HVAC-based. However, the established concepts and the developed methods are easily extendable to the HVDC transmission technology as well. In order to refine the scope of the PhD project further, breakdown of the export system CAPEX has been provided in Fig. 1.6 for a number of offshore windfarms in UK. This simplified analysis shows that offshore substations (including foundation and civil works) and the offshore section of the export cables (including installation and commissioning) constitute the major costs of the OWF export system. Therefore, optimal design and utilization of the electrical components relevant to these subsystems should supposedly have the highest influence on the overall business case.

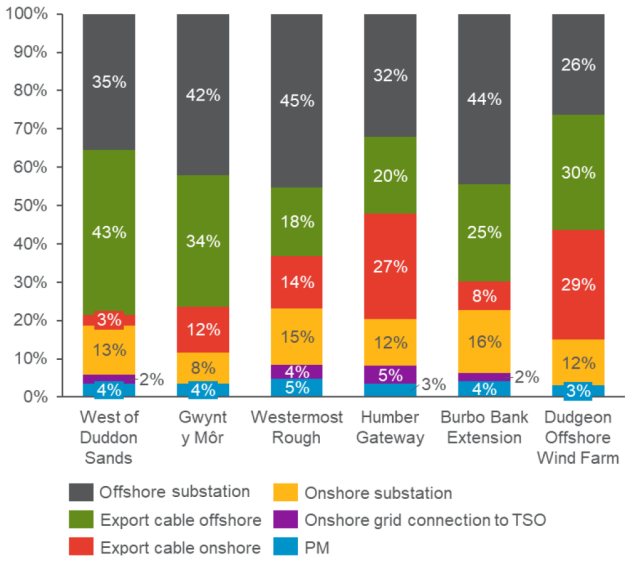

Figure 1.6: Breakdown of capital expenditures for transmission system of a number of commissioned offshore windfarms in UK [6]

Over the last decade, a number of publications have surfaced that present and analyse a number of techniques to optimize the design and utilization of the electrical network of the offshore windfarms [14, 16–26], which effectively address the efficiency of the electrical infrastructure, along with the investment costs and operational expenses. These publications are predominantly focused on the optimization of the cable routing and layout of the array cable network [16–20], while the rest of the OWF transmission network (HV export system) has been discussed in only a handful of the published research work. A substantial portion of this work has centred around optimization of HVAC submarine cables without the application of DTR [14, 21–23], while DTR has been used for cable design optimization in [24–26]. While on the contrary, the potential of optimizing the remaining HV components and systemic application of DTR on the complete export system is completely unexplored [12]. Furthermore, iterative coupling is predominantly used in defining the windfarm size and the ratings of HV transmission system components [22]. DTR-based optimization of transformer is given keen attention in this thesis, because these components are commonly over-dimensioned, are critical for security of supply, can outlive the OWF by tens of years, influence the business considerably and unlike cables, have not been addressed in the literature.

Even though, application of DTR for optimal utilization of transmission system components has been discussed in the literature [27], the application of this principle for OWFs during the design phase has been left untouched. This is because the uncertainty in wind generation profile over the OWF lifetime is a challenge, while the possible contingency of the system due to longer repair times and high capacity factors introduce reliability challenges [12, 17]. A number of probability-based methods ranging from analytical techniques [28] to Monte Carlo simulations [14, 17, 29] can be used to address these challenges. However, a balance needs to be maintained between problem complexity and computational efficiency for the design and utilization

problems. The state-of-the-art and the extensive literature review performed over the course of this project have been presented through out the thesis in the relevant sections.

1.3 Research Questions

Based on the scope of the PhD project, following research questions have been drawn up:

[Q1] What are the inherent thermal bottlenecks in the OWF export system and how can DTR facilitate resolution of major pinch-points?

[Q2] Can DTR be employed for operational and design optimization problems for offshore windfarms by using state-of-the-art thermal models for critical HV export system components? What modifications should be made to these models to make them fit for the relevant applications?

[Q3] How and why should machine learning and data analytics be used for dynamic thermal estimation and condition monitoring of OWF export system components? Is it possible to extract physical, operational insights about the components from the semi-physical grey-box and empirical black-box models?

[Q4] Is there a need to optimize the utilization of critical export system components by using DTR and/or by tracking their thermal and thermo-chemical ageing for reliable operation of the existing offshore windfarms? Can DTR facilitate the integration of OWFs in the transmission grid with minimal infrastructural investments?

[Q5] How can DTR be used to optimize the design of the complete OWF export system or its critical components over its entire lifetime, while accounting for uncertainty in generation and system availability/contingency?

[Q6] What are the economic and technical considerations needed for DTR-based design optimization of OWF export system? How can variables like efficiency of transmission, possibility of energy curtailment and reliability of design be used for economic optimization of offshore windfarm design based on DTR?

1.4 Contributions

The main contributions of the PhD project have been enumerated below:

(A) Comprehensive thermal assessment for identifying major bottlenecks in the HVAC-based export system for offshore windfarms considering energy availability, with focus on components and sub-components in offshore substations and export cable sections.

(B) Reformulation and validation of the relevant state-of-the-art thermoelectric models to prevent non-convexity of the developed optimization problems. The simplified models are based on:

  i) Temperature dynamics of transformer oil and winding under natural and forced cooling.

  ii) Data-driven parameter estimation and consolidation of thermoelectric nodes across cable cross-section.

(C) Development of data analytics based semi-physical grey-box and black-box models for dynamic thermal estimation of transformers and subsea export cables to account for variation in design and operational characteristics across portfolio projects. This is followed by validation and comparison of the developed models on actual offshore windfarm data and lab test setup.

(D) Evaluation of the potential condition-monitoring applications of the developed machine learning models including variation in surrounding characteristics along the subsea cable route and operating conditions of wind turbine transformers.

(E) Development and application of an iterative methodology for design and utilization of offshore windfarm transformers based on its cumulative loss-of-life. Two different approaches are used:

i) For operational and design optimization problems, standard Arrhenius reaction rate model is linearized.

ii) For iterative design problems, ageing models based on degree of polymerization are evaluated and benchmarked for accurate thermo-chemical decomposition considerations of cellulose-based insulation paper over the windfarm lifetime. The choice of end-of-life criterion and proposal of moisture/oxygen variation is performed on the basis of this analysis.

(F) Assessment of utilization of transformers from multiple actual OWFs under varying load conditions to recognize the potential for DTR-based optimal operation across portfolio projects and optimal design of pipeline projects.

(G) Development, testing and application of techniques for modeling of uncertainty in wind energy production and system availability over the OWF lifetime by adopting sophisticated trend analysis mechanisms. Following methods are utilized:

i) Stochastic ARIMA processes that account for daily and yearly seasonalities to model long-term time series for wind speed.

ii) Probabilistic discrete-time Markov chain processes for stochastic availability of wind turbines and contingency of export system circuits/components.

(H) Formulation, testing and application of an iterative technique for optimization of NPV and Transmission LCOE for offshore windfarms based on transformer DTR and thermo-chemical ageing, while accounting for contingency, system losses and possible curtailment over the OWF lifetime.

(I) Formulation and application of a lossy DC Optimal Power Flow (DCOPF) algorithm based on a Mixed Integer Quadratic Constrained Program (MIQCP) convex optimization problem that facilitates large-scale integration of offshore windfarms in the day-ahead market and allows deferring grid reinforcement costs by using DTR and lifetime-based transformer utilization. The problem is tested for actual load, weather and generation data from west-Denmark.

(J) Development, testing and application of an investment decision support tool for OWF sizing and export system design. This tool is based on a two-stage Mixed Integer Linear Program (MILP) stochastic optimization problem which uses DTR and thermal coordination of the relevant HV export system components for the optimization of windfarm business-case over the OWF lifetime, while accounting for load-dependent losses, energy curtailment and system reliability.

1.5 List of Publications

The work presented in this dissertation has been disseminated in a number of journal publication which are included in the Appendix. The relevant journal publications are listed below:

[**Pub. J1**] S. H. H.Kazmi, T. Laneryd, K. Giannikas, S. F. Ahrenfeldt, T. H. Olesen, T. S. Sørensen and J. Holbøll, **"Cost optimized dynamic design of offshore windfarm transformers with reliability and contingency considerations"**, *International Journal of Electrical Power and Energy Systems* Dec 2020.

[**Pub. J2**] S. H. H.Kazmi, N. Viafora, B. C. Pal, T. S. Sørensen, T. H. Olesen and J. Holbøll, **"Offshore Windfarm Design Optimization using Dynamic Rating for Transmission Components"**, submitted to *IEEE Transactions on Power Systems*, Nov 2020.

The scientific papers presented in a number of international conferences to publish the work presented in this thesis are enumerated below. These papers are also attached in the Appendix.

[**Pub. C1**] S. H. H.Kazmi, T. H. Olesen, T. S. Sørensen and J. Holbøll, **"Thermoelectric Modelling and Optimization of Offshore Windfarm Export Systems - State of the Art"**, *IEEE Global Power, Energy and Communication Conference (GPECOM)*, Nevsehir, Turkey, July 2019.

[**Pub. C2**] S. H. H.Kazmi, T. H. Olesen, T. S. Sørensen and J. Holbøll, **"Dynamic Thermoelectric Modelling of Oil-Filled Transformers for Optimized Integration of Wind Power in Distribution Networks"**, Paper 1744, *25th International Conference on Electricity Distribution (CIRED)*, Madrid, Spain, June 2019.

[**Pub. C3**] S. H. H.Kazmi, T. H. Olesen, T. S. Sørensen and J. Holbøll, **"Dynamic Thermoelectric Modelling of Oil-filled Power Transformers for Optimization of Offshore Windfarm Export Systems"**, *CIGRE Symposium*, Aalborg, Denmark, June 2019.

[**Pub. C4**] N. Viafora, S. H. H. Kazmi, T. H. Olesen, T. S. Sørensen and J. Holbøll, **"Load Dispatch optimization using Dynamic Rating and Optimal Lifetime Utilization of Transformers,"** *IEEE PES PowerTech*, Milan, Italy, July 2019.

[**Pub. C5**] S. H. H.Kazmi, T. H. Olesen, T. S. Sørensen and J. Holbøll, **"Machine Learning based Temperature Forecast of Offshore Windfarm Export Cables"**, *B1-109 CIGRE*, Paris, France, Aug 2020.

[**Pub. C6**] S. H. H.Kazmi, T. H. Olesen, T. S. Sørensen and J. Holbøll, **"Thermal Analysis and Debottlenecking of HVAC Export Cables for Offshore Windfarms"**, Accepted (awaiting presentation), *3rd CIGRE South East European Regional Council Conference*, Vienna, Austria, Nov 2021.

[**Pub. C7**] S. H. H.Kazmi, T. H. Olesen, T. S. Sørensen and J. Holbøll, **"Machine Learning based Dynamic Thermal Modelling of Offshore Wind Turbine Transformers"**, Accepted (awaiting presentation), *41st CIGRE Symposium*, Ljubljana, Slovenia, Jun 2021.

Other publications that have also been prepared during the course of the Industrial PhD project, but have been omitted because they are not directly related to the primary objective of the thesis, or because the scientific information has been partially covered in the remaining papers.

[**Pub. D1**] N. Viafora, K. Morozovska, S. H. H. Kazmi, T. Laneryd, P. Hilber and J. Holbøll, **"Day-ahead dispatch optimization with dynamic thermal rating of transformers and overhead lines"**, (2019) Electric Power Systems Research, Special Issue on Dynamic Rating 171, pp. 194-208.

[**Pub. D2**] S. H. H. Kazmi, **"Real-time Dynamic Rating and Condition Monitoring of Offshore Windfarm Export Systems"**, Poster Presentation, XIII *International Conference on Electrical Machines (ICEM)*, Alexandroupoli, Greece, Sep 2018.

[**Pub. D3**] K. Morozovska, S. H. H. Kazmi, F. Hajeforosh, P. Hilber and J. Holbøll, **"Net Present Value Optimization of Onshore Windfarm Design with Dynamically Rated Transformers"**, *Working Journal Paper*.

1.6 Thesis Structure

The rest of the PhD thesis has been divided into five parts. In order to draw an intelligible and transparent structure, the distribution of research questions, original contributions and relevant publications of the project is provided in Table 1.1 for the respective parts.

Table 1.1: Distribution of research questions, original contributions and relevant publications across Parts I-V of the dissertation.

Part	Research Question	Contribution	Publication
I	-	-	-
II	Q1 - Q3	A - D	C1 , C5 - C7
III	Q2 , Q4	E - F , I	C2 - C4
IV	Q2 , Q5 - Q6	G - H , J	J1 - J2
V	-	-	-

The contents of Parts II - V are briefly elaborated below:

- **Part II:** This part consists of chapters 2 and 3. The analysis is kicked-off in **Chapter 2**, where the layout and inherent thermal bottlenecks of the OWF export system are presented. The state-of-the-art dynamic thermal models using empirical differential equations based methods are discussed and then simplified for linear optimization applications. Furthermore, this chapter validates the DTR models for intermittent loading of components from multiple OWFs across the globe and provides the necessary background for discussion in the remaining chapters. Afterwards, the need for data-driven thermal estimation models for OWF components is elaborated in **Chapter 3**, which provides an exhaustive classification of relevant machine learning models used in this project. The difference in structure, estimation of parameters and key advantages of these models are highlighted, which is followed by validation and benchmarking of these models on measured temperature data from the relevant OWF components. The chapter finally touches upon the dynamic condition monitoring applications of these modern grey-box and black-box models for semi-physical estimation of HV export cable surroundings and thermal estimation of wind turbine transformers.
- **Part III:** This part deals with optimal utilization of offshore windfarm transformers in the operational frame work and it consists of chapters 4, 5 and 6. Firstly, in **Chapter 4** the thermal and thermo-chemical ageing of transformers using Arrhenius reaction rate and degree of polymerization models are benchmarked and their performance has been evaluated under different operating circumstances. Secondly, in **Chapter 5**, the shortlisted ageing models are used to identify the potential for DTR-based optimal utilization of OWF transformers using actual test case windfarms. Finally in **Chapter 6**, a dynamic ageing based utilization principle for a DCOPF algorithm is developed and tested for day-ahead dispatch optimization of IEEE 24-bus network by mapping the actual generation, load and wind production data from the transmission system of west-Denmark. The proposed technique is found to ease large-scale integration of offshore windfarms in the network by delaying grid-reinforcement costs.
- **Part IV:** This part of the thesis presents the optimization of export system components during the design and planning phase of offshore windfarms and it comprises of chapters 7, 8 and 9. In **Chapter 7**, methodologies for generation of set of scenarios are presented which are necessary to account for uncertainty in wind generation and system availability over the windfarm lifetime. In rest of the chapters, two techniques are developed and tested for economic optimization of actual test case offshore windfarm design which use DTR for rating of critical HV components of the export system. The first model (presented in **Chapter 8**) is an iterative algorithm, while the second model (presented in **Chapter 9**) is a two-stage stochastic optimization problem for investment decision support during the OWF planning phase. The developed methods are found to improve the business case considerably even after consideration of system losses and possible energy curtailment during contingency.
- **Part V:** The final part, comprising of **Chapter 10**, presents conclusions and outlines future research directions for the project. Furthermore, answers to the research questions and prospects of the developed methodologies are also discussed in this part.

PART II - THERMAL ASSESSMENT OF EXPORT SYSTEM AND EXPERIMENTAL VALIDATION OF MODERN THERMAL MODELS

This part has been split into two chapters: **Debottlenecking & Dynamic Thermal Modeling of OWF Transmission System** and **Dynamic Condition Monitoring using Data Analytics**. The details for this split are presented below.

It has been shown so far that the transmission system contributes extensively to the Capital Expenses (CAPEX) of the Offshore Windfarm (OWF) projects, with the highest investment costs being driven by the export cables and offshore/onshore substations. In order to identify the exact contributions of the relevant HV components and their performance under Dynamic Thermal Rating (DTR) based operation and design, it is important to distinguish the inherent thermal pinch points in the OWF export system. Afterwards, thermal modeling of the identified bottlenecks needs to be performed for real-time thermal estimation under dynamic load conditions. This is discussed in detail in Chapter 2

The thermodynamic behavior of these components is not only dependent on their physical attributes which are time-variant, but are also usually influenced by parameters that vary with environmental conditions. As an example, the thermal development of a test case OWF export cable is shown for its entire route over the period of 8 days in Fig. 1.7. The conventional thermal estimation mechanisms offer limited adaptability, while the data-analytics based machine learning algorithms, presented in Chapter 3, can potentially resolve these issues.

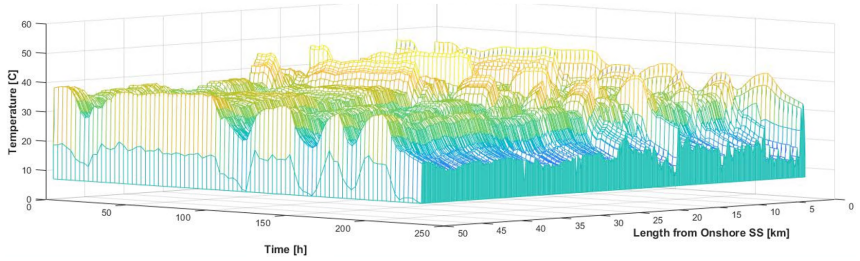

Figure 1.7: Variation of cable temperature over eight days along the entire length. The length is shown with respect to the onshore substation for the test windfarm. The thermal behavior is consistent along the route.

CHAPTER 2

Debottlenecking & Dynamic Thermal Modeling of OWF Transmission System

In order to employ dynamic rating on OWF export system components, it is critical to understand the system layout, design practices and inherent bottlenecks. In this project, HVAC-based transmission system is focused upon, but the concepts are extendable to HVDC technology as well. This chapter unfolds the export system and presents the state-of-the-art thermal models to be used for dynamic thermal estimation of the critical HV components. The discussion is focused on parameterization, benchmarking and modifications of the identified differential equations based Thermoelectric Equivalent (TEE) models, which is followed by validation of these models on actual test case windfarm components. The relevant non-linear, non-convex TEE models are simplified in this chapter to make them fit for linear optimization problems developed in the remaining chapters. A significant portion of this work has been presented in publications **[Pub. C1], [Pub. C2]** and **[Pub. C6]** by the author.

2.1 HVAC-based Offshore Windfarm Export System - Layout and Description

The energy produced by Offshore Windfarms (OWFs) is conventionally transmitted to the onshore grid using HVAC technology. The system responsible for this can be split into two subsystems: collection and transmission. The collection system gathers the energy from Wind Turbines (WTs) using a meshed network of subsea array cables and transfers it to the offshore substation(s); while the transmission system, also referred to as OWF export system in this project, is responsible for voltage step-up and transmission to the onshore grid. This project focuses primarily on the latter system.

As shown in Fig. 2.1(a) with two parallel circuits, the OWF export system usually consists of three types of substations: One or more Offshore Substations (OSS) close to the turbines, Onshore Substation (OnSS) on land serving as the interface between OWF and onshore transmission grid, and lastly, Reactive Compensation Station (RCS) close to the midpoint of the export cables. Even though HVAC technology is feasible for transmission up to 70 km length for large offshore windfarms, the intermediate shunt reactors placed in the RCS help increase the transmission distance. The exact number of substations for each type depend upon the location and size of OWFs, as governed by local design regulations and redundancy requirements. The OSS primarily consists of HV equipment which include oil-filled power transformers, HV/MV Switchgear (commonly gas-insulated), equipment for dynamic compensation, LV systems etc. While the OnSS commonly comprises of a range of additional HV components (incl. harmonic filters, static and variable compensation equipment etc.) which are necessary to fulfill grid-code requirements at the Point of Common Coupling (PCC). This is shown in Fig. 2.1(b) for a single-circuit OWF transmission system. It is important to clarify that system designers commonly employ multiple parallel circuits to improve system reliability and availability, but a balance has to be made between Capital Expenses (CAPEX), expected Operational Expenses (OPEX) and foreseen revenue during the design phase.

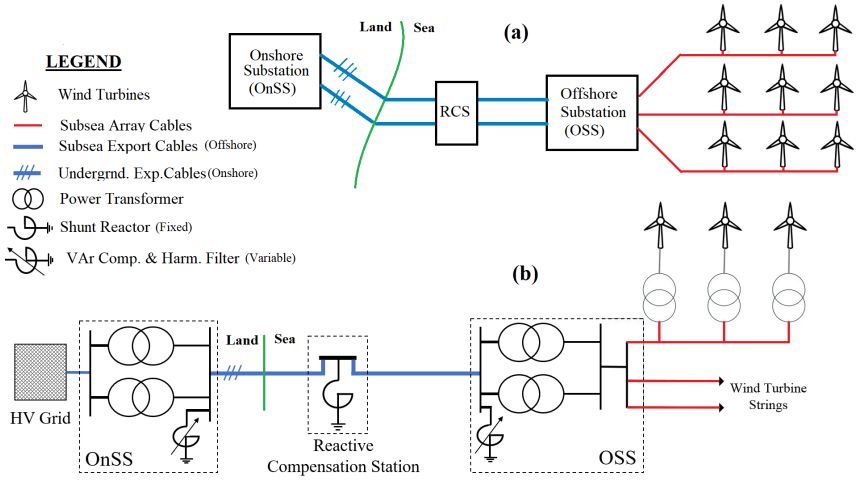

Figure 2.1: Simplified layout of offshore windfarms with focus on the HV export system. (a) Layout of onshore, reactor and offshore substations for export system with two parallel circuits. (b) Topology for connection of HV components in a typical circuit of HVAC-based export system.

One of the test case OWFs used in this project is Anholt windfarm located off the east coast of Jylland (Denmark) in the Kattegat sea. This 400 MW windfarm consisting of 111 3.6 MW turbines was jointly developed by Orsted and Energinet. The exact distribution of work scope for the two parties and the transmission system layout for Anholt are provided in Fig. 2.2. The export system topology for Anholt is unique as it comprises of three parallel transformers for the single-circuit transmission system, as compared to the other test-case OWFs studied in this project which usually consist of two parallel transformers per circuit.

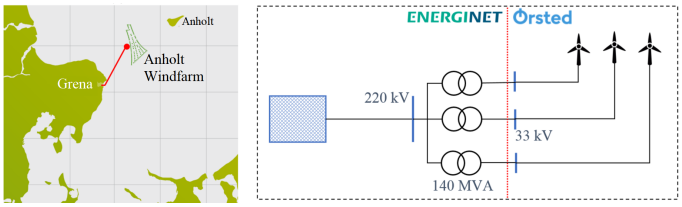

Figure 2.2: Layout for Anholt offshore windfarm in Denmark. (a) Location, wind turbine layout and onshore connection points for the windfarm [30]. (b) Layout of the HV export system and ownership/commissioning boundaries between Orsted and Energinet

2.2 Debottlenecking of HVAC-based OWF export system

It is important to identify the constraining HV components in the OWF export system for effective dynamic rating based design and operation. At the same time, it is critical to determine components that are either not affected by or have minimal influence under dynamic load conditions [31]. The business case for offshore windfarm export system design considers two system availability aspects: time and energy availability. Time availability determines the ability of the OWF export system to stay connected to the onshore PCC at all times without necessarily transmitting all the produced energy, while energy availability represents the ability to transmit the entire production capacity of the windfarm at all times. The first parameter allows compliance with local system operator regulations, while the latter influences the business case and revenue accumulation over the OWF lifetime. Simplified reliability block diagrams for a single-circuit OWF export system from Fig. 2.1(b) are provided for both time and energy availability considerations in Fig. 2.3. Under existing design mechanisms, all the export system components have to be available at all times for maximum energy transfer, whereas redundant components can be out-of-operation for certain duration for the system to comply with time availability requirements. The OWF export system components are classified into two categories in this

section because of their varying influence on energy transmission under dynamic load. Reliability diagrams and the relevance of highlighted blocks of Fig. 2.3 are further elaborated in the respective sub-sections.

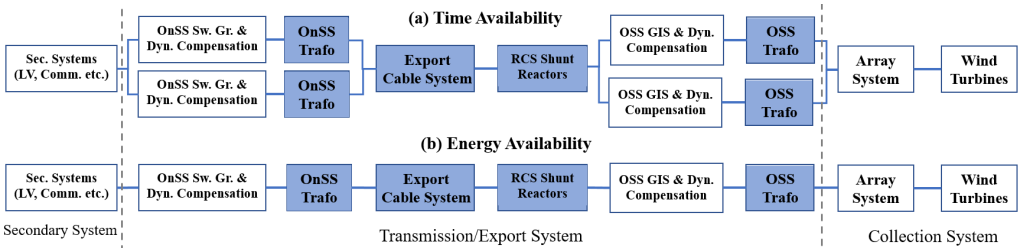

Figure 2.3: Simplified reliability block diagrams for each parallel circuit of the overall offshore windfarm HV export system from the perspectives of time and energy availability.

2.2.1 Substation Components

Even though HV export cables are known to be the primary bottlenecks in OWF export system because of the associated capital investment, some of the substation components can be just as important for system optimization during contingencies and planned/unplanned maintenance activities. Referring to Fig. 2.3, the system will fulfill the requirements of time availability if either of the two OSS transformers is available, but not for energy availability. In case of failure of any one of the these components, the export system will not be able to transmit the entire windfarm capacity and OSS transformers would become the primary system bottleneck. This is currently resolved by using over-sized transformers, such that overall transformer capacity is 120-140% of the windfarm's rated production. Such a practice allows the system operators to push up to 70% of the windfarm rated capacity during one transformer contingency scenario. However, under normal operation this extra transformation potential is left unused. Since transformers are the heaviest components on OSS, like the one in Fig. 2.4, its rating should be optimized to drive down CAPEX related to OSS foundation. Last but not the least, thermal time constants for transformers are considerably lower than cables which makes their thermal development to be more susceptible to load changes. Therefore, careful considerations are to be made if Dynamic Thermal Rating (DTR) is used for transformer operational and design optimization.

Unlike OSS transformers, shunt reactors located in the RCS are rarely the system bottlenecks under current design standards. However, the influence of their weight on RCS foundation costs and the direct dependence of their rating on the chosen cable design make them ideal for consideration in this study.

Figure 2.4: Offshore substation at Anholt windfarm in Denmark [30]

On the other hand, the need for optimization of ratings for OnSS transformers, OnSS/OSS switch gears and dynamic compensation equipment (harmonic filters, static compensators, variable reactors etc.) located in the onshore and offshore substations is found to be less critical for this project. The reason behind this

assessment is three-folds: Firstly, dynamic compensation components are mostly responsible for power quality at PCC and their respective locations over the entire range of dynamic load conditions with or without DTR considerations, which leaves less room for thermal design optimization. Secondly the influence of OnSS equipment's ratings on CAPEX and OPEX is minimal due to moderate weight-dependent foundation costs and ease of access to the substation. Lastly, the recorded experience for switch gears and compensation equipment suggests that load-dependent ageing accounts for only 10.3 % to 14.5 % failures for these components [32, 33]; which when combined with the difficulty to actively control their load and the inability to effectively assess the influence of temperature variation on loss of dielectric strength makes them less relevant for DTR-based design optimization in this project [34, 35].

2.2.2 Export Cable System

As mentioned earlier, export cables are the most expensive components of the OWF export system which is why they are designed close to the thermal limits. The associated CAPEX investment and the difficulty to identify and localize load-dependent thermal stress in cables means that the system operators are extra cautious during load management over the OWF lifetime by operating these cables conservatively. In conjunction, all of these factors make HV export cables the predominant bottlenecks in the OWF export system and thereby the primary candidates for Dynamic Thermal Rating (DTR) based design and operation in this project.

Temperature sensors like thermo-couples, PT-100 etc. can be used for temperature estimation for points along the export cable route point, but precision issues with these technique can potentially miss localized hotspot development [36].Therefore, real-time thermal monitoring of offshore windfarm cables can conventionally be performed using Distributed Temperature Sensing (DTS) equipment which uses fibre-optic cables (embedded in the HV cable or placed nearby) as linear sensors to obtain a continuous temporal variation of the cable temperature profile along the entire route [37]. This is considerably better than point-wise spectrum measurement equipment as the latest equipment can accurately measure ($\pm 1^{\circ}$C) with precision of up to 1 m, even for long cables (>70 km) [38] [39].

Besides being the major constraint in OWF transmission system, export cable system has inherent thermal bottlenecks which are not only influenced by seasonal variation of intermittent wind generation, sedimentation, ambient seabed temperature but are also highly dependent upon the cable installation and commissioning procedures [40]. In Fig. 2.5, maximum annual DTS measurements for the entire export cable route of an offshore windfarm in the UK have been provided for two different years, such that 0km mark represents the onshore substation entry point, while the OSS is located near the 47km mark. For the test case OWF location, 2016 was relatively colder than 2014 as the annual average ambient temperature was 2.6 $^{\circ}$C lower. More importantly, the intermittent wind generation in 2016 did not sustain long enough compared to 2014 thereby resulting in lower DTS measurements. Detailed explanation of this graph is provided later in this section, but two key observations are made here: hotspot detection can be performed using long-term DTS measurements and symmetric behavior of each point along the cable route is comprehensible.

In Fig. 2.6, standard layout of OWF export cables is provided, which consists of one 3-core Cross-Linked Poly-Ethylene (XLPE) insulated subsea cable between the OSS platform and the shore where a transition joint connects it to three 1-core XLPE insulated underground cables installed in ducts all the way to the OnSS. Before the termination of cable armor at the entrance of OSS platform hang-off, the export cable is passed through the J-tube and the Cable Protection System (CPS). CPS is responsible to maintain appropriate bending radius and to prevent additional mechanical stress on the export cable during commissioning, installation and operational lifetime [41]. The shallow burial depth in the sea quickly increases as the subsea cable approaches the sea defense wall to be passed through the Horizontal Directional Drilling (HDD) pipe. Hence, based on the observations of Fig. 2.5 and the distinctive laying conditions of Fig. 2.6, the OWF export cable can be divided into five sections: J-tube, CPS, Offshore (subsea, directly buried), HDD and Onshore (underground, buried in ducts).

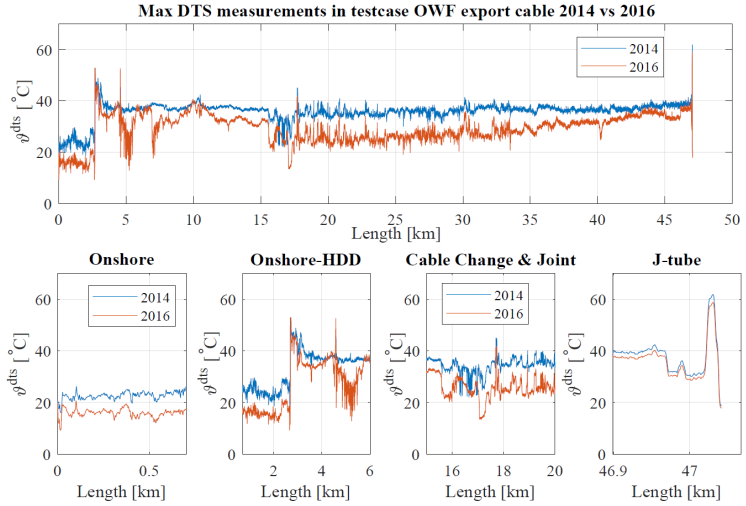

Figure 2.5: Maximum measured temperatures in years 2014 and 2016 for the export cable of the test case windfarm. Top: Measurements along the entire export cable length. Bottom: Closer look of different sections of interest

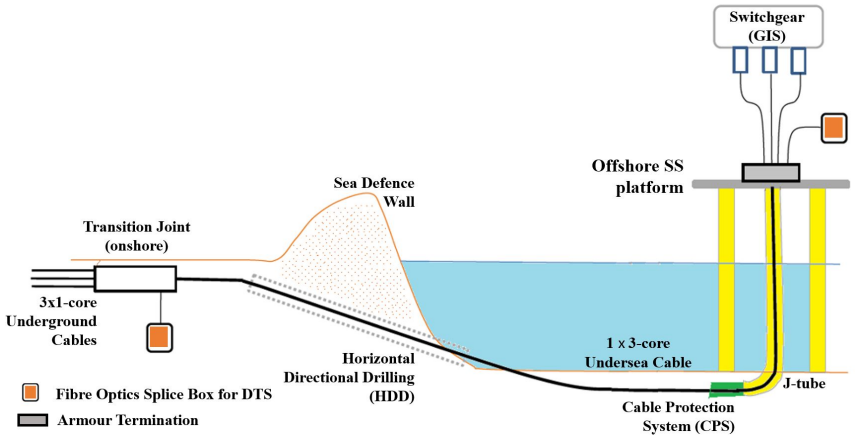

Figure 2.6: Overview of the main sections and sub-components for the HVAC-based export cable system in offshore windfarms.

The cable installation and commissioning conditions are considerably different in the sections mentioned above. As a result the temperature gradient and thermal time constants vary significantly along the export cable route. This is demonstrated further for the individual sections below:

- **J-tube Cable Section**

  J-tubes are commonly used in OWFs to provide the additional protection to the export cables from waves and tides. The three main segments of J-tubes incl. air, water and hang-off (termination for armour) are shown in Fig. 2.7 along with the DTS measurements for the respective section in test case OWF for a hot day in Summer 2014. Cable in the air segment is the hottest because of its exposure to the solar radiation and poor thermal dissipation characteristics compared to water. The temperature is observed to be highest in the middle of the air segment compared to the boundaries close to the water and OSS hang-off. This is due to the highest temperature gradient because of the longitudinal heat-flow at the boundaries [42]. This behavior is consistent during the daytime, which makes the J-tube air section one of the primary pinch-points along the export cable route, as shown in Fig. 2.5 earlier.

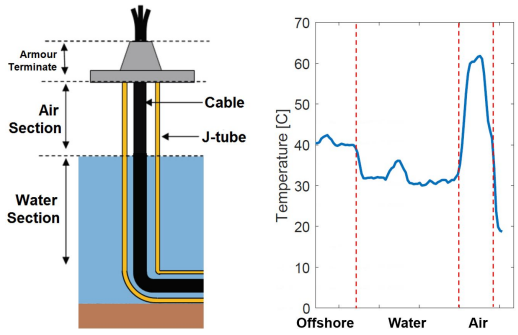

Figure 2.7: Left: Typical layout of the J-tube cable section [42]. Right: Temperature distribution in subsections of the test windfarm J-tube using DTS measurements

- **Onshore and HDD Cable Sections**

  The 1-core cables used in the Onshore section are not lined with optical-fibre cable, which is instead placed in a duct outside the cable carrying pipes. The DTS measurements are consistently lower for this section and a considerable offset needs to be added to obtain accurate conductor temperatures. On the other hand, onshore cables are laid in a relatively stable environment and are not designed as conservatively because of availability of large cable cross-sections by manufacturers at reasonable costs as compared to 3-core subsea cables [41]. Therefore onshore cable sections are seldom known to be the thermal pinch-points; in fact, the DTS data compiled for all the OWF projects in this study has not found the onshore section to be bottlenecks in any of the observed cases. The low and stable DTS measurements of onshore section are also demonstrated in Fig. 2.8 for another testcase windfarm off the west coast of UK.

  Between the onshore transition joint and the offshore section, the HDD section provides mechanical and environmental protection to the 3-core armored cable up to 1 km length. The significant burial depth in this section combined with high ambient temperatures and migration of soil moisture particularly in summer makes HDD environment to be thermally strenuous for cables [41]. The thermal pinch-points are resolved by using material like bentonite clay to fill up the HDD pipe due to its superior thermal dissipation qualities and by using cable with higher cross-sections in this segment [37]. Even with these provisions, HDD still returns high DTS measurements as shown in Fig. 2.8 for a hot summer day.

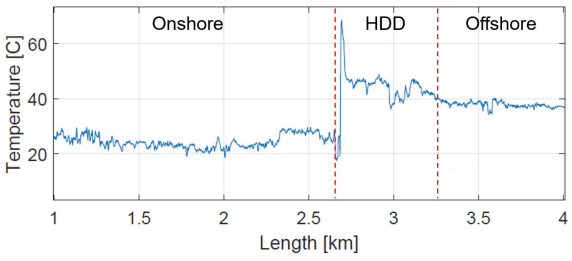

Figure 2.8: Temperature distribution in different sections of the test windfarm's export cable for a particular instant in 2014.

- **Offshore Cable Section**

  The longest cable section uses 3-core, armored cable which is buried directly in the seabed at the depth of 1 to 3 metres. The composition of the seabed material has a significant influence on cable's rating and its thermal performance in this section, as it varies considerably along the offshore cable route affecting the thermal resistivity and capacity of the cable surroundings. The variation in geological properties of seabed for an OWF cable in Denmark and its influence on the DTS measurements along the cable route are provided in Fig. 2.9. The sudden drop in observations near the 28 km mark can be explained

by transition from soft mud (clay) to gravel as the thermal resistivity ρ_{soil} of clay (0.56-2.5 m°C/W) is significantly higher than gravel (0.33-0.55 m°C/W) [43]. On the other hand, the volumetric specific heat capacity of soil ϖ_{soil} is similar for sand (1.09 to 3.04 $\times 10^6$ J/°C m^3) and soft mud (1.48 to 3.54 $\times 10^6$ J/°C m^3) as it depends on material porosity and vary with moisture content. Furthermore, natural offshore phenomena like sedimentation and seabed movement due to storms, sand wave migration, scouring etc. can change the cable burial depth over time. Therefore, new pinch-points may arise at local offshore segments due to change in thermal behavior over time.

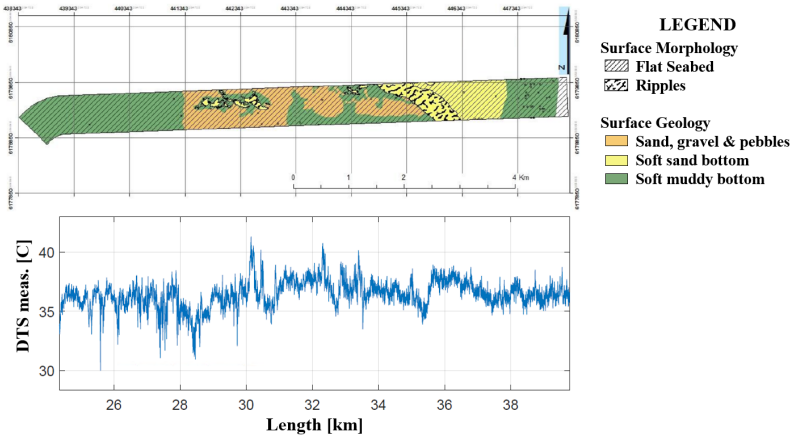

Figure 2.9: Top: Seabed surface geology of the offshore cable section for an offshore windfarm. Bottom: Cable temperature distribution (based on DTS measurements) for the same windfarm at an instant in time

2.3 Dynamic Thermal Modeling of HV Components

2.3.1 Thermal Modeling of Oil-filled Power Transformers

Transformer loadability depends directly upon two critical temperatures: Hot Spot Temperature (HST) and Top Oil Temperature (TOT) [44] [45]. Dynamic loadability of transformers for debottlenecking and optimization of OWF transmission system can be performed by real-time estimation of these temperatures. However, the thermodynamic behavior of transformers is considerably more complicated to design than cables [31]. During design phase, models based on computational fluid dynamics and thermo-hydraulic network are used extensively for dynamic thermal estimation of transformers [46]. But the complexity to design these models and the associated computational stress make them irrelevant for real-time operational and long-term design optimization applications. Therefore empirically derived TEE models are used in this project.

State-of-the-Art for Transformer TEE Modeling

The state-of-the-art is extensively presented in publication **[Pub. C1]**; whereas, only the relevant literature is briefly reviewed here. The analogy between thermodynamic principles and charge/discharge mechanism of RC circuit was originally introduced by Montsinger as the Exponential Law for temperature development in electrical machines [47]. This formulation has since been formalized into the existing structure presented as differential models in IEEE C57.91 [45], IEC 60076-7 [44], TEE models by Swift in [48], Tang in [49], Susa in [50] and many more. The experiments carried out in [51] and [52] facilitated the development of these empirical models which were later experimentally validated in [53–57]. The industry-wide accepted IEEE/IEC model of [44, 45] has improved significantly since 1990s by identification of error sources [58], accurate estimation of parameters [59] and application of statistical tools for restructuring [60]. Introduction of load-dependent losses and temperature-variant oil viscosity in Susa model [61] not just makes it unique and more reliable [62–64], but also offers a distinctive balance between design simplicity and accuracy [46]. Most of the recently proposed models explore data-analytics based designs with neural networks and fuzzy logic methods in the front [60, 65–68].

Relevant Models Considered in this Project

The dissipation of heat from winding to oil and oil tank to surrounding air is responsible for development of transformer HST and TOT respectively. The simplistic schematic for energy flow in transformers and fundamental TEE circuits for TOT and HST calculation are provided in Fig. 2.10. Two models are primarily considered in this project owing to their acceptance across the industry, flexibility of application and accuracy of estimation. As per IEEE C57.91 [45], transformer TOT and HST can be determined using (2.1), while the models by Susa *et al.* in [50, 61] are slightly more complicated as shown in (2.2).

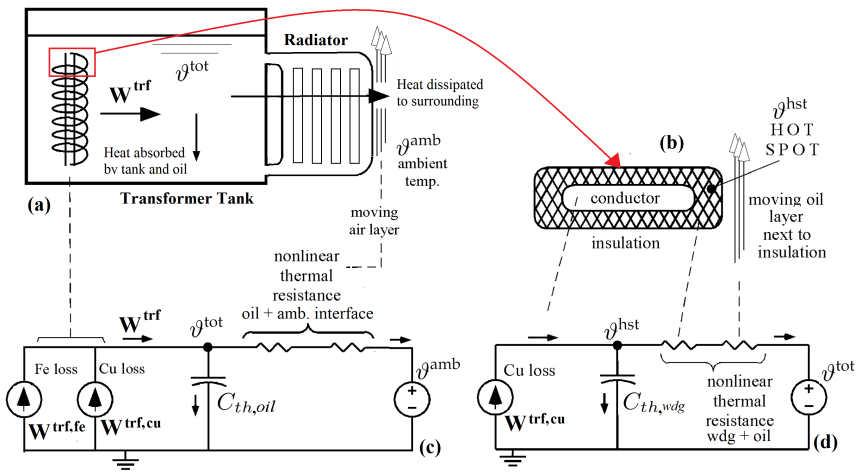

Figure 2.10: Schematic for heat dissipation in oil-filled power transformers from tank to surrounding air (a) and winding to oil (b). Thermoelectric model for top-oil temperature (c) and hot-spot temperature (d).

$$\textbf{IEEE C57.91} = \begin{cases} \tau_0 \dfrac{d\vartheta_t^{\text{tot}}}{dt} & = \Delta\vartheta_{rated}^{\text{tot}} \left(\dfrac{I_t^{\text{trf},\,pu\,2} W_{rated}^{\text{trf,cu,e},\,pu} + 1}{W_{rated}^{\text{trf,cu,e},\,pu} + 1} \right)^{\nu} - \left(\vartheta_t^{\text{tot}} - \vartheta_t^{\text{amb}} \right) \\ \tau_h \dfrac{d\vartheta_t^{\text{hst}}}{dt} & = \Delta\vartheta_{rated}^{\text{hst}} \left(I_t^{\text{trf},\,pu} \right)^{2\mu} - \left(\vartheta_t^{\text{hst}} - \vartheta_t^{\text{tot}} \right) \end{cases} \tag{2.1}$$

$$\textbf{Susa} = \begin{cases} \tau_0 \dfrac{d\vartheta_t^{\text{tot}}}{dt} & = \Delta\vartheta_{rated}^{\text{tot}} \left(\dfrac{I_t^{\text{trf},\,pu\,2}\, W_{rated}^{\text{trf,cu,e},\,pu} + 1}{W_{rated}^{\text{trf,cu,e},\,pu} + 1} \right) - \left(\dfrac{\vartheta_t^{\text{tot}} - \vartheta_t^{\text{amb}}}{\left[V_t^{pu}\, \Delta\vartheta_{rated}^{\text{tot}} \right]^{1-\nu}} \right)^{1/\nu} \\ \tau_h \dfrac{d\vartheta_t^{\text{hst}}}{dt} & = \Delta\vartheta_{rated}^{\text{hst}}\, I_t^{\text{trf},\,pu\,2}\, W_{t,\vartheta^{\text{hst}}}^{\text{trf},\,pu} - \left(\dfrac{\vartheta_t^{\text{hst}} - \vartheta_t^{\text{tot}}}{\left[V_t^{pu}\, \Delta\vartheta_{rated}^{\text{hst}} \right]^{1-\mu}} \right)^{1/\mu} \end{cases} \tag{2.2}$$

where ϑ^{tot} and ϑ^{hst} represent the calculated top oil and hot spot temperatures respectively [°C]; which are both dependent on per-unit transformer load $I^{\text{trf},\,pu}$, calculated as ratio between real-time and rated HV side currents in [A] $\left(\frac{I^{\text{trf}}}{I_{rated}^{\text{trf}}} \right)$. The time-variant, HST-dependent losses $W_{t,\vartheta^{\text{hst}}}^{\text{trf},\,pu}$ and ratio between rated load and no-load losses $W_{rated}^{\text{trf,cu,e},\,pu}$ are both expressed in [pu]. The temperature rises at rated load of 1 pu, i.e. $\Delta\vartheta_{rated}^{\text{tot}}$ representing TOT rise over ambient temperature ϑ^{amb} and $\Delta\vartheta_{rated}^{\text{hst}}$ representing HST rise over TOT are both presented in [°C]. The thermal time constants for oil τ_0 and winding τ_h [hr] are found to be dependent on the thermal capacitance of oil $C_{th,oil}$ and winding $C_{th,wdg}$ respectively, while the time-variant, temperature-dependent viscosity of oil V^{pu} is calculated in [pu]. Finally, ν and μ are dimensionless, empirically derived exponents which depend upon transformer's cooling mode. Some of these parameters require real-time calculation and are elaborated further in the next section.

Comparison and Parameterization of the Considered Models

The variation in viscosity of transformer oil with temperature has considerable influence on its thermodynamic behavior [51]. The transformer oil is known to operate frequently within the temperature range of 40 to 100

°C, while the fluctuation in oil viscosity is extreme at temperatures lower than 10 °C [44], which is why its influence is often ignored in the prevalent TEE models [45] [48] [49]. The variation in remaining physical properties of oil including conductivity, density, specific heat and volumetric expansion coefficient is rather trivial over the entire temperature range as compared to the kinematic viscosity [69]. This, when combined with the higher probability of low oil temperature operation for offshore windfarm transformers due to frequent exposure to sub-zero ambient temperatures, make it critical for OWF transformers' dynamic thermal estimation. The influence of oil viscosity variation on the convective cooling process is rightly introduced in the Susa model while ignored in the IEEE C57.91 model. The oil viscosity V^{pu} in (2.2) is the ratio between actual oil viscosity V^{oil} at time t and oil viscosity at rated TOT rise V^{oil}_{rated}, as mentioned in (2.3).

$$V_t^{pu} = \frac{V_t^{\text{oil}}}{V_{rated}^{oil}} = e^{\left(\frac{2797.3}{\vartheta_t^{\text{tot}} + 273} - \frac{2797.3}{\vartheta_{rated}^{\text{amb}} + \Delta\vartheta_{rated}^{\text{tot}} + 273}\right)} \tag{2.3}$$

Similarly, the inclusion of HST-dependent losses $W_{t,\vartheta^{\text{hst}}}^{\text{trf},\,pu}$ [pu] in the Susa model further adds to its accuracy. These losses can be empirically calculated using (2.4), where rated Copper losses $W_{rated}^{\text{trf,cu}\,pu}$ and rated Eddy current losses $W_{rated}^{\text{trf,e}\,pu}$ are expressed in [pu] with transformer total rated losses W_{rated}^{trf} [W] as base.

$$W_{t,\vartheta^{\text{hst}}}^{\text{trf},\,pu} = W_{rated}^{\text{trf,cu}\,pu}\left(\frac{235 + \vartheta_t^{\text{hst}}}{235 + \Delta\vartheta_{rated}^{\text{hst}}}\right) + W_{rated}^{\text{trf,e}\,pu}\left(\frac{235 + \Delta\vartheta_{rated}^{\text{hst}}}{235 + \vartheta_t^{\text{hst}}}\right) \tag{2.4}$$

Both the TEE models in (2.1) and (2.2) follow the same structure:

$$\text{Temperature Change} = f(\text{Heat-In}) - f(\text{Heat-Out}) \tag{2.5}$$

where, the term Heat-In is driven by the time varying load (and losses) as it is responsible for generating heat in the transformer tank, while the Heat-Out term is dependent on the difference in temperature between source and sink and models the convective process responsible for cooling during normal load operation. Even though, the structure is similar, there are distinctive differences between the two models. Firstly, the empirically-derived, convective-cooling exponents ν and μ are placed on the Heat-Out term in the Susa model which seems to be more accurate thermodynamically, in contrast to the IEEE model. The models attain a similar formation if these constants are set to 1, but diverge significantly in their original form. Secondly, the values for these exponents as defined by the respective models in Table 2.1 are fairly different.

Table 2.1: Empirical Constants for the considered TEE Models [45] [61]. On load represents circulating oil condition, while cold start means oil is not circulating at the start of loading interval.

Transformer Cooling Mode	**IEEE C57.91**		**Susa**			
			Cold Start		On load	
	ν	μ	ν	μ	ν	μ
Oil Natural Air Natural (ONAN)	0.8	0.8	1	0.33	0.8	0.67
Oil Natural Air Forced (ONAF)	0.9	0.8	0.67	0.33	0.83	0.67
Oil Forced Air Forced (OFAF)	0.9	0.8	0.67	0.33	0.83	0.67
Oil Directed Air Forced (ODAF)	1.0	1.0	0.67	0.33	0.83	0.67

Despite the differences, the two models have one common feature: they depend excessively on the parameters obtained through transformer heat-run tests performed during the Factory Acceptance Tests (FATs). Therefore, unavailability of any of these design parameters or any non-conformance of test protocols from the standards would poorly influence the transformer thermal estimation. Furthermore, the variation of these parameters with transformer age (e.g. degradation of cooler efficiency, accumulation of oil by-product deposits in transformer tanks etc.) can influence the estimation accuracy over the transformer life. One of these parameters is the transformer oil's thermal time constant τ_0 [h] calculated using (2.6), where C_{th} is the thermal capacitance of transformer tank [Wh/°C] which can be calculated using the long form of (2.7) [45] or can be

accurately estimated using the short form of (2.7), if relevant parameters are unavailable [50]. The masses of winding, iron core, metallic parts and oil represented by m are used, while the remaining parameters are described in Table 2.2. It has been observed that τ_0 can range between 1 and 3.5 hours for large and small transformers respectively, and has the tendency to change over operational lifetime.

$$\tau_0 = C_{th}\left(\frac{\Delta\vartheta^{\text{tot}}_{rated}}{W^{\text{trf}}_{rated}}\right) \tag{2.6}$$

$$C_{th} = c_{wdg}m_{wdg} + c_{fe}m_{fe} + c_{mp}m_{mp} + O_{oil}c_{oil}m_{oil} \approx 0.48m_{oil} \tag{2.7}$$

Table 2.2: Constants for determining thermal time constant for oil [50]

Symbol	Description	Value	Unit
c_{wdg}	Specific heat capacity of winding (Copper)	0.11	[Wh/kg° C]
	Specific heat capacity of winding (Aluminum)	0.25	[Wh/kg °C]
c_{fe}	Specific heat capacity of Iron core	0.13	[Wh/kg °C]
c_{mp}	Specific heat capacity of tank and metal parts	0.13	[Wh/kg °C]
c_{oil}	Specific heat capacity of oil	0.51	[Wh/kg °C]
O_{oil}	Correction factor for oil (ONAF, ONAN, OFAF)	0.86	-
	Correction factor for oil (ODAF)	1.0	-

The first-order ordinary differential equations of IEEE model in (2.1) are converted into discrete form using Backward Euler rule $\frac{dx_t}{dt} = \frac{x_t - x_{t-1}}{\Delta t}$ [70]. The resulting equations are provided in (2.8), where Δt is the time resolution. Alternatively, Forward Euler rule is preferred by the author to solve the Susa model of (2.2) and the results are provided in (2.9). It is important to note that the presence of temperature-dependent and time variant parameters (V^{pu} and $W^{\text{trf},\,pu}$) in the Susa model makes it non-linear and computationally stressful, particularly for optimization problems formulated in Chapters 6 and 9.

$$\textbf{IEEE} = \begin{cases} \vartheta^{\text{tot}}_t &= \dfrac{\tau_0}{\tau_0+\Delta t}\vartheta^{\text{tot}}_{t-1} + \dfrac{\Delta t}{\tau_0+\Delta t}\left[\Delta\vartheta^{\text{tot}}_{rated}\left(\dfrac{I_t^{\text{trf},\,pu\,2}W^{\text{trf,cu,e},\,pu}_{rated}+1}{W^{\text{trf,cu,e},\,pu}_{rated}+1}\right)^{\nu} + \vartheta^{\text{amb}}_t\right] \\ \vartheta^{\text{hst}}_t &= \dfrac{\tau_h}{\tau_h+\Delta t}\vartheta^{\text{hst}}_{t-1} + \dfrac{\Delta t}{\tau_h+\Delta t}\left[\Delta\vartheta^{\text{hst}}_{rated}\left(I^{\text{trf},\,pu}_t\right)^{2\mu} + \vartheta^{\text{tot}}_t\right] \end{cases} \tag{2.8}$$

$$\textbf{Susa} = \begin{cases} \vartheta^{\text{tot}}_t &= \vartheta^{\text{tot}}_{t-1} + \dfrac{\Delta t}{\tau_0}\left[\Delta\vartheta^{\text{tot}}_{rated}\left(\dfrac{I_{t-1}^{\text{trf},\,pu\,2}\,W^{\text{trf,cu,e},\,pu}_{rated}+1}{W^{\text{trf,cu,e},\,pu}_{rated}+1}\right) - \left(\dfrac{\vartheta^{\text{tot}}_{t-1}-\vartheta^{\text{amb}}_{t-1}}{\left[V^{pu}_{t-1}\,\Delta\vartheta^{\text{tot}}_{rated}\right]^{1-\nu}}\right)^{1/\nu}\right] \\ \vartheta^{\text{hst}}_t &= \vartheta^{\text{hst}}_{t-1} + \dfrac{\Delta t}{\tau_h}\left[\Delta\vartheta^{\text{hst}}_{rated}\,I^{\text{trf},\,pu\,2}_{t-1}\,W^{\text{trf},\,pu}_{t-1} - \left(\dfrac{\vartheta^{\text{hst}}_{t-1}-\vartheta^{\text{tot}}_{t-1}}{\left[V^{pu}_{t-1}\,\Delta\vartheta^{\text{hst}}_{rated}\right]^{1-\mu}}\right)^{1/\mu}\right] \end{cases} \tag{2.9}$$

Validation of the Considered TEE Models for Dynamic Load in Offshore Windfarms

The intermittent nature of offshore windfarm generation results in unique dynamic load for OWF transformers. Therefore performance of the considered models needs to be evaluated under different circumstances. The validation is performed for two test cases: **a)** 6.8 MVA, 0.69/34 kV, Dyn11, OFAF-cooled transformer located in the nacelle of a wind turbine 42 km off the east coast of UK. **b)** 140 MVA, 33/220 kV, ONAF-cooled export system transformer located in the OSS of the Anholt windfarm in Denmark, as shown in OWF layout of 2.2. The difference in cooling modes and construction of the two test case transformers makes the validation exhaustive for applications considered in this project. One year of operational data for 2017 has been used as inputs for both the transformers, which include 10-minute samples for transformer load and ambient/nacelle temperatures. It is important to note that only the measured TOT has been used for validation purposes

because HST measurements are not available for any of the transformers considered in this project. Further information about the test cases are available in publications **[Pub. C2]** and **[Pub. C3]**.

The validation results for the WT and OSS transformers are provided in Fig. 2.11 and 2.12 respectively for the months of January and July 2017 only to emulate the considerable difference in ambient conditions and production patterns, and to keep the elaboration intelligible. By reviewing the temporal evolution of the temperatures, it is perceivable that for both the test cases, the measured TOT is often close to or below the TOT calculated by the Susa model, which makes the Susa model slightly conservative due to its incorporation of temperature-dependent losses. As anticipated, the accuracy of the Susa model is higher at low ambient temperatures due to accurate modeling of oil viscosity variation. On the other hand, IEEE C57.91 model offers acceptable accuracy for both the test cases but often ends up underestimating the TOT and HST rise, which can lead to increased thermal stress if necessary precautions are not taken. The models are benchmarked using Normalized Mean Square Error (Chapter 3), which results in Susa model outperforming the IEEE model by 5 % and 3.5 % for the WT and OSS transformers respectively over the entire year.

Mention the validation for Lab transformer and other WTG transformers using ML etc.

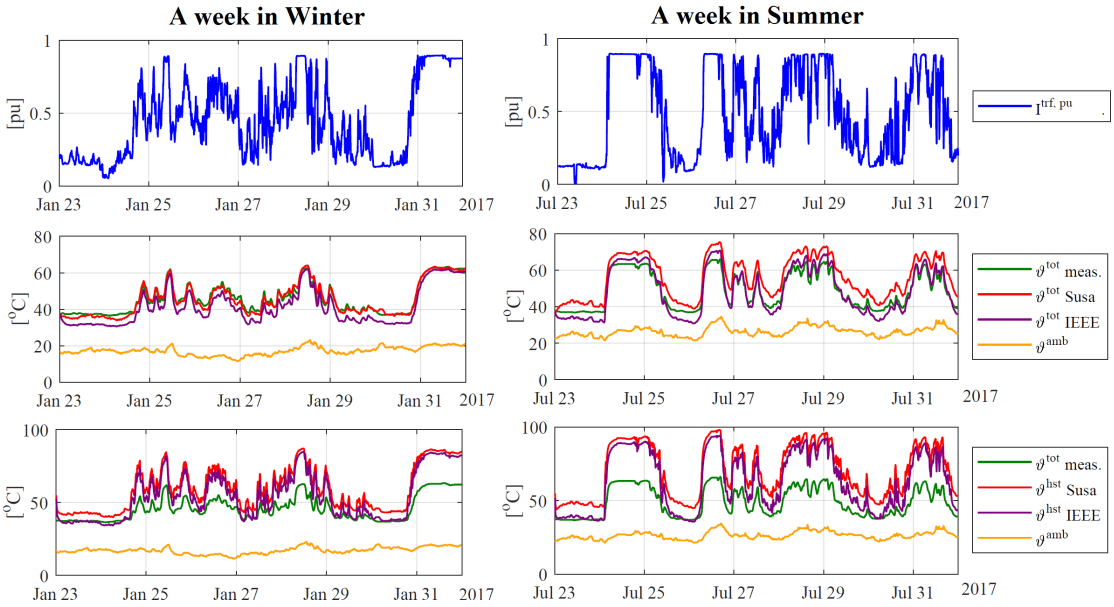

Figure 2.11: Validation of TEE models for the WT transformer in a UK OWF for a week in winter (left) and summer (right) 2017. Top: Load current in pu; Middle: Measured ambient temperature and TOT along with TOT calculated using Susa and IEEE model; Bottom: Measured ambient temperature and TOT along with HST calculated using Susa and IEEE model

Simplification of Transformer TEE models for Optimization

The TEE models considered for transformers are not suitable for the optimization problems developed in this project. Therefore further simplifications are needed to prevent non-convexity of the proposed optimization frameworks. The non-linearity arises due to the non-integer exponents ν and μ in both the models, but the presence of time variant, temperature-dependent parameters in the Susa model of (2.9) makes it specifically unfit for the problems in Chapters 6 and 8. Hence, despite the limitations of IEEE C57.91 model's accuracy, the formulation in (2.8) is simplified to achieve the models in (2.10) by making two approximations:

- The cooling mode for future transformer design is considered to be ODAF, which allows the exponents ν and μ to be set to 1, as per Table 2.1.
- The problems developed in this project deal with hourly operational time constraints. Since the thermal time constant of winding for HST estimation τ_h is in the range of 6 to 10 minutes [54], the ultimate

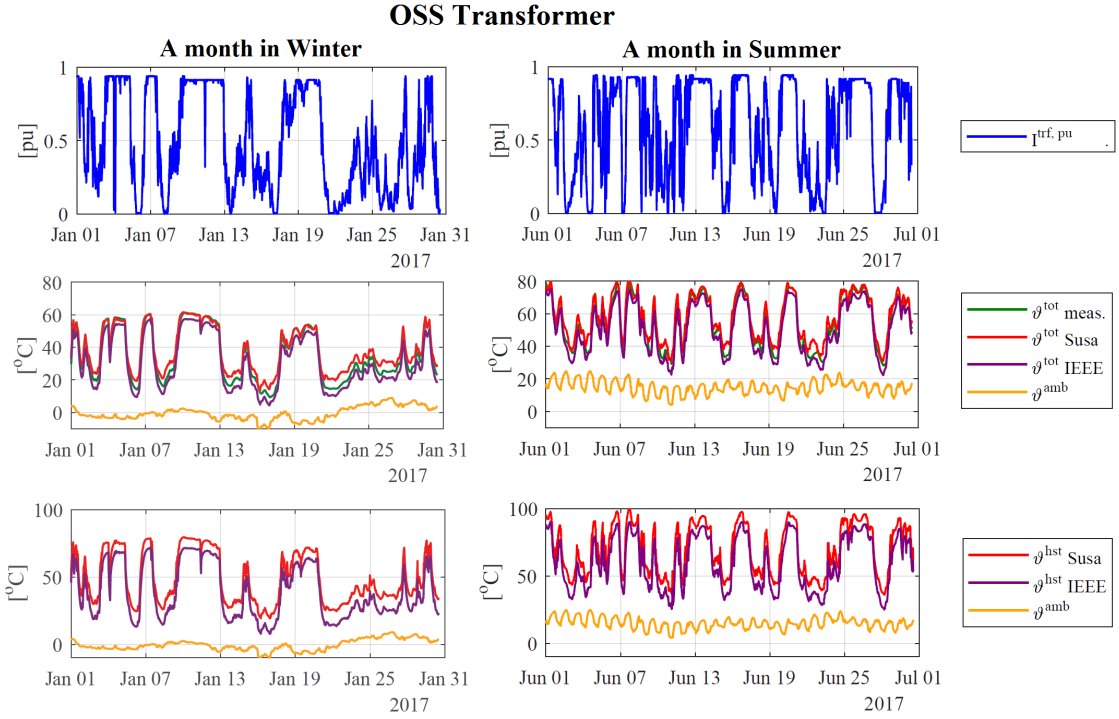

Figure 2.12: Validation of TEE models for the OSS transformer in Anholt windfarm for a month in winter (left) and summer (right) 2017. Top: Load current in pu; Middle: Measured ambient temperature and TOT along with TOT calculated using Susa and IEEE model; Bottom: Measured ambient temperature and calculated HST using Susa and IEEE models

steady-state HST rise (shown by the factor $\Delta\vartheta^{\text{hst}}_{rated}\, {I^{\text{trf},\,pu}}^2$) would be reached by the end of each hourly interval. This approximation is validated in Fig. 2.13 for the OWF OSS transformer from previous section, where a step response of HST rise ($\Delta\vartheta^{\text{hst}} = \vartheta^{\text{hst}} - \vartheta^{\text{tot}}$) to change in load current I^{trf} is compared to the steady-state rated HST rise in (2.10). The minimal difference between the two temperatures at the end of the 60-minute mark and the slight conservative estimation of the steady-state approximation irrespective of TOT and ambient temperatures are perceivable, which have also been verified for different transformers and hourly load variations. It must be mentioned that the thermal time constant for oil τ_0 can range between 60 to 200 minutes, which is why oil's thermal dynamic behavior over the hourly operational scale needs to accounted for.

$$\textbf{Simplified IEEE C57.91} = \begin{cases} \vartheta^{\text{tot}}_t &= b_1\vartheta^{\text{amb}}_t + b_2\left(\frac{I^{\text{trf}}_t}{I^{\text{trf}}_{rated}}\right)^2 + b_3\vartheta^{\text{tot}}_{t-1} + b_4 \\ \vartheta^{\text{hst}}_t &= \vartheta^{\text{tot}}_t + \Delta\vartheta^{\text{hst}}_{rated}\left(\frac{I^{\text{trf}}_t}{I^{\text{trf}}_{rated}}\right)^2 \end{cases} \tag{2.10}$$

where,

$$b_1 = \frac{\Delta t}{\tau_0 + \Delta t} \tag{2.11}$$

$$b_2 = b_1\frac{W^{\text{trf,cu,e},\,pu}_{rated}\,\Delta\vartheta^{\text{tot}}_{rated}}{(W^{\text{trf,cu,e},\,pu}_{rated} + 1)} \tag{2.12}$$

$$b_3 = 1 - b_1 \tag{2.13}$$

$$b_4 = b_1\frac{\Delta\vartheta^{\text{tot}}_{rated}}{(W^{\text{trf,cu,e},\,pu}_{rated} + 1)} \tag{2.14}$$

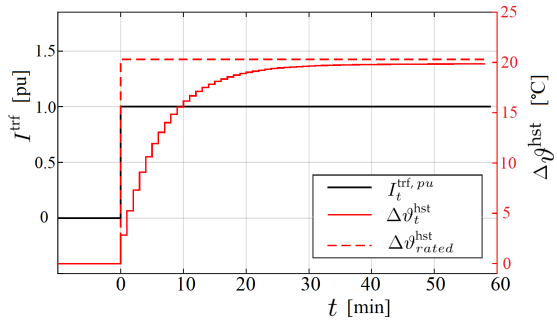

Figure 2.13: HST rise over TOT for a step change in load current I^{trf}. $\Delta\vartheta_t^{\text{hst}}$ is estimated using (2.8), while $\Delta\vartheta_{rated}^{\text{hst}}$ is calculated using the steady state approximation in (2.10).

2.3.2 Thermal Modeling of HV Export Cables

Like transformers, the loadability of export cables is defined by the operating temperature of insulation. The temperature is often limited to 90 C for XLPE insulated cables exposed to cyclic load conditions to prevent deterioration of cable's mechanical and dielectric strengths [71]. It is possible to calculate the continuous loadability of the cables by accurately modeling the thermodynamic behavior under different operating conditions like the Real Time Thermal Rating (RTTR) tool [72].

As mentioned earlier, the 1-core cables used in the underground section are not designed conservatively and are hardly ever the thermal pinch-points in the export system. Therefore, dynamic thermal modeling of rest of the export cable sections is focused upon in this work, all of which use 3-core, Separate Lead (SL) type, armored, subsea cables like the one shown in Fig. 2.14. Single core equivalent thermoelectric models are used in this project, the reasons for which are provided in the sections below.

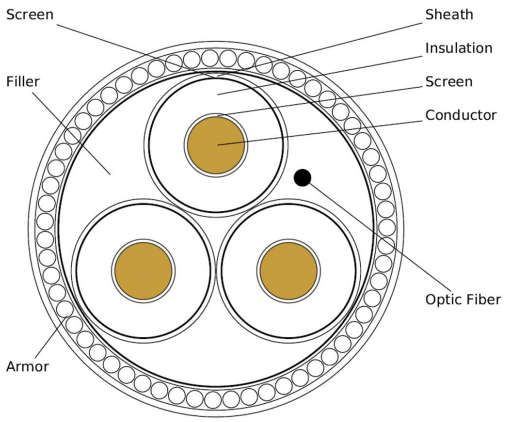

Figure 2.14: Cross section of the three-core XLPE insulated subsea cable - not to scale

State-of-the-Art for TEE Modeling for OWF export cables

Like transformers, the state-of-the-art for thermoelectric modeling of cables is reviewed extensively in publication **[Pub. C1]**. For steady state thermal rating calculations, internationally accepted IEC 60287-2 [73, 74] provides a range of analytical models. These methods are further complemented by the models for cyclic dynamic load conditions with emergency limits presented in IEC 60853 [71], which should be sufficient for standard cable installations and operation.

For the sake of commercial competitiveness, cable manufacturers and consultants have employed unique thermal modeling methods with minimal publicly available information [75–78]. For 3-core SL-type armored cables, the substantial research done in the field of single-core equivalent modeling over the years can be split

into three categories: Finite element models, Laplace transformation models relying on exponential integrals [71] [79–81] and Differential models relating physics to dynamic temperature rise [71, 74, 82, 83], the latter two qualifying as TEE models. The differential models are inherently similar in structure and mostly differ in parameter estimation techniques which can significantly influence the performance under long and short transients [84]. The assumptions of one-dimensional problem (no longitudinal heat flow) and symmetric nature of single-core equivalence for three-core cables have been challenged recently [85]. Furthermore, the model neglects the influence of cyclic load on thermal properties of the back-fill material [25, 86], but their simplicity of design, computational efficiency and fair accuracy are strongly favored [83]. The calculation of thermal parameters and thermal loss factors can be done using standard estimations [71, 74, 82, 87], which can result in overestimation of armor losses [13, 88] and a conservative design.

Non-conventional installation and commissioning practices for offshore windfarms, as discussed earlier, need more considerations. Some recent publications discuss implications of these practices including installation in high depths [89], shallow troughs [90], non-uniform surroundings of subsea [40, 41, 43] and underground cables [91]. For J-tubes and HDD, standard techniques for dynamic thermal modeling do not exist. However, efforts have been made over the years to address the complex three dimensional heat flow environment of J-tubes. These publications range from older empirical models of 1988 [81] which adopted the generic analytical methods for cable risers from 1983 [92] to new improvements in heat transfer coefficients in 1996 [93] and more recent work dealing with quasi-3D model for accounting of longitudinal heat flow [42] and accurate estimation of conduction, convection and radiation phenomena. The inclusion of variation in physical attributes for installations in free air [94] and without backfill [95] are also relevant for this project.

Approach for TEE Modeling of 3-core Subsea Cables

The three cable sections under consideration (incl. Offshore, J-tubes and HDD) differ considerably in installation practices. Therefore, it is easier to simplify the TEE model by splitting it into cable and installation blocks, as shown in Fig. 2.15. The directly buried cable in offshore section is exposed to the soil, but the HDD filling medium means that there needs to be an intermediate block for the HDD section. On the other hand, the constraining subsection of J-tube is exposed to ambient air temperature. Hence, by starting from the ambient sea ϑ^{sea} and air ϑ^{amb} temperatures, it is possible to find intermediate temperatures at the cable serving ϑ^{serv} and HDD surface ϑ^{hdd}, which can then lead to calculation of cable conductor temperature ϑ^{cond}.

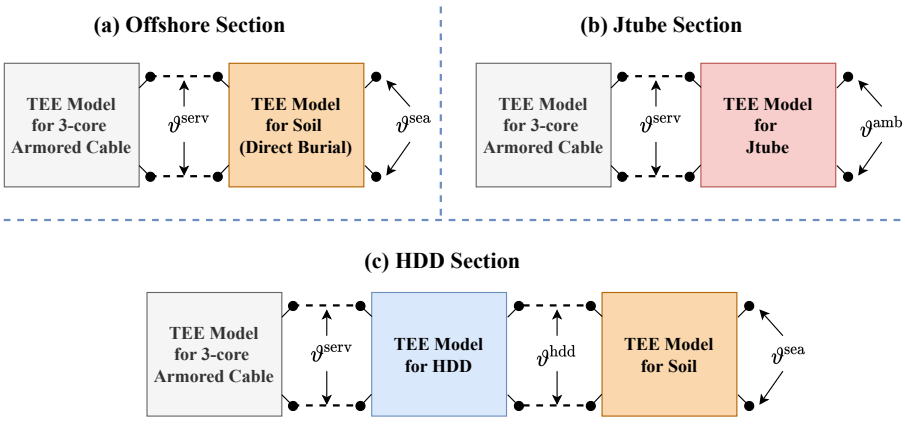

Figure 2.15: Block diagrams for thermoelectric modeling network of the cable sections under consideration

For grey-box in Fig. 2.15, the single core equivalent TEE model from [71] [82] relevant for dynamic thermal estimation of 3-core cables is presented in Fig. 2.16. The longitudinal heat flow along the cable is neglected even from the hotspots, which makes the problem one-dimensional. It is possible to calculate ϑ^{cond} and ϑ^{serv}, which represent cable conductor and serving temperature rise over ambient seabed temperature respectively, using this model. There are four sources of heat in the model: load-dependent and time-variant ohmic

conductor losses W^{cond} [W/m]; constant 3-phase dielectric losses W_d [W/m], which are distributed dependent on cable insulation's design; screen losses W^{s} and armor losses W^{a}. The latter two losses are both load dependent and time variant; and therefore, can be calculated by scaling W^{cond}. The dimensionless scaling factors λ_s and λ_a for calculation of W^{s} and W^{a} are defined as per IEC 60287 [73], out of which W^{a} are potentially overestimated [88], but the resulting cable design and operation is found to be conservative, which is acceptable for this project. The thermal parameters including capacitance [J/m°C] and resistance T_1, T_2 and T_3 [m°C/W] are treated as constants depending on cable construction and calculated using the formulation in IEC 60287-2 [74]. The three phase conductor losses are calculated as $W^{cond} = 3I^{\text{c}^2} r'^{\text{c}}_{ac}$ where I^{c} represents time-variant cable load current [A] and r'^{c}_{ac} represents conductor AC resistance [Ω/m] accounting for skin and proximity effects [96].

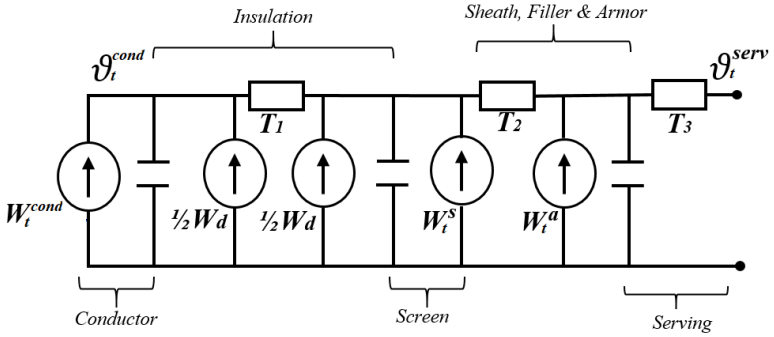

Figure 2.16: Single core equivalent TEE model for 3-core armored cables [71] [82]

The TEE models for the remaining blocks in Fig. 2.15 are readily available in the publications cited in the state-of-the-art review earlier. Efforts are not made to improve the models for J-tube and HDD sections because these sections are relatively small and there are alternate methods to optimize the cable ratings. For the longest cable section with directly buried cables in the offshore, the classical approach presented in CIGRE Elektra 143 [97] is used which employs concentric cylinders of soil surrounding the cable. The number of cylinders need to be optimized for calculation efficiency, with the outer-most and inner-most cylinders being exposed to the ambient seabed temperature and cable serving temperature respectively. For each cylinder, the thermal capacitance C_{soil} and resistance T_{soil} of the soil are calculated using (2.15)-(2.16). The parameters $D_{soil,inner}$ and $D_{soil,outer}$ representing the inner and outer diameter of each cylinder are to be defined in advance to balance the computational accuracy with required speed of calculation. The remaining parameters can be treated as constants at this stage with thermal resistivity of soil ρ_{soil} set to 0.7 m°C/W for saturated soil and volumetric specific heat capacity of soil ϖ_{soil} set to 2.5×10^6 J/°C m^3 for saturated and 1.8×10^6 J/°C m^3 for non-saturated soils. It will later be shown in Chapter 3 that the direct exposure of offshore cable section to the sea in some regions due to dynamic tidal movements, while increased burial depth in the other makes the surrounding of the offshore section of the export cable diverse in nature, which is further influenced by the presence of terrains with composition of mud, sand, silt and rocky soil. Therefore accurate parameterization of T_{soil} and C_{soil} will be possible using data-analytics based models.

$$C_{soil} = \frac{\pi}{4}\varpi_{soil}\left(D^2_{soil,outer} - D^2_{soil,inner}\right) \tag{2.15}$$

$$T_{soil} = \frac{1}{2\pi}\rho_{soil}\ln\left(\frac{D^2_{soil,outer}}{D^2_{soil,inner}}\right) \tag{2.16}$$

Simplified Lumped Model

The TEE model discussed so far is difficult to design and solve as it is highly non-linear and exceedingly dependent on the cable construction parameters. Simplifications are needed to make the models fit for the

linear optimization problems presented in Chapters 6 and 8. Therefore, a simplified lumped parameter model for calculation of cable conductor and serving temperature rise over ambient seabed temperature is proposed and validated in this section. The lumped parameter model presented in Fig. 2.17 merges the losses and the thermal parameters (incl. capacitance and resistance) of the model in Fig. 2.16, such that the total cable losses $W^{\text{tot c}}$ [W/m] are simply the sum of W^{cond}, W^{a}, W^{s} and W_d, as shown in (2.17). However, the lumped thermal capacitance C_x and resistance T_x are dependent on cable design and are determined by training the simplified model over a synthetic dataset using the principles described in Chapter 3 and Publication **[Pub. C5]**. The model shown in Fig. 2.17 is relevant for the offshore section only, but can easily be extended to HDD and J-tube sections as well. The temporal development of ϑ^{cond} and ϑ^{serv} can be calculated using (2.18) and (2.19).

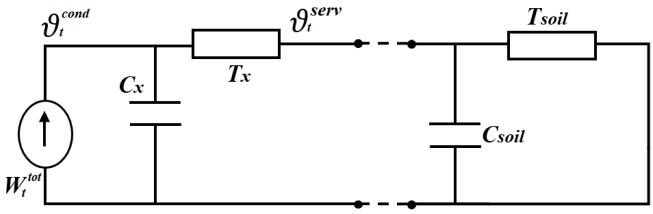

Figure 2.17: Simplified lumped 1-core equivalent TEE model for the 3-core subsea cables directly buried (offshore section)

$$W_t^{\text{tot c}} = W_d^{\text{c}} + 3(1+\lambda_a+\lambda_s) I_t^{\text{c}^2} r_{ac}^{\prime\,\text{c}} \tag{2.17}$$

$$\tau_x' \frac{d\vartheta_t^{\text{serv}}}{dt} = \frac{T_{soil}}{T_x + T_{soil}} \vartheta_t^{\text{cond}} - \vartheta_t^{\text{serv}} \tag{2.18}$$

$$\tau_x \frac{d\vartheta_t^{\text{cond}}}{dt} = T_x W_t^{\text{tot}} + \vartheta_t^{\text{serv}} - \vartheta_t^{\text{cond}} \tag{2.19}$$

where the time constants are calculated in seconds using the expressions $\tau_x = T_x C_x$ and $\tau_x' = \dfrac{T_x T_{soil}}{T_x + T_{soil}} C_{soil}$. This simplified lumped parameter model is conservative in nature as compared to the complex model of Fig. 2.16 as the losses are collectively referred to the conductor. Furthermore, conservatism of design is ensured by using constant values for conductor resistance $r_{ac}^{\prime\,\text{c}}$ at 90 °C. The models are solved using Backward Euler technique and the results are provided in (2.20) and (2.21), where Δt is the time-step and ϑ_{t-1} represents the calculated temperature at the previous time-step.

$$\vartheta_t^{\text{serv}} = a_1 \vartheta_{t-1}^{\text{serv}} + a_2 \vartheta_t^{\text{cond}} \tag{2.20}$$

$$\vartheta_t^{\text{cond}} = \frac{1}{a_3}\left[a_4 \vartheta_{t-1}^{\text{cond}} + a_5 \vartheta_{t-1}^{\text{serv}} + a_6 W_t^{\text{tot c}}\right] \tag{2.21}$$

where the constant coefficients a are calculated as:

$$a_1 = \frac{\tau_x'}{\tau_x' + \Delta t} \tag{2.22}$$

$$a_2 = \frac{T_{soil}}{T_x + T_{soil}} \left(\frac{\Delta t}{\tau_x' + \Delta t}\right) \tag{2.23}$$

$$a_3 = \frac{1}{1 - a_2 \frac{\Delta t}{\tau_x + \Delta t}} \tag{2.24}$$

$$a_4 = a_3 \frac{\tau_x}{\tau_x + \Delta t} \tag{2.25}$$

$$a_5 = a_1 a_3 \frac{\Delta t}{\tau_x + \Delta t} \tag{2.26}$$

$$a_6 = a_3 T_x \frac{\Delta t}{\tau_x + \Delta t} \tag{2.27}$$

The model has been validated by comparing its performance to the complex TEE model of Fig. 2.16. Referring to Fig. 2.18, similar cyclic load profiles are generated for two XLPE insulated cables with copper conductor of

different cross-sections. By scaling the load profiles to maximum current carrying capacities of the respective cables, similar thermal stress is exerted. It is seen that the conductor temperature estimated by the simplified model follows the complex model curve closely, but still results in overestimation. This can be due to the additional conservatism added to the design by resistance estimation at max operating temperature and by loss concentration to the conductor. The models are found to be acceptable due to the cautious nature needed for design and operation of OWF export cables. The tests have been repeated for a range of XLPE cables with Aluminum and Copper conductors with similar accuracies.

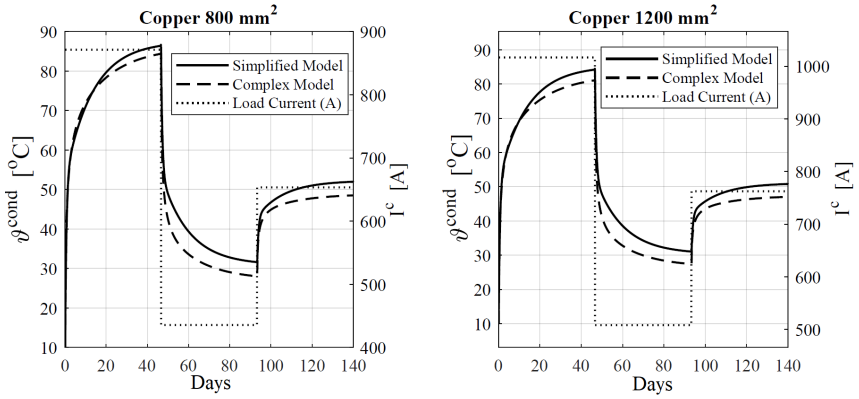

Figure 2.18: Performance comparison of simplified and complex TEE models for 220 kV subsea, XLPE-insulated, Copper cables under cyclic load. Left: 800 mm^2, Right: 1200 mm^2

Comments on Thermal Ageing and Limits of HV XLPE Cables

As discussed earlier, the loadability of HV cables is defined by the temperature of the insulating material [73]. For XLPE insulated cables, this limit is agreed to be set to 90 °C by manufacturers and international standards. This limit prevents deterioration of the dielectric and mechanical strength of the cable insulation and preserves its life [87]. The temperature-dependent properties of XLPE-insulated cables including specific heat, thermal resistivity, electrical resistivity, dielectric strength, tensile strength, electrical breakdown strength and tan delta losses have been investigated critically in the literature. Due to the limitation of available knowledge on the subject and the considerable CAPEX related to HV cables, the emergency and cyclic thermal limits for cables are not explored in this thesis. Instead, the design optimization tools developed in this project simply limit the conductor temperature to 90 °C.

2.3.3 Shunt Reactor Modeling

As discussed in Sec. 2.1, offshore windfarms that are further from the shore (> 80 km) and use HVAC technology for transmission often require additional reactive compensation near the middle point of the export cable. For this purpose, fixed HV shunt reactors located in the Reactive Compensation Station (RCS) are frequently used which are expensive to build [11]. The system is conventionally designed that 50 % of the compensation for export cables is performed by these shunt reactors, while dynamic compensation is performed from the OSS and OnSS ends of the cable. Hence, it is safe to assume stable system voltage for the export cable which results in static operation of these shunt reactors with constant reactive compensation load. The rating of RCS shunt reactors depends upon the export cable rating, as shown in (2.28)-(2.29).

$$I^{\mathrm{c}}_{\mathrm{Q}\,k} = \frac{1}{4}\left(2\pi f Q'^{\mathrm{c}}_{k} L^{\mathrm{c}} \frac{V_{ll}}{\sqrt{3}}\right) \times 10^{-3} \tag{2.28}$$

$$S^{\mathrm{SR}}_{k} = 2\left(\sqrt{3} V_{ll} I^{\mathrm{c}}_{\mathrm{Q}\,k}\right) \tag{2.29}$$

where $Q'^{\,\mathrm{c}}$ is the capacitance [μ F/m] of the export cable design and $I^{\mathrm{c}}_{\mathrm{Q}}$ is the peak charging current at the OSS, OnSS and RCS ends of the export cable. V_{ll} and f are transmission system voltage [kV] and frequency [Hz]; L^{c} is the length of export cable [m] and S^{SR} represents the rating of RCS shunt reactor [kVA] for design case k.

CHAPTER 3

Dynamic Condition Monitoring using Data Analytics

Over the last decade, the dramatic increase in computational capacity and data availability combined with monumental development in data analytics has prompted revolutionary applications across miscellaneous scientific fields, including image recognition [98], cognition in medical science [99] [100], natural language processing [101] etc.

Condition monitoring of HV transmission equipment exposed to dynamic rating operation requires estimation of critical temperatures in real-time. The first-principle TEE models discussed in Chapter 2 are difficult to develop as they require extensive knowledge about the component's mechanical and electrical design, along with accurate modeling of multiple heat transfer mechanisms. As an example, the 3-dimensional heat flow in J-tubes [42], elaborative design of cable-joints [82] and comprehensive information about the HDD backfill material etc. will be needed to solve the underlying equations resulting in both design complexity and computational stress. This is further complicated by the varying operational environment due to sedimentation and seabed movement for cables [40] or oil byproduct deposits in transformer tanks [56]. Self-learning, data-driven Machine Learning (ML) models can potentially solve these problems while offering more flexibility in operation with higher computational efficiency and better accuracy, owing to their adaptive nature [102]. Furthermore, monitoring of HV components generates extremely large datasets that can reveal underlying patterns and trends to ML-based models only, and can easily be overlooked by system operators or unintelligent monitoring algorithms [103]. The data generated by a typical offshore export cable section is manifested in Fig. 3.1, where 1.26 Million data points are needed to represent 35 days of operation.

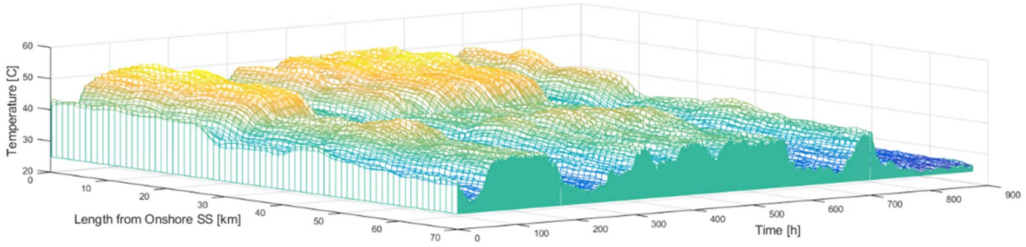

Figure 3.1: DTS measurements for 70 km long offshore cable section for a test case windfarm in UK. 1.26 Million data points are generated for 35 days of operation.

In this chapter, the third research question is answered such that dynamic thermal estimation models are developed, tested and applied for transformers and cables in offshore windfarms. Furthermore, the physical insights provided by some of the relevant models are used for dynamic condition monitoring of these components. The principal focus of this work revolves around empirical models due to their adaptive nature. As shown in the structure of the chapter provided in Fig. 3.2, the methodology behind the data-driven ML models is followed by validation of these models by applying them on actual test cases. These test cases include long and short term thermal prediction of export cables for Burbo Bank 2 (BB2) windfarm, validation for lab and wind turbine transformers. Finally, the potential application of these models are highlighted. A significant portion of this work has been presented in Publications **[Pub. C5]** and **[Pub. C7]** by the author.

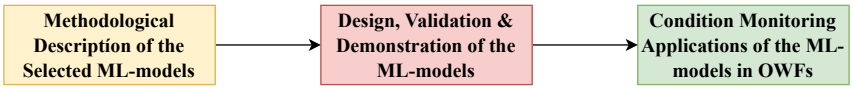

Figure 3.2: Structure of Chapter 3 and information flow to determine data-analytics based dynamic condition monitoring

3.1 Methodology of Data-Driven Modeling Approach

Data-driven ML models fit for approximation of time series data are considerably more complex than the well-established prevalent techniques [104, 105]. In order to build models for systems with dynamic responses, the core principles of *system identification* are used [106] [107]. The physical insights and knowledge about the dynamic thermal modeling of components have been utilized to correlate inputs, outputs and everything in between [108], [109]. Due to the computational stress posed by non-linear partial differential equations [110] [111] in combination with the complexity of their design [112], the underlying set of equations are linearized and necessary assumptions are made to obtain Ordinary Differential Equations (ODEs), where possible.

The prediction accuracy for the models developed in this project is evaluated by calculating the Normalized Mean Square Error (NMSE). This is shown in (3.1), where y_t and $\hat{y}_t$ are the measured and predicted values respectively and σ is the standard deviation. The normalization of Mean Square Error (MSE) by variance σ^2 offers a distinctive advantage for using NMSE as a benchmarking parameter, which is complemented by NMSE's simplistic interpretation [102]. This is true because the NMSE (%) can range between $-inf$ and 100; where 100 means a perfect fit, while 0 corresponds to a constant signal equivalent to the mean μ_t^y. Hence any model within the range 0 to 100 would perform better than a constant mean model [113]. More importantly, the evaluation criteria in this project also covers simplicity of design, flexibility of application and physical interpretability. The latter two parameters deal with application aspects such that flexibility means that the models can be used under varying operating circumstances, for e.g. thermal estimation of cables' HDD, offshore and J-tube sections; while physical interpretation means that the model parameters can be used for identifying the operating characteristics and circumstances. This is further discussed in Section 3.3.

$$NMSE = 100\left(1 - \frac{MSE}{\sigma^2}\right) = 100\left(1 - \frac{\|y_t - \hat{y}_t\|^2}{\|y_t - \mu_t^y\|^2}\right) \tag{3.1}$$

3.1.1 Classification of ML Models

The experiential nature of empirical models in combination with their computational efficiency and adaptability to varying operational circumstances make them ideal for data-analytics applications [102]. Depending upon the amount of physical insight needed for system design and how this knowledge blends with the empirically observed information, these models can be classified into different shades of grey, as shown in Fig. 3.3.

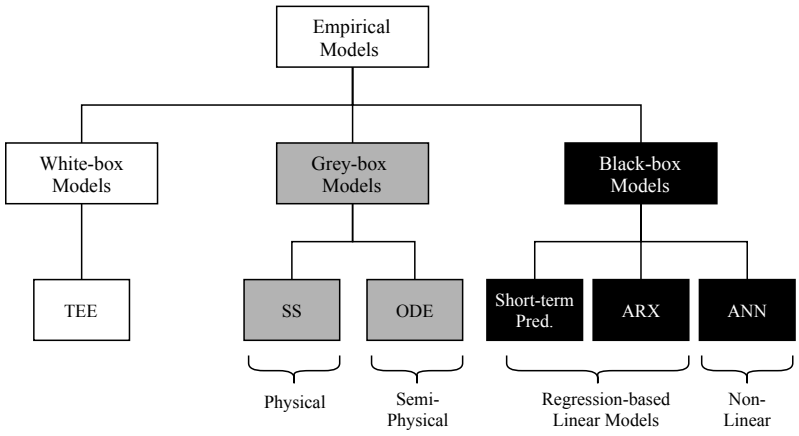

Figure 3.3: Classification of Empirical models with focus on data-analytics based models

White-box models can be constructed entirely based on prior system knowledge. For these models, the physical parameters and underlying equations are either perfectly known or can be accurately estimated, like the TEE models of Chapter 2. On the opposite end of the spectrum, system knowledge is either not available or not used for Black-box models. The Black-box models considered in this project are mostly regression-based and are selected based on their flexible structure and proven track record for identical applications [105, 114]. For systems where limited structural insights are available but parameters have the tendency to change over time, Grey-box models can be effectively used. These models require the user to define the basic problem framework, while the inconclusive parameters are determined by data-analytics [106]. Further classification of Grey-box models reveals that model structure can either be built on physical grounds alone (closer to white-box) or can be developed by trying-and-testing certain linear/non-linear combinations of the available data signals (semi-physical, black-box character) [115].

This is why, both the Black-box and Grey-box models need to be trained before the models are ready for predictions. The mechanism for training and testing of data-driven models is summarized in Fig. 3.4 using the test case of thermal estimation of cables and transformers in offshore windfarms. It can be seen that the variables used as input data remain the same during training and testing periods, for e.g. component load (I_t) and ambient temperatures (ϑ_t^{sea}, ϑ_t^{amb}); but prediction variables, including cable and transformer temperatures (ϑ_t^{c}, ϑ_t^{tot}, ϑ_t^{hst}) are only used for training the models. The measured prediction variables can later be used to check models' test accuracy and for benchmarking these models. All the relevant Black-box and Grey-box models that are considered in this project are discussed in detail in the following section, whereas the mechanism to determine the critical attributes of the respective models will be provided in Section 3.2.

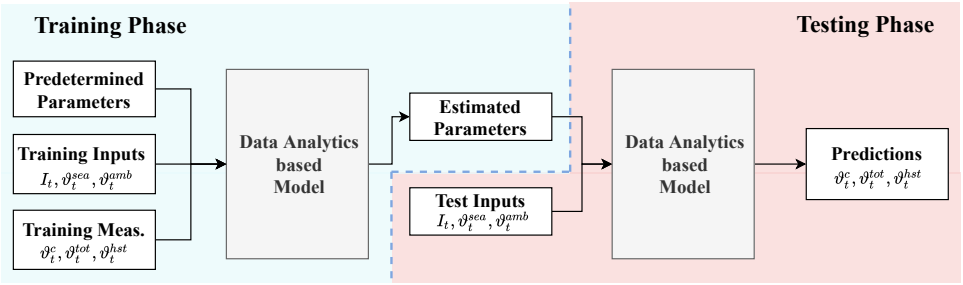

Figure 3.4: Training and testing mechanism of data-analytics based Grey-box and Black-box models. The test case of thermal estimation of cables and transformers is used for elaboration.

3.1.2 Description of Models

For dynamic rating based operation and design of HV components, it is imperative to be able to monitor and estimate the temporal development of critical temperatures over long and short periods. The relevant data-analytics based models shortlisted after extensive review and reconfigured as per the requirements of this project are discussed below. In these models, the signals $u_t \in \mathbb{R}$ and $y_t \in \mathbb{R}$ represent the input (load) and output (temperature) signals respectively.

Short-term Prediction Models

Short-term prediction of critical component temperatures is important for real-time applications in the operational domain. Three regression-based, linear, black-box models are found to be relevant in this project for their computational efficiency, accuracy and design simplicity as they do not require any additional inputs besides the measured temperatures. Moreover, the influence of seasonal variation on wind energy production and ambient conditions is not critical for design of these models.

- **General Linear Model (GLM):** This model can be expressed using a number of formulations which depend upon the available inputs and the required applications. The following model is based on the simplest form of linear regression:

$$\hat{y_t} = c_0 + c_1 t + \epsilon_t \tag{3.2}$$

where t is time step, $\hat{y_t}$ is the predicted response variable for each step, c_0 and c_1 are the parameters and ϵ_t is white noise, expressed using a sequence of mutually Independent and Identically Distributed (IID) random variables with zero mean value. GLM has not been implemented in this report due to its ineffectiveness for such applications [104], but it is still mentioned for effective comprehension of the models that follow.

- **Exponential Smoothing Model:** Unlike GLM, this model allows the most recent observations to influence the predictions more than the past ones by using a forgetting factor χ (s.t. $0 < \chi < 1$). A simple first-order exponential smoothing model is provided in (3.3).

$$\hat{y_t} = (1 - \chi)\, y_{t-1} + \chi\, \hat{y_{t-1}} + \epsilon_t \tag{3.3}$$

where the factor $1 - \chi$ is also called the smoothing constant as it defines the weight for the latest available observation, the influence of which diminishes over time depending on the chosen value of χ. The inherent drawback of this model is it can reliably perform one-step prediction only because it is a locally constant mean model. The l-step prediction formula ($\hat{y_{t+l|t}} = \hat{y_{t|t}}$) suggests that any future forecast will be the last one-step estimate, if further observations are not available.

- **Local Linear Trend Model:** This method combines the properties of the previous two models by forgetting the old observations of GLM in an exponential manner. The formulation is provided in (3.4).

$$y_{t+q} = \kappa^T(q)\, e + \epsilon_{t+q} \tag{3.4}$$

where $\kappa(q) = [\kappa_1(q), ..., \kappa_p(q)]^T$ represents the vector for known forecast functions, while $e = [e_1, ..., e_p]^T$ is the parameter vector and p is the order of approximation for observation instant q. The forecast functions are fixed for the problem type, and can be determined using transition matrices in [104]. The parameters e are to be recursively estimated after each time step or as soon as a new observation is available, which has been done using Weighted Least Square (WLS) approach. This is governed by (3.5), where Sum of Squared Errors SSE$(e;t)$ is calculated using (3.6) [113].

$$\hat{e_t} = arg\, min_e\, SSE(e;t) \tag{3.5}$$

$$\text{SSE}(e;t) = \sum_{q=0}^{t-1} \chi^q \left[y_{t-q} - \kappa^T(-q)e\right]^2, \quad 0 < \chi < 1 \tag{3.6}$$

where a suitable forgetting factor χ is to be chosen for optimal results. Theorem 3.3 from [104] has been used to solve the WLS problem, and the results are provided in (3.7) - (3.9). Afterwards, $l-$step prediction can be performed using (3.10).

$$\hat{e_t} = F_t^{-1} h_t \tag{3.7}$$

$$F_t^{-1} = \sum_{q=0}^{t-1} \chi^q \left[\kappa(-q)\kappa^T(-q)\right] \tag{3.8}$$

$$h_t = \sum_{q=0}^{t-1} \chi^q \left[\kappa(-q) y_{t-q}\right] \tag{3.9}$$

$$\hat{y_{t+l|t}} = \kappa^T(l)\, \hat{e_t} \tag{3.10}$$

Ordinary Differential Equation (ODE) Model

This grey-box model is semi-physical in nature which means that the limited physical knowledge about the system can be transformed into useful insights by *trying and testing* a number of linear/non-linear combinations of differential equations [70]. For dynamic thermal estimation of main HV components including cables and transformers, the model structures identified in (2.21) and (2.1) are a good starting point, and can be approximated using the first-order differential equation of (3.11) [116].

$$\tau_p \frac{dy_t}{dt} + y_t = K_p \, u_{t-\tau_d} \tag{3.11}$$

where y_t is the measured response variable which is to be predicted (relevant temperature ϑ in this case) and u_t are the available inputs (Load and ambient temperature in this case). The model parameters including gain K_p, time constant τ_p and dead-time τ_d are to be estimated by training the model. The transfer function is found by applying Laplace transformation, as shown in (3.12)-(3.13). For dynamic thermal modeling, the parameter τ_d is irrelevant and therefore not investigated further [117].

$$s\,\tau_p Y(s) + Y(s) = K_p \, U(s) e^{-s\tau_d} \tag{3.12}$$

$$G(s) = \frac{Y(s)}{U(s)} = \frac{K_p}{s\,\tau_p + 1} e^{-s\,\tau_d} \tag{3.13}$$

State Space (SS) Model

For the relevant applications in this project, the *single input single output* State Space (SS) model with order n^{ss} has been used. Unlike ODE model, this physical Grey-box model requires extensive system information as it represents a high-order linear physical system with n^{ss} first order differential equations [115], and has the following discrete form:

$$\dot{x_t} = Ax_t + Bu_t + K\epsilon_t \tag{3.14}$$

$$y_t = Cx_t + Du_t + \epsilon_t \tag{3.15}$$

where the state vector x_t with order $(n^{ss} \times 1)$, the output matrix C with order $(1 \times n^{ss})$ and the direct transition (feed-through) matrix D with order (1×1) are uniquely identified during system definition. While the state matrix A with order $(n^{ss} \times n^{ss})$, input matrix B with order $(n^{ss} \times 1)$ and state disturbance matrix K with order $(n^{ss} \times n^{ss})$ are to be estimated by the model. In this configuration, the process noise $K\epsilon_t$ is used to interpret the disturbance due to variation in ambient conditions of the component which is unpredictable in nature and thereby modelled as a random process [118]. One key assumption in this formulation is the time-invariance of parameters A and B, while experience suggests that these parameters can change over longer periods of time (due to sedimentation and sea-bed movement of offshore cables or oil byproduct deposits in transformer tanks). However, this formulation can also be used to detect these changes for improved condition monitoring of these components.

Auto-Regressive eXogenous (ARX) Model

This regression-based linear Black-box model uses the underlying assumption that a combination of random processes can be used to represent a system. Referring to (3.16), the linear combination of previously predicted values and stochastic inputs is used for future predictions [119].

$$\hat{y_t} = \boldsymbol{w}\, \boldsymbol{y_{t\hat{-}n^y}} + \boldsymbol{w'}\, \boldsymbol{u_{t-n^u}} + \epsilon_t \tag{3.16}$$

where the predicted output $\hat{y_t}$ is dependent on a linear combination of historic approximations $\boldsymbol{y_{t\hat{-}n^y}} = [y_{t\hat{-}1}, y_{t\hat{-}2}, ...y_{t\hat{-}n^y}]^T$ which are weighed linearly by the parameters $\boldsymbol{w} = [w_1, w_2, ...w_{n^y}]$. Similarly, the influence of input sequence $\boldsymbol{u_{t-n^u}} = [u_t, u_{t-1}, ...u_{t-n^u}]^T$ is weighed by $\boldsymbol{w'} = [w'_0, w'_1, ...w'_{n^u}]$. The optimal parameters $\boldsymbol{w}$ and $\boldsymbol{w'}$ are estimated by training the model over a sequence of available inputs and outputs, while the model order (n^y, n^u) is predetermined to balance prediction accuracy with computational stress.

Artificial Neural Network (ANN) Model

The models discussed so far are inherently linear, contrary to the thermodynamic behavior of the HV components in focus [112]. Artificial Neural Network (ANN) are regression-based, non-linear, black-box models which use similar inputs as the ARX model, but offer more flexibility than all the preceding models [120]. This is true because instead of using weighted-linear combinations, the variables are allowed to pass through three different layers of ANN (input, hidden and output layers) with non-linear cross-combinations. For input and output layers with n^I and n^o neurons, the ANN simply maps the input to output, as shown in (3.17). This property makes ANN suitable for non-linear multidimensional regressive applications [108].

$$f : \mathbb{R}^{n^I} \longrightarrow \mathbb{R}^{n^o} \tag{3.17}$$

A feed-forward ANN formulation consisting of one input layer, one output layer and n^H hidden layers, as shown in Fig. 3.5, has been used in this project. Input layer represents the input data, intermediate hidden layers performs computation, while the output layer produces results. Each arrow represents the weight $\boldsymbol{w}$, while each node in the hidden layer represents a variable H formed by the application of a non-linear activation function $h()$. One key property that the figure doesn't show are the *bias nodes* (w_{0j}) which act like regression intercepts or bias, but they are present for each layer in the ANN. The discussion so far has been summarized in (3.18)-(3.21) for the input/outputs layers and first/last hidden layers. The number of hidden layers n^H, along with the activation function and the number of neurons in the input (n^I), output (n^o) and the individual hidden (n^l) layers are design choices. This degree of freedom means that the performance of the model depends hugely on its chosen structure, and ANN has the tendency to overfit the data if not supervised. For a more detailed introduction to neural networks, the readers are directed to [102, 105, 120].

$$\text{Input :} \qquad U_j = u_j \tag{3.18}$$

$$\text{Hidden Layer 1 :} \qquad H_{1,\,j} = h\left(w_{0j}^{(0)} U_0 + \sum_{i=1}^{n^I} U_i w_{ij}^{(0)}\right) \tag{3.19}$$

$$\text{Hidden Layer } n^H \text{ :} \qquad H_{n^H,\,j} = h\left(w_{0j}^{(n^H-1)} H_{n^H-1,\,0} + \sum_{i=1}^{n^l} H_{n^H-1,\,i}\, w_{ij}^{(n^H-1)}\right) \tag{3.20}$$

$$\text{Output Layer :} \qquad Y = h\left(w_0^o H_{n^H,\,0} + \sum_{i=1}^{n^l} H_{n^H,\,i}\, w_i^o\right) \tag{3.21}$$

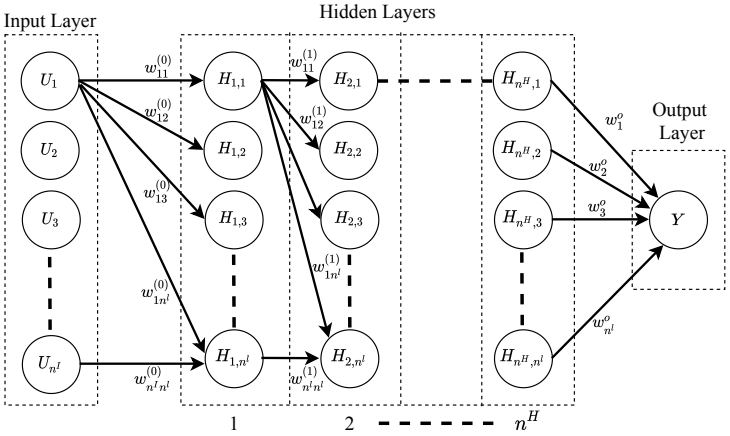

Figure 3.5: Illustration of the feed-forward Artificial Neural Network model with n^I neurons in input layer (U), n^H hidden layers (H) and 1 neuron in output layer (Y). The number of neurons in each hidden layer are fixed to n^l for illustration.

3.2 Dynamic Thermal Estimation of Cables and Transformers in OWF

In this project, data-driven Machine Learning (ML) models have primarily been used for DTR estimation of transformers and cables. Since these models can only be used for estimation of recorded temperatures, TOT measurements (ϑ_t^{tot}) for transformers and fibre-optics DTS measurements (ϑ_t^{dts}) for HV export cables are used as estimated outputs y_t or Y, instead of HST (ϑ_t^{hst}) and conductor ($\vartheta_t^{\text{cond}}$) temperatures. For input u_t, heat generated due to losses drive temperature development in the components; therefore, both load current square I_t^2 and losses W_t can be used equivalently with similar results. Additional inputs of ambient (ϑ_t^{amb}) and seabed (ϑ_t^{sea}) temperatures are not used in this formulation due to lack of availability of consistent data. Alternatively, these inputs are modelled as known disturbances where needed. Each of the models considered in this work is supposed to go through two steps before it is fit for temperature approximation: evaluation of predetermined parameters during model setup and estimation of remaining parameters by training over a range of available data.

Model setup step is considerably different for grey and black box models. The availability of physical insights is used to define the predetermined parameters such that they fit the grey-box process as much as possible, while a compromise between model's computational efficiency and accuracy is desired for in the latter. This is substantiated in Table 3.1, where the physics-based ODE and SS models are parameterized to reflect the order of differential equations driving component thermodynamics in (2.21) and (2.1) [117]. The higher order chosen for SS model was determined by testing upto 6^{th} order using *trial and error* approach in [121] which provided minimal improvement in prediction accuracy beyond the 3^{rd} order derivative for state x_t. The matrix D prevents direct transfer of input u_t to the temperature measurements.

Black-box models for long-term estimation, including ARX and ANN, are designed by testing over a range of parameters and selecting the lowest possible order which results in acceptable error. For both transformers and cables, same order of data available for prediction ($n^y = 10$ and $n^u = 8$) is used for both the ARX and ANN models, but the number of hidden layers (n^H) is different in ANN for each application with 8 nodes being suitable for the last hidden layer for transformers. All of these estimations can be handled automatically by the *System Identification Toolbox* in Matlab [121], using the principles in [106] [107]. The number of back-propagation epochs defines the number of times the training data is allowed to pass through the ANN model for parameter estimation. Considering the applications of the ANN model in this project, a non-linear ramp function called Rectified Linear Unit (ReLU) has been used as the activation function $h(x) = max(x, 0)$, because it can limit the minimum value which is critical for thermal estimation of HV components. Hence, it is observed that ANN offers a much larger range of design choices compared to linear regression, which start from the number of hidden layers to number of nodes per layer and goes all the way to epochs, batch size and activation functions. This makes ANN suitable for prediction of complex non-liner models, especially when exact relationship is not known beforehand, but consequently results in higher computational time and stress along with its tendency to overfit the data.

Moving on to short-term prediction models, forgetting factor χ of 0.2 is used for Exponential Smoothing model which allows the highest weight (smoothing factor of 0.8) to be allotted to the most recent observation; whereas, for the Local Trend Model, this factor is to be optimized by testing for minimum SSE in (3.6) over the range of $0 < \chi < 1$. This is demonstrated in Fig. 3.6 for BB2 export cable's J-tube section's thermal estimation, which gives optimal fit for $\chi = 0.67$. Both the variation of SSE with χ and exponential reduction in weight of observations further from the most recent one for optimal χ are provided in Fig 3.6.

The second step that deals with the estimation of remaining parameters, mentioned in the right-most column of Table 3.1, is trickier to deal with because regression-based (specially non-linear) models have the tendency to overfit the available data by adapting to noise and features specific to the training data, which fails as soon as new data becomes available [[122]]. One possible simplification that could be made is employment of Principal Component Analysis (PCA) which reduces the problem dimensions, but the applicability of this method on time-series data doesn't sit well with computational complexity and stress. Therefore, for the long-term prediction models, the available data series are split into training and testing sets following the cross-validation mechanism in [102]. For the training data set, the loss function in (3.22) is minimized by

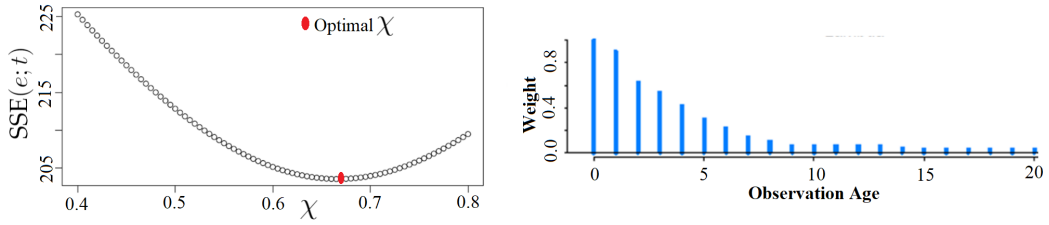

Figure 3.6: Left: Optimization of forgetting factorχ for Local Linear Trend model for BB2 J-tube. Right: Exponential reduction in weights of observations BB2 J-tube (0 means latest observation, 20 is the oldest in the given window)

adjusting the model parameters, where n^{train} represent the number of training observations, while $\hat{y}_t$ and y_t are the predicted and measured observations respectively.

$$L.F. = \frac{1}{n^{train}} \sum_{t=1}^{n^{train}} (\hat{y}_t - y_t)^2 \tag{3.22}$$

Table 3.1: Elaboration of predetermined and estimated parameters for the considered ML models

Models	Predetermined Parameters	Estimated Parameters
Exponential Smoothing	Forgetting Factor: $\chi = 0.2$	-
Local Trend	Forecast Function: $\kappa = [1 \quad q]^T$	Forgetting Factor: χ Forecast parameters: e Approx. order: p
ODE	Order of model = 1	Gain: K_p Time Constant: τ_p
SS	$C = [1 \quad 0 \quad 0]$ $D = [0 \quad 0 \quad 0]$ $x_t = [\vartheta_t^{\text{dts}} \quad \dot{\vartheta}_t^{\text{dts}} \quad \ddot{\vartheta}_t^{\text{dts}}]^T$ $x_t = [\vartheta_t^{\text{top}} \quad \dot{\vartheta}_t^{\text{top}} \quad \ddot{\vartheta}_t^{\text{top}}]^T$	Coefficient Matrices A, B, K
ARX	Model Order $n^y = 10$ $n^u = 8$	Weighing Parameters $\boldsymbol{w}, \boldsymbol{w}'$
ANN	Activation func. $h(x) = max(x, 0)$ no. of inputs: **10 + 8 + 1** no. of H layers : **2 / 3** no. of nodes : **5 + 20 + 8** back-prop epochs: **50 / 60**	Weighing Parameters $\boldsymbol{w}^{(n^H)}, \boldsymbol{w}^o$

* Relevant for WTG Transformers * Relevant for HV Export Cables

3.2.1 Validation of Models for Cable Thermal Estimation

In order to validate the applicability of the data-driven models for thermal estimation of HV cables, 220kV XLPE insulated export cable for 258 MW Burbo Bank Extension (BB2) which is 25 km off the west coast of UK has been used as test case. The total export cable length is 35.6 km and is divided in to HDD, J-tube, Offshore and Onshore sections as discussed in Chapter 2. The cable used along the route not only differs in rating (718-1080 A, 1000-1200 sq.mm), but the design is different as well (3-core for subsea and 3x1-core for land). In

total 27.5 days of DTS measurements are used with 30-min sampling rate, out of which 16.5 days of data has been reserved for training while the remaining 11 days for testing as per the 60-40 principle [123]. As shown in Fig. 3.7, the long-term prediction models have access to both the load (Current I^{c}) and ϑ^{dts} measurements during the training phase; whereas, only the temporal I^{c} information is provided to the models for testing. The predicted temperature $\hat{\vartheta^{\mathrm{dts}}}$ is then compared with the measured ϑ^{dts} represented by dashed-lines in Fig. 3.7 for validation. This entire process is repeated for each of the cable sections, therefore each model type is trained and tested four times to accurately model the difference in behavior of the respective sections. A quick view at the data reveals that the temperature varies more frequently for J-tube, while Onshore and HDD appears to have the largest thermal time constants.

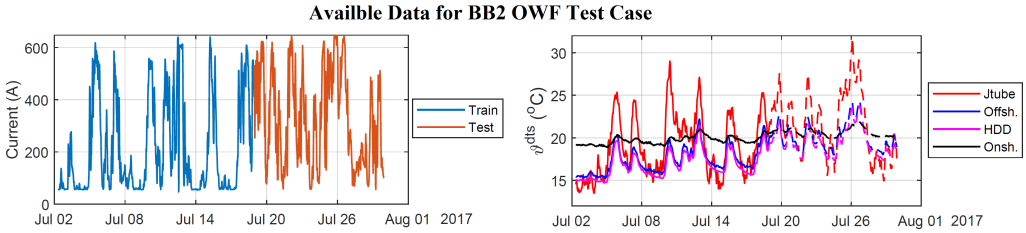

Figure 3.7: Training and test data for Burbo Bank 2 OWF export cable test case. Left: Cable current (I^{c}). Right: Temperature (ϑ^{dts}) for different cable sections (dashed lines represent test data which will only be used for validation and benchmarking)

Long-Term Prediction Models

The training and testing results for long-term prediction models are split for the four sections under focus. Fig. 3.8 - Fig. 3.11 present the performance of all the models for HDD, J-tube, Offshore and Onshore sections respectively. The grey-box and black-box models are fundamentally different, as the physics-based ODE and SS models treat the estimation mechanism as a process and do not care for long-term history of the measurements. While the ARX and ANN models solve the problem by statistically relying on historic load and temperature, as both the black-box models use the same order of 10 for ϑ^{dts} measurements. Hence, with 30-min sampling rate, these models can see upto 5-hours of historic DTS data which is considerably lower than the thermal time constants for the HDD and offshore sections of export cables (refer Chapter 2).

Table 3.2 provides the goodness-of-fit based on NMSE for all the test cases including testing and training periods. Unlike generalization error, the reason to include training fit results is to test the consistency in predictions and to check if the models overfit the training data or not. The highest variation between training and test results are found for ANN models which is expected because the degree of freedom offered by this model along with its non-linear characteristics can result in overfitting. However, it is possible to improve the performance of both the black-box models by tuning the parameters further (hyper-parameters in this case). Both the physics-based models perform well with SS resulting in better fit, higher consistency and greater flexibility which is also very important for this application. All of these models are expected to perform even better as more and more data becomes available for training and testing, with the exception of ANN due to its tendency to overfit.

Table 3.2: Goodness-of-fit results for long-term prediction Machine Learning (ML) models based on NMSE. 100 means perfect fit and 0 means inappropriate for prediction. The performance during training and test periods for all the cable sections for Burbo Bank 2 OWF test case is provided.

Long-term Pred. Models	**Cable Section**							
	HDD		**J-tube**		**Offshore**		**Onshore**	
	Train	Test	Train	Test	Train	Test	Train	Test
ODE	82.4	62.4	80.1	78.2	74.8	63.8	77.6	67.9
SS	90.2	88.5	88.7	82.5	92.5	90.8	84.8	83.6
ARX	70.2	68.8	79.9	78.2	85.5	82.3	68.2	62.4
ANN	59.5	41.5	64.4	44.4	69.9	38.1	52.9	31.8

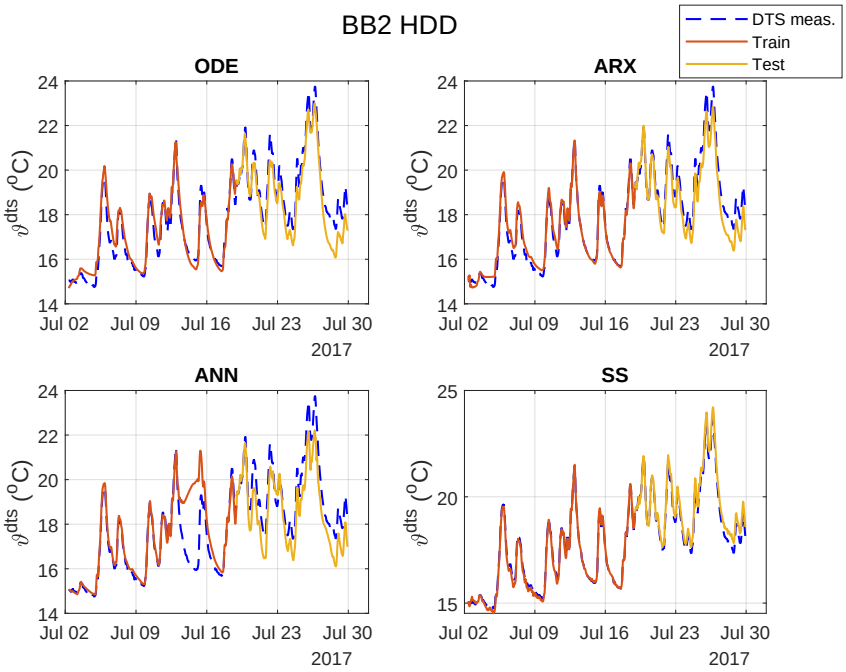

Figure 3.8: Machine learning based ϑ^{dts} forecast results for the HDD section of BB2 OWF test cases. All the long-term prediction models are presented. Training and test results are highlighted separately.

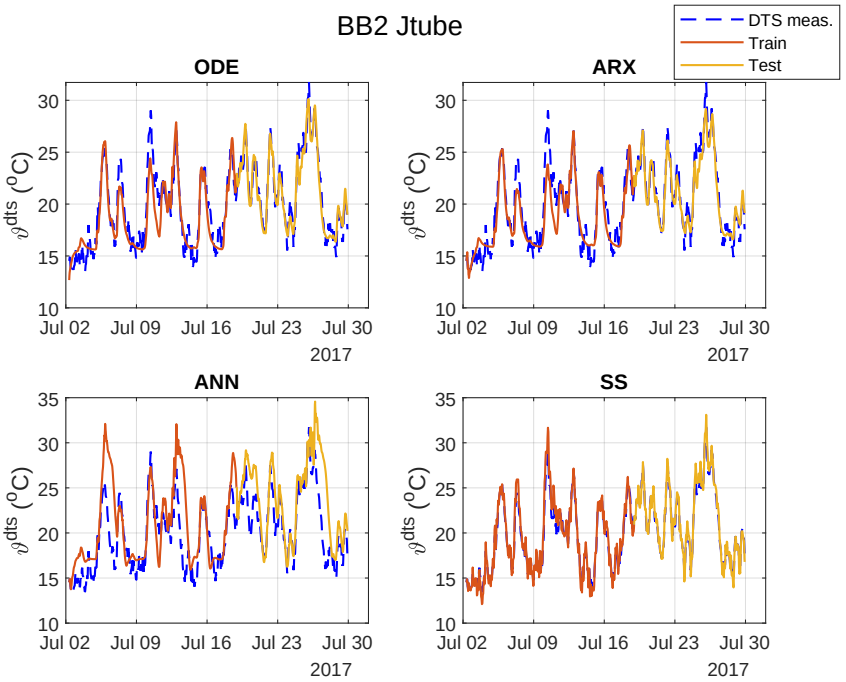

Figure 3.9: Machine learning based ϑ^{dts} forecast results for the J-tube section of BB2 OWF test cases. All the long-term prediction models are presented. Training and test results are highlighted separately.

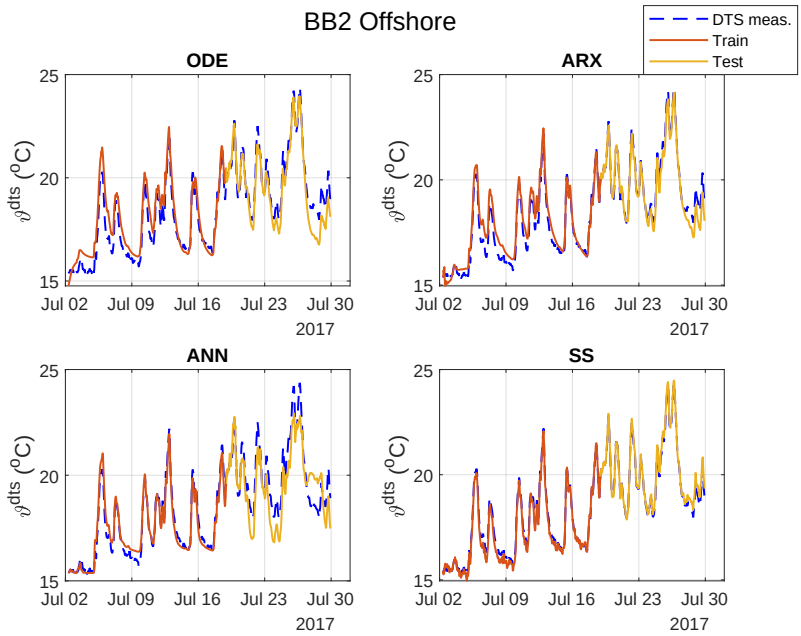

Figure 3.10: Machine learning based ϑ^{dts} forecast results for the offshore section of BB2 OWF test cases. All the long-term prediction models are presented. Training and test results are highlighted separately.

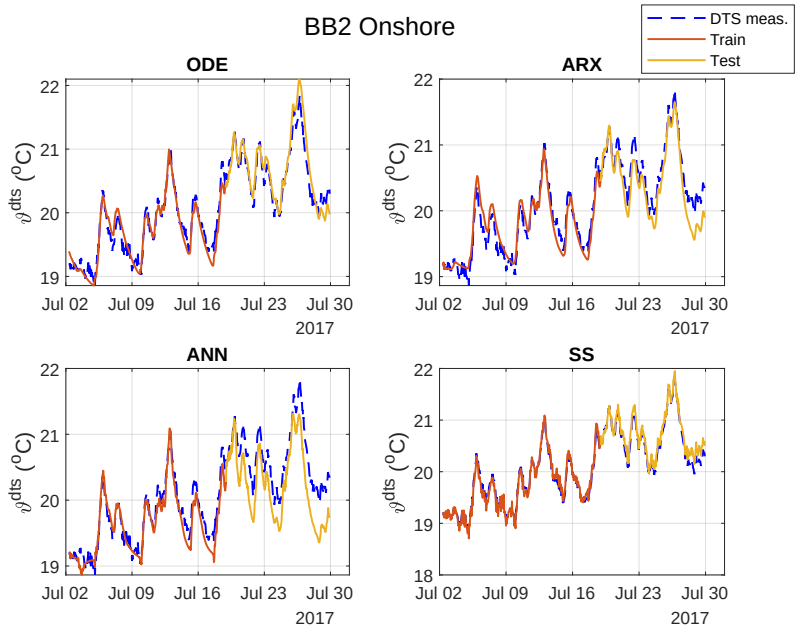

Figure 3.11: Machine learning based ϑ^{dts} forecast results for the onshore section of BB2 OWF test cases. All the long-term prediction models are presented. Training and test results are highlighted separately.

Short-Term Prediction Models

In contrast to long-term prediction models, these models have access to all the past measurements up until the time of prediction. In this test case, 24-step (12-hour ahead) predictions are performed by using real-time measurements represented by blue-dashed lines in Fig. 3.12. Hence, the prediction for July 08 (15:00) will be based on all the ϑ^{dts} measurements until July 08 (03:00). The entire process repeats as more observations

become available and this goes on for the entire duration. The prediction results for exponential smoothing and local linear trend models provided in Fig. 3.12 indicate that local trend model outperforms the smoothing model because the forgetting factor χ is optimized and due to its effectiveness for multi-step ahead predictions. However both the models are considerably better than constant-mean model. The performance of these models can further be improved if models are transformed to use I^{c} and ϑ^{sea} as inputs.

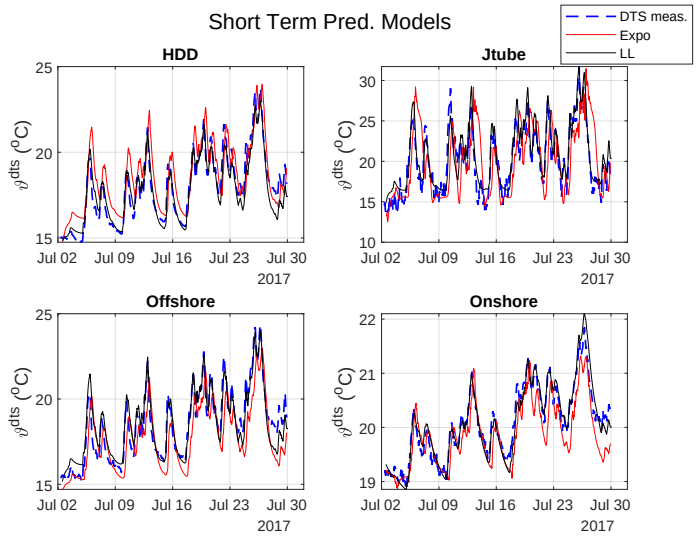

Figure 3.12: Machine learning based ϑ^{dts} forecast results for all the sections of BB2 OWF test cases. THe relevant short-term prediction models (Exponential smoothing - red, Local Linear Trend - black) are presented.

3.2.2 Thermal Validation for Lab Transformer

Hot spot temperature measurements are usually not available for OWF transformers, therefore validation of transformer TEE model from Chapter 2 and data-driven machine learning models is performed for the test transformer setup in Fig. 3.13 (a) at the DTU HV PowerLab. Controlled heat run tests have been performed on the test transformer (manufactured 1990) which was formerly operated in a distribution network. The transformer cooling mechanism along with its electrical and mechanical design, provided in Table 3.3 imply that the results of the heat run test can easily be scaled to offshore windfarm transformers.

Table 3.3: Specifications for Test transformer in DTU PowerLab

Parameter	Value
Rating	630 kVA
Voltage	0.4/10 kV $\pm$ 5%
Vector Group	Dyn11
Percentage Impedance	5 %
Frequency	50 Hz
Oil weight	460 kg
Winding Time Constant	6 min
Rated no-load/full-load losses	586/5064 W
Cooling mode	ONAN

In order to assess the thermal development in the transformer winding, core and tank during the heat run test, the oil was drained and the active part was removed (Fig. 3.13 b). Multiple Type-K thermocouple temperature sensors were installed at different positions inside and outside the transformer tank for temperature measurement, as shown in Fig. 3.13 (c). In total 6 sensors (T1-T6) were placed for TOT measurement (2 at the top of each phase winding), whereas the uncertainty in HST measurement was addressed by installing 7

sensors (H1-H7) close to the top of the LV and HV windings. The position of these sensors have been chosen based on experience and manufacturer's recommendations, which is why the majority of the sensors are located at the middle phase. The sensors T2 and H3 were later chosen for thermal validation of TOT and HST measurements respectively, Fig. 3.13 (d) (c). Furthermore, average values from multiple sensors placed around the lab transformer have been used to measure the ambient temperature, which was also provided as input to the relevant test models. To ensure the relevance of this exercise for dynamic rating of offshore windfarm transformers with intermittent loading, two different load profiles for the lab transformer heat run test have been chosen such that one profile stays within the transformer rated capacity, while the other pushes up to 1.4 pu rated current through the transformer HV winding.

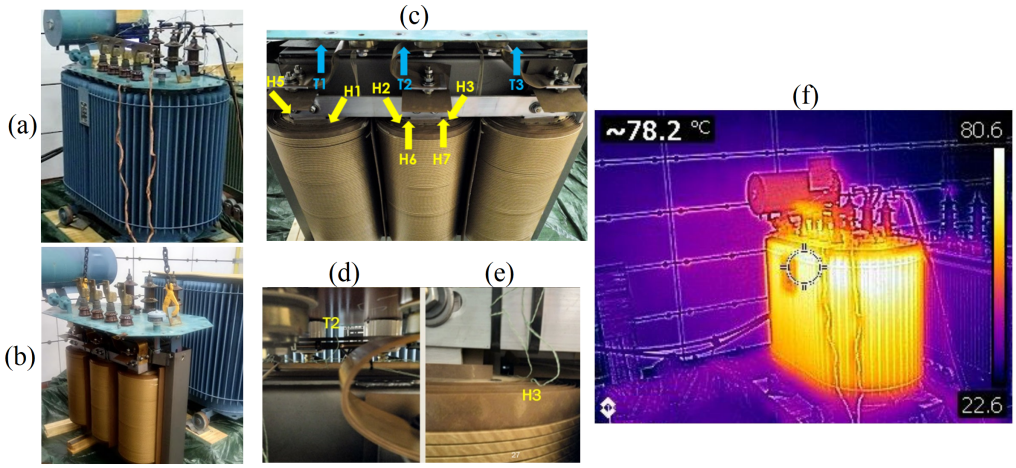

Figure 3.13: (a) Lab transformer energization setup for heat run test viewed from the LV side. (b) Active part of the lab transformer after oil drainage and before sensors' placement. (c) Position of TOT sensors T1-T3 (T4-T6 on the opposite sides) and HST sensors H1-H7 (except H4). (d) (e) Closeup of sensors T2 and H3 (these sensors are later chosen for thermal validation). (f) Thermal image of lab transformer during sustained overload (1.4 p.u) at 2.5 hour mark.

The measured TOT (T2) and HST (H3) when compared with the temperatures calculated using different TEE (Susa and IEEE) and Machine Learning (ML) models, as shown in Fig. 3.14 and 3.15, exhibit consistent behavior. The TEE models offer higher accuracy for both the load profiles, with the Susa model being the most accurate. The trends and peaks align for the measured and calculated values with maximum error of 2 °C. The consistent error could have been resolved by parameterizing the TEE model again for this old transformer because it has recently been refurbished, which may have affected some of the parameters in Table 3.3, but this was beyond the scope of this work. The intermittence of load prevent the temperatures to stabilize at a certain value, which is also observed in offshore windfarm transformers. The accuracy of the simulated temperatures proves that the tested model is reliable enough to be employed for intermittent dynamic load profiles of offshore windfarm transformers.

The entire dataset has been used for training the ML models and only long-term prediction models are considered for this application. Due to limited data-points, physics-based models (SS and ODE) do not perform efficiently in these tests; while the non-linear black-box ANN model fits the HST and TOT measurements quite well for both the load profiles. This is expected because the latter model can replicate the measurements by virtue of its inherent degree-of-freedom, but it is important to review these results under untrained environment before definite conclusions are made. Interestingly, the thermal image of the transformer after a sustained overload of 1.4 pu for 2.5 hours, as shown in Fig. 3.13 (f), provides an indicative concentration of high temperature in the top region of the transformer tank. The maximum temperature of 80.6 °C in Fig. 3.13 (f) is in coherence with TOT measurement at 2.5 hour mark in Fig. 3.15.

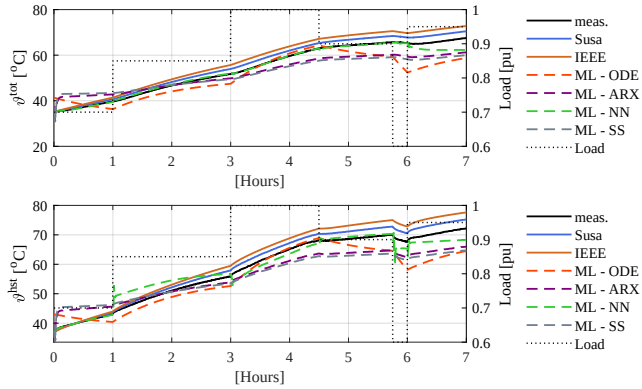

Figure 3.14: Comparison of calculated transformer temperatures (ϑ^{tot} and ϑ^{hst}) using TEE models from Susa [50], IEEE [45] and ML models with the measured values for the 630 kVA lab transformer for rated load condition ($\leq$ 1pu).

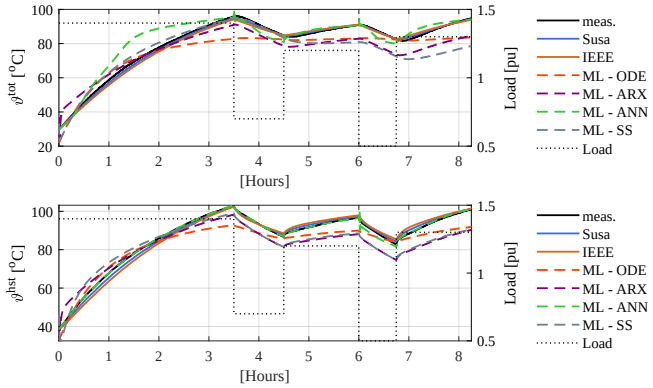

Figure 3.15: Comparison of calculated transformer temperatures (ϑ^{tot} and ϑ^{hst}) using TEE models from Susa [50], IEEE [45] and ML models with the measured values for the 630 kVA lab transformer for dynamic high load condition ($\geq$ 1pu).

3.2.3 Thermal Estimation of Wind Turbine Transformers

With the development of large-scale OWFs over the last decade, the number of Wind Turbine Generators (WTGs) per windfarm has increased significantly and it is observed that the recently built large-scale OWFs have as many as 200 WTGs. With each WTG consisting of at least one transformer, effective condition monitoring of these transformers has become arduous. This argument along with the lack of availability of consistent temperature data for offshore windfarm transmission transformers compelled the author to validate the developed machine learning models for WTG transformers. Ten different WTG transformers of similar size (7 MVA) and similar construction features from four OWF sites in UK and DK have been used. All of these transformers are located in the nacelle of the WTG and the temporal nacelle temperature has been used as ambient input for the relevant ML models, along with the transformer load information in real-time. 10-min sampled data for TOT (ϑ^{tot}) over the range of 2 to 3 years has been used for the tested WTG transformers. Two distinctive test approaches have been used, which are discussed in the following sections.

Train and Test on the same WTG Transformer

As the name suggests, the data from each WTG transformer is trained and tested on itself. Therefore, 10 models are trained for each of the considered model types for long-term prediction (ODE, ARX, ANN and SS), resulting in a total of 40 models. Moreover, the same 60-40 principle is used as per which 60% of the

available two-year ϑ^{tot}, I^{trf} and ϑ^{amb} data is used for training and rest for testing. The results for two WTG transformers are provided in Fig. 3.16 and 3.17 for a small sample size of the actual data. In contrast to the lab transformer setup, the performance of physics-based models is found to be considerably better than their black-box counterparts as the scale and quality of available data increases.

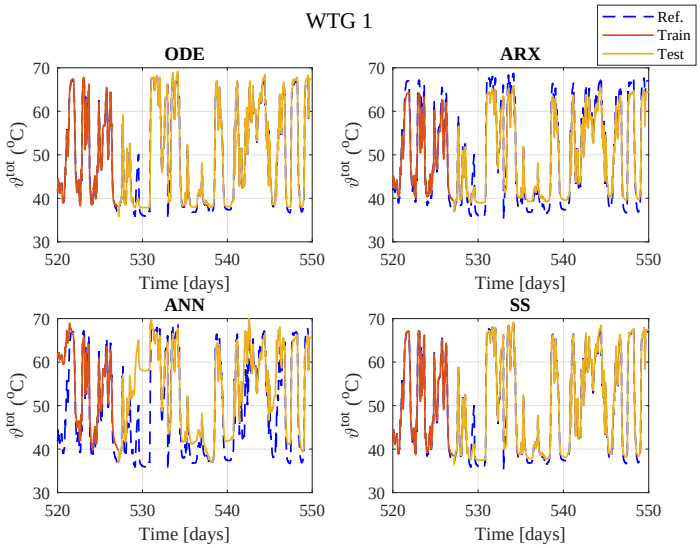

Figure 3.16: Thermal estimation results for WTG 1 transformer by training and testing on its own recorded ϑ^{tot} using 2 years of available data. All the long-term prediction models are presented for a 30-day window out of 730 days for ease of elaboration. Training and test results are highlighted separately.

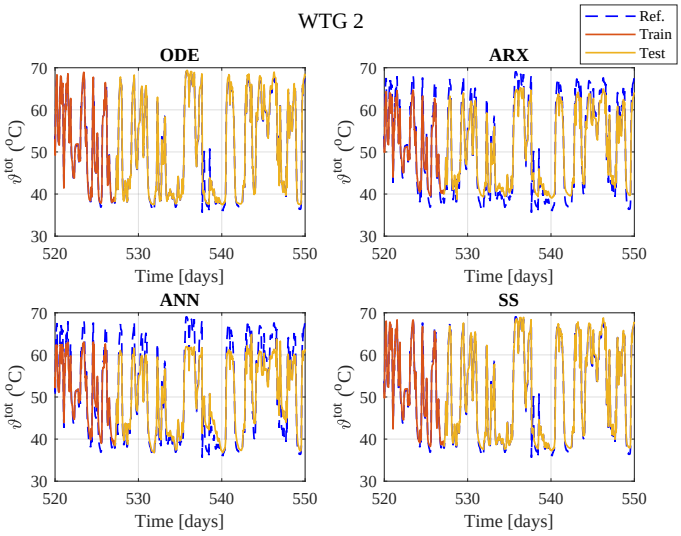

Figure 3.17: Thermal estimation results for WTG 2 transformer by training and testing on its own recorded ϑ^{tot} using 2 years of available data. All the long-term prediction models are presented for a 30-day window out of 730 days for ease of elaboration. Training and test results are highlighted separately.

The tested models are benchmarked using box-plots in Fig. 3.18 as per the NMSE parameters. Both the physics based models (SS and ODE) are not only considerably more accurate but also result in more consistent results. The linear black-box ARX models offer acceptable accuracy but can be improved by varying the model parameters. On the other hand, ANN models are least accurate but the consistency of estimation is similar for train and test data.

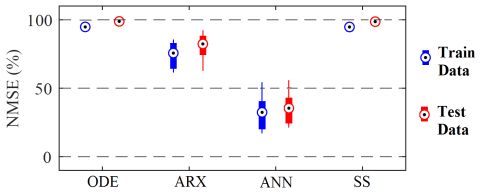

Figure 3.18: Boxplots for NMSE distribution when 10 WTG transformers are trained and tested on their own recorded ϑ^{tot}

3.3 Potential Applications of Data Driven Models

The models developed in this project can potentially be used for widescale applications in OWFs. These applications can range from improved cable system design and operation to transformation in predictive, preventive and condition-based maintenance of oil-filled components. Some of the applications explored in the project are presented below.

3.3.1 Apprehension of Cable Surroundings

As explained in Chapter 2, export cable's sections (incl. J-tube, HDD, Offshore etc.) exhibit different thermal behavior. The rationale behind these differences and the physics-based thermal modeling of these sections have been explored extensively in literature and are still being investigated [38, 40–42, 83]. The grey-box ODE ML model presented in this project can be a potential solution to this puzzle. By reviewing the estimated thermal time constant τ_p in ODE model for the entire BB2 cable, as shown in Fig. 3.19, the rapid thermal response of J-tubes (due to lowest τ_p distribution) compared to the remaining two sections is confirmed.

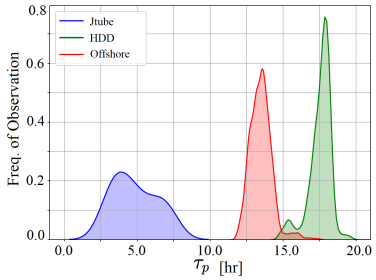

Figure 3.19: Normalized distribution of time constant τ_p for HDD, offshore and J-tube sections for BB2 export cable test case. The time constants were estimated with the ODE model.

The diverse nature of the offshore cable section has been discussed in detail in Section 2.2.2. By virtue of this diversity, the gain K_p and time constant τ_p parameters of the ODE model vary considerably along the offshore route. The temporal variation of ϑ^{dts} at four different locations along the test case cable's route with extreme estimated values of these parameters are provided in Fig. 3.20.

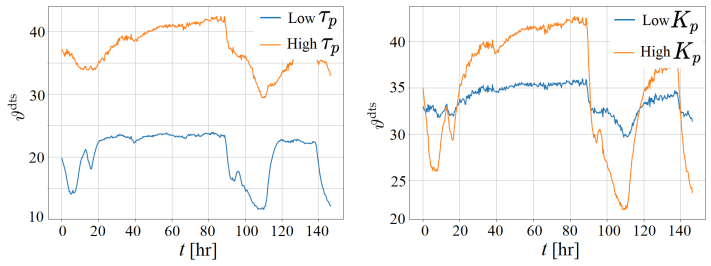

Figure 3.20: Measured temporal variation of ϑ^{dts} for 4 points along the offshore cable section with extreme values of τ_p (left), K_p (right). The parameters τ_p and K_p were estimated by training the ODE model over the 145-hour window of available data. The influence of these parameters on the test case OWF cable's temperature variation is expected.

The four test points High τ_p (15.9 hr), Low τ_p (1.7 hr), High K_p (0.25 °C/W) and Low K_p (0.06 °C/W) behave considerably different under the same load and ambient condition variation. Hence, it can be deduced that hidden information regarding the cable route can be gathered efficiently and any unexpected changes to this information can be identified by continuous training of physics-based ML models over a long period [117]. The observation so far has further been confirmed by performing sensitivity analysis of soil's resistivity ρ_{soil} and specific heat ϖ_{soil} for the ODE model parameters in Fig. 3.21. The inherent direct relation of thermal time constant with thermal resistance and capacitance ($\tau = TC$), (2.15) and (2.16) is accurately demonstrated, while the influence on gain K_p requires more elaboration [124]. Furthermore, unsupervised machine learning algorithms like clustering and classification can be used to identify troublesome sections along the offshore section's route.

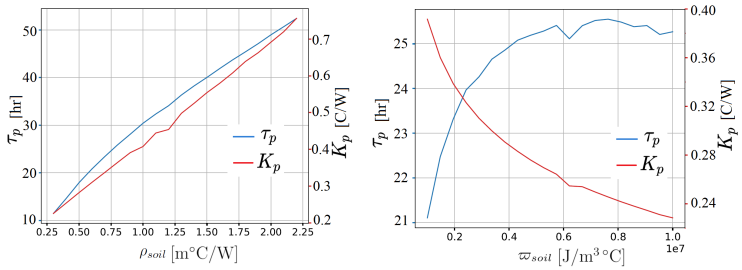

Figure 3.21: Estimated parameters for ODE model K_p and τ_p, versus soil resistivity (left) and soil specific heat (right). The parameters were estimated with the process model from synthetic data

One more important application of data-driven cable monitoring has been explored in the sub-project [124]. The feasibility to determine the offshore cable's burial depth along the entire route has been performed. The subsea cable burial depth, shown in Fig. 3.22, is not only different along the cable route but it also tends to change over time. As part of the sub-project, effective estimation of variation in this depth over longer periods due to sea-bed movement and sedimentation has been successfully demonstrated using linear regression models (less accurate) and non-linear ANN models (acceptable accuracy). This is shown in Fig. 3.23 for a synthetic dataset. Hence, by combining the properties of physics-based grey-box models for parameter estimation and black-box models for correlating these parameters with physical attributes, ML-based models can potentially revolutionize offshore cable monitoring.

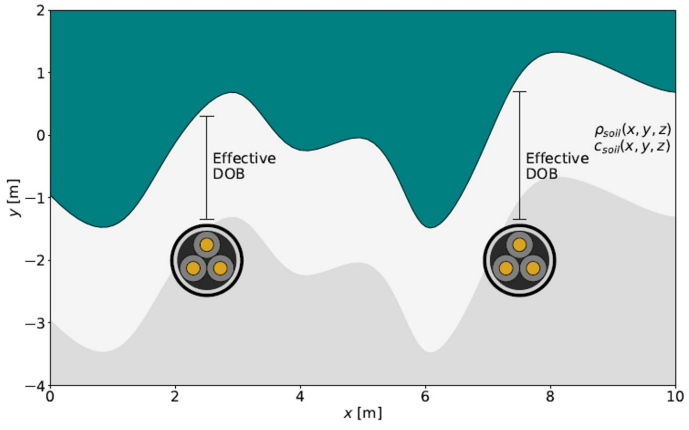

Figure 3.22: Depth of burial for two parallel subsea cables from a cross-sectional viewpoint. The soil resistivity and thermal capacity are identified to vary with location.

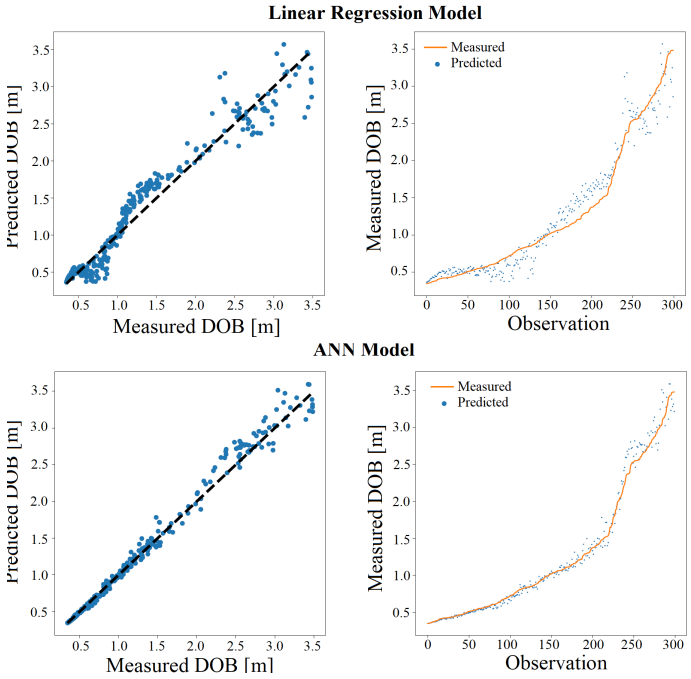

Figure 3.23: Predicted and measured depth of burial for HV export cables using synthetic dataset [124]. Top: burial depth estimation model is trained using linear regression. Bottom: burial depth estimation model is trained using ANN.

3.3.2 Monitoring of Offshore Wind Turbine Transformers

As the number of WTGs in OWFs increase, effective monitoring of transformers in these WTGs becomes more challenging. The large scale thermal monitoring data generated by these transformers has been used for a novel approach, which examines the potential for cross-application of the data analytics based models. This is done by training a model over the entire dataset for each WTG transformer and then testing it for the remaining transformers. Therefore, in total, 10 models are trained for each model type and each of these models are tested 9 times (90 tests per model type). The boxplots for benchmarking results in Fig. 3.24 confirms that the ODE, SS and ARX models can be used to stipulate thermal development of a large population of transformers by training the models over a smaller sample size of these transformers. The temperature plots in Fig. 3.25 presents one of these instances where Train WTG represents the training results for all the ML models, while the test results other than Train WTG are presented in the remaining three plots. All the models except ANN seem to perform appropriately which further proves the point that the tested formulation of ANN tends to overfit the training data. This demonstration can have wide-scale applications in condition monitoring of transformers.

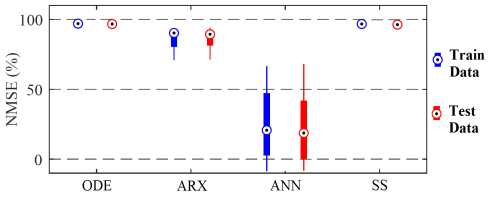

Figure 3.24: Boxplots for NMSE distribution when each of the 10 WTG transformers is trained on its own recorded ϑ^{tot} and tested on the remaining 9 WTG transformers. In total, 90 models are tested, 10 are trained.

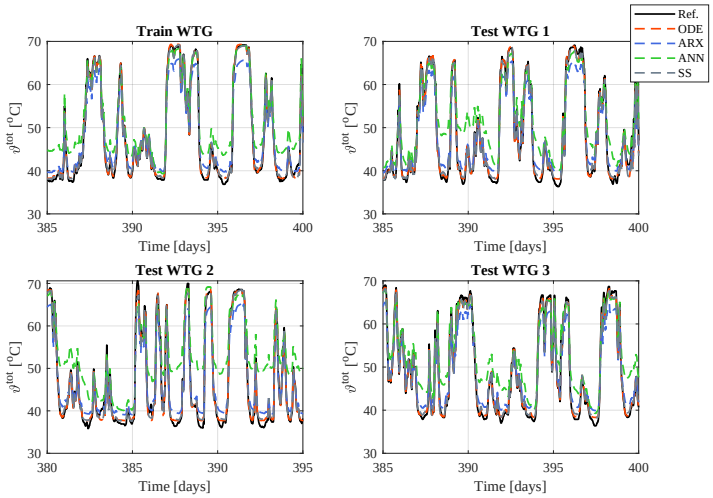

Figure 3.25: Thermal estimation results for the case where a WTG transformer is trained on its own recorded ϑ^{tot} and tested on three different WTG transformers using 2 years of available data. All the long-term prediction models are presented for a 15-day window out of 730 days for ease of elaboration.

Key Takeaways from Part II

In **Part II**, the foundation for thermal monitoring and estimation of critical HV components in the OWF export system has been established. The debottlenecking of the OWF export system has shown that OSS transformers and different subsections of the HV cables (incl. J-tubes, HDD and offshore/subsea) are the major thermal bottlenecks. Even though HV cables are conservatively designed and are known to be the primary thermal bottlenecks, the low thermal time constants of transformers can make them thermal pinch-points under fluctuating loads, which is the case for OWFs. The discussion in Chapter 2 has shown that the state-of-the-art TEE models can be used for dynamic thermal estimation of transformers and cables, but these models need to be modified to make them fit for the optimization problems presented later in the thesis. The validation of the simplified models on test case windfarm components and lab investigations has shown that the performance is acceptable. The utilization of data analytics and machine learning is uniquely addressed in Chapter 3, where two grey-box and multiple black-box models are tested for short-term and long-term thermal estimation of the relevant HV components. The first-order Ordinary Differential Equation (ODE) model and simplified SS model prove that the combination of physics with statistical estimation in grey-box models is the best way forward as it allows the developers to retrieve control of the model structure. On the other hand, the black-box models are found to over-fit the training data, particularly the non-linear Artificial Neural Network (ANN) models. The final applications of these machine learning models has shown that dynamic condition monitoring of the OWF export system and WTG transformers can be improved significantly if long-term data is available for these components. The results are published in **[Pub. C1]**, **[Pub. C5]**, **[Pub. C6]** and **[Pub. C7]**.

PART III - DYNAMIC THERMAL AGEING BASED OPTIMAL TRANSFORMER UTILIZATION

The discussion in **Part II** concluded that HV export cables account for the highest contributions to the Capital Expenditures (CAPEX) of Offshore Windfarm (OWF) export systems. It was further concluded that there is limited recorded experience of cable operation beyond designated thermal limits (90 °C for XLPE) and limited literature on thermo-chemical ageing beyond these limits. All of these arguments have compelled the OWF designers to optimize the cable design, while the operators are obliged to use these cables conservatively even with Dynamic Thermal Rating (DTR) operation. On the other hand, transformers are critical for operation, designed for contingency, have lower CAPEX footprint and offer more room for operational optimization under current design practices. Furthermore, the thermo-chemical ageing models for transformers under cyclic load and contrasting ambient conditions are also well-recorded.

Under Static Thermal Rating (STR) based operational philosophy, transformers can be operated between 1-1.3 pu of their nameplate ratings under continuous and cyclic loading conditions [45]. Instead of limiting transformer current, DTR allows manipulation of transformer thermal capacity for optimal loading under favorable ambient and load conditions. For oil-filled power transformers, the thermal capacity is defined by the maximum allowable stress on materials close to the hot-spot and top-oil temperature regions. The thermal stress is regulated by complying with the limits defined by international standards IEEE C57.91 [45] and IEC 60076-7 [44]. The HST limits defined by these standards are summarized in Table 3.4 for large power transformers (>100 MVA) with Kraft-based Thermally Upgraded Paper (TUP) insulation under different dynamic load conditions beyond the rated capacity. These dynamic load limits are applicable to transformers with lower thermal class insulation materials and low temperature rise requirements specified in IEC 60076-2 [125]

Table 3.4: Thermal limits for large power transformers with thermally upgraded Kraft paper [45] [44]

	Normal Cyclic Loading	**Emergency Loading** (long-term)	**Emergency Loading** (<30 min)
Hot Spot Temp.	120 °C	140 °C	160 / 180 °C
Top Oil Temp.	105 °C	115 °C	115 / 110 °C

Unlike HV cables, thermal time constants for transformers range between several minutes and few hours. This implies that for short-term operational loading, transformer DTR can not be performed a priori as historical loading patterns, thermo-chemical decomposition and environmental circumstances need to be taken into account. In this part of the thesis, research questions **(B)** and **(D)** are resolved as DTR and dynamic thermal ageing based utilization of transformers is examined. **Part III** starts off by presenting and evaluating transformer ageing models (Chapter 4), which is followed by assessment of potential of employing DTR-based optimal utilization on actual power transformers tested across ten different offshore windfarms (Chapter 5). Finally a novel transformer utilization technique is proposed, tested and applied using a multi-period lossy-DCOPF algorithm for day-ahead energy dispatch optimization for the transmission network of west-Denmark (Chapter 6). The methods developed in this chapter are tested on the meshed transmission network instead of the conventional radial OWF export system to allow active load balance and to ease large-scale integration of OWFs in future networks without the need for additional grid-reinforcements. The contributions of these chapters are elaborated in detail in publications **[Pub. C2], [Pub. C3]** and **[Pub. C4]** by the author.

CHAPTER 4

Load-dependent Thermal Ageing of Oil-filled Power Transformers

The application of dynamic rating on power transformers results in additional thermal stress particularly in the top region of the tank. As a result it can be deduced that for load-dependent ageing, the influence of mechanical, electrical and environmental stresses can be ignored and the process of multi-factor ageing involving the catalytic behavior of these stresses on the overall thermal ageing mechanism can be neglected [126] [127].

4.1 Background and Literature Review

The HV electrical insulation in oil-filled power transformers along with the mechanical substructure for winding support is made up of liquid impregnated cellulose materials like Kraft. Mineral oils have traditionally been used for paper impregnation and heat dissipation in the transformer tank [128]. Therefore, extensive state-of-the-art research exists for thermal ageing of mineral oil and paper systems, as numerous theories are postulated on chemical degradation mechanism and the driving kinetics [129–131]. The advent of natural and synthetic oil over the last few decades suggests that further investigation is needed to develop ageing models for generic oil-impregnated cellulose systems. This project, however, focuses on the long-established mineral oil and Kraft paper system only, with emphasis on TUP whose equivalent hot-spot design temperature is 110 °C.

Historically, hot spot temperature has been known to drive the ageing of paper insulation, as defined initially by the golden thumb rule presented by Montsinger in 1930, that every 6-10 degree rise in HST reduces the transformer life to half [132]. However, state-of-the-art research suggests that the degradation of Kraft paper is mainly influenced by temperature, water, oxygen and acids, as the main processes that drive the degradation mechanism are hydrolysis, oxidation and pyrolysis [44]. As all of these processes occur simultaneously, the ageing process is highly non-linear which makes the classic Arrhenius reaction model the primary candidate for ageing assessment of transformers [133]. The influence of these parameters primarily temperature, water and oxygen has been investigated extensively in the literature [129, 134, 135]. Non thermally upgraded Kraft paper are more prone to ageing acceleration due to moisture infusion compared to the thermally upgraded paper as the ageing rate doubles for each percent rise in moisture for non-TUP while minimal affects are seen for TUP. On the other hand, the influence of oxygen in oil is found to have similar influence on the ageing of TUP and non-TUP, as the ageing is accelerated by two to three times for both the papers in proportion to rise in diffused oxygen in transformer oil.

The residual mechanical strength (also called tensile strength) of the insulation paper is key in defining its residual lifetime, which strongly depends upon the length of cellulose molecules. Degree of Polymerization (DP), representing the average number of saccharide rings in these molecules, are commonly used to determine the mechanical strength, as it ranges from 1200 for new material (1000 for new transformer because of drying and other pre-commissioning processes) to 200 (20% tensile strength) over the transformer lifetime. The DP value decreases with the chain scission process which breaks the cellulose molecules under thermal stress, thereby reducing the mechanical strength.

The first-order differential kinetic model, originally proposed by Emsley in [133], reformulates the Arrhenius reaction rate theory to account for decrement in paper's DP. Several recent studies by Gilbert and Jalbert [136–138] have shown the experimental values obtained by Emsley, Lundgaard, Daniel and others [130, 139–142]

need to be tracked by using a pseudo-zero kinetic model that allows reduction of scission rate with time. This DP-based model which is also presented in the next section relies heavily on two factors: Activation energy E_a and pre-exponential factor A. The experimental results recorded in [134, 135, 139] recommend using constant E_a of 111 kJ/mol which has been backed by future work in [130, 140, 141, 143, 144] under constant oxygen conditions, but most of these publications [130, 136, 145] also discovered the variation of E_a with oxygen. Furthermore, the difference of temperature dependent degradation was later described in [130, 142, 145]. The reduction of influence of hydrolysis and relevance of oxidation on TUP's ageing is backed by the latest findings in [146, 147].

4.2 Thermal Ageing Models for Kraft Paper Insulation

The models considered in this project are classified in to two categories: Basic Arrhenius reaction based model and degree of polymerization based models. These model are elaborated in detail below.

4.2.1 Basic Arrhenius Reaction Rate Model

The ageing of transformers using basic Arrhenius reaction rate theory is customized in IEEE C57.91 [45] to calculate transformer ageing. In this model, thermal stress from HST location is assumed to drive the ageing of cellulose-based insulation paper, thereby defining the transformer lifetime. Transformer's cumulative Loss-of-Life (LL) λ in period $t_0 - t$ is determined using (4.2), where the ageing acceleration factor $\Delta\lambda$ (also called relative ageing rate) is calculated using (4.1) where ϑ^{hst} represents temporal development of hot-spot temperature, while rated HST $\vartheta^{\text{hst}}_{rated}$ depends on the type of insulation paper. Non thermally upgraded Kraft paper $\vartheta^{\text{hst}}_{rated} = 98°\text{C}$ and thermally upgraded Kraft paper (TUP) $\vartheta^{\text{hst}}_{rated} = 110°\text{C}$ are commonly used in the industry. For TUP, the variation of ageing acceleration factor $\Delta\lambda$ with respect to HST is provided in Fig, 4.1.

$$\Delta\lambda_t = e^{\left(\frac{15000}{\vartheta^{\text{hst}}_{rated}+273} - \frac{15000}{\vartheta^{\text{hst}}_{t}+273}\right)} \tag{4.1}$$

$$\lambda_t = \int_{t_0}^{t} \Delta\lambda_\tau \, d\tau \tag{4.2}$$

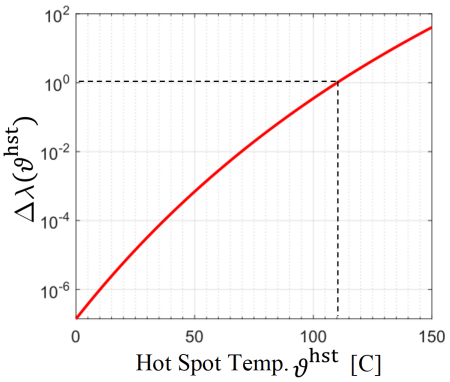

Figure 4.1: Variation of ageing acceleration factor $\Delta\lambda$ with respect to HST ϑ^{hst} for thermally upgraded Kraft insulation paper

4.2.2 Consideration of Chemical Decomposition using Degree of Polymerization based Models

The basic Arrhenius reaction based method from IEEE C57.91 does not model the impacts of oxygen development in transformer oil and residual moisture content in the insulation paper. As discussed earlier, the catalytic behavior of moisture in combination with the active reagent oxygen can accelerate the chemical decomposition of the cellulose-based insulation paper due to heat from HST. Since the Degree of Polymerization (DP) can represent the retained tensile strength of these papers, DP-based models are used in this project for applications where accurate considerations for transformer ageing are required and when the computational stress is not a challenge. The variation in insulation's DP can be calculated by reformulating the Arrhenius reaction rate theory using a first-order process, as shown in (4.3). It must be mentioned that experts suggest that this equation gives conservative estimates on transformer ageing [131].

$$\frac{1}{\mathrm{DP}_t} - \frac{1}{\mathrm{DP}_{t_0}} = A\, e^{\frac{-E_a}{R_g[\vartheta_t^{\mathrm{hst}} + 273]}} \quad t \tag{4.3}$$

where the DP values at start and end of the interval $t_0 - t$ are given by DP_{t_0} and DP_t, while R_g represents the ideal gas constant valued as 8.314 J/(mol K). The two important parameters that are found to be dependent on the chemical decomposition of insulation paper and transformer oil include pre-exponential factor A [1/hour] and activation energy E_a [kJ/mol], which represents the minimum energy needed to start the decomposition reaction. As discussed in the literature review, the variation of content of oxygen in oil (defined as volumetric parts per million - ppm) and content of moisture in the paper (defined as percentage mass) has considerable influence on the evolution of these parameters for TUP and non-TUP insulation over the transformer lifetime. Results from the most relevant state-of-the-art experiments [44, 130, 139–141] are summarized in Table 4.1. For the Monash model from 2012 [140] [141], the development of A with paper moisture variation under different oxygen concentration in oil is fitted to polynomial curves which have been reproduced in Fig. 4.2. One important point to note is that the IEC 60076-7 Annex A model [44] adopts the proposal by Lundgaard in [128].

Table 4.1: Comparison of parameters dependent on insulation material and decomposition process from state-of-the-art DP-based ageing models [44, 130, 139–141] refined using experimental data for thermally upgraded and non-upgraded Kraft Paper. Activation energy (E_a) is in kJ/mol. Pre-exponential acceleration factor (A) is in 1/hour

Paper Type	Model	Activation Energy E_a [kJ/mol]		Preexponential Factor A [1/hour]			
		Low O2	High O2	Low H20, Low O2	1.5% H20, Low O2	3.5% H20, Low O2	Low H20, High O2
Non Thermally Upgraded Kraft Paper	Emsley (2000) [139]	111		1.07×10^8	3.5×10^8	35×10^8	2.0×10^8
	Lundgaard (2004) [130]	111		2.0×10^8	6.2×10^8	21×10^8	8.3×10^8
	Monash (2012) [140, 141]	111		1.42×10^8	6.8×10^8	see Fig. 4.2	9.33×10^8
	IEC 60076-7 Annex A (2018) [44]	128	89	4.1×10^{10}	1.5×10^{11}	4.5×10^{11}	4.6×10^5
Thermally Upgraded Kraft Paper	Emsley (2000) [139]	111		3.65×10^7	-	-	-
	Lundgaard (2004) [130]	111		6.7×10^7	1.1×10^8	2.6×10^8	3.5×10^8
	Monash (2012) [140], [141]	111		6.92×10^7	2.61×10^8	see Fig. 4.2	4.29×10^8
	IEC 60076-7 Annex A (2018) [44]	86	82	1.6×10^4	3.0×10^4	6.1×10^4	3.2×10^4

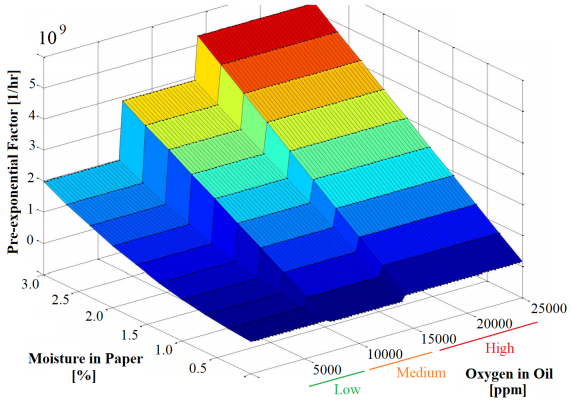

Figure 4.2: Variation in the pre-exponential factor A with change in oxygen and water content. These values are calculated using the fitted polynomial curves of [148]

The first three models that calculate values for A using the same activation energy E_a irrespective of oxygen content in oil are found to be in agreement with each other. This is shown for low oxygen level circumstances in Fig. 4.3 for Emsley [139], Lundgaard [130] and Monash [140] models. The polynomial curve fitted to these observations in order to make the calculations more generic is also provided. Hence, this analysis reveals that these models can be used interchangeably with acceptable degree of agreement, which is why the discussion from this point onward will use the Monash model as the representative of this group of models.

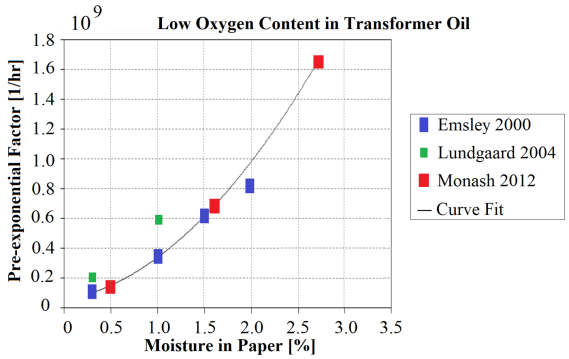

Figure 4.3: Under low oxygen levels, the variation in A with paper moisture content is compared for Emsley [139], Lundgaard [130] and Monash [140] models which are based on activation energy of 111 kJ/mol. The polynomial curve providing the best fit for the observed data is also shown.

4.3 Comparison and Sensitivity Analysis of the Considered Models

The discussion so far reveals that the models considered for analysing load-dependent thermal ageing of oil-filled power transformers in this project can be classified as: Basic Arrhenius reaction based IEEE C57.91 model [45], DP-based Monash model [130, 139, 140] and DP-based IEC 60076-7 Annex A model [44]. In order to compare the acceleration of transformer ageing for these models under different thermal operating conditions, transformer's Expected Lifetime (EL) is calculated using (4.4)-(4.5).

$$\mathrm{EL_{IEEE}} = \frac{150000}{8760 \times \Delta\lambda(\vartheta^{\mathrm{hst}})} \quad \text{[years]} \tag{4.4}$$

$$\mathrm{EL_{DP}} = -\frac{\frac{1}{\mathrm{DP_{start}}} - \frac{1}{\mathrm{DP_{end}}}}{A \times 24 \times 365}\, e^{\frac{E_a}{R_g\,(\vartheta^{\mathrm{hst}} + 273)}} \quad \text{[years]} \tag{4.5}$$

where EL is calculated in years, the hot spot temperature [°C], ideal gas constant R_g and the HST-dependent ageing acceleration factor $\Delta\lambda(\vartheta^{\text{hst}})$ are treated as constants, while E_a and A are considered to be dependent on oxygen and moisture contents. For the IEEE model, 20% retained tensile strength for the cellulose-based insulation paper is considered to be the transformer end-of-life which translates to the numerator of 150000 hours in (4.4). For the DP-based models, DP value at the time of transformer's first energization (DP_{start}) can simply be set to 1000, but the difference in opinion of technical experts [44] [128] [131] for end-of-life criterion with 20% and 30% retained tensile strength for Kraft paper suggests that DP_{end} can either be set to 200 or 300. Therefore, the sensitivity of the three models are assessed by varying some of these parameters in the discussion below.

- **Sensitivity to the end-of-life criterion:** The influence of using DP_{end} of 200 and 300 on the expected transformer lifetime predicted by the two DP-based models is shown in Fig. 4.4 for a range of continuous HST operation under low oxygen and moisture conditions. The analysis for both the thermally upgraded $\vartheta^{\text{hst}}_{rated} = 110°\text{C}$ (right) and non-upgraded $\vartheta^{\text{hst}}_{rated} = 98°\text{C}$ (left) Kraft-based insulation papers is presented in the figure. As expected, both the DP-based models show similar behavior with logarithmic change in EL for the two end-of-life criteria. Higher activation energy E_a and lower pre-exponential factor A for the IEC 60076-7 Annex A model results in more conservative results, which is why this model with 20% retained tensile strength criteria will be used for the further analysis in Chapter 8.

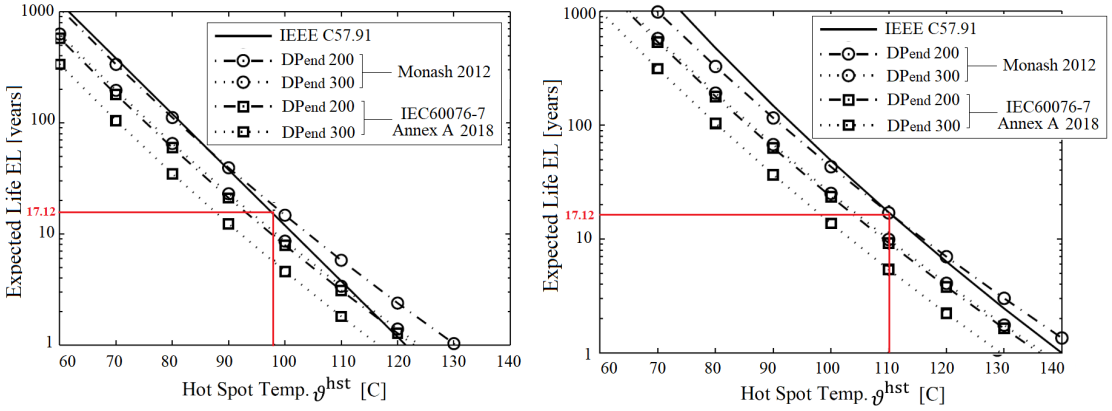

Figure 4.4: Influence of different end-of-life criterion with retained tensile strength of 30 % (DP_{end} = 300) and 20 % (DP_{end} = 200) for the DP-based models by Monash [140] and IEC 60076-7 Annex A [44]. Left: Non-thermally upgraded Kraft paper. Right: Thermally upgraded Kraft paper. Test case with low oxygen ($\leq$ 7000 ppm) and moisture (0.5-1%) is presented. The basic Arrhenius model from IEEE C57.91 is also presented for comparison

- **Sensitivity to the oxygen and moisture contents:** Since the two main parameters of DP-based models E_a and A depend primarily upon the moisture content in paper and oxygen saturation in oil, the influence of varying these parameters on EL calculation by IEC 60076-7 Annex A model is presented in Fig. 4.5. It is observed that the increase in oxygen and moisture contents can decrease the expected lifetime considerably even if the transformer stays within the normal cyclic HST thresholds. However, under normal conditions of low moisture (0.5-1%) and low oxygen ($\leq$ 7000 ppm) the calculated EL is as expected and is found to be in agreement with the IEEE C57.91 model which suggests that both these models can be used if normal operating conditions are expected. Readers are reminded that uncharacteristically high oxygen ($\geq$ 7000 ppm) and moisture ($\geq$ 2%) represent serious quality issues in transformer manufacturing and maintenance, which is beyond the scope of work done in this project.

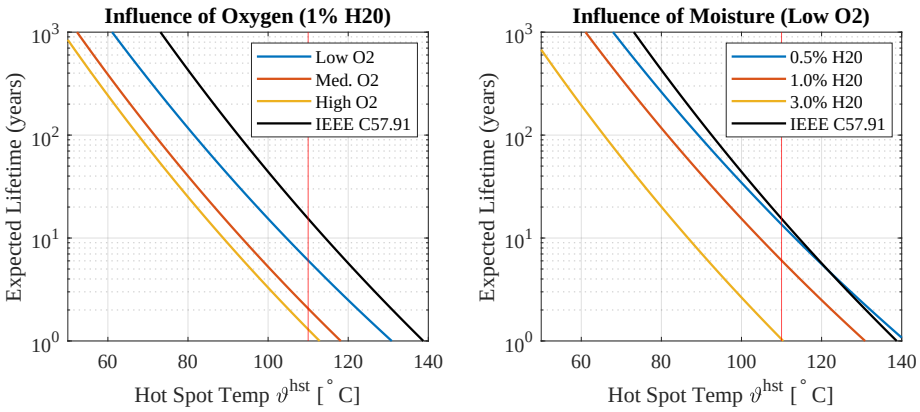

Figure 4.5: Sensitivity of transformer expected lifetime to Moisture and Oxygen variation for the IEC 60076-7 Annex A (Lundgaard) model. Left: constant moisture (1%) and varying oxygen. Right: constant oxygen (low) and varying moisture. The basic Arrhenius model from IEEE C57.91 is also presented for comparison

The discussion so far has shown that the IEEE C57.91 model continuously returns less conservative results at low temperatures but the required conservatism is achieved at higher HST, which means that the basic Arrhenius based model can be used when the transformers are expected to operate continuously at higher temperatures. This gives the simplified model a distinctive edge over the considered DP-based models, especially for applications where simplicity of design and high computational efficiency are desired. Therefore, the optimization problems developed in this project use the basic Arrhenius model based on IEEE C57.91 for tracking transformer lifetime utilization.

CHAPTER 5

Potential for Dynamic Rating Operation for OWF Transformers

Over the course of this project, it has been deduced that transformers in offshore windfarms are over-dimensioned. In this section, the extent of this over-sizing is investigated by studying the load and lifetime utilization of ten different power transformers installed on OSS platforms, in the WTG nacelles and in the base of WTG towers. The OWF projects included in this study are mostly located in the North Sea in Europe and on the west coast of UK. For detailed design assessment, the test case of Anholt windfarm (Denmark) also presented in publication **[Pub. C3]** has been used, the details for which were provided in Section 2.1. Similar results are elaborated in detail for WTG transformers in publication **[Pub. C2]**.

5.1 Assessment of Transformer Loading in OWFs

As introduced in Chapter 1, the intermittent nature of wind generation means that electrical components in OWF export system are seldom loaded to their nameplate capacity. This, when combined with the over-sizing of these components, implies that a significant portion of the OWF transmission capacity is unutilized. Anholt windfarm is an exception to this design methodology as three 140 MVA, 225/33 kV, YNd11, ONAN cooled OSS transformers with thermally upgraded kraft paper insulation are used to transmit the generation from the 400 MW rated windfarm shown in Fig. 2.2, which makes the total transformer capacity of 420 MVA. It is important to note that if conventional design practices for transformer rating were used, the total transformer capacity would have been 500 MVA with each transformer rated at 167 MVA.

Referring to Fig. 5.1, it can be deduced that even with the strict design practices, the OSS transformer in Anholt is underutilized. The histograms for transformer load and critical temperatures for 2017, which look like the probability density function of Beta distribution with uniform parameters, suggest that over the course of an entire year the transformer does not reach its rated capacity of load current (1 pu) and temperatures (normal cyclic limits in Table 3.4). The temperatures are calculated using the Susa model from (2.9) and the calculations have already been validated in Section 2.3.1. The utilization of transformer lifetime (λ) is calculated using the basic Arrhenius reaction rate model from IEEE C57.91 [45] because of the expected low-moisture, low-oxygen conditions due to strict regulations for design quality, operation and condition monitoring. The discussion in IEEE C57.91 suggests that under constant operation at rated ϑ^{hst} (110 °C for TUP), the expected design lifetime EL_{rated} of transformers should be 17.12 years (150000 hours). Under ideal conditions, OWF transformers should last 25 years of windfarm lifetime which translates to rated yearly loss of life $\lambda_{y,rated}$ of 0.685 years (17.12/25). The analysis in Fig. 5.1(d) reveals that the Anholt OSS transformer lost close to 23 days (0.063 years) of its life λ_y in 2017, which is significantly lower than $\lambda_{y,rated}$ of 0.685 years. Hence, there is substantial room to employ dynamic rating and optimize the utilization of Anholt offshore windfarm's OSS transformers.

In order to validate the relevance of this analysis across offshore windfarms located in different regions with contrasting wind production and ambient condition patterns, the process is repeated for 9 more transformers for yearly observations and the results are compiled in Fig. 5.2. Besides Anholt, OSS transformers from the following offshore windfarms are used: 367 MW Walney (WOW) and 348 MW Burbo Bank (BBW) off the west coast of UK, 573 MW Race Bank (ROW) off the east coast of UK and 582 MW Gode Wind in the German

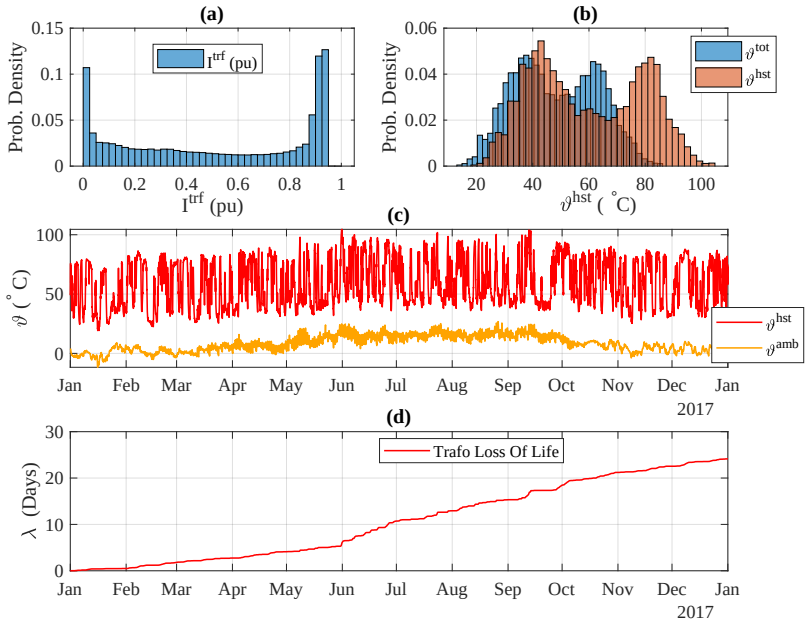

Figure 5.1: Utilization of OSS transformer in Anholt offshore windfarm in 2017. (a) Histogram for transformer load current in pu. (b) Histograms for transformer top-oil and hot-spot temperatures. (c) Temporal development of ambient and hot-spot temperature. (d) transformer loss-of-life calculated using thermal ageing formula from IEEE C57.91

sector of the North Sea. Furthermore, wind turbine transformers from OWFs in the Netherlands, UK and Germany for WTGs rated between 3.6 - 8 MW are also used. The box-plots for HST suggest that none of the examined transformers reached the rated design HST of 110 °C for the observed yearly duration, and are found to be far from crossing the normal cyclic load limit of 120 °C from [125]. The per-unit yearly loss of transformer life with respect to the rated yearly lifetime utilization $\lambda_y/\lambda_{y,rated}$ has also been presented in the figure and found to be considerably below the rated 1 pu mark for all the test case transformers.

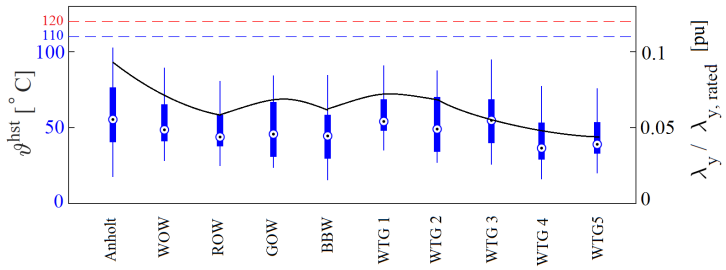

Figure 5.2: Assessment of loading for the 10 test case transformers using box-plots for year-round distribution of calculated hotspot temperatures (blue) and per-unit yearly loss of transformer life $\lambda_y/\lambda_{y,rated}$ (black). The dashed lines represent thermal design and cyclic load limits for ϑ^{hst}

5.2 Influence of OWF Expansion on Optimal Transformer Utilization

Based on the discussion so far, power transformers are significantly underutilized in offshore windfarms. Therefore, an attempt has been made to inspect how much extra energy can these test case transformers push, if optimal yearly lifetime utilization is desired. This exercise is relevant as the findings can allow operators to maximize energy transmission by using dynamic rating during contingency and other demanding conditions, given that the remaining export system components can withstand the additional load during n-1 contingencies. For this purpose, the recorded instantaneous wind energy generation for all the test case windfarms has been scaled by an up-scaling factor 'U' for the entire year.

The influence of up-scaling Anholt windfarm OSS transformer's load on its temporal HST development for a short period in summer has been provided in Fig. 5.3. In order to find the optimal up-scaling factor, two considerations are made: Firstly, the cumulative yearly loss-of-life λ_y is calculated and secondly a probability function ψ_{hst} to prevent violation of long-term emergency loading limits of Table 3.4 is used. The parameter ψ_{hst} returns the value of 1 if the calculated temperatures ϑ^{tot} and ϑ^{hst} do not violate the respective thermal limits for more than 2 hours, while it is zero if the limits are violated for more than 25 percent of the overall simulated time period. This prevents the adverse ageing impacts due to extensive bubbling and acidic formations at $\vartheta^{\text{hst}} \geq 140°\text{C}$. The detailed results for the Anholt test case are provided in Fig. 5.4. It can be seen that the optimal up-scaling factor lies near the 1.52 mark, and even though the lifetime utilization λ_y is not exactly equal to $\lambda_{y,rated}$ at this point, further load up-scaling results in reduction of the probability factor ψ_{hst}. The expected λ_{rated} parameter is calculated as $0.685t$ in the lifetime utilization plots of Fig. 5.3(c).

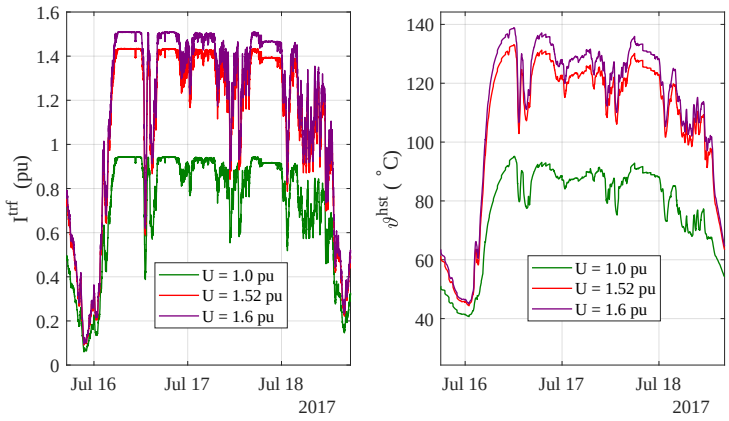

Figure 5.3: Up-scaling power generation in Anholt windfarm. Left: Up-scaled transformer load for three days in summer 2017. Right: Calculated hot-spot temperature for different up-scaling factors for the same period.

These calculations are repeated for the remaining test case transformers and the parameters for the optimal up-scaling results for the individual transformers are provided in Fig. 5.5. The HST box-plots for the respective optimal results show a uniform spread up to the emergency thermal limits as dynamic rating

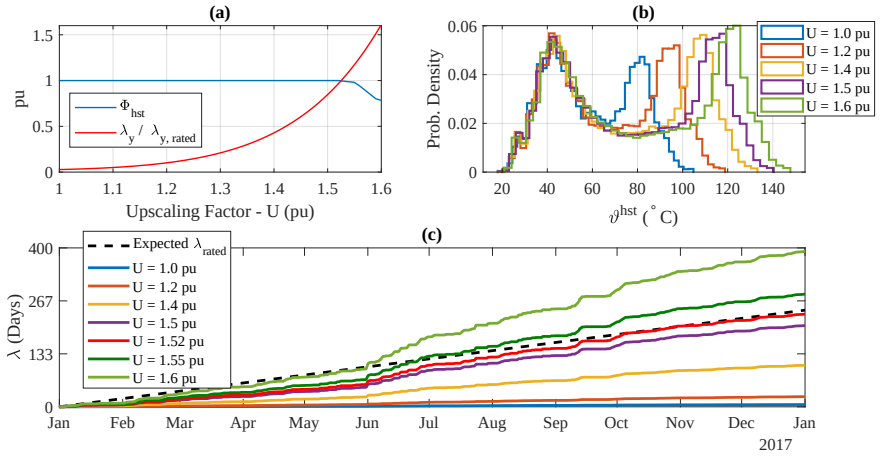

Figure 5.4: Influence of up-scaling wind generation on utilization of Anholt OSS transformer in 2017 (a) per-unit yearly loss of transformer life and probability function to prevent violation of emergency thermal limits of [44]. (b) Histograms for year-round HST distribution for different up-scaling factors. (c) Thermal lifetime utilization for increased wind generation. 'U' represents the up-scaling factor of wind generation in pu with actual generation in 2017 as base.

is used in day-to-day operations. The per-unit yearly loss of transformer life $\lambda_y/\lambda_{y,rated}$ is around 0.9 for all the test case transformers and the respective wind farm load can optimally be up-scaled by up to 50 %. The analysis has confirmed that OWF transformers are under-utilized and a novel methodology based on combination of dynamic rating and optimal lifetime utilization can potentially be developed to optimize the operation of these components.

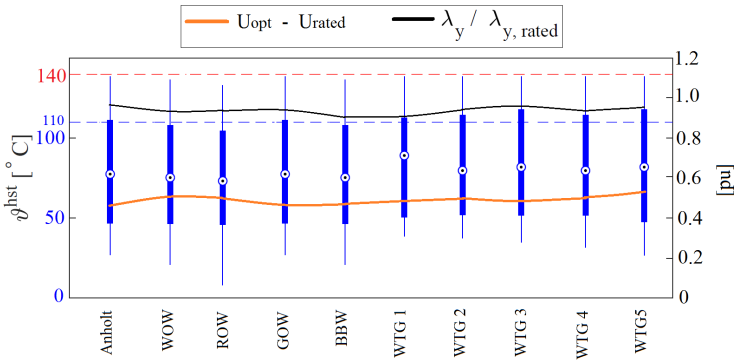

Figure 5.5: Assessment of loading for the 10 test case transformers after up-scaling the respective windfarm load to the optimal value. Box-plots for year-round distribution of calculated hotspot temperatures (blue), per-unit yearly loss of transformer life (black), value of optimal up-scaling for the respective test case transformer (orange). The dashed lines represent thermal design and long-term emergency load limits for ϑ^{hst}

CHAPTER 6

Optimal Transformer Utilization based on DTR & Dynamic Ageing Principle

As discussed earlier, DTR allows better utilization of transformers as compared to STR. It has also been shown that if the operational thermal limits under DTR operation are changed from normal limits to long-term emergency cyclic limits of Table 3.4, the transformers can be even better utilized [149–151]. However, such an operational methodology can not ensure reliable transformer operation as historic transformer utilization and real-time accelerated ageing under higher thermal stress are not tracked. Furthermore, it has also been shown that OSS and WTG transformers in the offshore windfarms are over-dimensioned and significantly underutilized. This means that at the time of windfarm decommissioning, usually after 25-35 years of operation, there will be significant residual life for transformers. Therefore, an improved transformer utilization technique, termed as Enhanced Dynamic Thermal Rating (DTR^{+}), has been proposed in this project which can potentially resolve these issues.

It must be mentioned that residual transformer lifetime after 35 years of operation is not necessarily a problem in the conventional transmission systems as the Transmission System Operators (TSOs) continue to use these transformers with increased condition monitoring. However, for OWF applications with limited asset life (25-30 years design lifetime), a transformer design optimization procedure that can reduce the abundant residual life at the time of OWF decommissioning can influence the business case and the Levelized Cost of Energy (LCOE) for offshore wind significantly. This is further clarified in Chapter 8. On the other hand, smart transformer utilization based on the proposed methodology can allow the system planners and TSOs to defer investments in case of large-scale rapid integration of renewable energy sources as a trade-off against truncated transformer lifetime. This application has been demonstrated successfully in the discussion below.

6.1 Overview and Background of the Proposed Methodology

The methodology proposed in this section redefines the hourly thermal limits for transformer operation in real-time by evaluating its consumed thermal lifetime λ until that instant. These thermal limits ensure that the transformer is optimally utilized, while complying with the ageing rate defined in IEEE C57.91 [45]. The methodology is graphically demonstrated in Fig. 6.1 for an oil-filled power transformer with thermally upgraded Kraft insulation paper, which can withstand 110 °C of continuous HST operation.

The transformer in Fig. 6.1 is assumed to operate continuously at ϑ^{hst} = 98 °C until time t_0, which is a fairly conservative assumption compared to the operating HST of OWF transformers discussed earlier. This translates to a constant relative ageing rate (or ageing acceleration factor) of $\Delta\lambda = 0.282$, represented by the black line's slope. The utilized transformer lifetime at this stage would be $\lambda_A = 0.282t_0$, which is far lower than the design utilization λ_D, as shown in the figure. The transformer would continue to be underutilized and the difference $\lambda_D - \lambda_A$ would increase further if this loading strategy persists. On the other hand, if the conventional DTR strategy is used for rest of the transformer design life which operates the transformer close to the design HST limit of 110 °C more often, the utilization would improve but there would still be significant

residual lifetime at the time of decommissioning, as shown in Fig. 6.1(a). The proposed methodology resolves this issue by considering both the temperature and ageing dynamics at the same time for the DTR$^+$ strategy. Referring to Fig. 6.1(b), it is perceivable that instead of using ϑ^{hst} limit of 110 °C for the period $t_0 - t_1$, optimal transformer utilization would have been achieved if $\vartheta^{\text{hst}} = 122°\text{C}$ which results in $\Delta\lambda = 3.29$ and allows the blue line to touch the red dashed line representing the rated transformer lifetime utilization within the given operation period. As a result of this dynamic thermal setting, the operator can load the transformer higher under contingency, grid congestion and other demanding situations.

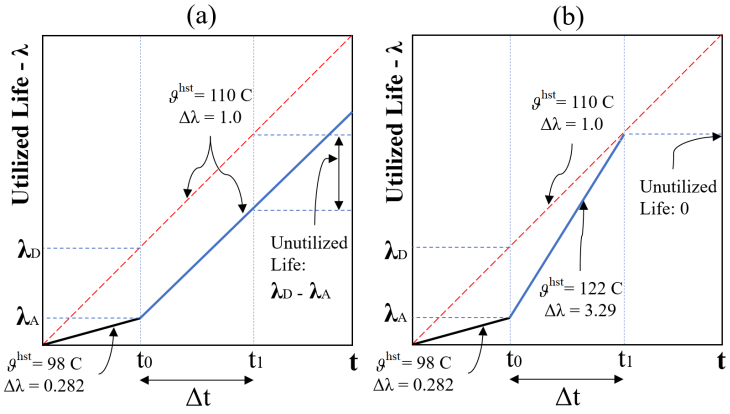

Figure 6.1: Methodology for optimal transformer utilization. (a) Conventional approach for DTR: Fixed HST limit ($\overline{\vartheta^{\text{hst}}}$ = 110 C). (b) Proposed enhanced DTR$^+$ approach: Variable HST limit dependent on utilized lifetime λ ($\overline{\vartheta^{\text{hst}}}$ = 140 C).

6.1.1 Problem Overview and Schematic Description

A dynamic DC Optimal Power Flow (DCOPF) problem with multi-period formulation is developed to test the concept presented above. The problem optimizes the cost of energy dispatch over a 24-hour period in a power system for the day-ahead market. The mechanism of the day-ahead market clearance are demonstrated in Fig. 6.2, along with the schematic for the proposed problem framework. The 24-hour schedule for day 'd' in this market is usually cleared around mid-day the day before ('d-1') [152]. The optimization problem uses static, dynamic and enhanced dynamic rating mechanisms for the preselected bottleneck transformers to minimize the cost of energy dispatch by maximizing the utilization of energy from low-cost wind resources and unlocking the flexibility potential of the transmission network.

The power system considered in this problem is divided into following sets: conventional generators ($\mathcal{G}$), wind farms ($\mathcal{W}$), buses ($\mathcal{B}$) and branches ($\mathcal{A}$) with number of elements $|\mathcal{G}|$, $|\mathcal{W}|$, $|\mathcal{B}|$ and $|\mathcal{A}|$, respectively. The last set for branches include the overhead transmission lines, cables and transformers in the network. All the overhead lines and cables are statically rated, whereas only a subset of transformers is to be considered for DTR. These transformers are to be preselected based on debottlenecking of the considered system if further windfarms are installed in one specific region of the system. Hence, the transformer subsets are identified as $\mathcal{A}^{\text{STR}}$, $\mathcal{A}^{\text{DTR}}$ and $\mathcal{A}^{\text{DTR}^+}$ for STR, DTR and DTR$^+$ test cases. The results are benchmarked by comparing the change in performance of the algorithm for DTR and DTR$^+$ with respect to the STR test case.

The optimal scheduling problem primarily includes unit commitment from conventional generation $P^{\text{conv}}_{g,t}$ for source $\forall g \in \mathcal{G}$ and intermittent renewable energy $P_{w,t}$ from wind resource $\forall w \in \mathcal{W}$. Moreover, possible load shedding $P^{\text{sh}}_{\beta,t}$ at bus $\forall \beta \in \mathcal{B}$ that might be needed under extreme conditions is also considered. The forecast for load demand $\widehat{P^{\text{load}}_{\beta,t}}$ for each bus and average wind generation $\widehat{P^{\text{av}}_{w,t}}$ for day 'd' are to be made available before the time of market clearance the day before ('d-1'). System parameters and ratings of transmission components are needed as well. It is known that besides the integration of large-scale distributed renewable energy sources, the load forecasting models can lead to uncertainty in unit commitment [153]. However, this formulation does not account for uncertainties in load and wind forecasts, but these can easily be added by

using the principles discussed in [154] [155]. It must be mentioned that the discussion in Chapter 9 presents decision-support tools which accurately account for uncertainty during the design phase.

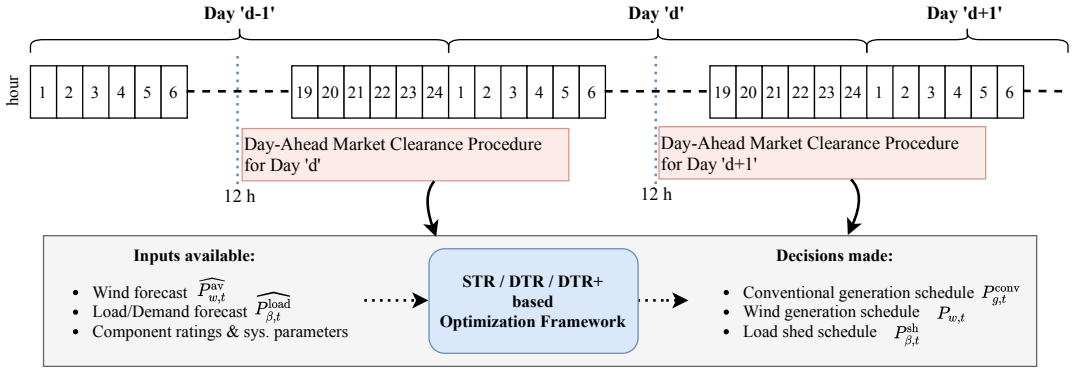

Figure 6.2: Overview of the day-ahead market and schematic representation of the developed methodology.

6.1.2 Common Formulations and Prerequisite Information

The formulation of the proposed problem has a number of substructures and designs that have either been originally developed or adapted from different studies during this project. Among these substructures, the most important ones include the utilization of piecewise linearized ageing model for transformers, the inclusion of power losses in a DCOPF problem based on an iterative process and simplification of non-linear TEE models to quadratic inequality constraints for keeping the optimization problem convex. The mechanism behind each of these contributions are briefly described in this section before the actual framework for the optimization problem is provided.

- **Power Flow and Load Calculations:** In this study, DC approximation of the full AC power flow equations is adopted. A Power Transfer Distribution Factor matrix (PTDF) $\boldsymbol{M}$ is used to model the flow of active power on each branch in $\mathcal{A}$ [156]. This approach neutralizes the need for introduction of bus voltage angles in the decision variables set. The relation between power injected at each bus and power flow in the respective branches can be linearly related by using the constant coefficients of matrix $\boldsymbol{M} = \boldsymbol{B}_\alpha \boldsymbol{B}_\beta^{-1}$, such that $\boldsymbol{M} \in \mathbb{R}^{|\mathcal{A}|\times|\mathcal{B}|}$, while $\boldsymbol{B}_\alpha$ and $\boldsymbol{B}_\beta$ are the branch admittance and bus admittance matrices respectively. Finally, the per-unit temporal power flow $F_{\alpha,t}$ on each line α is calculated using (6.1), where $\boldsymbol{M}_\alpha$ is the $\alpha - th$ row of matrix $\boldsymbol{M}$ and $\boldsymbol{P}^{\text{inj}}_t$ is the column vector representing temporal power injection at each bus in pu. The per-unit transformer load $I^{\text{trf},pu}_{\alpha,t}$ on branch α depends on the respective transformer size S^{trf}_α, as shown in (6.2). This is true because if smaller transformers are used or if the transformers are derated (as done in this formulation to create bottlenecks in the system), the power flow $F_{\alpha,t}$ in the respective branch needs to be scaled with respect to the base system rating S^{base}.

$$F_{\alpha,t} = \boldsymbol{M}_\alpha \boldsymbol{P}^{\text{inj}}_t \tag{6.1}$$

$$I^{\text{trf},pu}_{\alpha,t} = F_{\alpha,t} \frac{S^{\text{base}}}{S^{\text{trf}}_\alpha} \tag{6.2}$$

The nodal power injection at bus β can then be written in its extensive form

$$P^{\text{inj}}_{\beta,t} = P^{\text{conv}}_{g,t} + P_{w,t} - \left(P^{\text{load}}_{\beta,t} - P^{\text{sh}}_{\beta,t} + W^{\text{bus}}_{\beta,t}\right) \tag{6.3}$$

where $P^{\text{conv}}_{g,t}$ and $P_{w,t}$ represent conventional and wind power generation; $P^{\text{load}}_{\beta,t}$ and $P^{\text{sh}}_{\beta,t}$ represent net load demand and possible load shedding; while $W^{\text{bus}}_{\beta,t}$ expresses nodal power losses. The last term is

used to identify the branch power losses $\boldsymbol{W}$ that are dissipated on transmission lines and transformers, which are expressed in terms of additional load demand $\boldsymbol{W_t^{\text{bus}}}$ at each bus. This is explained further below.

- **Losses Estimation**: In DCOPF problems, estimation of losses is rather abstruse which is why it is explored extensively in the literature. The method developed in this project uses quadratic inequality constraints to estimate branch power losses $\boldsymbol{W}$ and models them as additional load demand on the individual busses $\boldsymbol{W_t^{\text{bus}}}$ in the system. The overarching concept is based on the considerations of [157], where the losses in branch α are divided between the sending and receiving buses equally. A loss allocation matrix $\boldsymbol{Y} \in \mathbb{R}^{|\mathcal{B}|\times|\mathcal{A}|}$ is used for this purpose whose (β,α) component is defined in (6.4). Consequently, $\boldsymbol{W_t^{\text{bus}}}$ is then calculated as $W_{\beta,t}^{\text{bus}} = \boldsymbol{Y}_\beta \boldsymbol{W}$, where $\boldsymbol{Y}_\beta$ is the $\beta - th$ row of $\boldsymbol{Y}$.

$$Y(\beta,\alpha) = \begin{cases} 0.5 & \text{if line } \alpha \text{ is connected to bus } \beta \\ 0 & \text{otherwise} \end{cases} \tag{6.4}$$

As a result of congestion in the test transmission network which can produce negative locational marginal prices, the method presented in [157] has the tendency to introduce additional fictitious losses leading to inaccurate conservative loss estimation [158] [159]. Therefore, in order to resolve this issue while preserving the convexity of the proposed optimization problem under the consideration of quadratic power losses, the iterative process of [157] is bounded at each step. This upper bound is lowered at each iteration if the losses are overestimated. The step-by-step process is explained below:

1. The maximum power flow in the respective branch and its resistance r are used to set the upper bound for power losses $W^{\max}$ which is complemented by a tolerance δ to ensure convergence.

$$W_{(1)}^{\max} = r\, F^{\max^2} \tag{6.5}$$

2. The DCOPF problem of (6.12) is solved and the resulting power flows $F_{(k)}$ and losses $W_{(k)}$ are obtained for the *k*-th iteration.

3. The difference between the estimated and the actual losses are calculated and compared to the tolerance δ. If the difference is within the tolerance, the solution is accepted, otherwise the Step 4 is considered.

$$\Delta W_{(k)} = W_{(k)} - r F_{(k)}^2 \tag{6.6}$$

4. If the solution is not produced in Step 3, $W^{\max}$ is updated with the power flow at iteration k and an additional margin ε is added. Afterwards, Steps 2 and 3 are repeated.

$$W_{(k+1)}^{\max} = r F_{(k)}^2 + \varepsilon \tag{6.7}$$

Hence, the iterative process can guarantee a unique solution, which is achieved by a gradual reduction of size of the feasible region for branch losses. A graphical representation of the iterative algorithm is given in Fig. 6.3 where different shades of gray indicate the gradual restriction of the feasible domain. The method needs to be tested comprehensively over different test cases to assess the generality of its application.

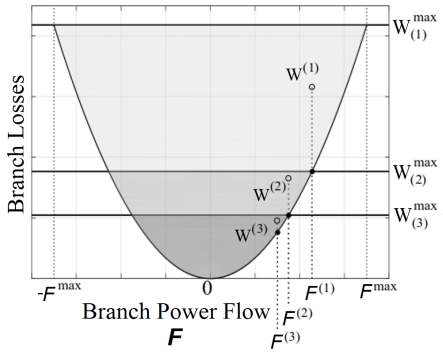

Figure 6.3: Graphical representation of the iterative approach to approximate quadratic power losses by iteratively reducing the feasible region

- **Dynamic Thermal Estimation of Transformers:** As discussed in Chapter 2, DTR modeling of transformers in hourly operational time frames is difficult not just due to the temporal coupling of ϑ^{tot} and ϑ^{hst}, but also because the dynamic behavior of transformer top-oil spans across multiple hours. This means that for accurate DTR modeling, influence of historic transformer load and ambient conditions are to be accounted for and steady state estimation of ϑ^{tot} and ϑ^{hst} is not possible unless empirical assumptions are made. Fortunately, the work-arounds discussed in Section 2.3.1 for hourly operational time-frame are valid for this application, particularly because the candidate transformers for DTR and DTR $^{+}$ considerations are identified to be the system constraints and therefore operated at ODAF cooling mode continuously. The resulting simplified equations for TOT and HST estimation from Section 2.3.1 are repeated in (6.8)-(6.9).

$$\vartheta_t^{\text{tot}} = b_1 \vartheta_t^{\text{amb}} + b_2 \left(I_t^{\text{trf},\,pu}\right)^2 + b_3 \vartheta_{t-1}^{\text{tot}} + b_4 \tag{6.8}$$

$$\vartheta_t^{\text{hst}} = \vartheta_t^{\text{tot}} + \Delta\vartheta_{rated}^{\text{hst}} \left(I_t^{\text{trf},\,pu}\right)^2 \tag{6.9}$$

- **Resolution of Non-linear Constraints for Ageing Dynamics:** In order to keep the optimization problem convex, the non-linearities that arise due to the exponential relation in the HST-dependent transformer ageing model by IEEE C57.91 as shown in (4.1)-(4.2) need to be resolved. Hence a set of linear inequality constraints are used for the estimation of ageing acceleration factor $\Delta\lambda$ to form a convex piece-wise linear approximation in the base DCOPF problem of (6.12). This formulation is shown in (6.10), where the coefficients m_l and q_l represent the slope and intercept values for the l-th tangent line belonging to the set $\mathcal{L}$. Hence, by using this technique the real-time transformer HST ϑ_t^{hst} can be linearly related to the corresponding incremental lifetime utilization $\Delta\lambda_t$, as shown in Fig. 6.4. For cumulative lifetime utilization λ_t can then be calculated using (6.11).

$$\Delta\lambda_t = \max_l \{m_l \vartheta_t^{\text{hst}} + q_l\} \tag{6.10}$$

$$\lambda_t = \lambda_{t-1} + \Delta\lambda_t \tag{6.11}$$

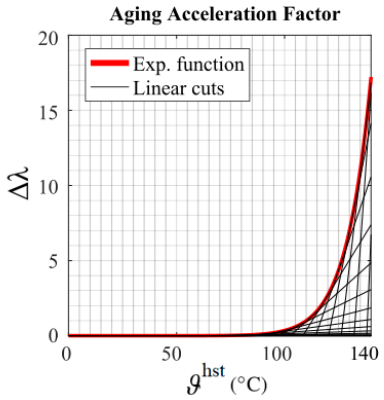

Figure 6.4: Piecewise linear approximation of non-linear exponential function for transformer lifetime utilization dependent on hot-spot temperature with $\mathcal{L} = 30$ cuts

6.2 Formulation of the Multi-Period DCOPF Problem

6.2.1 Proposed Framework

The proposed optimization problem is a multi-period DCOPF problem for the day-ahead market whose objective is to minimize the total cost of generation over the period $\mathcal{T}$. The framework for the developed multi-period DCOPF problem is provided in (6.12). The total cost of conventional generation C^{conv}, wind generation C_t^{W} and possible load shedding C_t^{sh} along with all the constraints that follow have to hold $\forall t \in \mathcal{T}$. The first three sets of constraints are relevant for all the test cases, while the last three constraints will only be applicable to the individual test cases for STR, DTR and DTR$^+$ which are to be run independently for benchmarking the results. In short, the problem is solved three times: first by considering STR operation of the chosen transformer subset in $\mathcal{A}^{\text{STR}}$, then for DTR of the subset $\mathcal{A}^{\text{DTR}}$ and finally for enhanced DTR operation of $\mathcal{A}^{\text{DTR}^+}$. All the remaining parameters and conditions are kept the same for these test cases.

In the proposed methodology, the linear objective function is complemented by a set of standard equality and inequality constraints. By using the multi-period structure, the incorporation of transformer's temporal temperature development which includes conic quadratic inequality constraints is accurately accounted for. The Matlab-based CVX [160] is used in this project to model the optimization problem using Mosek.

$$\min_{\Xi} \quad \sum_{t\in\mathcal{T}} \left(C_t^{\text{conv}} + C_t^{\text{W}} + C_t^{\text{sh}}\right) \tag{6.12a}$$

s.t.	(6.14),	Power Balance,	$\forall g, \forall w, \forall \beta, \forall t$
	(6.15) – (6.19),	Generational & Operational Limits,	$\forall g, \forall \alpha$
	(6.20),	Losses approximation,	$\forall \alpha, \forall t$
	(6.21),	Load Limits (for STR only),	$\forall \alpha \in \mathcal{A}^{\text{STR}}, \forall t$
	(6.22) – (6.23),	Thermal dynamics (for DTR only) ,	$\forall \alpha \in \mathcal{A}^{\text{DTR}}, \forall t$
	(6.24) – (6.26),	Ageing and Thermal dynamics (for DTR$^+$ only) ,	$\forall \alpha \in \mathcal{A}^{\text{DTR}^+}, \forall t$

where Ξ is the list of decision variables. The sections below provide detailed description of these variables along with the associated constraints.

6.2.2 Objective Function

The objective function to minimize the overall cost of energy dispatch over a 24-hour period in the day-ahead market is provided in (6.13).

$$\min_{\Xi} \quad \sum_{t\in\mathcal{T}} \left(\sum_{g\in\mathcal{G}} c_g P_{g,t}^{\text{conv}} + \sum_{w\in\mathcal{W}} c_w P_{w,t} + \sum_{\beta\in\mathcal{B}} c_\beta^{\text{sh}} P_{\beta,t}^{\text{sh}} \right) \tag{6.13}$$

where the set of decision variables $\Xi = [P_{g,t}^{\text{conv}}, P_{\beta,t}^{\text{sh}}, P_{w,t}, W_{\alpha,t}]$ for each time step t represents the scheduled conventional generator's output for every generator, possible load to be shed for every bus, and dispatched wind power $P_{w,t}$ for every wind farm respectively. Lastly, an auxiliary decision variable is used to model the power losses in the branches $W_{\alpha,t}$, as shown earlier. The parameters c_g, c_w and c_{sh} respectively represent the cost of dispatching conventional generation, cost of wind energy dispatch and the cost of preemptive corrective load shedding actions. These parameters are treated as constants in this project, but can be treated as variable to model the unit commitment problem more accurately which was not the goal here.

6.2.3 Definition of Constraints

Constraints for Power Balance

The constraint in (6.14) ensures power balance in the system for each individual hour in the 24-hour period of the day-ahead dispatch market. It is important to mention that the parameter $W_{\beta,t}^{\text{bus}}$ is a design feature of this problem and models the branch losses as additional load, as explained earlier.

$$\sum_{g\in\mathcal{G}} P_{g,t}^{\text{conv}} + \sum_{w\in\mathcal{W}} P_{w,t} - \sum_{\beta\in\mathcal{B}} (P_{\beta,t}^{\text{load}} - P_{\beta,t}^{\text{sh}} + W_{\beta,t}^{\text{bus}}) = 0, \qquad \forall t \in \mathcal{T} \tag{6.14}$$

Constraints for Generational & Operational Limits

The constraints (6.15) - (6.16) ensure that the generational limits for the conventional generator and the available production capacity of the windfarms are not violated. The modeling of the wind power available at each bus P_w^{av} is explained in Section 6.3. The decision variable P_w is key here as the amount of wind to be dispatched out of the total P_w^{av} would depend upon the load demand and grid congestions because of lack of consideration of flexible load, storage or cross-border transmission in the considered problem. This optimally dispatched P_w will be determined by the optimization problem.

$$\underline{P_g^{\text{conv}}} \leq P_{g,t}^{\text{conv}} \leq \overline{P_g^{\text{conv}}}, \qquad \forall g \in \mathcal{G}, \quad \forall t \in \mathcal{T} \tag{6.15}$$

$$0 \leq P_{w,t} \leq P_w^{\text{av}}, \qquad \forall w \in \mathcal{W}, \quad \forall t \in \mathcal{T} \tag{6.16}$$

Similarly, the constraint (6.17) allows compliance with the ramping capabilities of the conventional generators. The power flow in each branch is limited within the rated capacity by the constraint (6.18), while the amount of load to be shed at each bus is constrained to the actual load of that bus by (6.19). The sign of line power flow F represents the direction of power flow between buses.

$$-\overline{\Delta P_g^{\text{conv}}} \leq P_{g,t}^{\text{conv}} - P_{g,t-1}^{\text{conv}} \leq \overline{\Delta P_g^{\text{conv}}}, \qquad \forall g \in \mathcal{G}, \quad \forall t \in \mathcal{T} \tag{6.17}$$

$$-\underline{F} \leq F_{\alpha,t} \leq \overline{F}, \qquad \forall \alpha \in \mathcal{A}, \quad \forall t \in \mathcal{T} \tag{6.18}$$

$$0 \leq P_{\beta,t}^{\text{sh}} \leq P_{\beta,t}^{\text{load}}, \qquad \forall \beta \in \mathcal{B}, \quad \forall t \in \mathcal{T} \tag{6.19}$$

Constraint for Losses Approximation

The approximation of losses is performed according to the principle explained earlier. The power losses in each branch are bounded by (6.20). The lower bound is modeled correctly by quadratic representation using resistance of the respective branch r_α; whereas the upper bound is uniquely modelled to prevent the inclusion of fictitious losses in the network.

$$r_\alpha F^2_{\alpha,t} \leq W_{\alpha,t} \leq W^{\max}_{(k)}, \qquad \forall \alpha \in \mathcal{A}, \quad \forall t \in \mathcal{T} \tag{6.20}$$

Additional Constraint for the STR Test Case

This additional constraint is valid for the subset $\mathcal{A}^{\text{STR}}$ of transformers that are statically rated as the maximum transformer load in the corresponding branch α is limited to the rated capacity of 1 pu, as shown in (6.21).

$$-1 \leq I^{\text{trf},\,pu}_{\alpha,t} \leq 1, \qquad \forall \alpha \in \mathcal{A}^{\text{STR}}, \quad \forall t \in \mathcal{T} \tag{6.21}$$

Additional constraints for the DTR Test Case

For the test case where the identified transformer is to be dynamically rated as per conventional methods, the limits for top-oil and hot-spot temperatures represented by $\overline{\vartheta^{\text{tot}}}$ and $\overline{\vartheta^{\text{hst}}}$ are set below the normal cyclic limits of Table 3.4, as shown in (6.22)-(6.23). These limits are chosen to be 100 and 110 °C for ϑ^{tot} and ϑ^{hst} respectively in this section in order to comply with the conventional design practices at all times. The estimation of these temperatures are performed using the quadratic inequality constraints of (6.8)-(6.9) which keep the resulting optimization problem convex.

$$\vartheta^{\text{tot}}_{\alpha,t} \leq \overline{\vartheta^{\text{tot}}}, \qquad \forall \alpha \in \mathcal{A}^{\text{DTR}}, \quad \forall t \in \mathcal{T} \tag{6.22}$$

$$\vartheta^{\text{hst}}_{\alpha,t} \leq \overline{\vartheta^{\text{hst}}}, \qquad \forall \alpha \in \mathcal{A}^{\text{DTR}}, \quad \forall t \in \mathcal{T} \tag{6.23}$$

Additional constraints for the DTR+ Test Case

The third and final loading strategy has been originally proposed in this project. This technique not only takes into account the thermal dynamic behavior of the transformer, but its ageing rate as well. The constraints (6.24) and (6.25) make use of the long-term emergency limits of Table 3.4 by setting the limits $\overline{\overline{\vartheta^{\text{tot}}}}$ and $\overline{\overline{\vartheta^{\text{hst}}}}$ to 115 and 140 °C respectively, which are significantly higher than the normal cyclic limits in consideration to accelerated ageing at high temperatures. As a result, the transformer ageing is expected to be much higher in this method. Therefore, the constraint (6.26) is added to the problem which ensures that the lifetime utilization of the transformer at all operational hours stays below the design limit set by IEEE C57.91 in [45]. The parameter $\overline{\Delta\lambda}$ represents the desired maximum ageing rate which is set to '1' in this study. The parameter t is used as a time counter during the simulation.

$$\vartheta^{\text{tot}}_{\alpha,t} \leq \overline{\overline{\vartheta^{\text{tot}}}}, \qquad \forall \alpha \in \mathcal{A}^{\text{DTR}^+}, \quad \forall t \in \mathcal{T} \tag{6.24}$$

$$\vartheta^{\text{hst}}_{\alpha,t} \leq \overline{\overline{\vartheta^{\text{hst}}}}, \qquad \forall \alpha \in \mathcal{A}^{\text{DTR}^+}, \quad \forall t \in \mathcal{T} \tag{6.25}$$

$$\lambda_{\alpha,t} \leq \lambda_{\alpha,t-1} + \overline{\Delta\lambda}\, t, \qquad \forall \alpha \in \mathcal{A}^{\text{DTR}^+}, \quad \forall t \in \mathcal{T} \tag{6.26}$$

The ultimate outcome of this approach is that the transformer utilization can be accelerated when needed, depending on its historic load profile and operating conditions. As soon as the upper boundary of transformer lifetime utilization is reached, the conventional settings for DTR are followed as the binding constraint switches from following HST to cumulative utilization lifetime λ_t.

6.3 Test Case of the West-Denmark Transmission System with Increased Offshore Wind Generation

For demonstration of the effectiveness of the proposed methodology, the IEEE RTS-24 bus network of [161] has been modified. The main modifications made to the system include: addition of increased offshore wind power generation, application of actual load and generation patterns from the transmission network of West Denmark (DK1) and application of dynamic rating on selected transformer in the network. These alterations are elaborated in detail below.

Additional offshore wind generation units are strategically added to Bus 16, 21 and 23 of the test case IEEE RTS-24 bus network, shown in Fig. 6.5. One of the reasons for these placements is the existing concentration of the load demand in the lower region of the network which suggests that for optimal utilization of additional wind generation, long distance transmission would be needed resulting in system congestions and additional strain on the components in the middle section of the network. This also complies with the developments foreseen in the Danish transmission network with more and more offshore windfarms being planned near the west coast and concentration of load in the east. Preemptive power flow simulations suggest that the transformer between Bus 3 and 24 (original rating 250 MVA) can be a bottleneck in the system. In addition to this, three transformer ratings of 200, 175 and 150 MVA are tested to increase the thermal stress on the selected transformers; the DTR modeling parameters for which are provided in Table 6.1. Therefore, DTR will have to be used for integration of additional OWF generation to the lower half of the system. It must be mentioned that the operational constraints of the system which can limit the load of the chosen bottleneck transformer including protection settings, ratings of switchgear components etc. are ignored in this study.

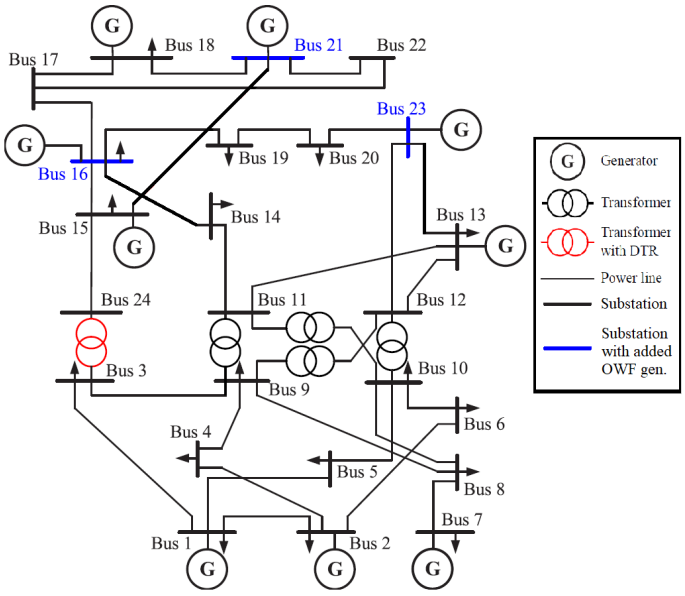

Figure 6.5: IEEE RTS 24-bus system modified with increased wind generation, bottleneck transformer and load demand scaling [161]

Table 6.1: Parameters for DTR modeling of test case transformers.

Parameter	Symbol	Unit	Test Case Transformers		
			200 MVA	175 MVA	150 MVA
Rated Load Losses	$W_{rated}^{trf,cu}$	[kW]	411.8	394.2	367.7
Rated No-Load Losses	$W_{rated}^{trf,e}$	[kW]	72.9	68.8	69.1
Rated HST Rise	$\Delta\vartheta_{rated}^{hst}$	[° C]	38.3	36.6	37.7
Rated TOT Rise	$\Delta\vartheta_{rated}^{tot}$	[° C]	20.3	21.1	20.4
Thermal Capacitance	C_{th}^{trf}	[kWh/°C]	59.6	56.1	53.3
Thermal Time Constant (wdg.)	τ_h	[min]	7	6.75	7.6

In order to improve the practical applicability of the test results, the actual patterns of load demand and generation from the DK1 system in Denmark are used for the years 2014, 2015 and 2016. Moreover, historical wind generation from DK1 for the same period has been used to demonstrate the behavior of a power system with increased penetration of wind generation. The aggregate wind generation in West Denmark is shown in Fig. 6.6 as a function of average windspeed across the DK1 region for the three years. The fitted P^{W} has been used to convert the time series for wind speed (and direction) to the wind power production for the entire duration. The procedure has originally been developed in [162] which is based on the mesoscale down-scaling method presented in [163] and utilized by the authors in **[Pub. C4]** and **[Pub. J1]**. Lastly, the actual ambient temperature time series $\vartheta_t^{\mathrm{amb}}$ from the DK1 has been used for DTR calculation to account for the correlation between mean wind speed and $\vartheta_t^{\mathrm{amb}}$.

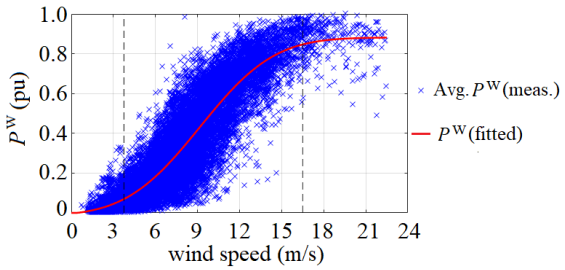

Figure 6.6: Overall wind power production in the transmission network of West Denmark (DK1) for the considered 3-year period. The wind speed and average wind production P^{W} are shown as a scatter plot (blue); while the fitted function demonstrates average spatio-temporal power curve to represent the correlation of wind speed and P^{W} (red) **[[Pub. D1]]**

Finally, the actual load demand is increased for each day by 25 % during the peak load interval in order to take the possible changes in network utilization over the next decade into account. This is shown in Fig. 6.7. The utilization of additional wind generation has to be met by some additional load and the need to employ DTR on the selected components is further enhanced by this step.

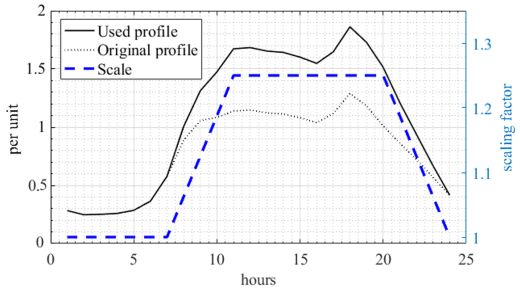

Figure 6.7: Linear scaling of DK1 load during peak hours to increase the stress on cyclic loading of transformer

6.4 Performance Evaluation under Actual Conditions

The DCOPF problem developed using a multi-period formulation has been solved in a 24-hour moving window for 3 years (2014, 2015 and 2016). The three loading strategies are used: STR with rated transformer load limits, DTR with conventional $\overline{\vartheta^{\mathrm{hst}}} = 110°\mathrm{C}$ limit, DTR^{+} with $\overline{\vartheta^{\mathrm{hst}}} = 140°\mathrm{C}$ limit along with the optimal lifetime utilization constraint. Prior to running the test cases, the transformer is assumed to have been operated for 3 years and assumed to have lost half of its lifetime during that period ($\lambda_0 = 1.5$ years), which is a conservative presumption based on the recorded operational experience as discussed earlier. The results for the 175 MVA transformer test case are discussed in detail below, while the outcomes for all the tested transformer sizes are compared in Section 6.4.2.

6.4.1 Transformer Utilization and System Performance

The utilization of transformers is significantly different for the three test cases. Referring to the histograms in Fig. 6.8, it can be seen that the 175 MVA transformer operates more often around $\vartheta^{\text{hst}} = 115°\text{C}$ for the proposed test case of DTR$^+$, while the conventional DTR operation results in frequent operation at $\vartheta^{\text{hst}} = 110°\text{C}$ limit over the 3-year simulated period. Under STR conditions, the transformer is found to be significantly underutilized even though it is the main system bottleneck. These observations are further demonstrated by plotting the cumulative transformer lifetime utilization in Fig. 6.9. The STR test case causes insignificant ageing over the simulated period because the consistent operation at low HST is coupled with the exponential ageing rate relation. This is found to be in compliance with the conventional conservative practices of transformer utilization. Whereas, under the DTR$^+$ operation strategy, the transformer is pushed to its design limit curve within the first year and it continues to operate in a fashion that uses the available lifetime at disposal. The conventional DTR methodology is found to be better than STR, but still results in significant unconsumed transformer life, as originally expected.

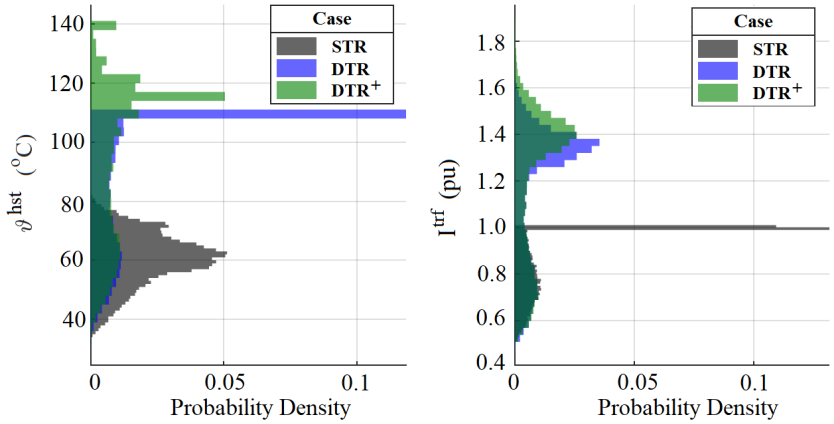

Figure 6.8: Histograms for the normalized probability distribution for 3-years simulation of transformer HST and load for the STR DTR and DTR+ loading strategies

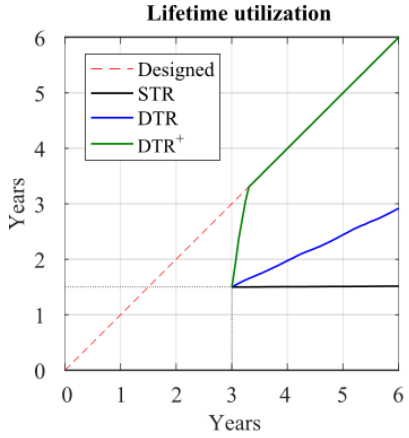

Figure 6.9: Cumulative lifetime utilization of the bottleneck transformer over the 3-year period for the STR, DTR and DTR$^+$ loading strategies

The three-day period with high wind production is considered in Fig 6.10 to present the transformer load along with its corresponding HST. The favorable ambient conditions suggest that under STR operation, the transformer HST is well below the design limits. These limits are pushed by the DTR$^+$ strategy when the load

demand is high during the day and the high offshore wind energy production in the upper region needs to be transmitted to fulfill this demand due to its commercial and sustainable merits. Furthermore the evaluation of transformer and system losses for the STR, DTR and DTR$^+$ loading strategies are also presented in the figure, where the system and transformer losses are found to be highest for the proposed methodology. Hence, as expected, additional losses are created in the system when grid congestions are relieved using DTR and DTR$^+$ as a result of additional power flows across the grid.

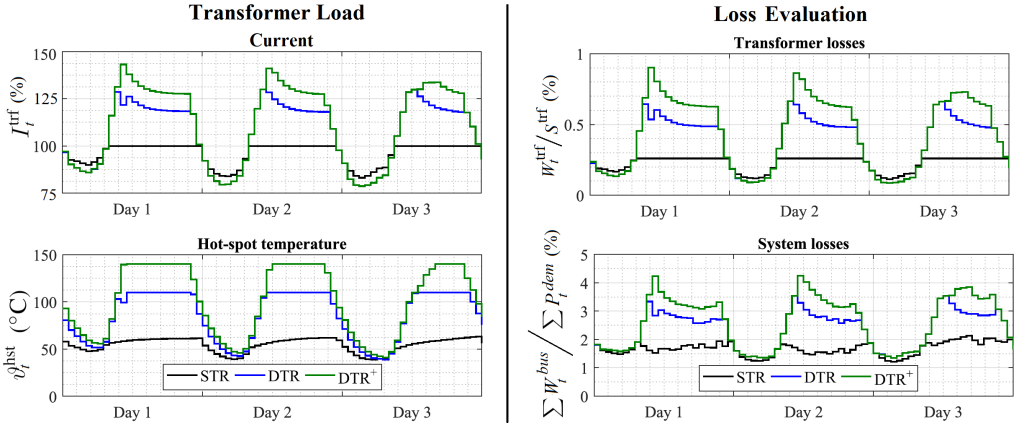

Figure 6.10: Evaluation of transformer utilization and system losses for the STR, DTR and DTR$^+$ loading strategies with focus on three days of operation. Left: Transformer load (%) and hot-spot temperature. Right: Losses (%) in bottleneck transformer and the overall system.

6.4.2 Energy Dispatch and Wind Integration

The plots in Fig. 6.11 are crucial for this study. Firstly, the dispatched wind energy (P^{W}) is compared for the STR, DTR and DTR$^+$ test cases and the total available wind energy generation in the system. It is seen that the conventional STR operation results in lowest utilization of the available wind energy for the entire duration compared to the other test cases. DTR and DTR$^+$ often result in similar wind energy dispatch, with DTR$^+$ (represented by green line) taking the lead during certain periods. Similarly, the figure also presents total load injection for the system along with conventional power generation schedule for the three test cases. STR is found to allocate the highest share of conventional generation, with DTR$^+$ being the lowest.

The overall results compiled in Table 6.2 present the complete picture where utilization of wind energy, reduction in cost of energy dispatch and the increase in transformer utilization are presented for a 1-year simulation period with respect to the figures for the STR loading strategy. DTR$^+$ consistently results in the highest utilization of wind energy which is also reflected in the lowest cost of energy dispatch while accounting for the additional system losses. Smaller the transformer size, higher the potential to improve system performance. Hence, it is observed that despite the increase in system losses, the overall economic benefits outweigh the negatives as proven by the multi-period DCOPF problem. The reduction in dispatch cost by up to 11.5% is significant and can potentially motivate the system operator to integrate more low-cost renewable generation, while deferring the grid reinforcement costs.

Table 6.2: Assessment of results with respect to the STR test case after 1 year of simulations. Increase in wind energy utilization, decrease in energy dispatch cost in the day-ahead market & increase in transformer lifetime utilization.

Transformer Size (MVA)	**Wind Utilization (%)**		**Cost Reduction (%)**		**Used Lifetime (%)**	
	DTR	DTR$^+$	DTR	DTR$^+$	DTR	DTR$^+$
150	+8.9	+10.2	-10.1	-11.5	+41.5	+166
175	+7.1	+9.1	-8.1	-8.8	+31.1	+166
200	+6.2	+8.1	-6.4	-7.1	+24.2	+166

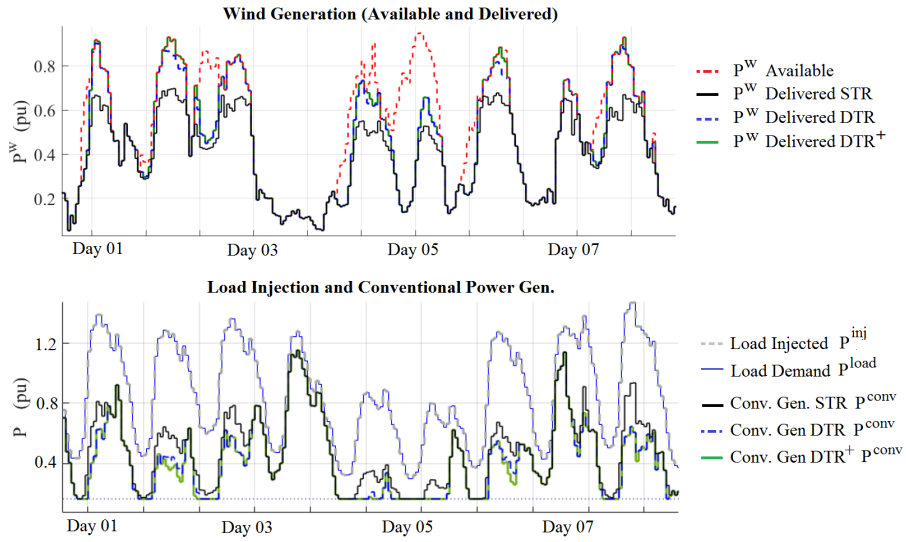

Figure 6.11: Influence of the STR, DTR and DTR $^+$ loading strategies on energy dispatch for one-week of operation. Top: Temporal variation of total wind generation available and dispatched under the three tested methodologies. Bottom: Contribution of conventional generation in load fulfillment (no load shedding observed).

6.4.3 Final Deductions

It has been shown that the transformer operation and utilization, while staying within the operational security limits set by IEEE and IEC standards of [45] [44], can potentially unlock the hidden capacity of the transmission system. While delaying the grid reinforcement and infrastructure upgrade costs, the higher utilization of transformers based on enhanced DTR can be matched with the high load periods during the day to maximize wind and renewable integration. The two potential pitfalls of the utilitarian methodology, which include unreliable transformer operation and higher system losses, are not found to constitute major problems in the proposed formulation. This technique can be used in synergy with the algorithms developed as part of this project and proposed in publication **[D1]**. The utilization of dynamic network rating, i.e. simultaneously employing coordinated DTR on multiple system components incl. transformers and overhead lines, is proven to make the most optimal use of the system in publication **[D1]**.

Key Takeaways from Part III

The discussion in Part III has shown that power transformers in offshore windfarms are over-dimensioned and the optimal utilization needs to be performed by employment of DTR. For this purpose, the extensive review of load-dependent thermal ageing of transformers is performed in Chapter 4, where basic Arrhenius reaction rate models are compared with the extensively explored DP-based thermo-chemical ageing models. In Chapter 5, the utilization and loading of ten test case transformers from a number of portfolio OWF projects across the globe are compared with the expected rated ageing. The analysis shows that the windfarms can be expanded by 40 to 50 % for the transformer utilization to match the rated ageing. Hence, based on this investigation, the novel optimization problem developed in chapter 6 introduces the Enhanced Dynamic Thermal Rating (DTR^{+}) principle that generates adaptive thermal limits for each operational duration depending on the utilized transformer lifetime. The developed lossy dynamic DC Optimal Power Flow (DCOPF) methodology is then adjusted to accommodate the day-ahead energy dispatch optimization in the IEEE 24-bus RTS network with increased offshore wind generation and load/generation patterns replicating the actual readings from west-Denmark. The findings of this study has shown that DTR^{+} based optimal transformer utilization can facilitate large scale integration of OWFs and delay the investments related to required grid infrastructure improvements. The costs for power losses are modeled as additional load demand, therefore indirect costs are included only. The efficiency of networks is to be maintained by the system operations, which would require additional ad hoc measures. In conclusion, the investigation has shown that for OWFs in particular, DTR can improve export system utilization during contingency and allow operators to maximize power transmission in case of failures etc. The DTR^{+} methodology presented in Publication **[Pub. C4]** has been extended in **[Pub. D1]** to incorporate dynamic rating on multiple system components at the same time, also termed as dynamic network rating.

PART IV - DTR-BASED OPTIMAL DESIGN OF OWF EXPORT SYSTEM COMPONENTS WITH RELIABILITY AND UNCERTAINTY CONSIDERATIONS

The discussion so far has shown that the major HV components in the Offshore Windfarm (OWF) export system, like the one in Fig. 6.12, are over-dimensioned. For portfolio projects, optimal utilization of these components can be performed under certain circumstances. However, the potential to improve the OWF business case by using Dynamic Thermal Rating (DTR) based design of these components during the planning phase of OWFs is considerable for the pipeline projects. **Part IV** of the PhD thesis deals with this subject, while accounting for uncertainty in wind generation over the OWF lifetime and reliability of system availability for the same period, the mechanism for which is explained in Chapter 7.

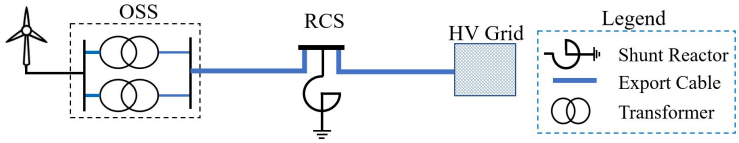

Figure 6.12: Simplified layout of an OWF HV export system with one radial circuit. The highlighted components are to be optimally designed.

The design optimization of OWF array cable system has been presented extensively in [16–20], but limited work has been done on DTR-based export cable design [24–26]. One of the techniques presented in [164] uses a step-load profile generated via long-term assessment of wind generation profile, like the one shown in Fig 6.13. The step-load profile represents the worst-case load that the export cable experiences over the OWF lifetime and the thermal estimation suggests the maximum continuous duration the load can be sustained to ensure compliance with cable thermal limits.

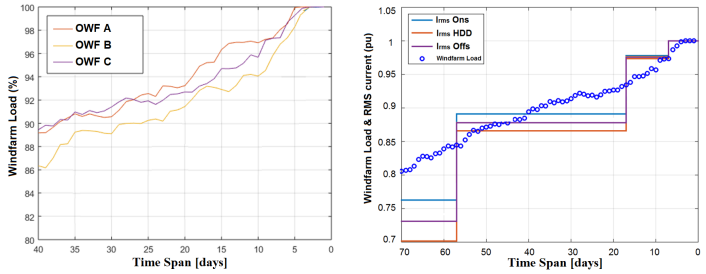

Figure 6.13: Cable sizing methodology for offshore windfarms based on step-load profile [164]. Left: Load duration curves for three test case windfarms in UK. Right: Step-load profile for HDD, Onshore and Offshore cable sections along with load duration curve (blue dots) for one of the test case windfarms.

However, little to no work addressing the optimization of the remaining OWF export system components including transformers, reactors etc. is available in the literature. Furthermore, the systemic approach to export system optimization by using electro-thermal coordination of all the relevant HV components in the export system has not been addressed either. In this part, DTR-based design optimization of transformers to match the operational lifetime of windfarms has been addressed in Chapter 8, which is followed by design optimization of the entire system in Chapter 9. The work is presented in publications **[Pub. J1]** and **[Pub. J2]** by the author.

CHAPTER 7

Scenario Generation for Uncertainty and Reliability Considerations

In order to design the OWF export system on the basis of DTR operation under intermittent wind generation, it is important to consider the uncertainty of wind speed and production profile over the entire OWF lifetime. Furthermore, the reliability of such a design has to be ensured by considering availability and contingency of the relevant components that generate and transmit the energy to the grid. Both these considerations not only ensure that the designed ratings for critical export system components (cables, transformers, reactors etc.) can outlast the OWF lifetime, but are also needed to assess the influence of the design on energy availability and system efficiency. In this project multiple OWF lifetime scenarios are generated for the OWF test site's wind speed profile, time series for availability of wind turbines A_t^{W} [pu] and time series for availability A_t^{c} [pu] and load-scaling A_t^{SF} [pu] of export system components. The steps for scenario generation and the intermediate power after each step are set forth in Fig. 7.1, which is followed by a detailed elaboration of the individual blocks.

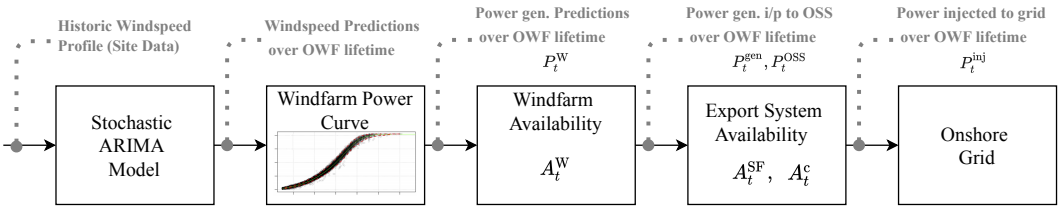

Figure 7.1: Block representation of scenario generation process from historic site data to power injection time series.

7.1 Modeling of Wind Speed using Stochastic ARIMA Process

Modeling of wind power for offshore windfarms has conventionally been done using stochastic Auto Regressive Integrated Moving Average (ARIMA) models [25] [165] [166], where long-term historic wind speed profiles for the site under consideration are used to identify the underlying physical processes. These models take into account non-stationarity and have proven to be more efficient and generic to design compared to discrete time Markov processes of [167] [168]. Therefore in this project ARIMA modeling is used to generate long-term wind speed time series for the test case windfarms.

The long-term hourly wind speed site data for an offshore windfarm site off the east coast of UK has been obtained from [169]. Since the 14-year data is found to have an inherent trend, the procedure defined in [170] has been used for identifying the model of non-stationary time series. First of all, the raw time series is transformed to remove the underlying long-term trend (> 1 year) by using differencing operation, and the resulting data is plotted in Fig. 7.2 along with the monthly average to further ensure that no long-term trends exist in the data. Afterwards, following steps are followed to fit the correct ARIMA model:

- **Stationarity Test:** In order to make sure that the statistical properties of the detrended time series for wind speed are independent of time in the long-term (>1 year), stationarity tests are performed including **kpss** and **adf** [104]. All of these tests combined with the visual inspection performed earlier indicate stationarity over long-term.

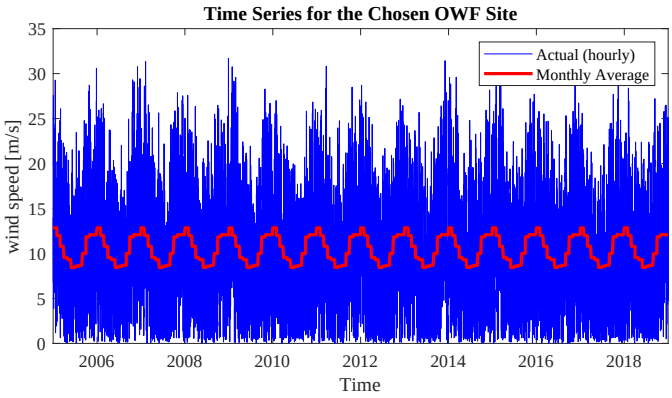

Figure 7.2: Hourly wind speed data for an offshore windfarm location off the east coast of UK [169]. Outliers, missing data and long-term trend in the data have been removed. Monthly average values are also plotted.

- **Seasonal Differencing:** Referring to the monthly average plot in Fig. 7.2, there is a clear yearly seasonal trend that needs to be removed. This is further confirmed by plotting the Auto Correlation Function (ACF) of the original time series in Fig. 7.3 for lags spanning across multiple years. Following long-term seasonal lags (hours) are identified: 2200 (quarterly) and 8760 (yearly), which are further analysed by splitting the yearly trend in 4 seasons: Winter (December-February), Spring (March-May), Summer (June-August) and Autumn (September-November). A closer look at the data also reveals a daily trend at lower lags (24-hours) which is not shown in the figure. Both these seasonal trends are removed through differencing, and the resulting ACF and Partial ACF values are plotted in Fig. 7.3 for the data without seasons. PACF plot has not changed (as expected), but the seasonality from the ACF plot has definitely been removed. This data is found to be fit for ARIMA model fitting.

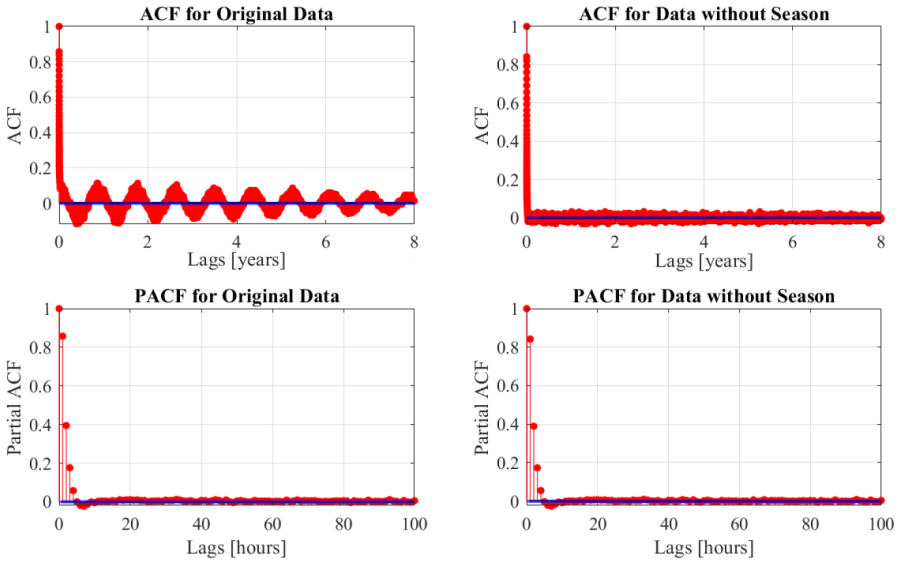

Figure 7.3: Auto Correlation Function (ACF) plots for long-term and Partial ACF plots for short term. Left: Original de-trended data. Right: Data after yearly and daily seasons are removed.

- **ARIMA Model Fitting:** Since the seasonal trends for lags 24 hours have been removed, ARIMA model fitting for the remaining data is performed by observing the ACF and PACF at lower lags. In this project, the forecast model in R [171] has been used and ARIMA (2,0,2) for the lower lags is found to result in optimal fit.
- **Residual Analysis:** In this step the difference between actual and fitted values (residuals) are analysed to check if any underlying pattern exists. This is a standard process in ARIMA model fitting, and several methods are used to ensure the quality of the fit as shown in Fig. 7.4. Visual inspection of the scatter plot reveals that the residuals are random in nature and found to be independent and identically distributed. This is further confirmed by the normal distribution analysis, the QQ plot of residuals, sign tests [172] and Ljung box test [104]. Furthermore, the ACF and PACF plots for lower lags do not reveal any irregular spikes or missing peaks. Therefore, the model deduced in the previous step is found to be good enough for wind speed forecast for the selected OWF site.

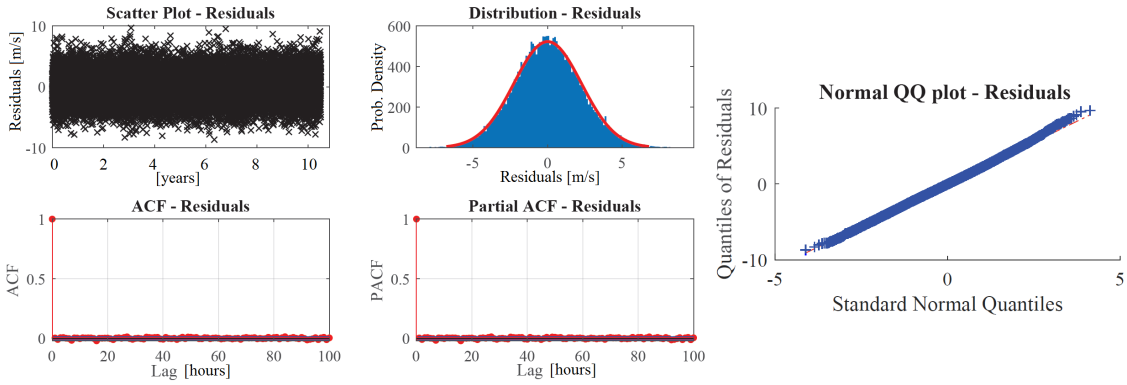

Figure 7.4: Residual analysis of the fitted ARIMA model to the long-term wind speed data. The analysis includes scatter plots, distribution fit, Normal QQ plot along with Auto Correlation and Partial Auto Correlation analysis plots.

- **Wind Speed Profile Predictions:** The fitted ARIMA model can be used to generate stochastic scenarios of wind speed profile. Three scenarios are simulated in Fig. 7.5 for 15-year each, while a small sample size of the simulations is provided for ease of observation. The histograms shed more light on the likeliness of similarity on the overall distribution of the wind speeds, while the scatter plot determine the temporal variation.

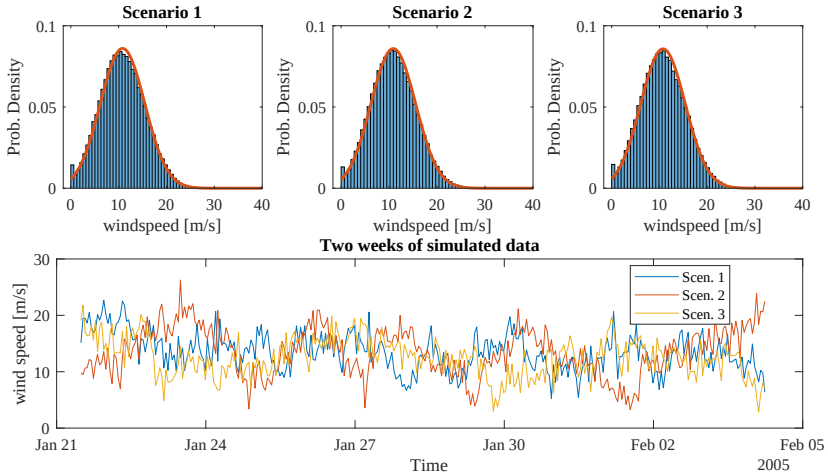

Figure 7.5: Simulated scenarios of 15 year wind speed time series for the test site. Histograms on wind speed distribution for each scenario at the top. A small sample of the simulated data is plotted in the bottom figure.

7.2 Stochastic Modeling of Wind Farm Availability

The hourly power generated by the OWF which needs to be transmitted to the shore depends not only on the wind profile but also on the number of wind turbines available for operation for that given hour. Since, WTGs are susceptible to failure and maintenance activities due to continuous mechanical stress, it is important to account for WTG down time [8]. Furthermore, WTGs are frequently operated higher than their rated capacities by using the recently introduced *power-boost* function which resolves wake effect and other phenomena that restrict energy production under certain wind characteristics [173].

The prediction of hourly WTG availability over the OWF lifetime can be difficult to model due to the presence of innumerable influential parameters. In this project a simplistic statistical WTG availability technique is developed which combines simple distribution functions to simulate multiple scenarios for the time series of availability factor $A^{\mathrm{W}}_{t,s}$ [pu], as shown in (7.1). Firstly, two normally distributed functions ($\mathcal{N}_{act}$ and $\mathcal{N}_{out}$) are used to generate random numbers to respectively represent the actual expected availability of windfarm and the unexpected outliers which may arise due to natural events and other anomalies leading to common failures. Both the normal distribution functions are averaged around the mean availability of wind turbines $\mu_{A^{\mathrm{W}}_{av}}$, but with varying standard deviations (σ_{act} and σ_{out}). Afterwards, a random number generator is used to generate X which is limited between 0 and 1. A special function ψ depending on the random number X is used to activate the normal distribution functions, such that the first function (actual) represents 95% of the samples, while the outliers are limited to 5%. Hence, by using this hourly WTG availability $A^{\mathrm{W}}_{t,s}$ in cooperation with the hourly OWF generated wind power $P^{\mathrm{W}}_{t,s}$ [MW] is simulated using ARIMA model and the OWF power curve, it is possible to calculate the power at the entrance of the OSS ($P^{\mathrm{gen}}_{t,s}$ or $P^{\mathrm{oss}}_{t,s}$), as shown in (7.2).

$$
\begin{aligned}
A^{\mathrm{W}}_{t,s}(\tau_{\mathrm{w}}) \sim & \psi\left(0 \leq X(\tau_{\mathrm{W}}) < 0.95\right) \cdot \mathcal{N}_{act,s}(\mu_{A^{\mathrm{W}}_{av}},\, \sigma^2_{act}) + \\
& \psi\left(0.95 \leq X(\tau_{\mathrm{w}}) \leq 1.0\right) \cdot \mathcal{N}_{out,s}(\mu_{A^{\mathrm{W}}_{av}},\, \sigma^2_{out}) \\
& \text{s.t.} \\
& \{X \in \mathbb{R} \mid 0 \leq X \leq 1.0\} \\
& \{\psi(z) = 1 \mid z = true\} \\
& \{\psi(z) = 0 \mid z = false\} \\
& A^{\mathrm{W}}_{min} \leq \mathcal{N}_{act,s}(\mu_{A^{\mathrm{W}}_{av}},\, \sigma^2_{act}) \leq A^{\mathrm{W}}_{max} \\
& 0 \leq \mathcal{N}_{out,s}(\mu_{A^{\mathrm{W}}_{av}},\, \sigma^2_{out}) \leq A^{\mathrm{W}}_{max} \\
& \sigma^2_{out} = 5\sigma^2_{act}
\end{aligned}
\tag{7.1}
$$

$$
P^{\mathrm{gen}}_{t,s} = A^{\mathrm{W}}_{t,s} \cdot P^{\mathrm{W}}_{t,s} \tag{7.2}
$$

where each availability value $A^{\mathrm{W}}_{t,s}$ is held for a roll-over period τ_{WTG} (set to 24 hours) as it defines the duration for how long a given number of WTGs will be available as it is influenced by wind turbine repair rate and other factors. The variance of outliers σ^2_{out} are set to be five times higher than the variance of actual windfarm availability σ^2_{act} to reproduce the WTG availability figures in [8], while the mean availability $\mu_{A^{\mathrm{W}}_{av}}$ can be set to 96% based on practical experience reported in [174]. The upper and lower bounds for the distribution functions $\mathcal{N}_{act}$ and $\mathcal{N}_{out}$ are defined by A^{W}_{max} and A^{W}_{min} respectively. The former term is set higher than 100% (105 % for this test case [173]) as it accounts for *power-boost* characteristics for the WTG, while the lower bound is predefined to comply with the maintenance targets of the OWF operator [9]. The simulation results for one of the scenarios realized using this formulation is shown in Fig. 7.6.

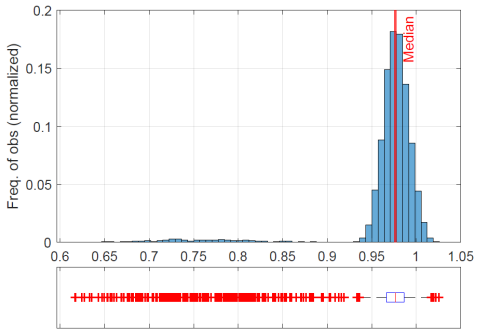

Figure 7.6: Simulation of one of the scenarios for availability of OWF turbines $A^{\mathrm{W}}_{t,s}$ (horizontal axis) over the OWF design lifetime of 30 years using a histogram and a box-plot. The simulations are based on (7.1)

7.3 Contingency Assessment for HV Export System using Stochastic Markov Process

The assessment of export system's reliability and contingency is crucial for OWF design, particularly for components located off the shore because of inherent nuisances like accessibility issues leading to longer repair times [12]. As the capacity factor demand for offshore projects increase, the availability characteristics are bound to become even more critical [17]. A number of probabilistic methods are available in the literature that can be used to model the stochastic nature of export system's availability over the OWF lifetime. These methods can rely on analytical techniques [28] or Monte Carlo simulations [14, 17, 29]. However, the applicability of these techniques depends heavily on the problem to be solved as the computational stress on the design optimization problem can be challenging.

The transmission of power generated by offshore windfarms is dependent on the availability of the HV export system. As already discussed, the export system commonly consists of more than one parallel radial circuits interlinked at the offshore and onshore substation points. These interlinks allow diversion and redistribution of power in case one or more parallel circuit components face contingency. Hence, it can simply be assumed that for an export system equipped with n^{c} parallel radial circuits, the power generated by the OWF P^{gen}_t is equally divided between all circuits $\left(\frac{P^{\mathrm{gen}}_t}{n^{\mathrm{c}}}\right)$ under normal operating circumstances. The number of available circuits reduce during contingency, which would require redivision of the load to maximize energy transfer during these abnormal circumstances. Two important time-variant parameters are introduced in this project to scale the load of components in HV export system at all operational hours: A^{c}_t (number of available circuits at time t) and A^{SF}_t (load scaling factor at time t).

Discrete Time Markov Chain (DTMC) models are found to be most appropriate for design applications and contingency simulations in this project. The progression of the export system between normal and contingency operation has been modelled using the state transition principle based on DTMC's probabilistic determination approach [28] using the reliability indices like Mean Time To Failure (MTTF) [hour] and Mean Time To Repair (MTTR) [hour]. At any given instant, each radial circuit in the export system (or any of its relevant HV components) is assumed to be either available (UP state) or unavailable due to failure, planned maintenance etc. (DOWN state). The simplified transitional process of the circuit between UP and DOWN states has been presented in Fig. 7.7, where the failure rate Λ [1/hr] and repair rate Υ [1/hr] are calculated as $\frac{1}{\mathrm{MTTF}}$ and $\frac{1}{\mathrm{MTTR}}$ respectively . In the state transition diagram, the arrows represent the probability of the system to move from the existing state to the other state within the time interval Δt [12, 175]. This is also shown in the State Transition Matrix **P** in Fig 7.7, where the diagonal elements represent the probability of staying in the respective state in period Δt and off-diagonal elements in each row indicate the probability of jumping from that state to the respective state of the column [176].

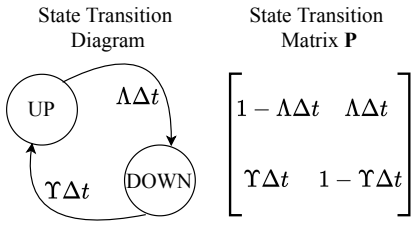

Figure 7.7: State transition diagram and matrix **P** for a two-state system governing the probabilistic discrete time Markov chain process.

The principle for a one-circuit, two-state system in Fig. 7.7 needs to be extended to a system with n^{c} parallel circuits. The total Markov states for this system can be $2^{n^{\mathrm{c}}}$ if Common Cause Failures (CCF) due to natural events etc. are considered and $n^{\mathrm{c}}+1$ for No Common Cause Failure (NCCF) considerations. Therefore a generic state transition diagram is presented in Fig. 7.8 (common cause failures are not considered). In total, the considered system has $n^{\mathrm{c}}+1$ possible states, each state represented by a circle. The value inside the circle represents the number of available circuits A^{c} in the respective state as it ranges from n^{c} (normal operation) to 0 (all parallel circuits failure). The probability of transition between matrices, represented by arrows, is governed by the same failure and repair rates but are scaled to account for the number of available circuits that can possibly fail or be repaired in the time step. Hence, it is concluded that if the relevant information (incl. reliability indices and number of parallel circuits) is available in the design phase, it can be possible to simulate probabilistic scenarios of system availability over the OWF lifetime.

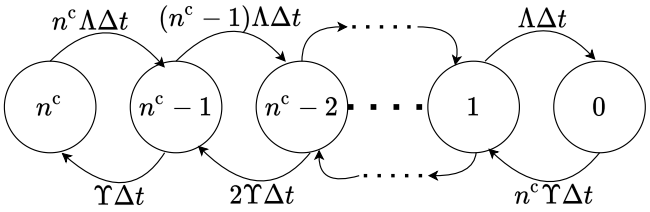

Figure 7.8: State transition diagram for a system with n^{c} parallel radial circuits using Discrete Time Markov Chain (DTMC) process. Each circle represents a state, values inside the circle present the number of available circuits A^{c} in that state, while arrows represent the probability of transition between the respective states in time step Δt.

7.3.1 Consideration of System Design Concepts: *n-1* and *non contingent* designs

Offshore windfarm developers and electrical system designers generally use two design concepts: *n-1 contingent* and *non-contingent*. The former approach allows normal system operation even when one of the system (or its sub-components) is out of operation, while the latter behaves normally only when all the systems and their sub-components are fully (or partially) available. The discussion can be simplified by dividing the possible Markov states in to three categories: Normal (system and components are loaded within their name plate ratings), Abnormal (dynamic rating is necessary beyond nameplate rating to maximize power transmission) and Fail (no power flow possible because all critical components/circuits are out of operation). This can be illustrated in Fig. 7.9 for NCCF considerations for a system with three parallel radial circuits ($n^{\mathrm{c}}=3$) and 4 possible operating states: 3UP (all circuits in operation), 2UP (one circuit failure), 1UP (two circuits failure) and 0UP (all circuits or critical sub-component failure). The two design concepts are shown to provide different degrees of freedom for the normal and abnormal system operation.

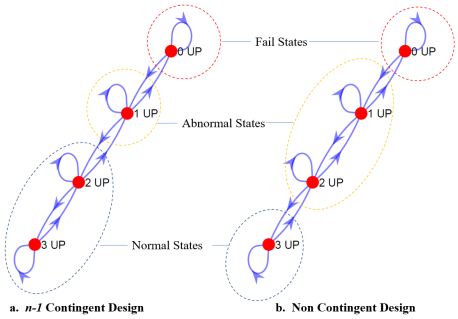

Figure 7.9: Classification of Markov states for normal, abnormal and fail operation for *n-1 contingent* and *non-contingent* design concepts using a system with three parallel radial circuits. Common cause failures are not considered.

The concept has been generalized in Table 7.1 for considerations of NCCF and CCF. It is conceivable that *n-1 contingent* design generally allows higher number of states in normal operation as the system is designed to withstand one failure. The availability of energy, also perceived as the capability of the export system to transmit the rated generation capacity of the OWF, during abnormal system operation is dependent on employment of dynamic rating as the components will have to be loaded beyond their respective nameplate ratings. Hence, as the transition between system normal, abnormal and fail states are simulated over time using the DTMC principle, the parameter A_t^{SF} allows the scaling of load for the individual components to ensure maximum power transfer under all operating circumstances. This concept is elaborated further for the individual test cases in Sections 8 and 9.

Table 7.1: Classification of Markov states and design concepts for a system with n^{c} parallel radial circuits and sub-components.

Name	**No. of States in the Considered Design Concepts**				**Energy Availability**		**Load Scaling Factor $A_t^{\mathbf{SF}}$**
	$n-1$ **Contingent Design**		**Non Contingent Design**				
	CCF	**NCCF**	**CCF**	**NCCF**	w/o DTR	DTR	(DTR)
Normal	$1+n^{\mathrm{c}}$	2	1	1	Full *	Full	Rated (≤ 1)
Abnormal	$2^{n^{\mathrm{c}}}-(n^{\mathrm{c}}+2)$	$(n^{\mathrm{c}}+1)-3$	$2^{n^{\mathrm{c}}}-2$	$(n^{\mathrm{c}}+1)-2$	Partial	Full ^{o}	Increased (≥ 1)
Fail	1	1	1	1	Nil	Nil	No Load (0)

CCF - Considering common cause failures and limited repair resources
NCCF - Not considering common cause failures and repair resources are not limited
* Full energy available unless curtailment needed due to extreme ambient conditions or thermal limitations

CHAPTER 8

Cost-optimized Dynamic Design of Offshore Windfarm Transformers

The discussion in Chapter 5 has shown that offshore windfarm transformers, particularly the ones located in the OSS, are over-dimensioned and under-utilized. Since, it is not always possible to control the utilization of these transformers due to the intermittent nature of the wind, the hypothesis that OWFs should be over-planted or OSS transformer ratings should be optimally reduced is tested in this section. However, this optimal reduction based on DTR has to account for not only reliability of design and uncertainty of operation, but the overall economic impacts on the OWF business (incl. OPEX, CAPEX and possible revenue loss) must be considered. The findings of this section are based on the methodology and results presented in publication **[Pub. J1]** by the author.

8.1 Problem Development and Overview of the Test Case

For the purpose of using a real-life test case, a 1200 MW offshore windfarm in the North Sea is used as inspiration, whose export system layout is provided in 8.1. The export system consists of two parallel circuits with two 66/220 kV offshore transformers per circuit spread across two OSS. The export cables and other relevant HV equipment in the export system are assumed to be over-dimensioned to allow the debottlenecking problem remain relevant for the OSS transformers during all the considered operating circumstances. The test case windfarm is designed for 30 years ($\Pi^{\text{WF}} = 30$), while the available wind speed [169], ambient temperature[177], substation modeling [178] and power curve data are elaborated in publication **[Pub. J1]**.

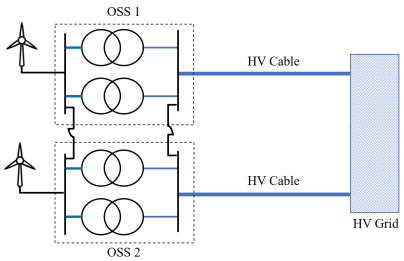

Figure 8.1: Simplified export system layout for the 1200 MW test case offshore windfarm.

In order to assess the commercial influence of OSS transformer optimization, the complete economic picture is painted using Net Present Value (NPV) assessment. If the transformer size is changed from the base case (k, base) to any of the smaller size in design case $k \in \mathcal{K}$, the NPV will either increase (positive business case), decrease (negative business case) or stay the same (neutral business case) with respect to the base design. This is shown in $\text{NPV}_k = \text{NPV}_{k,\text{base}} + \Delta\text{NPV}_k$, where ΔNPV_k [M €] represents the change in NPV for design case k with respect to base design and can be calculated using (8.1). The equation shows that OSS transformer size reduction will have two major influences: CAPEX reduction at year '0' (ΔC_k) [€] and Revenue change

(ΔR_k) [€] over the windfarm lifetime Π^{WF} (years), as OPEX is assumed to remain constant irrespective of transformer size. For each design case, the reduction in CAPEX is driven primarily by decrement in cost of transformers ΔC_k^{trf} [€] and reduction in cost of OSS and foundations ΔC_k^{oss} [M €] due to change in overall OSS weight. On the other hand, revenue over the OWF lifetime will change because of variation in load-dependent transformer losses $\Delta W_{t,k}^{\text{trf}}$ [MW] and possible curtailment due to bottlenecks $P_{t,k}^{\text{cut}}$ [MW], which are scaled using the discount factor i and the price at which energy is sold γ [€/MWh]. It is perceivable that only the parameters in the revenue term are dependent on time $t \in \mathcal{T}$, year $y \in \mathcal{Y}$ and the simulated scenario $s \in \mathcal{S}$ (averaged using probability of each scenario π_s). The CAPEX terms are only dependent on the transformer size and therefore do not vary over the OWF lifetime.

$$\Delta\text{NPV}_k = \Delta C_k^{\text{trf}} + \Delta C_k^{\text{oss}} - \sum_{s\in\mathcal{S}} \pi_s \Delta R_{s,k} \qquad \forall k \in \mathcal{K} \tag{8.1}$$

$$\Delta R_{s,k} = \sum_{y=1}^{\Pi^{\text{WF}}} \frac{\gamma}{(1+i)^y} \sum_{t=1}^{8760} \left(P_{t,y,s,k}^{\text{cut}} + \Delta W_{t,y,s,k}^{\text{trf}}\right) \qquad \forall k \in \mathcal{K} \tag{8.2}$$

For this particular test case, the discount rate of 6.75% [179], and γ of 44.99 €$/MWh$ are used. These values are based on the strike price of the 1.2 GW Doggerbank Creyke Beck A as per the latest Contract for Differences (CfD) auction results [1]. The two terms in CAPEX need more explanation:

- **OSS Cost Reduction** ΔC_k^{oss} (€): As the transformer weight and footprint reduces, so does the overall steel needed to build the offshore substation. This reduction can cause the overall foundation costs to decrease substantially because transformers are the heaviest components on the OSS. Therefore ΔC_k^{oss} can be calculated empirically by using the reduction in transformer mass Δm_k^{trf} [tonne] as governed by the relation $\Delta C_k^{\text{oss}} \sim 2\ c^{\text{oss}} n^{\text{trf}} \left(\Delta m_k^{\text{trf}}\right)$, where c^{oss} represents the weight dependent cost of OSS [€/tonne] and n^{trf} represent the number of transformers in the OSS. This relationship is perceivable because a unit change in transformer weight is complemented by the same change in steel weight [11]
- **Reduction in Transformer Cost** ΔC_k^{trf} (€): Smaller transformers are cheaper to procure due to savings in raw material costs, so total transformer cost savings become $\Delta C_k^{\text{trf}} = n^{\text{trf}} \Delta c_k^{\text{trf}}$, where c^{trf} is the cost reduction of each transformer. However, the reduction in these costs is not linear and it is difficult to model the exact values. For this project, the relationship from [180] is used which derives the transformer scaling relation by fixing four critical parameters: magnetic flux density, frequency of operation, basic insulation level and current density, whereas the dimensions of the core including the cross-section of the winding are allowed to vary with transformer rating. The relationship is provided in (8.3), where the transformer rating for the base design case $S_{k,\text{base}}^{\text{trf}}$ [MVA] and for the design case under consideration S_k^{trf} [MVA] are used to derive the relevant parameter Z. These parameters are summarized in Table 8.1, where the exponential e for the respective parameters are also mentioned.

$$\Delta Z_k^{\text{trf}} = Z_{k,\text{base}}^{\text{trf}} \left[1 - \left(\frac{S_k^{\text{trf}}}{S_{k,\text{base}}^{\text{trf}}}\right)^e\right] \tag{8.3}$$

Table 8.1: Scaling exponents for (8.3) for oil-filled HV power transformers [180]

Symbol for Z^{trf}	Transformer Parameter	Value of Exponent e
m^{trf}	Mass	3/4
c^{trf}	Cost	3/4
$W_{rated}^{\text{trf, cu}}$	Load loss (rated)	4/5
$W_{rated}^{\text{trf, e}}$	No-load loss (rated)	4/5

8.2 Formulation of the Iterative Algorithm for Optimal Transformer Design

The optimization of OSS transformer rating in offshore windfarms can be efficiently performed by using the novel algorithm of Fig 8.2. The overall framework is simple as it consists of four major blocks: Available data, reliability, DTR and output (post processing and economic evaluation). The main idea is that for the test case windfarm, the relevant transformer ratings should be tested by loading them over the entire OWF lifetime and assessing their loss of life and economic influence by the end of windfarm lifetime. The transformer rating that presents the best business case while complying with the lifetime requirements of the windfarm is chosen to be the optimal design case. The individual blocks are explained in detail below:

- **Scenario Generation:** The first two blocks are part of the scenario generation steps to account for uncertainty and reliability considerations. Long-term available site data for wind speed and ambient temperature are used to fit the ARIMA models identified in Section 7.1. This step allows simulation of likely windfarm generation patterns by using the OWF power curve and the fitted ARIMA models. For this test case, the same 14 year data is used to generate 100 scenarios of wind speed and ambient temperature profiles for 1.2 GW windfarm over its lifetime (Π^{WF}) of 30 years. The uncertainty of availability of WTGs in the test case OWF are modeled as per the principle described in Section 7.2. Finally, the hourly load of transformer needs to be adjusted in case of contingency. These contingency scenarios are simulated over the entire OWF lifetime by using the DTMC-based principle developed in Section 7.3. Each scenario of wind generation P_t^{W} is associated with one scenario of wind turbine availability (A_t^{W}) and one scenario of DTMC-based load scaling factor due to contingency (A_t^{SF}), which means 100 realizations of transformer load for the given test case are tested over the entire OWF lifetime. One of the extreme scenarios of contingency will be explained in detail in Section 8.2.1, while 10 worst-case scenarios are elaborated in Publication **[Pub. J1]**.

- **Transformer DTR and Lifetime Utilization:** The third block is responsible for calculating the transformer thermal stress and ageing over the course of OWF lifetime. This block is expanded in Fig. 8.3, where two sub-blocks can be seen: Thermal estimation block to calculate and monitor critical transformer temperatures and lifetime assessment block to assess chemical decomposition of the transformer insulation. The critical transformer temperatures for top-oil (TOT) and hot-spot (HST) are calculated using the Susa model from (2.9). These calculations are repeated for each scenario $s \in \mathcal{S}$ and for all the design case transformer ratings $k \in \mathcal{K}$. Management of transformer load and possible energy curtailment are also performed by this block, in case the long-term emergency thermal limits of Table 3.4 are violated by the calculated TOT and HST.

  The calculation of transformer's thermal ageing with respect to the temporal load variation is performed using the DP-based models presented in Section 4.2.2 because they allow for consideration of thermo-chemical decomposition. Transformer lifetime utilization (LL) is calculated using the IEC 60076-7 Annex A (2018) model because of its relative conservative results and compliance with the major state-of-the-art models. Another reason to use the IEC 60076-7 Annex A model by Lundgaard over other models is the utilization of different activation energies E_a for low and high Oxygen conditions, which directly influences the expected lifetime calculations using DP, as shown in (4.5). For the developed framework, the cumulative loss of transformer life over the windfarm lifetime $\text{LL}_{\Pi^{\text{WF}}}$ [%] is calculated by summing the yearly loss-of-life LL_y [%] as formulated in (8.4). Loss-of-life in a particular year depends upon the expected life for that year EL_y [years] which is normally known to be a function of the hot-spot temperature only. However, in this formulation EL_y is expected to change every year as it depends on two important factors: Firstly, the transformer load for that year which drives its HST ϑ^{hst} and secondly, the chemical decomposition (oxygen and moisture contents) for that year which drive the yearly values for activation energy $E_{a\,y}$ and pre-exponential factor A_y. Based on extensive literature review of transformer post-mortem analysis and reliability statistics [181], conservative assumptions are made for yearly development of oxygen and moisture over the OWF lifetime. According to these assumptions, the oxygen content in oil increases linearly from 2000 to 7000 ppm, while moisture content

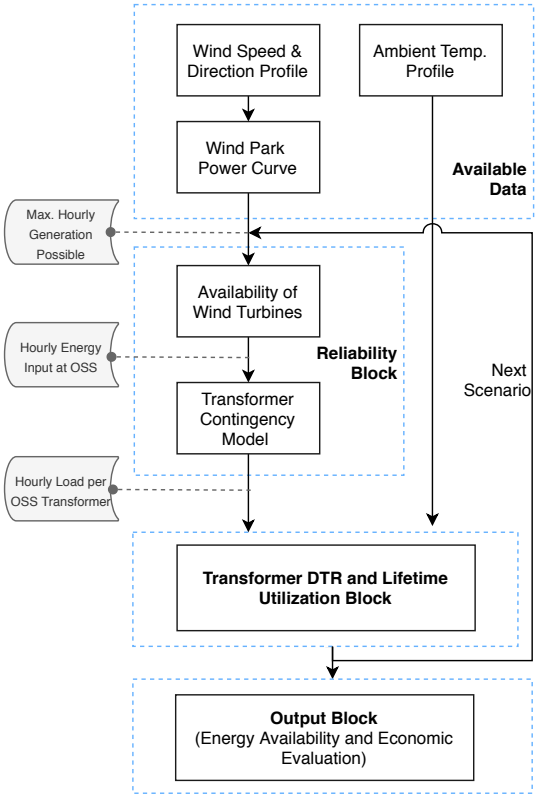

Figure 8.2: Main algorithm for cost-effective dynamic optimization of OWF transformers with reliability and uncertainty considerations

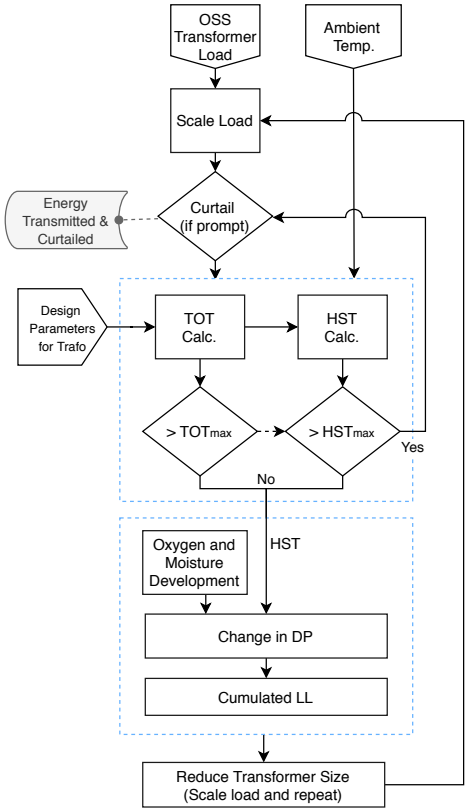

Figure 8.3: Expansion of DTR and lifetime utilization block for the developed methodology

in the insulation increases from 0.5% to 3% in the same manner over the OWF lifetime Π^{WF}. More test cases for oxygen and moisture development are tested in 8.3.4. Finally, another important proposal in this formulation is the use of weighted yearly HST $\vartheta_y^{\mathrm{hst_W}}$ for EL_y calculation because the hourly $\vartheta_t^{\mathrm{hst}}$ varies continuously throughout the year, and utilization of a mean value for HST does not result in appropriate ageing impact. Hence, by using the exponential factors, (8.6) allows calculation of $\vartheta_y^{\mathrm{hst_W}}$ which can accurately model the overall transformer ageing in the respective year. Lastly, it should be noted that the end-of-life criterion of $\mathrm{DP_{start}} = 1000$ and $\mathrm{DP_{end}} = 200$ is used.

$$\mathrm{LL}_{\Pi^{\mathrm{WF}}} = \sum_{y=1}^{\Pi^{\mathrm{WF}}} \mathrm{LL}_y = \sum_{y=1}^{\Pi^{\mathrm{WF}}} \frac{1}{\mathrm{EL}_y} \quad \frac{[\text{years}]}{[\text{years}]} \times 100 \quad [\%] \tag{8.4}$$

$$\mathrm{EL}_y = -\frac{\frac{1}{1000} - \frac{1}{200}}{A_y \times 24 \times 365} e^{\frac{E_{a\,y}}{R_g\,(\vartheta_y^{\mathrm{hst_W}} + 273)}} \quad [\text{years}] \tag{8.5}$$

$$\vartheta_y^{\mathrm{hst_W}} = \frac{1}{-\frac{R_g}{E_{a\,y}}\, ln \frac{\sum_{t=1}^{8760} e^{-\frac{E_{a\,y}}{R_g[\vartheta_t^{\mathrm{hst}} + 273]}}}{8760}} - 273 \quad [^{\circ}C] \tag{8.6}$$

- **Output Block:** The final block is responsible for compiling the results from economic and lifetime assessment. The values for CAPEX, revenue loss due to curtailment and losses over the OWF lifetime and transformer's yearly loss-of-life are stored, while the appropriate test case that results in the best business is taken forward. It must be mentioned that the variation in transformer rating and winding

temperature results in the change in load and no-load losses, which are modelled using the parameters in Table 8.1 and the principles elaborated in Publication **[Pub. J2]**.

8.2.1 Overview of Simulated Scenarios

Offshore windfarm design is an iterative process, particularly when optimization of cost and system design is desired. The developed mechanism takes care of the large degree of uncertainty through scenario generation of wind speed, windfarm availability and transformer contingency. The examples for the first two have been provided in the respective sections before, but the DTMC-based simulation of transformer availability is dependent on the system topology. Furthermore, the two design concepts of *n-1 contingency* and *non-contingent* designs require distinctive elaboration of this step.

For this purpose, the transformer reliability survey from [181] has been used to obtain reliability indices for large power transformers in OWFs. The recorded indices including MTTF of 25 years are made more conservative for this design because DTR-based operation tend to load the transformers more rigorously thereby increase the probability of downtime. Hence, MTTR of 10 years (failure rate $\Lambda = 0.1$ fail/year) [12] and MTTR of 73 days (repair rate $\Upsilon = 5$ repairs/year) are conservatively used in this analysis. The four parallel transformers in the test case export system of Fig. 8.1 can have 5 possible states: 4UP, 3UP, 2UP, 1UP and 0UP, if NCCF considerations are used with unlimited repair resources as shown in Table 7.1. The resulting state transition matrix **P** is provided in (8.7) where $\Delta t = 1$ hour ($1/8760$ years), while Fig. 8.4 graphically presents the probability of transition between these states for both the design concepts. It should be mentioned that these probabilities are so low that the chances of having more than one failure at a given instant are extremely low [17].

$$\mathbf{P} = \begin{bmatrix} 1-4\Lambda(\Delta t) & 4\Lambda(\Delta t) & 0 & 0 & 0 \\ \Upsilon(\Delta t) & 1-(\Upsilon+3\Lambda)(\Delta t) & 3\Lambda(\Delta t) & 0 & 0 \\ 0 & 2\Upsilon(\Delta t) & 1-(2\Upsilon+2\Lambda)(\Delta t) & 2\Lambda(\Delta t) & 0 \\ 0 & 0 & 3\Upsilon(\Delta t) & 1-(3\Upsilon+\Lambda)(\Delta t) & \Lambda(\Delta t) \\ 0 & 0 & 0 & 4\Upsilon(\Delta t) & 1-4\Upsilon(\Delta t) \end{bmatrix} \tag{8.7}$$

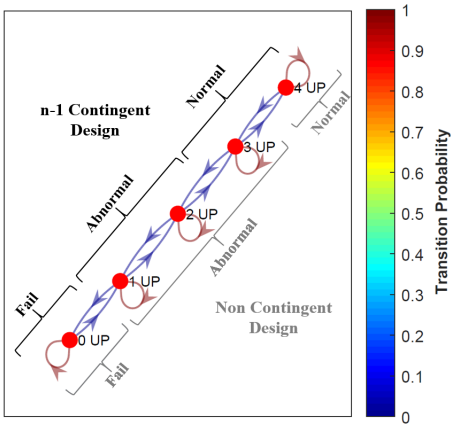

Figure 8.4: DTMC-based state transition diagram and probability of transition between states for the four transformer OWF test case. Classification of states in Normal, Abnormal and Fail states for the two design concepts.

It is important to consider that for the 1200 MW test case windfarm with four transformers, the *n-1 contingency* design would employ a base transformer size of 400 MVA, while the *non contingent* design would conventionally use 300 MVA transformers. The scaling of transformer load to ensure maximum energy availability of these design concepts will be considerably different. The main differences are highlighted in Table 8.2, including the need for possible energy curtailment and change in transformer losses.

Table 8.2: Influence of design concepts on load scaling for different system states for the four-transformer export system. The explanation for influence of possible curtailment and losses are also provided.

n-1 Contingent Design Concept				Non-Contingent Design Concept			
State Name	State Description	Load Scaling Factor A^{SF}	Total Power Curtailment and Losses	State Name	State Description	Load Scaling Factor A^{SF}	Total Power Curtailment and Losses
4 UP	Low load	0.75	$P_t^{cut} = 0$ $W_t < W_{rated}$	**4 UP**	Rated load	1.0	$P_t^{cut} = 0$ $W_t \leq W_{rated}$
3 UP	n-1 contingency (rated load)	1.0	$P_t^{cut} = 0$ $W_t \leq W_{rated}$	**3 UP**	n-1 contingency (high load)	1.33	P_t^{cut} and W_t calc. by simulation
2 UP	2 transformers share total load	1.5	P_t^{cut} and W_t calc. by simulation	**2 UP**	2 transformers share total load	2.0	P_t^{cut} and W_t calc. by simulation
1 UP	1 transformer supplies total load	3.0	P_t^{cut} and W_t calc. by simulation	**1 UP**	1 transformer supplies total load	4.0	P_t^{cut} and W_t calc. by simulation
0 UP	All transformers offload	0	$P_t^{cut} = P_t^{gen}$ $W_t = 0$	**0 UP**	All transformers offload	0	$P_t^{cut} = P_t^{gen}$ $W_t = 0$

Out of the 100 simulated scenarios, one of the extreme scenarios (with high thermal stress over the entire OWF life and largest number of simulated contingencies) is shown in Fig. 8.5 for the first 15 years of operation. It can be seen that the system reaches the state 3UP (one transformer failure) quite often and even results in 2 simultaneous transformer failures (2UP) for a short duration in Year 8. Furthermore, the distribution of power at different stages of generation and transmission over the entire OWF lifetime is provided using histograms in Fig. 8.6 for the same extreme scenario. The maximum possible generation is multiplied by temporal WTG availability A_t^W to obtain the power entering the OSS. The transformer load over the OWF life for the two design concepts is considerably different as the 300 MVA transformers for *non-contingent* design is found to experience higher load stress compared to the 400 MVA transformers for *n-1 contingent* design, as expected.

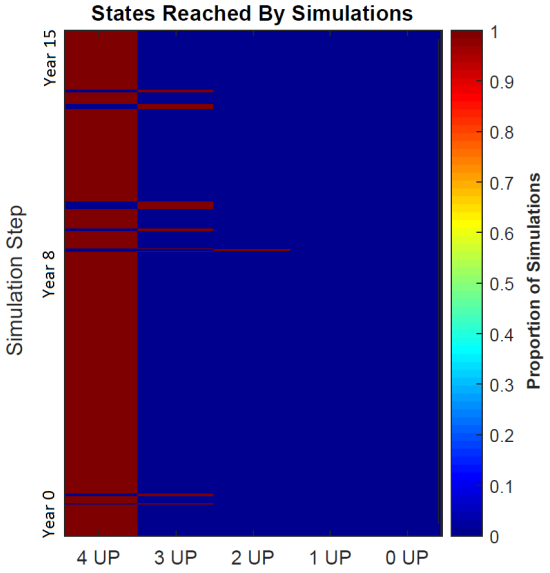

Figure 8.5: Time series for states reached in the first 15 years of simulation for the worst case scenario out of 100 simulated scenarios. A singular 2 transformer failure state (2UP) is briefly observed around the Year8 mark.

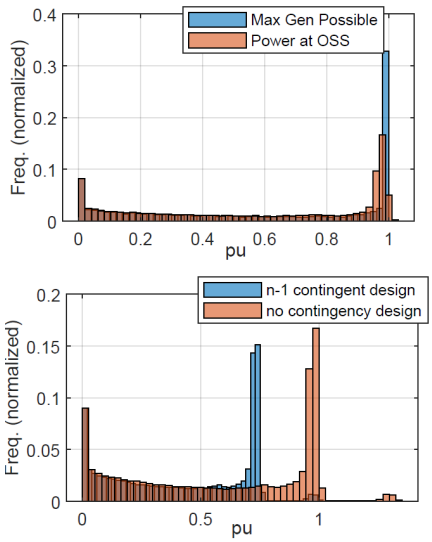

Figure 8.6: Power at different stages along the export system for the worst case scenario of Fig. 8.5 over the OWF lifetime. Top: Simulated wind power (max gen possible) and power after availability of WTGs (power at OSS). Bottom: Transformer loading for the two design concepts.

8.3 Evaluation of the Proposed Framework and Sensitivity Analysis

All the necessary inputs and test case parameters have been defined. In order to run the analysis, a dedicated test machine (i7-9850H 2.6 GHz with 6 cores, 64 GB RAM and 64-bit Windows 10 OS) has been used which performed the complete end-to-end simulations in 5.5 hours. The results from this assessment are summarized below.

8.3.1 Thermal Assessment During Critical Periods

The developed algorithm curtails load when the emergency loading limits of Table 3.4 for HST or TOT are violated. For the worst case scenario of Fig 8.5, transformer load and thermal development for one transformer contingency (3UP) event of Year 13 is shown for the base transformer sizes in Fig. 8.7. As one of the transformer fails in August and November, the additional load is passed through the remaining transformers which result in higher HST and TOT during these periods. However, even during this period the thermal stress is far from the defined limits and no curtailment is seen for *n-1 contingent design*. For the *n-1 contingent* design with 300 MVA base transformer rating, some curtailment is needed during the contingency in November because HST touches the 140 °C limit. The transformer load and temperature development during the high thermal stress period of 2UP state is provided in the Appendix. The overall HST distribution for different transformer sizes over the OWF lifetime for the *n-1 contingent* is provided in histograms of Fig. 8.8.

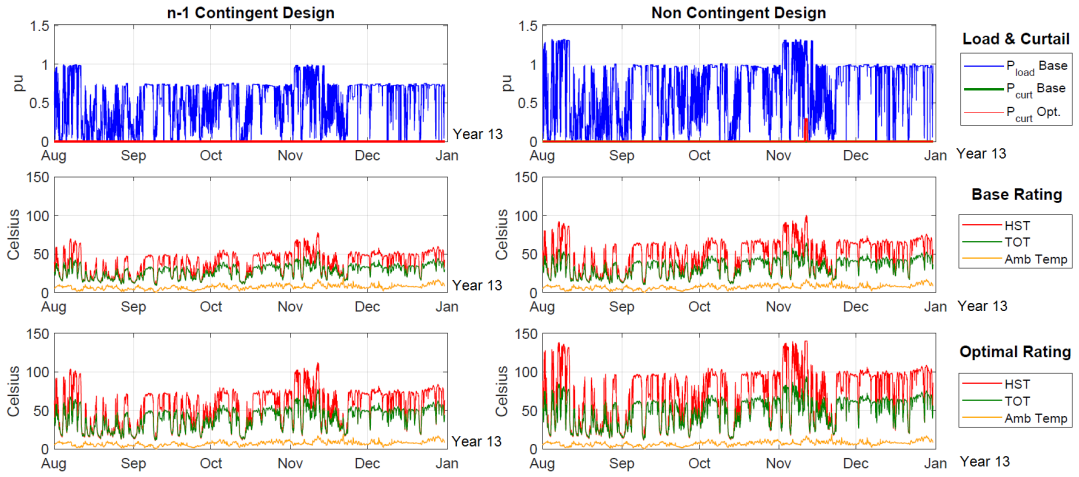

Figure 8.7: Transformer load and thermal performance during one transformer failure (3UP) state in Year 13 for the scenario in Fig. 8.5. Top: transformer load, curtailed power for the base and optimal transformer rating cases. Thermal development for base (middle) and optimal (bottom) ratings.

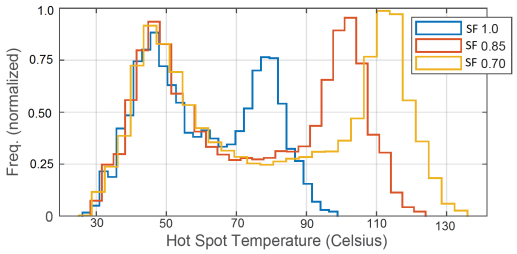

Figure 8.8: Distribution of HST over for 30 years of simulated operation for different transformer ratings for the test case OWF. Only *n-1 contingent* design case is presented.

8.3.2 Transformer Lifetime Utilization for Size Optimization

Fig. 8.9 provides the cumulative lifetime utilization of different transformer ratings over the OWF operational life of 30 years for the worst case scenario. Highest thermal stress resulting in highest weighted average HST (HSTw), highest DP reduction and highest lifetime utilization is observed in 2 different years over the entire lifetime. These years coincide with long-contingency periods and are found to make use of transformer DTR efficiently. Referring to Fig. 8.10, HSTw and cumulative LL at the end of OWF life are analysed for different transformer sizes for the two design concepts. Based on this analysis it can be concluded that transformer

size reduction to 70% of the base capacity is possible for the *n-1 contingent* design and up to 90% for the *non-contingent* design case.

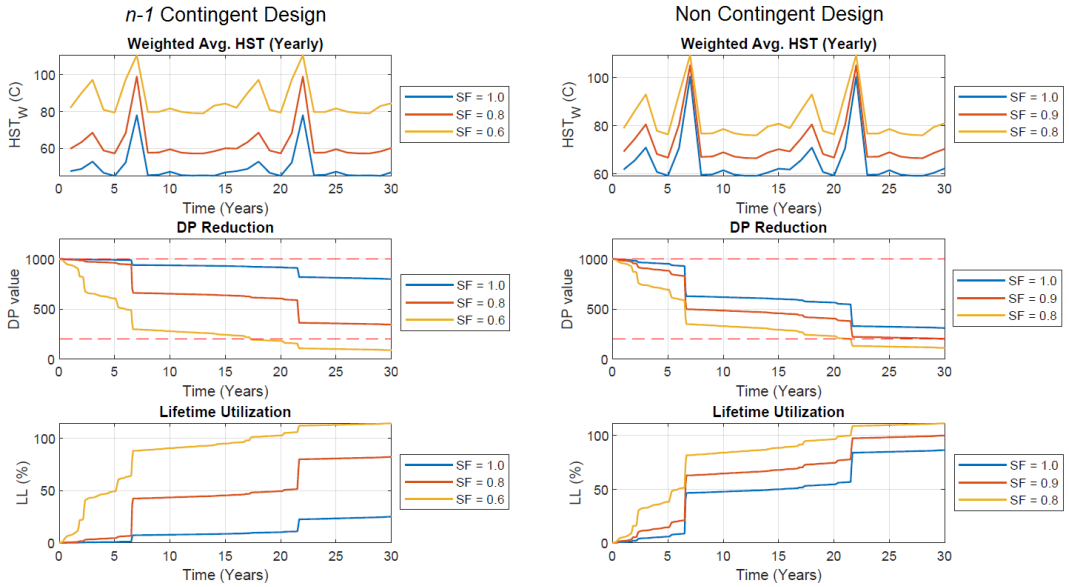

Figure 8.9: Assessment of transformer lifetime utilization over 30 years of operation for the chosen worst case scenario for different transformer ratings. Top: Yearly weighted HST, Middle: Yearly change in degree of polymerization. Bottom: Cumulative yearly loss-of-life (100 % means transformer should be discarded).

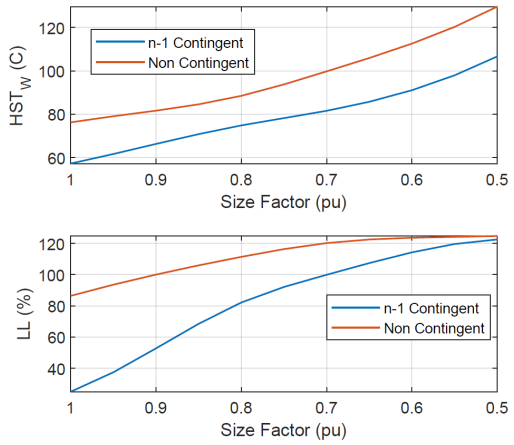

Figure 8.10: Influence of transformer size reduction on utilization for the two design concepts. Top: weighted hot spot temperature over 30 years of operation. Bottom: cumulative loss-of-life after 30 years of operation.

8.3.3 Economic Evaluation for Optimal Transformer Rating

The analysis so far has revealed that the transformer rating can be reduced significantly while complying with OWF's lifetime requirements. However, a business case assessment is still needed which accounts for revenue loss due to additional losses and possible energy curtailment. Therefore total energy curtailment $E_{\text{curt},\,k} = \sum_{t\in\mathcal{T}} \frac{P^{\text{cut}}_{t,k}}{P^{\text{gen}}_{t}}$, losses $E_{\text{loss},\,k} = \sum_{t\in\mathcal{T}} \frac{W^{\text{exp}}_{t,k}}{P^{\text{gen}}_{t}}$ and total energy delivered $E_{\text{del},\,k}$ in (8.8) for each transformer rating $k \in \mathcal{K}$ are plotted in 8.11 for the two design concepts, along with the change in NPV (ΔNPV) for the worst case scenario out of the 100 scenarios. For the given test case under worst-case scenario, the total NPV increase can optimally be around 5 M€ if transformer size is reduced to 85% of its base rating for the *n-1*

contingency case which exhibits a positive business case upto 65% of the base rating. The *non-contingent* design results in minor reduction as both losses and energy curtailment increase dramatically below 85% transformer capacity of its base rating. On average, the 100 scenarios result in NPV increment of 7.6 M€ at 75% of the base size for the *n-1 contingent* design concept and 1.5 M€ at 85% of the base size for the other.

$$E_{\text{del},\,k} = \sum_{y=1}^{\Pi^{\text{WF}}} \sum_{t=1}^{8760} \left(\frac{P_{t,y}^{\text{gen}} - P_{t,y,k}^{\text{cut}} + W_{t,y,k}^{\text{exp}}}{P_{t,y}^{\text{gen}}} \right) \qquad \forall k \in \mathcal{K} \tag{8.8}$$

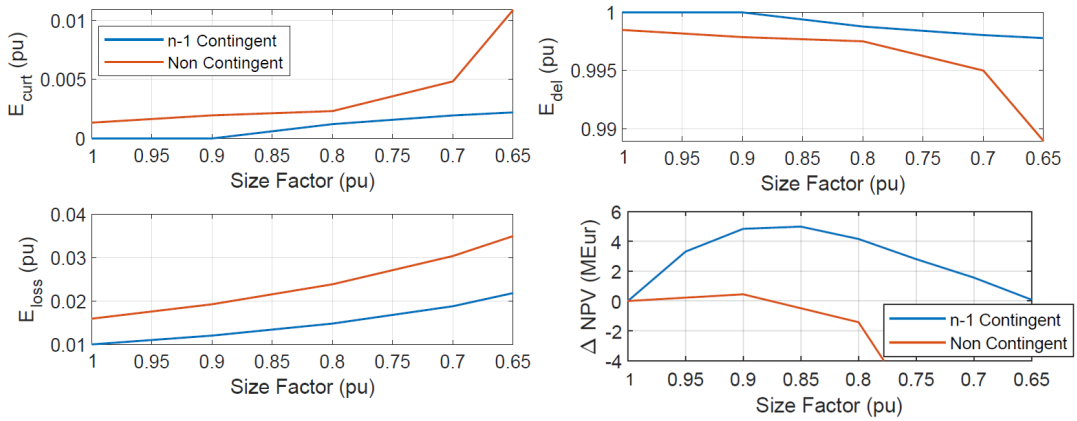

Figure 8.11: Transformer size reduction impact on cumulative energy curtailment E_{curt}, energy losses E_{loss}, cumulative delivered energy E_{curt} and change in NPV over the OWF lifetime for the two design concepts. Per unit valuation is used for conventional *n-1 contingent* design concept transformer size (400 MVA) as base.

8.3.4 Sensitivity to Oxygen and Moisture Variation over Transformer Lifetime

The development of oxygen and moisture over the transformer operational life has been defined conservatively for the simulations so far. Under poor quality standards, the chemical decomposition will be worse as both oxygen and moisture content may vary considerably more than the conservative assumptions, as previously shown in Fig. 4.5. To generalize the applicability of this methodology and assess its sensitivity to different manufacturing standards in the algorithm of Fig. 8.3, two additional test cases of oxygen and moisture development besides the originally tested 'Conservative' case are defined in Table 8.3.

Table 8.3: Three test cases for development of oxygen (in oil) and moisture (in paper) over 30 years of transformer operation.

Scenario	**Moisture (%)**		**Oxygen (ppm)**	
	Initial	Final	Initial	Final
Conservative	0.5	3	2000	7000
High Moisture	2	5	2000	7000
High Oxygen	0.5	3	20000	40000

The average expected transformer lifetime for the simulated scenarios are compiled in Fig. 8.12 for the high oxygen, high moisture and the originally tested conventional test case. As expected, the influence of oxygen content in oil on thermal ageing of transformer insulation paper is found to be more extravagant than the influence of high moisture in paper. The conservative test case results in expected lifetime of more than 30 years for all the shown transformer sizes, but the remaining two cases the room for transformer optimization is minimum as minor change in size results in sudden drop in the expected lifetime.

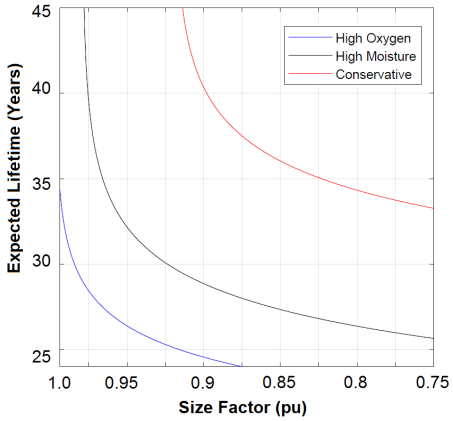

Figure 8.12: Expected transformer lifetime for the *n-1 contingent* design concept for the three test cases (conservative, high moisture, high oxygen) for different transformer ratings.

8.3.5 Sensitivity to OWF Capacity Factor and Ambient Temperature

The developed methodology is found to be driven by the loading characteristics of the transformer and its ambient circumstances. Therefore, the entire process is repeated for two more actual test case windfarms **(OWF A and OWF B)** located in substantially different environments at the opposite ends of the globe. The 15 years of site data available for **OWF A** shows consistently low ambient temperature and low capacity factor 41.4% (meaning wind generation is less consistent), while **OWF B** with 12 years of available site data shows much higher ambient temperature distribution and consistent generation with high capacity factor of 48.7%. The distribution of ambient temperatures for the two test sites are provided in Fig. 8.13.

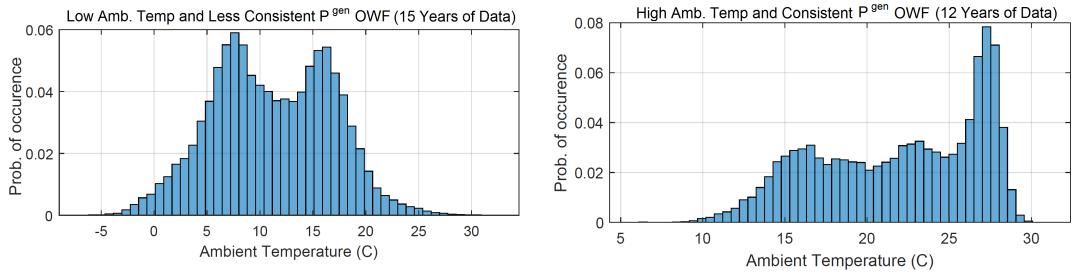

Figure 8.13: Histograms for ambient temperature distribution for **OWF A** (left) and **OWF B** (right)

For **OWF A** (Low ambient temp and less consistent P^{gen}), both the generation and temperature profiles are found to be more favorable for transformer optimization than **OWF B** (High ambient temp and consistent P^{gen}). This is shown in Fig. 8.14, where the respective transformers are found to last more than 40 years of operation under the worst scenario, even if the base size for **OWF A** is decreased by 27.8 % (180 to 130 MVA), while **OWF B** shows the potential of 14% reduction from the base size only (360 to 310 MVA). The business case assessment performed in Fig. 8.15 using the same cost of wind energy shows that despite being much smaller in size, **OWF A** achieves a higher NPV increase than **OWF B** if the OSS transformer ratings for the respective windfarms is changed to the identified optimal size. This assessment proves that the developed methodology is susceptible to site characteristics and individual assessment should be performed for each for identifying its OSS transformers' optimal size reduction potential.

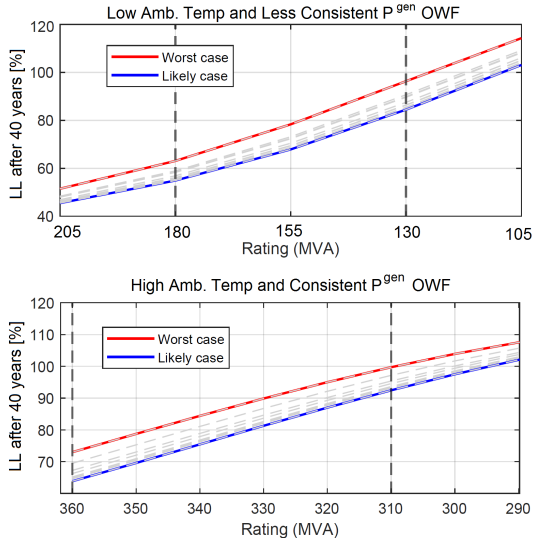

Figure 8.14: Transformer cumulative lifetime utilization after 40 years of operation using different OSS transformer ratings for **OWF A** (top) and **OWF B** (bottom)

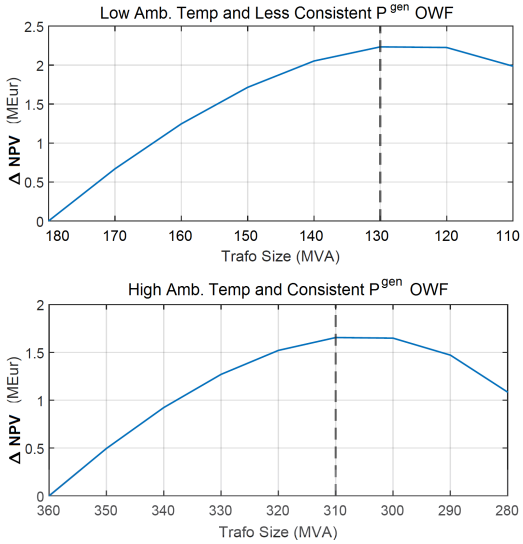

Figure 8.15: NPV change after 30 years of production using different OSS transformer ratings for **OWF A** (top) and **OWF B** (bottom)

CHAPTER 9

Export System Design Optimization using a DTR-based, Multi-Stage, Stochastic Investment Decision Tool

The problems and algorithms presented so far have focused on optimization of OSS transformer rating primarily because over the course of this project it was deduced that offshore substations offer the largest room for cost-effective optimization. On the other hand, the topics of DTR-based optimal sizing and design of HV export cables for OWFs have been addressed in detail in the literature [24–26]. Based on this discussion, the missing piece of the puzzle would be dynamic optimization of the entire export system by using DTR for network analysis. In this section, a comprehensive two-stage optimization framework has been developed which uses DTR for design of all the major HV components of OWF export system and can be used as an investment decision tool for OWF sizing. Detailed description of the developed tool and the analysis of the identified test case are discussed in detail in this section, which is based on the publication **[Pub. J3]** by the author.

9.1 Problem Overview and Schematic Description

The two-stage stochastic optimization problem proposed in this project optimizes the design of offshore windfarm export system using dynamic rating and electro-thermal coordination of all the relevant HV components. The goal of the proposed methodology is to use DTR-based operation to find the optimal windfarm size and design ratings of export system components that result in highest NPV, while accounting for CAPEX at year '0' and operating costs due to higher losses and possible curtailment over the entire windfarm lifetime. Reliability and uncertainty considerations are key features of this problem. The overview of the novel framework is shown using the schematic representation of Fig. 9.1, which is based on the following four basic steps:

- **Step 1: Pre-selection of relevant candidate design cases** $\mathcal{K}$. These design cases include unique combinations of transformer, shunt reactor and export cable ratings which are chosen based on the windfarm size window, topology of the export system and other predefined parameters.
- **Step 2: Generation of hourly scenarios** $\mathcal{S}$ **for uncertainty and reliability considerations**. This step is necessary to generate the load profile for individual components in the OWF export system over the entire lifetime. It accounts for stochasticity of the OWF site's wind speed using ARIMA-based trend analysis of long-term historic site data (incl. wind speed and direction profiles) from Section 7.1. Furthermore, temporal stochastic availability of turbines in the windfarm (Section 7.2) and availability of HV components in the export system (Section 7.3) are also accounted for as possible failures and contingency conditions are pre-simulated based on component reliability indices Λ and Υ [1/hr]. In

contrast to the discussion in the previous section, these indices are to be calculated for the entire export system circuit. Hence individual values for subsea cables, transformers and shunt reactors connected in series are used as shown in (9.1) and (9.2) [175].

$$\Lambda = \Lambda^{\mathrm{c}} + \Lambda^{\mathrm{trf}} + \Lambda^{\mathrm{SR}} \tag{9.1}$$

$$\Upsilon = \Upsilon^{\mathrm{c}} + \Upsilon^{\mathrm{trf}} + \Upsilon^{\mathrm{SR}} \tag{9.2}$$

- **Step 3: Solution of the two-stage optimization problem over the OWF lifetime**. This step is solved separately for all the pre-selected design cases. All the decision variables are stored, while only the two main decision variables including NPV and windfarm size (represented by number of WTGs n^{tur}) are considered for the next step.
- **Step 4: Selection of the optimal design case.** Out of all the pre-selected design cases, the one which results in highest NPV is selected.

The first two steps are responsible for generating the inputs for the optimization problem, which are shown by the grey dotted lines in Fig. 9.1. Hence, as a result of these steps, component costs, ratings and thermal parameters for each design case along with multiple scenarios of OWF site's temporal wind speed and availability over the entire OWF lifetime are readily available for the optimization framework. Since, the ratings for HV components are commonly available in discrete steps, design iterations can be used to shortlist relevant design cases in step 1, which can thereby reduce the number of times step 3 is to be run.

The optimization problem in step 3 maximizes the windfarm's business case over its lifetime for each of the pre-selected design case, as defined by the objective function. The term 'Cost', which includes all the CAPEX figures for year '0', is assumed to be dependent on design case $k \in \mathcal{K}$ and independent of the generation and availability realizations in scenario $s \in \mathcal{S}$. The 'Revenue' term on the other hand is dependent on both k and s. Besides the investment decision support, the decision variables in the upper level (Stage 1) define the degree of freedom for energy injection over the windfarm design lifetime by determining the optimal wind farm size n^{tur}; whereas yearly utilization of the transformer thermal lifetime is also addressed at this level. On the other hand, the lower level (Stage 1) is responsible for operational scenarios and hourly constraints. The decision variables at this level include component load, critical temperatures of the components, component ageing, system losses and possible energy curtailment.

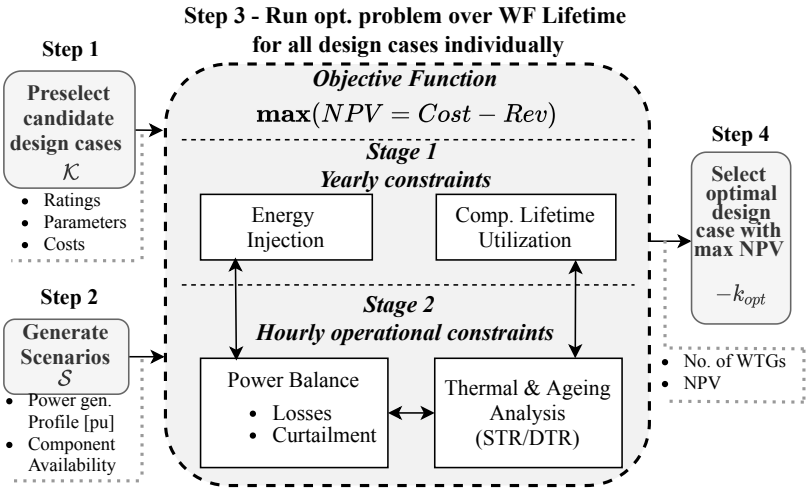

Figure 9.1: Schematic description of the optimization strategy for the novel investment decision support tool for dynamic rating based design of the OWF export system HV components

9.2 Formulation of the DTR-based, Two-Stage Stochastic Optimization Model

9.2.1 Proposed Framework

The novel stochastic optimization problem is compactly formulated in (9.3), where the objective function is followed by the relevant constraints. The problem consists of two-stages: the first stage provides the investment decision support by determining the optimal number of wind turbines n^{tur} for the respective design case, while each of the hourly operational scenarios is modelled in the second stage using the index t. The objective function maximizes the NPV for each design case k as it includes a term for investment/costs at year '0' C_0 and a term for revenue over windfarm lifetime R_s associated with the probability π_s. The first term is dependent on the design case under consideration k, while the latter term depends not only on k, but also on the energy sold to the grid in each scenario s. The problem is developed as a Mixed-Integer Linear Programming model (MILP), as the quadratic and non-linear constraints are resolved using linear inequalities. The model is implemented in MATLAB using the YALMIP toolbox [182] for the high-level problem structure, while GUROBI solver [183] is used for solving the mixed-integer convex optimization problem.

$$\max_{\Xi} \quad \left(\text{NPV}_k = -C_{0\,k} + \sum_{s \in \mathcal{S}} \pi_s R_{s,\,k} \right) \tag{9.3a}$$

$$\begin{aligned}
\text{s.t.} \quad & (9.7), && \text{Wind farm size,} && \\
& (9.8) - (9.12), && \text{Power balance and component load,} && \forall s, \forall t \\
& (9.16) - (9.17), && \text{Losses approximation,} && \forall s, \forall t, \forall j \\
& (9.24) - (9.26), && \text{Thermal dynamics,} && \forall s, \forall t \\
& (9.27) - (9.28), && \text{Ageing dynamics,} && \forall s, \forall t, \forall l, \forall y
\end{aligned}$$

where the decision variables are compiled as a list in Ξ. These variables are described together with the associated constraints in the discussion that follows.

9.2.2 Objective Function

The objective function in (9.3) consists of two main terms. The first term models the total investment cost of the OWF at year '0'. This cost can further be broken down into three sub-costs: cost of all wind turbines $n^{\text{tur}} c^{\text{tur}}$, cost of export system C_k^{exp} and fixed costs C^{fix} covering all the remaining cost functions (incl. development expenses, balance of plant, commissioning, decommissioning etc.), as shown in (9.4). C_k^{exp} is dependent on the preselected design case, while the fixed costs can be assumed to be constant for all the design cases as these are not influenced by minor changes in OWF size and transmission system. On the other hand, since n^{tur} is the only decision variable in C_0 and it defines the size of OWF (plus the power flow in the operational time frame), the output of the optimization problem directly affects the investment decision support.

$$C_0 = n^{\text{tur}} c^{\text{tur}} + C_k^{\text{exp}} + C^{\text{fix}} \tag{9.4}$$

$$\begin{aligned}
C_k^{\text{exp}} = {} & n^{\text{c}} L^{\text{c}} c_k^{\text{c}} + n^{\text{trf}} c_k^{\text{trf}} + n^{\text{SR}} c_k^{\text{SR}} + \\
& 2 c^{\text{oss}} \left(n^{\text{trf}} m_k^{\text{trf}} + n^{\text{SR}} m_k^{\text{SR}} \right)
\end{aligned} \tag{9.5}$$

where the superscripts for turbines (tur), cables (c), transformers (trf) and shunt reactors (SR) are used to classify the number of respective components n and cost functions c [€] (with the exception of cable costs c^{c} [€/km] and weight-dependent costs of OSS/RCS c^{oss} [€/tonne]). Length of cable circuit L^{c} is used to scale the cable costs c^{c}, while respective component masses m [tonnes] are used to scale c^{oss}, which are used to model the total weight-dependent foundation costs for substations.

The second term in the objective function, modelled with R_s, represents the overall revenue stream for each scenario, as shown in (9.6). This revenue is directly dependent on the total yearly injected energy $\sum P^{\text{inj}}$ over

the OWF lifetime $\Pi^{\text{WF}} = \text{length}\,(\mathcal{Y})$ and it is scaled using the yearly weighted factors for NPV calculation, where the windfarm lifetime Π^{WF} is presented in years.

$$R_s = \sum_{y \in \mathcal{Y}} \frac{\gamma}{(1+i)^y} \sum_{t \in \mathcal{T}} P^{\text{inj}}_{t,s} \tag{9.6}$$

where the energy selling price γ [€/MWh] is assumed to be constant over the OWF lifetime, but can be modeled to follow the spot-price market if needed. The discount rate i is used in per-unit, while the respective scenario's injected hourly power $P^{\text{inj}}_{t,s}$ [MW] is the decision variable of the developed problem. In this approach, the computational efforts are preserved by assuming that the yearly revenues which are dependent on the total energy sold to the grid are repeated every year over the OWF lifetime. However, this can easily be remodelled if the right computational resources are available.

9.2.3 Definition of Constraints

Constraints for Wind Farm Size

The number of turbines n^{tur}, which is a decision variable in the first stage, determines the size of the windfarm. This variable is limited between the minimum $\underline{n^{\text{tur}}}$ and maximum $\overline{n^{\text{tur}}}$ number of turbines that can be installed in the project.

$$\underline{n^{\text{tur}}} \leq n^{\text{tur}} \leq \overline{n^{\text{tur}}} \tag{9.7}$$

Constraints for Power Balance and Component Load

The power balance in the system for each operational hour is ensured by the constraints (9.8) - (9.9), while the hourly generated wind energy $P^{\text{gen}}_{t,s}$ [MW] from the OWF is calculated as a function of the realized Availability of wind turbines $A^{\text{w}}_{t,s}$ for each scenario [pu] and the realized per-unit OWF generation profile $P^{\text{w}}_{t,s}$ for the respective scenario.

$$P^{\text{gen}}_{t,s} - P^{\text{cut}}_{t,s} - A^{\text{c}}_{t,s}\left(W^{\text{c}}_{t,s} + 2W^{\text{trf}}_{t,s} + W^{\text{SR}}\right) - P^{\text{inj}}_{t,s} = 0 \tag{9.8}$$

$$0 \leq P^{\text{cut}}_{t,s} \leq P^{\text{gen}}_{t,s} \tag{9.9}$$

$$P^{\text{gen}}_{t,s} = A^{\text{w}}_{t,s} P^{\text{w}}_{t,s} S^{\text{tur}} n^{\text{tur}} \tag{9.10}$$

where the hourly power curtailed $P^{\text{cut}}_{t,s}$ and injected $P^{\text{inj}}_{t,s}$ are decision variables calculated in MW. While the hourly load dependent losses [MW] for transformers, cables and shunt reactors, represented by $W^{\text{c}}_{t,s}$, $W^{\text{trf}}_{t,s}$ and $W^{\text{SR}}_{t,s}$ respectively, are also the decision variables. The remaining parameters including number of available circuits for each operational hour in each scenario $A^{\text{c}}_{t,s}$ [pu] (to consider contingency of the export system components) and the rating of WTG S^{tur} [MW] are predefined during the scenario generation and pre-design phases respectively.

For each scenario, the calculation of hourly load current for cables $I^{\text{c}}_{t,s}$ and transformers HV side $I^{\text{trf}}_{t,s}$ in [A] is performed using the Kirchhoff's current law, as shown in (9.11)-(9.12). The S^{trf}_{rated} and I^{trf}_{rated} representing transformer MVA rating and rated HV-side current [A] respectively are known for each design case, while the line-to-line voltage of the transmission system V_{ll} is defined in advance. It must be mentioned that this formulation only presents the DTR design mechanism, therefore neither $I^{\text{c}}_{t,s}$ nor $I^{\text{trf}}_{t,s}$ is constrained here. It must be mentioned that this formulation only works when there is at least one circuit available $A^{\text{c}} \geq 1$, which is the most probable scenario for systems with low failure probabilities [14].

$$I^{\text{c}}_{\text{P}\,t,s} = \frac{1}{A^{\text{c}}_{t,s}} \frac{(P^{\text{gen}}_{t,s} - P^{\text{cut}}_{t,s})}{\sqrt{3}V_{ll}} \tag{9.11}$$

$$I^{\text{trf}}_{t,s} = \frac{1}{2A^{\text{c}}_{t,s}} \frac{(P^{\text{gen}}_{t,s} - P^{\text{cut}}_{t,s})}{S^{\text{trf}}_{rated}} I^{\text{trf}}_{rated} \tag{9.12}$$

Losses Approximation using Linear Inequality Constraints

The losses are quadratically related to the load current. In order to evaluate the losses over the entire length of HV export cables, (2.17) is used and total cable losses over the entire length L^{c} are simply calculated as $W^{\mathrm{c}}_{t,s} = W^{\mathrm{tot\,c}}_{t,s} L^{\mathrm{c}}$, where $W^{\mathrm{tot\,c}}_{t,s}$ are losses per unit length [W/m], as explained in Section 2.3.2. However, as discussed in Section 2.3.3, the cable current I^{c} is not only dependent on the load but it also varies along the cable length due to capacitive charging. For the topologies considered in this project, the capacitive charging current peaks at the offshore, onshore and reactive compensation substations. The load dependent current component $I^{\mathrm{c}}_{\mathrm{P}\,t,s}$ [A] is time-variant and depends on the realized scenario, while the peak charging current $I^{\mathrm{c}}_{\mathrm{Q}}$ [A] is treated as constant for each design case as it depends on the capacitance of the cable design. For estimation of cable losses, utilization of peak charging current $I^{\mathrm{c}}_{\mathrm{Q}}$ can overestimate these losses by up to 100 % [96]. Therefore the formulation of second approximation proposed in [13] is used in this project, and the resulting equation is provided in (9.13). In this formulation, the total cable resistance over the entire length r^{c} is calculated conservatively at 90 °C using (9.14), the dielectric losses W^{c}_{d} [W/m] are cable design dependent, while the armor and screen loss factors (λ_a and λ_s) are treated as constants

$$W^{\mathrm{c}}_{t,s} = 3r^{\mathrm{c}} \left(I^{\mathrm{c}^2}_{\mathrm{P}\,t,s} + \frac{1}{2} I^{\mathrm{c}^2}_{\mathrm{Q}} \right) + W^{\mathrm{c}}_{d} L^{\mathrm{c}} \tag{9.13}$$

$$r^{\mathrm{c}} = (1 + \lambda_a + \lambda_s) r'^{\mathrm{c}}_{ac} L^{\mathrm{c}} \tag{9.14}$$

The losses in OSS transformers, on the other hand, are calculated by the HV side referred current $I^{\mathrm{trf}}_{t,s}$ [A] in (9.15). In this formulation, the design-dependent transformer winding resistance referred to the HV side r^{trf} [Ω] is treated as constant and defined conservatively at 110 °C, while the design-dependent no load losses W^{trf}_{nl} [W] are time-invariant as well. The losses in shunt reactors are calculated in the same manner.

$$W^{\mathrm{trf}}_{t,s} = 3r^{\mathrm{trf}} I^{\mathrm{trf}^2}_{t,s} + W^{\mathrm{trf}}_{nl} \tag{9.15}$$

The discussion so far reveals that the quadratic relation between losses need to be simplified to prevent the MILP problem from becoming mixed-integer quadratic constrained. Therefore, convexity and linearity of the problem is preserved by using piecewise linear approximation of losses with respect to the currents. The losses $W^{\mathrm{c}}, W^{\mathrm{trf}}$ are expressed as sets of $j \in \mathcal{J}$ linear inequality constraints related to currents I^{c} and I^{trf} with slope p and intercept q in (9.16)-(9.19), where the intercept term q_j is responsible to account for no-load losses. This process has been explained in detail in Section 6.1.2.

$$W^{\mathrm{c}}_{t,s} \geq p^{\mathrm{c}}_{j} I^{\mathrm{c}}_{\mathrm{P}\,t,s} + q^{\mathrm{c}}_{j} \tag{9.16}$$

$$W^{\mathrm{trf}}_{t,s} \geq p^{\mathrm{trf}}_{j} I^{\mathrm{trf}}_{t,s} + q^{\mathrm{trf}}_{j} \tag{9.17}$$

$$q^{\mathrm{c}}_{j} = q^{\mathrm{c}}_{j0} + \frac{3}{2} I^{\mathrm{c}^2}_{Q} r^{\mathrm{c}} + W^{\mathrm{c}}_{d} L^{\mathrm{c}} \tag{9.18}$$

$$q^{\mathrm{trf}}_{j} = q^{\mathrm{trf}}_{j0} + W^{\mathrm{trf}}_{nl} \tag{9.19}$$

Constraints for Thermal Dynamics of Components

The development of cable conductor temperature $\vartheta^{\mathrm{c}}_{t,s}$ and transformer hot-spot $\vartheta^{\mathrm{hst}}_{t,s}$ and top-oil temperatures $\vartheta^{\mathrm{tot}}_{t,s}$ over each operational hour is calculated by reformulating (2.20)-(2.21) and (2.10), as shown in (9.20)-(9.23). The reformulation is key because it makes use of the losses calculated in (9.13) and (9.15) to remove the quadratic current constraints from these equations. In this way the thermodynamic constraints for both cables and transformers are linearized and the limits for these critical temperature constraints are defined in (9.24)-(9.26), where ϑ^{sea} is the nominal sea-bed temperature.

The limits are defined such that overall cable temperature rise is limited conservatively to $\overline{\vartheta^{\mathrm{c}}} = 90°\mathrm{C}$, while the emergency loading limits from Table 3.4 are used for transformers with $\overline{\vartheta^{\mathrm{top}}} = 115°\mathrm{C}$ and $\overline{\vartheta^{\mathrm{hst}}} = 140°\mathrm{C}$.

$$\vartheta^{\text{serv}}_{t,s} = a_1 \vartheta^{\text{serv}}_{t-1,s} + a_2 \vartheta^{\text{c}}_{t,s} \tag{9.20}$$

$$\vartheta^{\text{c}}_{t,s} = \frac{1}{a_3}\left(a_4 \vartheta^{\text{c}}_{t-1,s} + a_5 \vartheta^{\text{serv}}_{t-1,s} + \frac{a_6}{L^{\text{c}}} W^{\text{c}}_{t,s}\right) \tag{9.21}$$

$$\vartheta^{\text{tot}}_{t,s} = b_1\left(\frac{W^{\text{trf}}_{t,s} - W^{\text{trf}}_{nl}}{3r^{\text{trf}} I^{\text{trf2}}_{rated}}\right) + b_2 \vartheta^{\text{amb}}_{t,s} + b_3 \vartheta^{\text{tot}}_{t-1,s} + b_4 \tag{9.22}$$

$$\vartheta^{\text{hst}}_{t,s} = \vartheta^{\text{tot}}_{t,s} + \vartheta_{\text{hr}}\left(\frac{W^{\text{trf}}_{t,s} - W^{\text{trf}}_{nl}}{3r^{\text{trf}} I^{\text{trf2}}_{rated}}\right) \tag{9.23}$$

$$\vartheta^{\text{c}}_{t,s} \leq \overline{\vartheta^{\text{c}}} - \vartheta^{\text{sea}} \tag{9.24}$$

$$\vartheta^{\text{top}}_{t,s} \leq \overline{\vartheta^{\text{top}}} \tag{9.25}$$

$$\vartheta^{\text{hst}}_{t,s} \leq \overline{\vartheta^{\text{hst}}} \tag{9.26}$$

Constraints for Ageing Dynamics of Transformers

Building upon the formulation of DTR^{+} design mechanism of Section 6, the reliability of transformer design is ensured by tracking and limiting the overall transformer lifetime utilization. This is done by constraining the yearly cumulative loss-of-life $\lambda_{y,s}$ for each of the simulated scenario to rated value of $\overline{\lambda} = 8760 \times 17.12/\Pi^{\text{WF}}$, as shown in (9.28). The design lifetime of the OWF Π^{WF} [yr] and rated design lifetime of the transformer (17.12 years) at constant $\vartheta^{\text{hst}}_{rated}$ as per [45] are used here. As discussed earlier in Section 6.1.2, the convexity of the problem is preserved by linearizing the exponential function for transformer ageing calculation in (4.1) by using sets of $l \in \mathcal{L}$ linear inequality constraints with slope p and intercept q, as shown in (9.27).

$$\Delta\lambda_{t,s} \geq p_l \vartheta^{\text{hst}}_{t,s} + q_l \tag{9.27}$$

$$\lambda_{y,s} = \sum_{t \in \mathcal{T}} \Delta\lambda_{t,s} \leq \overline{\lambda} \tag{9.28}$$

9.3 Test Case of a Large OWF with Three Parallel Circuits

In order to demonstrate the applicability of the proposed methodology, the design of an actual windfarm off the east coast of UK has been used, as shown in Fig. 9.2. There are three interlinked parallel circuits in the test case OWF, with each circuit comprising of one 100 km long 3-core XLPE insulated subsea cable with copper conductor and two parallel 66/220 kV transformers. For reactive compensation at the midpoint of the export cable, one three-phase shunt reactor is placed in the Reactive Compensation Station (RCS) per circuit. Hence, the total components in the considered export system spread across three OSS and one RCS are $n^{\text{trf}} = 6$, $n^{\text{SR}} = 3$ and $n^{\text{c}} = 3$. The design lifetime of this test case is set to $\Pi^{\text{WF}} = 30$ years. For uncertainty and reliability induction, a total $\mathcal{S} = 30$ scenarios with unique time series of P^{w}, WT availability A^{w} and number of available export circuits A^{c}_t have been simulated using the principles of Section 7 for duration of $\mathcal{T} = 8760$ hr (1 year) each.

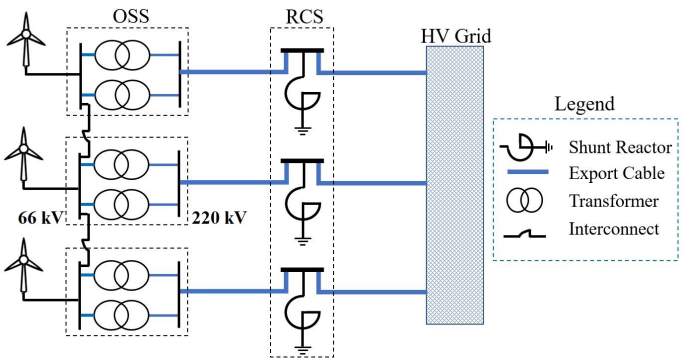

Figure 9.2: Simplified HV export system layout for the 1200 MW test case offshore windfarm (excl. Onhore Substation)

9.3.1 Constraints for Base Case with STR (Base$_{\text{STR}}$)

The developed algorithm uses coordinated DTR for all the relevant HV components in the export system. In order to benchmark the results with respect to conventional practices based on Static Thermal Rating (STR), the base test case has been run with STR and the results are compiled in Base$_{\text{STR}}$. The constraints in (9.3) have to be updated for the Base$_{\text{STR}}$ test case. The main changes include discarding constraints (9.24)-(9.28) because neither component thermal dynamics nor ageing dynamics are relevant for STR operation. On the other hand, some additional constraints are introduced, as shown in (9.29)-(9.31). The windfarm size for the Base$_{\text{STR}}$ is rated to its original size of 1197 MW ($n^{\text{tur}}_{base} = 171$, $S^{\text{tur}} = 7$ MW), while the components are rated as 250 MVA OSS transformers and 1600 mm^2 cables and the load I in (9.11)-(9.12) are constrained to 1 pu.

$$n^{\text{tur}}_{k} = n^{\text{tur}}_{base} \qquad \forall k \in \mathcal{K}_{\text{Base}_{\text{STR}}} \tag{9.29}$$

$$I^{\text{c}}_{t,s,k} \leq I^{\text{c}}_{rated} \qquad \forall k \in \mathcal{K}_{\text{Base}_{\text{STR}}}, \quad \forall s \in \mathcal{S}, \quad \forall t \in \mathcal{T} \tag{9.30}$$

$$I^{\text{trf}}_{t,s,k} \leq I^{\text{trf}}_{rated} \qquad \forall k \in \mathcal{K}_{\text{Base}_{\text{STR}}}, \quad \forall s \in \mathcal{S}, \quad \forall t \in \mathcal{T} \tag{9.31}$$

9.3.2 Pre-selected Design Cases for DTR Test Cases

For the DTR methodology in (9.3), a total of 20 candidate design cases (5 transformer ratings and 4 cable sizes) are considered, the relevant parameters for which are provided in Table 9.1. This analysis is performed by considering the configuration of network, base OWF size and availability of components by manufacturers. Each design case consists of a unique combination of cable and transformer rating, and the 20 candidate designs are classified as $\mathcal{K}$ = {Trafo [MVA], Cable [mm^2]} are considered: {T250, C1600}, {T250, C1400}... {T150, C1000}. For all the DTR test cases, n^{tur} is limited between 143 (1001 MW) and 200 (1400 MW). The mentioned OWF ratings do not include the *power-boost* function, which is considered during the scenario generation process of Section 7.

Table 9.1: Relevant parameters for selected sizes of HV components for candidate design cases

Component	Parameter		Design Cases				
Transformer	S^{trf}_{rated}	[MVA]	**250**	**225**	**200**	**175**	**150**
	r^{trf} at 110C	[Ω]	1.64	2.49	2.98	3.65	4.12
	W^{trf}_{nl}	[kW]	74.14	67.33	61.42	55.63	49.18
Cable	Cond. Size	[mm^2]	**1600**	**1400**	**1200**	**1000**	-
	S^{c}_{rated} (STR)	[MVA]	417	404	387	370	-
	I^{c}_{rated} (STR)	[A]	1095	1060	1016.5	971	-
	r'^{c}_{ac} at 90C	[$\mu\Omega$/m]	16.02	17.31	19.11	21.18	-
	Q^{c}	[μF/km]	0.214	0.201	0.190	0.178	-
Shunt Reactor	S^{SR}_{rated}	[MVAr]	**165**	**152**	**143**	**135**	-

9.3.3 Cost Functions and Relevant Predefined Parameters

The relevant economic parameters are defined as per the latest information available in the literature. The latest CfDstrike price of the 1.2 GW Doggerbank Creyke Beck A offshore windfarm ($\gamma = 44.9$ [€/MWh]) has been used, while the discount rate i is set to 6.75% [1]. The cost for XLPE insulated subsea cables is calculated using (9.33), where nominal voltage dependent coefficients are found to be $g_1 = 1.991 \times 10^6$, $g_2 = 0.5 \times 10^6$ and $g_3 = \sqrt{3}\dfrac{3.16 \times 220}{1 \times 10^6}$ for the 220 kV cable design with Copper conductor [16]. The cost and mass of the oil-filled components (transformer and shunt reactors) are derived empirically, as shown in Section 8 and (8.3) earlier. This is driven by (9.32) for large power transformers, such that Z is replaced by the relevant parameter (c or m) [180]. All of the remaining cost parameters which include c^{tur}, c^{oss} and C^{fix} are derived from [11].

$$Z^{\text{trf,SR}}_{k} = Z_{base}\left(\frac{S^{\text{trf,SR}}_{rated,k}}{S^{\text{trf,SR}}_{base}}\right)^{3/4} \tag{9.32}$$

$$c^{\text{c}}_{k} = L^{c}\left(g_1 + g_2\, e^{g_3 I^{c2}_{rated,k}}\right) \tag{9.33}$$

9.4 Performance Evaluation using Economic and Efficiency Analysis

In order to highlight the benefits of the proposed methodology, the optimization problem is first allowed to run for the {T250, C1600} design case with STR constraints and the results are recorded in Base_{STR}. Afterwards, the originally proposed optimization framework is solved for all the 20 design cases in $\mathcal{K}$, as specified in Table 9.1. Out of these DTR test cases, the first design is similar to the Base_{STR} case ({T250, C1600}), which is why this design case is referred to as Base_{DTR} from this point onward. Base_{DTR} design case implies using the same infrastructure as the base case and applies DTR to optimize utilization of components over the OWF lifetime while optimizing the OWF size. Out of the 20 design cases, the design case that results in the highest NPV is termed as 'Optimal' in the discussion that follows.

9.4.1 Economic Assessment and Efficiency of Transmission

First and foremost, the Optimal design case is identified by calculating the NPV for the 20 design cases. The results are recorded in Fig. 9.3, where the change in NPV with respect to the Base_{STR} test case ($\Delta\text{NPV}_k = \text{NPV}_k - \text{NPV}_{\text{Base}_{\text{STR}}}$) is recorded, along with the optimal number of turbines n^{tur} for each design case. The results reveal that by merely considering DTR for the same infrastructure, the NPV increases by 327 M€ for Base_{DTR}, while the optimal n^{tur} are set to their max value of 200 compared to 171 for Base_{STR}. It is further shown in Fig. 9.3 that the design case {T200, C1400} (Optimal) results in the highest NPV increase, which is 51 M€ higher than Base_{DTR}. The Optimal design case employs 191 turbines, but still gives out the best business case. It is important to mention that a number of tested design cases result in negative NPV change (which suggests a poor business case compared to Base_{STR}), because of higher energy losses and higher curtailment needed due to transmission bottlenecks.

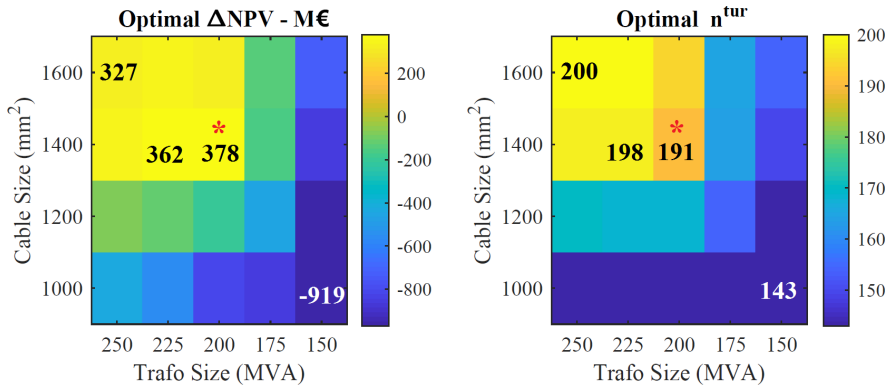

Figure 9.3: Final results of the optimization problem for all the shortlisted design cases $\mathcal{K}$. Left: Change in NPV (ΔNPV) with respect to Base_{STR} design case. Right: Optimal number of turbines. Values for four different design cases are mentioned for elaboration, with special mention to the Optimal design case {T200, C1400} marked with *

The results are further compiled in Table 9.2, where the following three parameters are recorded for the Base_{STR}, Base_{DTR} and Optimal design cases: Levelized Cost of Energy (LCOE) [$\frac{€}{\text{MWh}}$], loss of transformer life (LL) over the OWF lifetime [%] and efficiency of energy transfer (η) [%] representing the ratio between total injected and generated energy over the OWF lifetime. The last parameter accounts for energy losses and curtailment for the three design cases. It can be seen that even though the Optimal case has lower η than Base_{DTR}, it still results in the lowest LCOE. This is observed because the energy not delivered over the OWF lifetime is weighed yearly using the discount factor and also because the lower investment cost of Optimal case, due to reduction in export system costs and total turbine costs, outweighs the energy delivered over the OWF lifetime. Finally, it is shown that the transformer is utilized at a much better rate for the Optimal design case compared to the other two cases.

Table 9.2: Parameters for economic and efficiency assessment for Base_{STR}, Base_{DTR} and Optimal design cases

Parameter			Design Case		
Label	Unit	Formula	Base_{STR}	Base_{DTR}	Optimal
LCOE	$[\frac{€}{\text{MWh}}]$	$\frac{C_o(1+i)^y}{\sum_{y\in\mathcal{Y}} \pi_s \sum_{s\in\mathcal{S}} \sum_{t\in\mathcal{T}} P^{\text{inj}}_{t,s}}$	32.62	30.45	29.56
η	[%]	$\frac{\sum_{y\in\mathcal{Y}} \sum_{s\in\mathcal{S}} \sum_{t\in\mathcal{T}} P^{\text{inj}}_{t,s}}{\sum_{y\in\mathcal{Y}} \sum_{s\in\mathcal{S}} \sum_{t\in\mathcal{T}} P^{\text{gen}}_{t,s}}$	97.15	98.61	98.13
LL	[%]	$\frac{\sum_{y\in\mathcal{Y}} \pi_s \sum_{s\in\mathcal{S}} \lambda_{y,s}}{8760\ \Pi^{\text{WF}}}$	4.25	9.5	72.5

9.4.2 Evaluation of DTR and Component Utilization during Contingency

As mentioned earlier, the emergency cyclic limits of 140 °C for ϑ^{hst} [45] and normal cyclic limits of 90 °C for ϑ^{c} [71] are used in this study. The overall temperature recorded for Base_{STR}, Base_{DTR} and Optimal design cases are compiled in Fig. 9.4 using histograms for two scenarios: with contingency and without contingency. Contingency means that one or more circuits of the export system are simulated to be unavailable for certain periods over the OWF lifetime. It can be seen that both the cables and transformers operate closer to their respective thermal limits more often for the Optimal case compared to the Base_{STR} and Base_{DTR} cases. Moreover, the thermal stress is even higher for both Base_{DTR} and Optimal design cases for the scenario with simulated contingency, as the components are utilized to their limits in order to maximize the energy transfer during contingency.

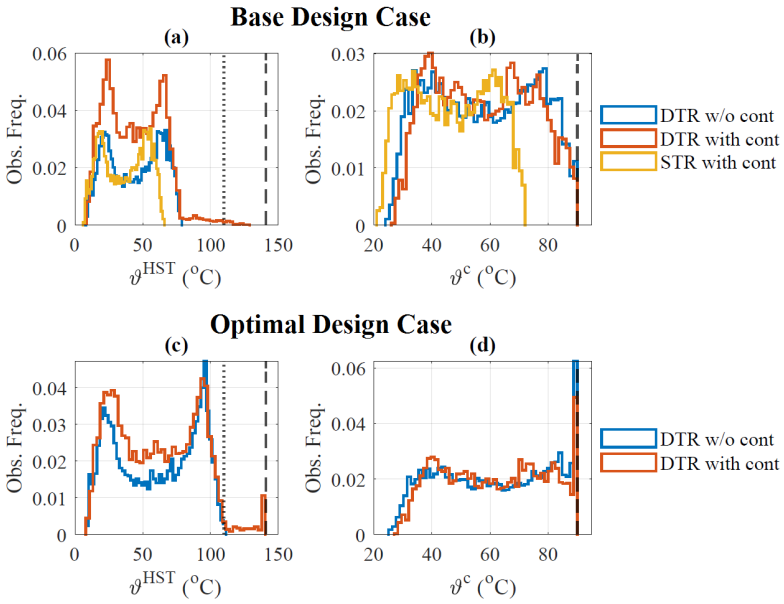

Figure 9.4: Histograms for critical temperatures for transformer (ϑ^{hst}) and Cable ϑ^{c} (incl. seabed temp. ϑ^{sea}) for two scenarios in $\mathcal{S}$ (with & without contingency). The results for Base_{STR}, Base_{DTR} and Optimal design cases are provided for simulated period of 30 years.

The optimal yearly loss-of-life (LL) for transformers λ [Days] is recorded in Fig. 9.5 for one of the simulated scenarios in $\mathcal{S}$ for Base_{STR}, Base_{DTR}, Optimal design cases. Furthermore, results for the 'Non-Optimal' design case {T175, C1600} which leads to maximum transformer utilization are also provided for comparison. It can be seen that during contingency, the number of available circuits reduce to 2 for a limited duration, during

which the Optimal transformer lifetime is utilized extraordinarily compared to the Base_{STR} and Base_{DTR} cases. This is performed by the optimization problem to maximize the energy transfer during contingency. It must be mentioned that for the entire duration, the thermal limits of all the relevant components are not violated.

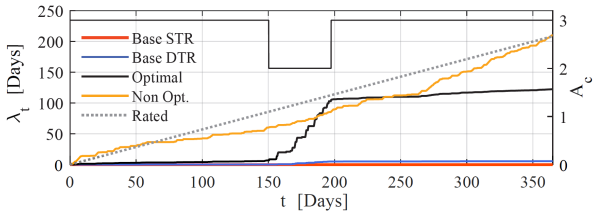

Figure 9.5: Number of available circuits A^c and cumulative loss-of-life (days) for transformer for a scenario with contingency.

9.4.3 Power Balance and Component Load during Contingency

The load current for cable I^c and power curtailment P^{cut} are recorded in Fig. 9.6 for a short duration before and after the contingency event for the scenario mentioned above. As the number of available circuits reduces to 2, the available export cables are loaded beyond their rated capacity for the Base_{DTR} and Optimal cases only, while additional energy needs to be curtailed for the Base_{STR} case. A closer look at the figure reveals that some curtailment is needed around the 155^{th} day for the Optimal and Base_{DTR} cases because ϑ^c and ϑ^{hst} reach their respective limits, as shown in Fig. 9.7.

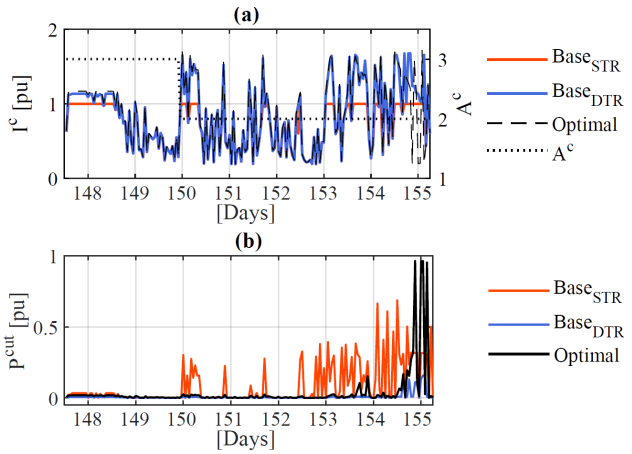

Figure 9.6: Difference in loading for Base_{STR}, Base_{DTR} and Optimal design cases during contingency as the number of available circuits A^c decreases from 3 to 2 around day 150. Bottom: load curtailment (P^{cut} [pu] with P^{gen} as base) for these design cases due to thermal bottlenecks.

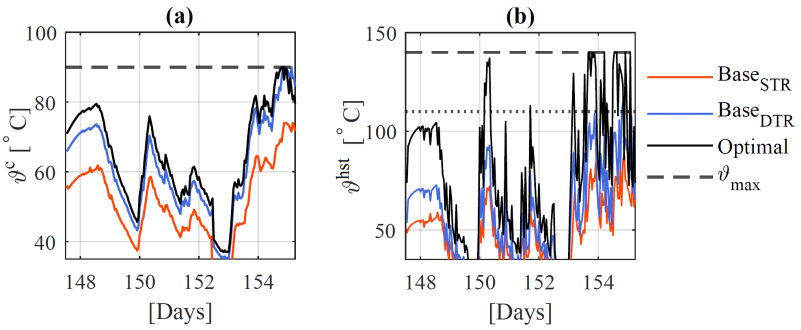

Figure 9.7: Development of critical temperature for transformer ϑ^{hst} (left) and cable ϑ^c (incl. seabed temp. ϑ^{sea}) for the same period and scenario as Fig. 9.6 for Base_{STR}, Base_{DTR} and Optimal design cases (incl. respective thermal limits).

Key Takeaways from Part IV

In Part IV, it has been shown that the optimization of design of critical HV components in the OWF export system can be facilitated by employment of DTR in the planning phase. The utilization of stochastic Auto Regressive Integrated Moving Average (ARIMA) processes and probabilistic DTMC principles allow consideration of uncertainty due to intermittent wind generation and system availability/contingency respectively, as shown in Chapter 7. These techniques are used to deploy multiple operational scenarios over the OWF lifetime, which ensure reliability of system design. The iterative technique for optimization of transformer rating presented in Chapter 8 has proven to be cost-effective even when revenue loss due to increase in temperature-dependent transformer losses and energy curtailment are considered. The test case of a large offshore windfarm off the east coast of UK has shown that this iterative technique can increase the Net Present Value (NPV) by a few million €. On the other hand, the two-stage stochastic optimization problem presented in Chapter 9 uses DTR for optimization of the entire OWF export system. This novel methodology resolves the hourly operational constraints in the first stage, while the constraints related to windfarm sizing and overall energy injection are handled in the second stage. The convexity of the optimization problem is maintained by mathematical manipulation of the non-linear functions and the problem is designed to account for uncertainty, losses and curtailment. The test case of large OWF has shown that the developed methodology can increase the business case by 10s and 100s of M€ for large-scale offshore windfarms. The iterative technique is presented in Publication **[Pub. J1]**, while the stochastic optimization problem is published in **[Pub. J2]**

PART V - CONCLUDING REMARKS

CHAPTER 10

Conclusion and Future Work

The discussion spread across parts I to IV and chapters 1 to 9 has extensively explained the values created during the Industrial PhD project. The last chapter compiles the analysis and findings presented so far. The chapter is structured as follows: the general comments and concluding remarks for the thesis are summarized in Section 10.1, the research questions drafted for the PhD project in Chapter 1 are briefly answered in Section 10.2 and finally the future research direction stemming from the outcome of this thesis are touched upon in Section 10.3

10.1 General Comments

The decarbonization targets for 2050 set by nations across the globe would not be accomplished without the development of large-scale Offshore Windfarms (OWFs). These targets hinge on continuous reduction in OWF's Levelized Cost of Energy (LCOE) which has already been squeezed significantly by optimization of the entire value chain by developers and manufacturers alike. In this PhD thesis, it has been shown that the utilization of Dynamic Thermal Rating (DTR) for design and operation of the OWF transmission system and its HV components can further facilitate this process substantially. The thesis presents the work from a windfarm developer's standpoint and has been structured in a way that all the relevant condition and thermal monitoring tools are presented initially. Afterwards, the developed methodologies are bifurcated into the following aspects: Firstly, the operational framework which addresses the DTR-based utilization of critical OWF transmission components. Secondly, the design framework which optimizes the design of the OWF transmission system components during the planning phase.

In conclusion, the results accomplished in this thesis suggest that the intermittent nature of the wind and the favorable ambient conditions in the offshore environment allow effective application of DTR in OWFs. The utilization of portfolio projects and the design of pipeline projects are positively influenced in terms of reliability and cost-effectiveness by the employment of DTR. The novel operational and design methodologies presented in this thesis are not only technically feasible, but are also carefully developed for practical considerations of the offshore projects. The applications of machine learning, data analytics and modern optimization tools demonstrated in this project compel the developers and operators to evolve their traditional processes with the available technologies.

10.2 Answers to the Research Questions

[Q1] *What are the inherent thermal bottlenecks in the Offshore Windfarm (OWF) export system and how can Dynamic Thermal Rating (DTR) facilitate resolution of major pinch-points?*

As per the discussion in Chapter 2 and Publication **[Pub. C6]**, there are two categories of thermal bottlenecks in the OWF export system. Power transformers located in the Offshore Substation (OSS) and sub-sections of the export cables (particularly J-tubes, HDD and subsea/offshore sections) can be thermally limiting under certain operating conditions, which include system/component contingency, sustained wind generation for long periods etc. These bottlenecks arise due to low thermal time constants, susceptibility to load variation and variable environmental circumstances. Referring to the discussion in Publication **[Pub. J2]**, the resolution of relevant bottlenecks can be performed by taking a systemic approach and by using electro-thermal coordination for all the components when application of DTR is considered. Finally, it has been shown that effective debottlenecking is possible by employing DTR on transformers and offshore/subsea section of the export cables only.

[Q2] *Can DTR be employed for operational and design optimization problems for offshore windfarms by using state-of-the-art thermal models for critical HV export system components? What modifications should be made to these models to make them fit for the relevant applications?*

The discussion in Chapter 2 and Publication **[Pub. C1]** suggests that state-of-the-art differential equations based non-linear Thermo-electric Equivalent (TEE) models are more suitable for the applications considered in this thesis due to their empirical nature, adaptability to varying operating circumstances and balance between accuracy and efficient computation. However, for the DTR-based novel operational and design optimization problems proposed in Chapters 6 and 8 respectively, the identified models require following modifications to ensure convexity of solution and low computational stress: data-driven parameter estimation for consolidated export cable models (shown in Publication **[Pub. C5]**) and continuous forced cooling operation for transformer winding and oil (shown in Publication **[Pub. C4]**). Nevertheless, for the novel iterative techniques presented in Publications **[Pub. J1]**, **[Pub. C2]** and **[Pub. C3]**, the chosen models can be used in their true form.

[Q3] *How and why should machine learning and data analytics be used for dynamic thermal estimation and condition monitoring of OWF export system components? Is it possible to extract physical, operational insights about the components from the semi-physical grey-box and empirical black-box models?*

It has been demonstrated that the empirical TEE models do not account for the time-variant physical attributes of the HV components and they require detailed insights regarding the design/operational circumstances. The discussion in Chapter 3 has shown that a series of novel self-learning grey-box and black-box Machine Learning (ML) models can efficiently perform thermal estimation of HV cables and transformers. The difference in thermal time constants and uniquely varying environmental conditions of transformers (Publication **[Pub. C7]**) and all the subsections of the export cables (**[Pub. C5]**) are efficiently analysed by the semi-physical Ordinary Differential Equation (ODE) models, physical State Space (SS) models and black-box Auto Regressive eXogenous (ARX) models. The non-linear black-box Artificial Neural Network (ANN) models are found to over-fit the training data in most cases, but the discussion has touched upon the means to fix these issues. These results are based on long-term thermal measurements of relevant components from multiple OWFs around the globe, along with experimental measurements acquired from transformers in the DTU HV lab. The combination of semi-physical ODE models and flexible ANN models allow extraction of physical insights for the test cases. On one hand, information related to subsea cable surroundings is accurately extricated; while on the other, real-time thermal condition monitoring of multiple wind turbine transformers is performed by training and testing on different test case turbines.

[Q4] *Is there a need to optimize the utilization of critical export system components by using DTR and/or by tracking their thermal and thermo-chemical ageing for reliable operation of the existing offshore windfarms? Can DTR facilitate the integration of OWFs in the transmission grid with minimal infrastructural investments?*

For optimal utilization, OSS transformers are given keen attention in this thesis, because these components are found to be over-dimensioned across all the analysed portfolio projects, as shown in the discussion in Chapter 5 and Publications **[Pub. C2]** and **[Pub. C3]**. Furthermore, OSS transformers are critical for security of supply, can outlive the OWF by tens of years, have considerable economic impacts and unlike cables, have not been addressed in the literature. In order to employ emergency thermal limits for DTR-based transformer utilization, it is found to be critical to use Degree of Polymerization (DP) thermo-chemical ageing models for cellulose-based insulation paper. DP-based models are extensively analysed and benchmarked in Chapter 4 for sensitivity to end-of-life criterion and moisture/oxygen decomposition. The novel methodology that proposes linearized Arrhenius reaction based thermal ageing model for dynamic transformer utilization in real-time has shown successful results in Chapter 6 and Publication **[Pub. C4]**. The methodology is tested via a unique lossy-DCOPF algorithm for a quadratically-constrained day-ahead energy dispatch optimization problem, by mapping the actual generation, load and wind production data from the transmission system of west-Denmark. The results

prove that the concept can ease large-scale integration of offshore windfarms in the network, while delaying grid-reinforcement costs. The concept is further extended to employment of DTR on multiple components (including transformers and overhead lines) across the test network, and the results are found to improve even further if systemic DTR is used as shown in Publication **[Pub. D1]**.

[Q5] *How can DTR be used to optimize the design of the complete OWF export system or its critical components over its entire lifetime, while accounting for uncertainty in generation and system availability/contingency?*

It has been deduced over the course of this study that in order to optimize the design of the complete export system for OWFs, employment of DTR needs to be considered during the planning phase for all the critical thermal bottlenecks simultaneously. The discussion in Chapter 9 and Publication **[Pub. J2]** has presented a novel two-stage stochastic design optimization problem based on mixed-integer linear programming that uses electro-thermal coordination of the components that are the major thermal pinch-points in the OWF export system. On the other hand, when systemic design optimization is not needed (for e.g. in cases where cable rating design is subject to local regulations or when developers use established techniques for cable rating optimization), the ratings of transformers located in the offshore substations can be optimized using the iterative framework presented in Chapter 8 and Publication **[Pub. J1]**. Design optimization problems are found to face unique challenges due to operational uncertainty over the OWF lifetime. In order to account for the uncertainty in hourly system/component load due to stochasticity of possible contingencies and for the uncertainty in hourly generation due to the stochastic nature of the wind and availability of wind turbines, the concepts in Chapter 7 and Publications **[Pub. J1]** and **[Pub. J2]** use probabilistic scenario generation principles. These principles are developed using non-linear stochastic trend analysis models like *ARIMA processes* that account for daily and yearly seasonalities to model long-term time series for wind wind generation and probabilistic *discrete time Markov processes* for component availability. Furthermore, the reliability of design is ensured by considering conservative operational and thermo-chemical ageing assumptions. All of the developed methodologies have been employed for design optimization of actual test case windfarms, while considering their operation over the entire OWF lifetime.

[Q6] *What are the economic and technical considerations needed for DTR-based design optimization of OWF export system? How can variables like efficiency of transmission, possibility of energy curtailment and reliability of design be used for economic optimization of offshore windfarm design based on DTR?*

The optimized ratings of OWF export system components obtained using the design optimization problems developed in this study are found to have extensive economic impacts on the OWF operation. The reduction in component size results in higher losses as the components operate closer to their thermal limits for sustained periods. The economic losses due to reduction in temperature-dependent transmission efficiency have been accounted for by using Net Present Value (NPV) assessment at the operational time-frame over the course of entire OWF lifetime. Furthermore, the thermal and ageing constraints can enforce energy curtailment to prevent over-utilization of components. The novel investment decision support tools (one iterative and one two-stage stochastic optimization model developed in this project) account for the revenue loss due to energy losses and curtailment, while ensuring reliability of design. The optimal design case is selected based on the overall positive influence on the economics (i.e. when the savings made in investments outweigh the discounted revenue loss over the OWF lifetime). The cost-effectiveness of the developed methodologies has been demonstrated in this thesis using actual large-scale test case windfarms. All of this is presented in Publications **[Pub. J1]** and **[Pub. J2]**.

10.3 Future Research Directions

The following points can be addressed in the future research work to be performed in this field:

[R1] The analysis in this thesis has been focused on High Voltage AC technology for the OWF transmission system. The development of large-scale offshore windfarms further from the shore using High Voltage DC (HVDC) transmission technology is becoming more prevalent. The results of this thesis should be just as relevant for HVDC, if not more, as it offers better transmission system control. However, the additional thermal stress on components due to increased power-electronics based control should be addressed in the future.

[R2] Besides the employment of HVDC, it is also foreseen that the development of more OWFs (plus energy islands) and efforts to improve cross-border trading will eventually result in the development of offshore grids. These grids would experience continuous evolution as more renewable energy sources need to be connected over time. DTR will facilitate the deferral of grid reinforcements in such cases and will be even more relevant compared to the radial circuits analysed in this thesis. Furthermore, the integration of OWF with other renewable technologies (incl. solar, hydrogen, onshore windfarms etc.) should be performed for these grids.

[R3] The utilization of machine learning in assessment of cable surroundings (incl. burial depth estimation of subsea cable) is found to be technically feasible in this thesis. However, further efforts are needed to develop tools that utilize a combination of semi-physical, grey-box models and empirical black-box models for these assessments.

[R4] The non-linear machine learning tools developed in this project (particularly artificial neural networks) tend to over-fit the training data. These tools are extremely adaptable and efforts should be made to improve their performance before these tools are used for other applications.

[R5] The DTR-based stochastic optimization tools developed in this project for design and operation of OWF export system should be extended to include the following:

i) OWF collection system (meshed and radial) consisting of MV/HV array cables (incl. cable routing and optimal layout)

ii) Secondary HV components in the OWF export system (incl. power converters, switchgear sub-components etc.)

iii) Transmission grid beyond the point of common coupling to employ dynamic network rating, as shown in Publication **[Pub. D1]**. The inclusion of wide-area monitoring, high-resolution numerical weather prediction across the network etc. should be analysed for this application.

Bibliography

[1] Colin Walsh and Daniel Fraile. Offshore wind in europe - key trends and statistics 2019 (wind europe). https://windeurope.org/, Feb 2020.

[2] Jessica Elgot, Fiona Harvey and Jillian Ambrose. Boris Johnson to unveil plan to power all UK homes with wind by 2030, 05-Oct-2020. *The Guardian*, 2020.

[3] KYODO. Japan aims to be world's No. 3 offshore wind power producer in 2040, 16-Dec-2020. *Japan Times*, 2020.

[4] Brady Dennis. The U.S. will soon rejoin the Paris climate accord, 22-Dec-2020. *The Washington Post*, 2020.

[5] EU Energy Commission. A Clean Planet for all - A European strategic long-term vision for a prosperous, modern, competitive and climate neutral economy. *European Commission*, 2018.

[6] Navigant, Tennet TSO (Netherlands), RTE TSO (France). Connecting offshore wind farms - a comparison of offshore electricity grid development models in northwest europe. https://guidehouse.com/news/energy/2019/navigant-compares-offshore-grid-connection-models, July 2019.

[7] Peng HOU, Jiangsheng ZHU, Guangya YANG, and Zhe CHEN. A review of offshore wind farm layout optimization & electrical system design methods. *Jour. of Modern Power Systems & Clean Energy*, 7:975–986, 2019.

[8] Catapult Offshore Wind Energy. System performance, availability and reliability trend analysis portfolio review. https://ore.catapult.org.uk/stories/system-performance-availability-and-reliability-trend-analysis-sparta/, 2019.

[9] Rodrigo Viera and Miguel Sanz-Bobi. Failure risk indicators for a maintenance model based on observable life of industrial components with an application to wind turbines. *IEEE transactions on Reliability*, 62(3):569 to 582, 2015.

[10] Andrew ZP Smith. UK offshore wind capacity factors. https://energynumbers.info/uk-offshore-wind-capacity-factors, November 2020.

[11] BVG Associates. Guide to an offshore wind farm (updated) - the crown estate and ore catapult. https://ore.catapult.org.uk/app/uploads/2019/04/BVGA-5238-Guide-r2.pdf, April 2019.

[12] Jiashen Teh and Ian Cotton. Reliability impact of dynamic thermal rating system in wind power integrated network. *IEEE Trans. on Reliability*, 65(2):1081 to 1089, 2016.

[13] H. Brakelmann. Loss determination for long three-phase high-voltage submarine cables. *Eur. Trans. Elect. Power*, 13(3):193–197, Nov 2003.

[14] Heejung Park, Ross Baldick, and David Morton. A stochastic transmission planning model with dependent load and wind forecasts. *IEEE Trans. on Power Systems*, 30(6):3003–3011, Jan 2015.

[15] Dan Zhou, Zhongdong Wang, and Chengrong Li. Data requisites for transformer statistical lifetime modelling part i: Aging-related failures. *IEEE transactions on Power Delivery*, 28(3):1750 to 1757, 2013.

[16] J.A. Perez-Rua, M. Stolpe, K. Das, and N. A. Cutululis. Global optimization of offshore wind farm collection systems. *IEEE Trans. on Power Systems*, 35(3):2256–2267, May 2020.

[17] Marcos Banzo and Andres Ramos. Stochastic optimization model for electric power system planning of offshore wind farms. *IEEE Trans. on Power Systems*, 26(3):1338–1348, Aug 2011.

[18] Shurong Wei, Lu Zhang, Yao Xu, and Fangxing Li. Hierarchical optimization for the double-sided ring structure of the collector system planning of large offshore wind farms. *IEEE Trans. on Sustainable Energy*, 3(8):1029–1039, Jul 2017.

[19] Javier Gonzalez, Manuel Payan, and Jesus Santos. A new and efficient method for optimal design of large offshore wind power plants. *IEEE Trans. on Power Systems*, 28(3):3075–3084, Aug 2013.

[20] Hakan Ergun, Dirk Van Hertem, and Ronnie Belmans. Transmission system topology optimization for large-scale offshore wind integration. *IEEE Trans. on Sustainable Energy*, 3(4):908–917, Oct 2012.

[21] Mohsen Sedighi, Mohammad Moradzadeh, and Murat Fahrioglu. Simultaneous optimization of electrical interconnection configuration and cable sizing in offshore wind farms. *Jour. of Modern Power Systems & Clean Energy*, 6:749–762, 2018.

[22] Heejung Park and Ross Baldick. Transmission planning under uncertainties of wind and load: Sequential approximation approach. *IEEE Trans. on Power Systems*, 28(3):2395–2402, Aug 2013.

[23] Adelaide Cerveira, Amaro Sousa, E. J. Solteiro Pires, and Jose Baptista. Optimal cable design of wind farms: The infrastructure and losses cost minimization case. *IEEE Trans. on Power Systems*, 31(6):4319–4329, Nov 2016.

[24] J.A. Perez-Rua, K. Das, and N. A. Cutululis. Optimum sizing of offshore wind farm export cables. *International Journal of Electrical Power & Energy Systems*, 113:982 to 990, Dec 2019.

[25] Simon Catmull, Richard D. Chippendale, and James A. Pilgrim. Cyclic load profiles for offshore wind farm cable rating. *IEEE Trans. on Power Delivery*, 31(3):1242–1250, June 2016.

[26] M. A. H. Colin and J. A. Pilgrim. Offshore cable optimization by probabilistic thermal risk estimation. In *Proceedings of IEEE International Conference on Probabilistic Methods Applied to Power Systems (PMAPS)*, USA, 2018.

[27] Oscar David Rocha, Kateryna Morozovska, Tor Laneryd, Ola Ivarssonc, Claes Ahlrotc, and Patrik Hilbera. Dynamic rating assists cost-effective expansion of wind farms by utilizing the hidden capacity of transformers. *Electrical Power and Energy Systems*, 123 (2020), 2020.

[28] R. Billinton and R. N. Allan. *Reliability Evaluation of Engineering Systems: Concepts and Techniques*. Plenum, New York, USA, 1992.

[29] Yuan-Kang Wu, Po En Su, Yu-Sheng Su, and Wen Shan Tan. Economics and reliability-based design for an offshore wind farm. *IEEE Trans. on Industry Applications*, 53(6):5139–5149, Jan 2018.

[30] PensionDenmark, PKA and Orsted. Anholt offshore wind farm - Denmark's largest offshore windfarm. https://stateofgreen.com/files/download/5199, June 2013.

[31] M. H. Banakar, N. Alguacil, and F. D. Galiana. Electrothermal coordination I: theory and implementation schemes. *IEEE Transactions on Power Systems*, 20(2):798–805, 2005.

[32] Work Group A3.12. Failure survey on circuit breaker control systems. *CIGRE Technical Brochure*, -(259):94, Aug 2004.

[33] Work Group A3.06. Final report of the 2004-2007 international enquiry on reliability of high voltage equipment, part 2 reliability of high voltage sf6 circuit breaker. *CIGRE Technical Brochure*, -(510):94, Aug 2012.

[34] IEC 62271-203. High-voltage switchgear and controlgear part 203: Gas-insulated metal-enclosed switchgear for rated voltages above 52 kv. *IEC Standard*, 2011.

[35] IEC 62539:2007. Guide for the statistical analysis of electrical insulation breakdown data. *IEC standard*, 2007.

[36] T. Igi, H. Komeda, and S. Mashio. Study of the dynamic rating of a 138kv xlpe cable system by optical fiber monitoring. In *Proceedings of Jicable: 8th International Conference on Insulated Power Cables*, 2013.

[37] Work Group B1.45. Thermal monitoring of cable circuits and grid operators use of dynamic rating systems. *CIGRE Technical Brochure*, page 94, Feb 2019.

[38] Erdmann Matthias, James Pilgrim, and et. al. Towards active cable reburial monitoring using distributed fiber-optic sensing over 40km of a high voltage marine interconnector. In *Proceedings of Jicable: 10th International Conference on Insulated Power Cables*, Versailles, France, 2019. IEEE.

[39] Jane Rowsell and Etienne Rochat. Condition monitoring and optimization of subsea energy cables using optical fiber sensing, Omnisens SA, December 2013.

[40] Timothy J Hughes, T. Henstock, JA Pilgrim, and Charlotte EL Thompson. Effect of sediment properties on the thermal performance of submarine HV cables. *IEEE Trans. on Power Delivery*, 30(6):2443–2450, Nov 2015.

[41] Thomas Worzyk. *Submarine power cables: design, installation, repair, environmental aspects*. Springer, 2009.

[42] RD Chippendale, JA Pilgrim, KF Goddard, and Priank Cangy. Analytical thermal rating method for cables installed in J-tubes. *IEEE Trans. on Power Delivery*, 32(4):1721–1729, Nov 2016.

[43] Timothy J Hughes, T. Henstock, JA Pilgrim, and Charlotte EL Thompson. Thermal ratings of submarine hv cables informed by environmental considerations. In *Proceedings of Jicable: 9th International Conference on Insulated Power Cables*, Versailles, France, 2015.

[44] IEC 60076-7. *Loading guide for oil-immersed power transformers*. IEEE, 2018.

[45] IEEE C57.91-2011. *Guide for Loading Mineral-Oil-Immersed Transformers and Step-Voltage Regulators - Redline*. IEEE, Mar 2011.

[46] J. Lapworth, P. Picher, and J. Channet. Technical report by Work Group A2.38 on Transformer thermal modelling. *CIGRE TB*, pages 0–94, Aug 2016.

[47] V.M Montsinger. Effect of load factor on operation of power transformers. *Transactions on Electrical Engg.*, 59(11):632–636, 1940.

[48] Glenn Swift, Tom S Molinski, and Waldemar Lehn. A fundamental approach to transformer thermal modeling. I. theory and equivalent circuit. *IEEE transactions on Power Delivery*, 16(2):171–175, 2001.

[49] W.H. Tang and Q.H. Wu. A simplified transformer thermal model based on thermal-electric analogy. *IEEE Transactions on Power Delivery*, 19(2):1112–1119, 2004.

[50] Dejan Susa, Matti Lehtonen, and Hasse Nordman. Dynamic thermal modelling of power transformers. *IEEE Trans. on Power Del.*, 20(1):197–204, 2005.

[51] H. Nordman, N. Rafsback, and D Susa. Temperature responses to step changes in the load current of power transformers. *IEEE Transactions on Power Delivery*, 18(1):107–112, 2003.

[52] Glenn Swift and Tom Molinski. Power transformer life-cycle cost reduction. In *Proceedings of the Minnesota Power Systems Conference (MIPSYCON), Minneapolis, USA*, volume 111, 1996.

[53] Glenn Swift, Tom S Molinski, and Waldemar Lehn. A fundamental approach to transformer thermal modeling. II. field verification. *IEEE transactions on Power Delivery*, 16(2):176–180, 2001.

[54] Dejan Susa and Matti Lehtonen. Dynamic thermal modeling of power transformers: further development part II. *IEEE Transactions on Power Delivery*, 21(4):1971–1980, 2006.

[55] M. Djamali and S. Tenbohlen. Real-time evaluation of the dynamic loading capability of indoor distribution transformers. *IEEE Transactions on Power Delivery*, 33(2):1134–1142, 2018.

[56] Lida Jauregui-Rivera, Xiaolin Mao, and Daniel J Tylavsky. Improving reliability assessment of transformer thermal top oil model parameters estimated from measured data. *IEEE Transactions on Power Delivery*, 24(1):169–176, 2009.

[57] N. Alguacil, M. H. Banakar, and F. D. Galiana. Electrothermal coordination II: case studies. *IEEE Transactions on Power Systems*, 20(4):1738–805, 2005.

[58] D.J. Tyalvsky and Q. He. Sources of error in substation distribution transformer dynamic thermal modeling. *IEEE Transactions on Power Delivery*, 15(1):178–185, 2000.

[59] D Susa and H Nordman. Iec 60076–7 loading guide thermal model constants estimation. *International Transactions on Electrical Energy Systems*, 23(7):946–960, 2013.

[60] Daniel J Tylavsky, Xiaolin Mao, and Gary A McCulla. Transformer thermal modeling: Improving reliability using data quality control. *IEEE Transactions on Power Delivery*, 21(3):1357–1366, 2006.

[61] Dejan Susa and Matti Lehtonen. Dynamic thermal modeling of power transformers: further development part I. *IEEE Transactions on Power Delivery*, 21(4):1961–1970, 2006.

[62] Oluwaseun A. Amoda, Daniel J Tylavsky, and Wesley A. Knuth. Acceptability of three transformer hottest-spot temperature models. *IEEE Transactions on Power Delivery*, 27(1):13–22, 2012.

[63] L. Jauregui-Rivera and D. J. Tylavsky. Acceptability of four transformer top-oil thermal models part 1 defining metrics. *IEEE Transactions on Power Delivery*, 23(2):860–865, April 2008.

[64] X Mao, DJ Tylavsky, and GA McCulla. Assessing the reliability of linear dynamic transformer thermal modelling. *IEEE Proceedings-Generation, Transmission and Distribution*, 153(4):414–422, 2006.

[65] Q. He, J. Si, and D. Tylavsky. Prediction of tot for transformers using ann. *IEEE Transactions on Power Delivery*, 15(2):1205–1511, 2000.

[66] M. Djamali and S. Tenbohlen. Hundred years of experience in the dynamic thermal modelling of power transformers. *IET Generation, Transmission and Distribution Journal*, 11(3):2731–2739, 2017.

[67] M. Hell and P.J. Costa. Participatory learning in powertransformers thermal modeling. *IEEE Transactions on Power Delivery*, 24(4):2058–2067, 2008.

[68] Lida Jauregui-Rivera and Daniel J Tylavsky. Acceptability of four transformer top-oil thermal models part 2 comparing metrics. *IEEE Transactions on Power Delivery*, 23(2):866–872, 2008.

[69] F. P. Incropera and D. P. DeWitt. *Fundamentals of Heat and Mass Transfer*. Wiley, New York, USA, 2008.

[70] A. Iserles. *A first course in the numerical analysis of differential equations*. Cambridge University Press, 2009.

[71] IEC Standard 60853-2. *Calculation of the Cyclic and Emergency Current Rating of Cables. Part 2: Cyclic Rating of Cables Greater Than 18/30 (36) kV and Emergency Ratings for Cables of all Voltages*. IEC, AD:2017.

[72] Work Group B1.40. Offshore generation cable connections. *CIGRE Technical Brochure 610*, page 94, Feb 2015.

[73] IEC Standard 60287-1-1. *Electric cables - Calculation of the current rating (100 percent load factor) and losses*. IEC, AD:2006.

[74] IEC Standard 60287-2-1. *Calculation of the current rating Part 2-1: Calculation of Thermal Resistance*. IEC, AD:2006.

[75] ABB. Network Manager SCADA DMS, ABB Sweden, December 2015.

[76] Siemens. Energy, Jul 2018.

[77] Areva T&D. E-Terraplatform - The power to adapt, Dec 2008.

[78] CYMCAP. Cable Optimization Tool, CYMCAP, Nov 2017.

[79] R. J. Millar. A comprehensive approach to real time power cable temperature prediction and rating in thermally unstable environments, PhD Dissertation, Helsinki University of Technology, Finland Dec, 2006.

[80] G. J. Anders. Improvement in cable rating calculations by consideration of dependence of losses on temperature. *IEEE Transactions on Power Delivery*, 19(4):919–925, Nov 2004.

[81] M. Coates. Rating cables in J tubes (88-0108), ERA technology Dec, 1988.

[82] Rasmus Olsen, George Anders, Joachim Holboll, and Unnur Stella Gudmundsdottir. Modelling of dynamic transmission cable temperature considering soil-specific heat, thermal resistivity and precipitation. *IEEE Transactions on Power Delivery*, 28(3):1909–1917, July 2013.

[83] Dimitrios Chatzipetros and James A. Pilgrim. Review of the accuracy of single core equivalent thermal model for offshore wind farm cables. *IEEE Trans. on Power Delivery*, 33(4):1913–1921, August 2018.

[84] Rasmus Olsen, George Anders, Joachim Holboll, and Unnur Stella Gudmundsdottir. Electrothermal coordination in cable based transmission grids. *IEEE Transactions on Power Systems*, 28(4):4867 – 4874, Nov 2013.

[85] G. Anders and G. Georgallis. Transient analysis of 3-core sl-type submarine cabes with jacket around each core. In *Proceedings of Jicable: 9th International Conference on Insulated Power Cables*, Paris, France, 2015. IEEE.

[86] Ossama Gouda, Gomaa Fahmey Osman, Waleed A. Salem, and Shawky H. Arafa. Cyclic loading of underground cables including the variations of backfill soil thermal resistivity and specific heat with temperature variation. *IEEE Trans. on Power Delivery*, 33(6):1242–1250, Jan 2019.

[87] X. Qi and S. Boggs. Thermal and mechanical properties of EPR and XLPE cable compounds. *IEEE Electrical Insulation Magazine*, 22(3):24, June 2006.

[88] K. Goddard, J. A. Pilgrim, R. Chippendale and P. Lewin,. Induced losses in three-core sl-type high voltage cables. *IEEE Transactions on Power Delivery*, 30(3):1505–1513, Nov 2015.

[89] E. Dorison, G. J. Anders and F. Lesur. Ampacity calculations for deeply installed cables. *IEEE Transactions on Power Delivery*, 25(2):524–533, June 2010.

[90] G. J. Anders, M. Coates and M. Chaaban. Ampacity calculations for cables in shallow troughs. *IEEE Transactions on Power Delivery*, 25(4):2064–2072, June 2010.

[91] M. Diaz-Aguilo and F. de Leon. Introducing mutual heating effects in the ladder-type soil model for the dynamic thermal rating of underground cables. *IEEE Transactions on Power Delivery*, 30(4):1958–1964, June 2015.

[92] R. A. Black and W. Hartlein. Ampacity of electric power cables in vertical protective rises. *IEEE transaction on power apparatus and systems*, 102(6):–, June 1983.

[93] G. Anders. Rating of cables on riser poles, in trays, in tunnels and shafts - a review. *IEEE transactions on power delivery*, 11(1):3–11, Aug 1996.

[94] A. Sedaghat and F. d. Leon. Thermal analysis of power cables in free air: Evaluation and improvement of the iec standard ampacity calculations. *IEEE Transactions on Power Delivery*, 29(5):2306–2314, June 2014.

[95] M. Terracciano, S. Purushothaman, F. de Leon and A. Farahani. Thermal analysis of cables in unfilled troughs: Investigation of the iec standard and a methodical approach for cable rating. *IEEE Transactions on Power Delivery*, 27(3):142, June 2012.

[96] Ander Madariaga, Jose Martin, and Olimpo Anaya Lara. Effective assessment of electric power losses in three-core xlpe cables. *IEEE Trans. on Power Systems*, 28(4):4488–4495, Nov 2013.

[97] Work Group 21.08. Cigre elektra 143 - calculation of temperatures in ventilated cable tunnels - part i. *CIGRE Technical Brochure*, page 14, Feb 1992.

[98] A. Krizhevsky, I. Sutskever, and G. E. Hinton. Imagenet classification with deep convolutional neural networks. *Advances in neural information processing systems*, 20(2):1097 to 1105, May 2017.

[99] LB. M. Lake, R. Salakhutdinov, and J. B. Tenenbaum. Human-level concept learning through probabilistic program induction. *Science*, 350(2):1332 to 1338, July 2015.

[100] B. Alipanahi, A. Delong, M. T. Weirauch, and B. J. Frey. Predicting the sequence specificities of dna-and rna-binding proteins by deep learning. *Nature biotechnology*, 33(1):831 to 838, July 2016.

[101] Y. Le Cun, Y. Bengio, and G. Hinton. Deep learning. *Nature*, 521(7):436 to 444, Oct 2015.

[102] Geron and Aurelien. *Hands-on machine learning with Scikit-Learn and TensorFlow: concepts, tools, and techniques to build intelligent systems*. O Reilly Media Inc, Massachusetts, United States, 2017.

[103] M. Sakata and S. Iwamoto. Genetic algorithm based real-time rating for short-time thermal capacity of duct installed power cables. In *Proceedings of International Conference on Intelligent Systems Applications to Power Systems*. ISAP, 2006.

[104] Henrik Madsen. *Time Series Analysis*. Chapman & Hall CRC, New York, USA, 2008.

[105] Christopher M Bishop. *Neural Networks for Pattern Recognition*. Ozford University Press, UK, 1995.

[106] Lennart Ljung. *System Identification and Simple Process Models*. Linkoping University, Linkoping, Sweden, 2013.

[107] Lennart Ljung. *System Identification - Theory for the User*. Prentice-Hall Inc., Linkoping, Sweden, 1999.

[108] K Zhang, A. Guliani, and G. Memik. Machine learning-based temperature prediction for runtime thermal management across system components. *IEEE Transactions on Parallel and Distributed Systems*, 29(2):2079–2107, July 2017.

[109] M. Hezri, F.L Rahiman, and M. N. Taib. Performance of multi-step-ahead-prediction arx for steam temperature in a self-refilling distillation essential oil extraction system. In *Proceedings of IEEE International Conference on Control, Automation and Systems*, Seoul, Korea, 2007.

[110] M. Raissi, P. Perdikaris, and G. E. Karniadakis. Hidden physics models: Machine learning of nonlinear partial differential equations. *Journal of Computational Physics*, 357(1):125 to 141, Nov 2018.

[111] S. H. Rudy, S. L. Brunton, J. L. Proctor, and J. N. Kutz. Data-driven discovery of partial differential equations. *Science Advances*, 3(1):683 to 693, Nov 2017.

[112] M. Raissi, P. Perdikaris, and G. E. Karniadakis. Numerical gaussian processes for time-dependent and non-linear differential equations. *Journal of Computational Physics*, 356(1):683 to 693, Jan 2018.

[113] Gavin C Cawley and Nicola LC Talbot. On over-fitting in model selection and subsequent selection bias in performance evaluation. *Journal of Machine Learning Research*, pages 2079–2107, Nov 2010.

[114] M Raissi, P. Perdikaris, and G. E. Karniadakisa. Physics-informed neural networks: A deep learning framework for solving forward and inverse problems involving nonlinear partial differential equations. *Elsevier Journal of Computational Physics*, 378(2):686 to 707, Feb 2019.

[115] T. Herlau, M. N. Schmidt, and M Morup. *Introduction of Machine Learning - Neural Networks*. Technical University of Denmark, Denmark, 2018.

[116] M. Raissi, P. Perdikaris, and G. E. Karniadakis. Machine learning of linear differential equations using gaussian processes. *Journal of Computational Physics*, 348(1):683 to 693, Nov 2017.

[117] Gerald Teschl. *Ordinary differential equations and dynamical systems*. American Mathematical Society, Providence, USA, 2012. Ed: 140.

[118] M. Raissi, P. Perdikaris, and G. E. Karniadakis. Inferring solutions of differential equations using noisy multi-fidelity data. *Journal of Computational Physics*, 335(1):736 to 746, July 2017.

[119] J. Fulcher, D. Martin, and O. Krause. Developing simplified thermal models for 11 kv underground cables in australia. In *Proceedings of IEEE PES Asia-Pacific Power and Energy Engineering Conference*, Brisbane Australia, 2015. IEEE.

[120] Ravid Shwartz-Ziv and Naftali Tishby. Opening the black box of deep neural networks via information, 2017.

[121] Natick. *MATLAB and System Identification Toolbox Release 2019b*. The Mathworks Inc., Massachusetts, United States, 2019.

[122] Gavin C Cawley and Nicola LC Talbot. On over-fitting in model selection and subsequent selection bias in performance evaluation. *Journal of Machine Learning Research*, 11(1):2079 to 2107, Nov 2010.

[123] Christopher M Bishop. *Pattern recognition and machine learning*. Springer, 2006.

[124] Benjamin Cordes. *MSc Thesis - Machine learning based real-time monitoring of offshore windfarm cables using distributed temperature sensing,*. Technical University of Denmark, 2020.

[125] IEC 60076-2:1993. *Power transformers - Part 2: Temperature Rise*. IEC, 2011.

[126] . IEC 60505-11:2011 evaluation and qualification of electrical insulation systems. *IEC*, 2011.

[127] . IEC 60216-3:2007 electrical insulating materials - thermal endurance properties - part 3: Instructions for calculating thermal endurance characteristics. *IEC*, 2007.

[128] Work Group D1. Ageing of cellulose in mineral-oil insulated transformers. *CIGRE TB*, page 94, Aug 2007.

[129] A. M. Emsley and G. C. Stevens. Kinetics and mechanisms of the low-temperature degradation of cellulose,. *Cellulose*, 01:26–56, Mar 1994.

[130] L Lundgaard, W Hansen, D Linhjell, and T Painter. Aging of oil-impregnated paper in power transformers. *IEEE Transactions on Power Delivery*, 19(1):230–239, 2004.

[131] Work Group D1.53. Ageing of liquid impregnated cellulose for power transformers. *CIGRE TB*, page 94, Aug 2018.

[132] V. W. Montsinger. Loading transformers by temperature. *Transactions of AIEE*, pages 776–792, Jun 1930.

[133] A. M. Emsley, R. J. Heywood, M. Ali, and C. M. Eley. On the kinetics of degradation of cellulose. *Cellulose*, 01:1–5, Mar 1997.

[134] A. M. Emsley and G. C. Stevens. Review of chemical indicators of degradation of cellulosic electrical paper insulation in oil-filled transformers. *IEE Proceedings-Science Measurement and Technology*, 15:324–334, Sep 1994.

[135] A. M. Emsley. The kinetics and mechanisms of degradation of cellulosic insulation in power transformers. *Polymer Degradation and Stability*, 44:343–349, Dec 1994.

[136] R. Gilbert, J. Jalbert and Y. Denos. Kinetics of the production of chainend groups and methanol from the depolymerization of cellulose during the ageing of paper/oil systems. part 1: Standard wood kraft insulation. *Cellulose*, 16:327–338, Apr 2009.

[137] R. Gilbert, J. Jalbert and Y. Denos. Kinetics of the production of chainend groups and methanol from the depolymerization of cellulose during the ageing of paper/oil systems. part 2: Thermally-upgraded insulating papers. *Cellulose*, 17:253–269, Apr 2010.

[138] J. Jalbert, E. Rodrigues-Celis, M. Ryadi, and R. Gilbert. Kinetics of the production of chain-end groups and methanol from the depolimerization of cellulose during the ageing of paper/oil systems. part 3: extension of the study under temperature conditions over 120 c. *Cellulose*, 22:829–848, July 2015.

[139] A Emsley, X Xiao, R Heywood, and M Ali. Degradation of cellulosic insulation in power transformers. part 3: effects of oxygen and water on ageing in oil. *IEE Proceedings - Science, Measurement and Technology*, 147(3):115–119, 2000.

[140] Nick Lelekakis, Daniel Martin, and Jaury Wijaya. Ageing rate of paper insulation used in power transformers part 1: Oil/paper system with low oxygen concentration. *IEEE Transactions on Dielectrics and Electrical Insulation*, 19(6):1999–2008, 2012.

[141] Nick Lelekakis, Daniel Martin, and Jaury Wijaya. Ageing rate of paper insulation used in power transformers part 2: Oil/paper system with medium and high oxygen concentration. *IEEE Transactions on Dielectrics and Electrical Insulation*, 19(6):2009–2018, 2012.

[142] M. H. G. Ese, K. B. Liland, and L. E. Lundgaard. Oxidation of paper insulation in transformers. *IEEE Transactions on Dielectrics and Electrical Insulation*, 17:939–946, Jun 2010.

[143] S. Soares, N. M. P. S. Ricardo, F. Heatley, and E. Rodrigues. Low temperature thermal degradation of cellulosic insulating paper in air and transformer oil. *Polymer International*, 50:303–308, Mar 2001.

[144] P. Calvini, A. Gorassini, and A. L. Merlani. On the kinetics of cellulose degradation: looking beyond the pseudo zero order rate equation. *Cellulose*, 15:193–203, Apr 2008.

[145] K. B. Liland, M. Kes, L. E. Lundgaard, and B. E. Christensen. Study of oxidation and hydrolysis of oil impregnated paper insulation for transformers using a microcalorimeter. *IEEE Transactions on Dielectrics and Electrical Insulation*, 18:2059–2068, Dec 2011.

[146] L. E. Lundgaard, W. Hansen, and D. Linhjell. Ageing of kraft and thermally upgraded oil impregnated paper. *Proceedings of Nord-IS 05, Trondheim*, pages 45–49, Dec 2005.

[147] K. B. Liland, M. H. G. Ese, C. M. Selsbak, and L. Lundgaard. Ageing of oil impregnated thermally upgraded papers. oxidation and hydrolysis. *presented at the 2011 IEEE International Conference on Dielectric Liquids*, Jun 2011.

[148] Daniel Martin, Yi Cui, Chandima Ekanayake, and Tapan Saha. An updated model to determine the life remaining of transformer insulation. *IEEE Transactions on Power Delivery*, 30(1):395–403, 2015.

[149] M. Humayun, M.Z. Degefa, A. Safdarian, and M. Lehtonen. Utilization improvement of transformers using demand response. *IEEE transactions on power delivery*, 30(1):202–210, Feb 2015.

[150] M. Humayun, M. Ali, A. Safdarian, M.Z. Degefa, and M. Lehtonen. Optimal use of demand response for lifesaving and efficient capacity utilization of power transformers during contingencies. In *2015 IEEE power energy society general meeting*, pages 1–5, Jul 2015.

[151] G. Bajracharya et al. Optimization of transformer loading based on hot-spot temperature using a predictive health model. In *Int. Conf. on Condition Monitoring and Diagnosis, Tokyo, Japan*, pages 914–917, 2010.

[152] J. M. Morales et al. *Integrating Renewables in Electricity Markets, International Series in Operations Research & Management Science 205*. Springer Science+Business Media New York, 2014.

[153] H. Hahn, S. Meyer-Nieberg, S. Pickl. Electric load forecasting methods: Tools for decision making. *European Journal of Operational Research*, 199:902–907, 2009.

[154] E.A. Feinberg, D. Genethliou . *Load Forecasting in Applied Mathematics for Restructured Electric Power System*. Springer, 2005.

[155] A. Keyhani, M.N. Marwali and M. Dai. *Integration of Green and Renewable Energy in Electric Power Systems*. Wiley, 2010.

[156] B. Wollenberg R. Christie and I. Wangensteen. Transmission management in the deregulated environment. *Proc. of the IEEE*, 88(02):170 – 195, Feb. 2000.

[157] R. A. Jabr. Modeling network losses using quadratic cones. *IEEE Transactions on Power Systems*, 20(1):505–506, Feb 2005.

[158] O. W. Akinbode and K. W. Hedman. Fictitious losses in the dcopf with a piecewise linear approximation of losses. In *IEEE PES GM*, pages 1–5, July 2013.

[159] A. Tosatto, T. Weckesser, and S. Chatzivasileiadis. Market integration of HVDC lines: Internalizing HVDC losses in market clearing. *IEEE Transactions on Power Systems*, 35(1):451–461, Jan 2020.

[160] Michael Grant and Stephen Boyd. CVX: Matlab software for disciplined convex programming, version 2.1. http://cvxr.com/cvx, March 2014.

[161] Christos Ordoudis, Pierre Pinson, Juan Miguel Morales González, and Marco Zugno. *An Updated Version of the IEEE RTS 24-Bus System for Electricity Market and Power System Operation Studies.* Technical University of Denmark, 2016.

[162] N. Viafora, S. Delikaraoglou, P. Pinson, and J. Holboll. Chance-constrained optimal power flow with non-parametric probability distributions of dynamic line ratings. *International Journal of Electrical Power and Energy Systems*, 2019.

[163] A Hahmann, C Vincent, A Pena, J Lange, and C Hasager. Wind climate estimation using WRF model output: method and model sensitivities over the sea. *International Journal of Climatology*, 35:3422–3439, 2015.

[164] T. Kvarts, I. Arana, R. Olsen and P. Mortensen. Systematic description of dynamic load for offshore wind farms: Method and experience. *B1-303 CIGRE*, -:1–10, 2016.

[165] Peiyuan Chen, Troels Pedersen, and Birgitte Bak-jensen. Arima-based time series model of stochastic wind power generation. *IEEE Trans. on Power Systems*, 25:667–676, 2010.

[166] J. W. Taylor, P. E. McSharry and R. Buizza. Wind power density forecasting using ensemble predictions and time series models. *IEEE Transactions on Energy Conversion*, 24:775–782, 2009.

[167] A. Shamshad, M. A. Bawadi and S. A. M. Sanusi. First and second order markov chain models for synthetic generation of wind speed time series. *Energy*, 30(3):1 to 22, 2005.

[168] N. B. Negra, O. Holmstrom, B. Bak Jensen and P. Sorensen. Model of a synthetic wind speed time series generator. *Wind Energy*, 11(11):193 to 209, 2008.

[169] MO. Wind speed and direction, england north sea, met office uk. https://www.metoffice.gov.uk/research/climate/maps-and-data/uk-and-regional-series, 2020.

[170] W. W. S. Wei. *Time Series Analysis Univariate and Multivariate Methods*. Redwood City, CA Addison-Wesley, 1990.

[171] Rob J Hyndman and Yeasmin Khandakar. Automatic time series forecasting: the forecast package for R. *Journal of Statistical Software*, 26(3):1 to 22, 2008.

[172] G. E. P. Box, G. M. Jenkins, and G. C. Reinsel. *Time Series Analysis Forecasting and Control*. Englewood Cliffs, NJ Prentice-Hall, 1994.

[173] Siemens Gamesa. Energy thrust. energy output upgrade for wind turbines. https://www.siemensgamesa.com/products-and-services/service-wind/energy-thrust, 2019.

[174] Andrew Henderson, Nick Baldock, Ivan Arana Aristi, and Chris Newton. Low hanging fruit for reducing the cost of energy: Optimising the electrical export capacity. In *Proceedings of EWEA Offshore Wind 2015*. EWEA, 2015.

[175] Jan Jurgensen, Lars Nordstrom, and Patrik Hilber. Estimation of individual failure rates for power system components based on risk functions. *IEEE transactions on Power Delivery*, 34(4):1599 to 1607, 2019.

[176] Wang Yong and Xueshan Han. Power system operational reliability equivalent modeling and analysis based on the markov chain. In *Proceedings of 2012 IEEE International Conference on Power System Technology (POWERCON)*, Auckland, New Zealand, 2012. IEEE.

[177] MOI. Mercator ocean international ambient temperature european north west shelf seas. https://resources.marine.copernicus.eu/, 2020.

[178] Jarmo Elovaara and Angela Klepac. *Impact of Ambient Conditions on Substations*. Number 2018:37 in TRITA-EECS-AVL. Springer, Cham, 2019. QC 20180423.

[179] G. Thornton. Clean energy pipeline - renewable energy discount rate survey results 2017. http://www.cleanenergypipeline.com/Resources/CE/ResearchReports/, Jan 2018.

[180] DOE. US department of energy - energy conservation program: Energy conservation standards for transformers. https://www1.eere.energy.gov/buildings/appliance_standards/pdfs/dt_final_rule.pdf, June 2019.

[181] Work Group A2.37. Transformer reliability survey. *CIGRE Technical Brochure*, page 122, Aug 2015.

[182] Johan Lofberg. Yalmip: A toolbox for modeling and optimization in matlab, 2020.

[183] LLC Gurobi Optimization. Gurobi optimizer reference manual, 2020.

Appendix - Additional plots for the *n-1* contingent design

For further demonstration of the iterative design optimization of OWF transformers in Chapter 8, this appendix presents the output of the optimization tool for the extreme case of multiple transformer contingency, as discussed in Section 8.3.1. Out of the two design concepts, the base n-1 contingent design results in zero energy curtailment during the worst case scenario of 2 simultaneous transformer failures (n-2 contingency) in year 8 as shown in Figure 1. But some curtailment is observed if the transformer size is reduced to the optimal rating because HST has to be limited to the 140 C limit [45] [44]. On the other hand, Figure 2 reveals that the non-contingent design concept results in some curtailment for both the base and optimal ratings during n-2 contingency situation.

Figure 1: Assessment of *n-1 contingent* design during n-2 contingency. Top: transformer load and power curtailment (base and optimal rating). Middle: thermal performance for base rating. Bottom: thermal performance for optimal rating

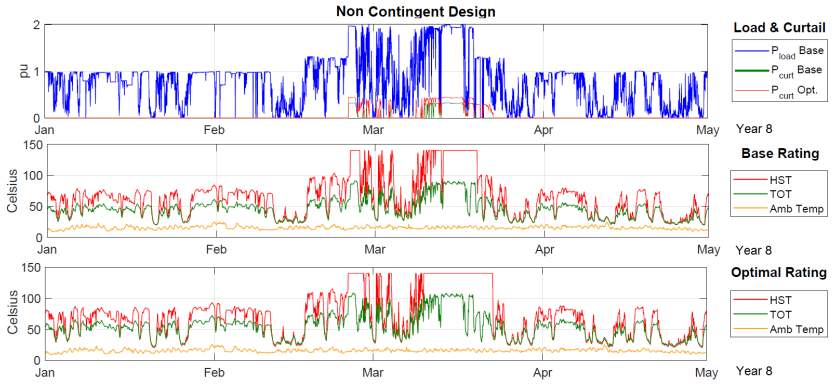

Figure 2: Assessment of *non-contingent* design during n-2 contingency. Top: transformer load and power curtailment (base and optimal rating). Middle: thermal performance for base rating. Bottom: thermal performance for optimal rating

Collection of relevant publications

[**Pub. J1**] S. H. H.Kazmi, T. Laneryd, K. Giannikas, S. F. Ahrenfeldt, T. H. Olesen, T. S. Sørensen and J. Holbøll, **"Cost optimized dynamic design of offshore windfarm transformers with reliability and contingency considerations"**, *International Journal of Electrical Power and Energy Systems* Dec 2020.

[**Pub. J2**] S. H. H.Kazmi, N. Viafora, B. C. Pal, T. S. Sørensen, T. H. Olesen and J. Holbøll, **"Offshore Windfarm Design Optimization using Dynamic Rating for Transmission Components"**, submitted to *IEEE Transactions on Power Systems*, Nov 2020.

[**Pub. C1**] S. H. H.Kazmi, T. H. Olesen, T. S. Sørensen and J. Holbøll, **"Thermoelectric Modelling and Optimization of Offshore Windfarm Export Systems - State of the Art"**, *IEEE Global Power, Energy and Communication Conference (GPECOM)*, Nevsehir, Turkey, July 2019.

[**Pub. C2**] S. H. H.Kazmi, T. H. Olesen, T. S. Sørensen and J. Holbøll, **"Dynamic Thermoelectric Modelling of Oil-Filled Transformers for Optimized Integration of Wind Power in Distribution Networks"**, Paper 1744, *25th International Conference on Electricity Distribution (CIRED)*, Madrid, Spain, June 2019.

[**Pub. C3**] S. H. H.Kazmi, T. H. Olesen, T. S. Sørensen and J. Holbøll, **"Dynamic Thermoelectric Modelling of Oil-filled Power Transformers for Optimization of Offshore Windfarm Export Systems"**, *CIGRE Symposium*, Aalborg, Denmark, June 2019.

[**Pub. C4**] N. Viafora, S. H. H. Kazmi, T. H. Olesen, T. S. Sørensen and J. Holbøll, **"Load Dispatch optimization using Dynamic Rating and Optimal Lifetime Utilization of Transformers,"** *IEEE PES PowerTech*, Milan, Italy, July 2019.

[**Pub. C5**] S. H. H.Kazmi, T. H. Olesen, T. S. Sørensen and J. Holbøll, **"Machine Learning based Temperature Forecast of Offshore Windfarm Export Cables"**, *B1-109 CIGRE*, Paris, France, Aug 2020.

[**Pub. C6**] S. H. H.Kazmi, T. H. Olesen, T. S. Sørensen and J. Holbøll, **"Thermal Analysis and Debottlenecking of HVAC Export Cables for Offshore Windfarms"**, Accepted (awaiting presentation), *3rd CIGRE South East European Regional Council Conference*, Vienna, Austria, Nov 2021.

[**Pub. C7**] S. H. H.Kazmi, T. H. Olesen, T. S. Sørensen and J. Holbøll, **"Machine Learning based Dynamic Thermal Modelling of Offshore Wind Turbine Transformers"**, Accepted (awaiting presentation), *41st CIGRE Symposium*, Ljubljana, Slovenia, Jun 2021.

[Pub. J1]

S. H. H. Kazmi, T. Laneryd, K. Giannikas, S. F. Ahrenfeldt, T. H. Olesen, T. S. Sørensen and J. Holbøll, **"Cost optimized dynamic design of offshore windfarm transformers with reliability and contingency considerations"**, *International Journal of Electrical Power and Energy Systems*, Volume 128, 2021, 106684, ISSN 0142-0615

The published version of the paper is attached and also available at https://doi.org/10.1016/j.ijepes.2020.106684

Electrical Power and Energy Systems 128 (2021) 106684

Contents lists available at ScienceDirect

International Journal of Electrical Power and Energy Systems

journal homepage: www.elsevier.com/locate/ijepes

Cost optimized dynamic design of offshore windfarm transformers with reliability and contingency considerations

Syed Hamza Hasan Kazmi [a,*], Tor Laneryd [b], Konstantinos Giannikas [a], Søren Frost Ahrenfeldt [a], Troels Stybe Sørensen [a], Thomas Herskind Olesen [a], Joachim Holbøll [c]

[a] Transformers & HV Components, Ørsted Wind Power A/S, Gentofte, Denmark
[b] Hitachi ABB Power Grids Research, Västerås, Sweden
[c] Dept. of Electrical Engineering, Technical University of Denmark, Lyngby, Denmark

ARTICLE INFO

Keywords:
Dynamic transformer rating
Offshore windfarm optimization
Transformer lifetime utilization
Contingency based design

ABSTRACT

Application of Dynamic Thermal Rating (DTR) for optimal utilization of transmission system components has been addressed in several studies. For Offshore Wind Power Plants (OWPPs), as a consequence of intermittent wind generation combined with favorable ambient conditions and strict design regulations, power transformers tend to be over-dimensioned. Experience suggests that transformer lifetime exceeds OWPP life by tens of years, therefore DTR-based design of transformers can facilitate the optimization of OWPP export system.

The recent breakthroughs in Thermo-Electric Equivalent (TEE) and aging models of transformers suggest that temporal development of Top Oil (TOT) and Hot Spot (HST) temperatures can be calculated efficiently, which when combined with monitoring of moisture and oxygen development can accurately assess the transformer health in real-time using Degree of Polymerization (DP). However, the economic optimization of offshore windfarms substations using DTR and lifetime utilization-based transformer design during the OWPP planning phase has not been addressed in the literature due to the risks involved in balancing system reliability with windfarm profitability.

In this paper, a novel strategy is proposed to utilize transformer DTR for cost optimization of offshore windfarm export system during the OWPP design phase. Net Present Value (NPV) is used to assess capital cost impacts on transformer and Offshore Substation (OSS) design in year 0, and yearly revenue change over OWPP lifetime due to increased losses and possible energy curtailment as a result of smaller transformers. The unique methodology accounts for varying wind turbine availability due to maintenance and concurs with OWPP design requirements for OSS transformer contingency by generating statistical scenarios based on distribution functions and Markov Chain (MC) models respectively. Moreover, the MC models are adapted for two fundamentally different design concepts for OWPP export system: *n-1 contingent* and *non-contingent*. The implementation of probabilistic Markov models to resolve stressful periods with increased transformer loading is distinctive to this paper and offers a unique perspective for DTR-based transformer size optimization. Long-term site assessment data for OWPP including historical wind generation is used for transformer thermal assessment (TOT and HST) based on its load and ambient conditions. Furthermore, the reliability of design for varying construction and commissioning conditions is ensured by tracking DP-based transformer lifetime utilization over the operation period for three scenarios of oxygen and moisture development: conservative, high moisture and high oxygen.

The case study of a 1200 MW offshore windfarm with two 220 kV parallel export circuits and four 33/220 kV transformers in one OSS located 50 km off the east coast of UK has been used in this paper. 100 scenarios of wind turbine availability and transformer contingency are simulated and the optimal design is determined for the worst-case scenario. Results indicate that optimal transformer rating can result in high thermal stress and minor energy curtailment during extreme contingency conditions for both the design concepts. However, the reduction in transformer size to align with OWPP operation life can reliably improve the windfarm business case significantly, particularly for the n-1 contingent design concept with conservative transformer moisture and oxygen conditions.

* Corresponding author at: Nesa Alle 01, DK-2820 Gentofte, Denmark.
E-mail address: syeka@orsted.dk (S.H.H. Kazmi).

https://doi.org/10.1016/j.ijepes.2020.106684
Received 4 August 2020; Received in revised form 12 October 2020; Accepted 28 November 2020
Available online 8 January 2021

Nomenclature

Acronyms

CCF	Common Cause Failures
DP	Degree of Polymerization, no unit
DTMC	Discrete Time Markov Chain
DTR	Dynamic Thermal Rating
HST	Hot Spot Temperature
LCOE	Levelised Cost of Energy
LL	Loss of Life [%]
MTTF	Mean Time To Failure
NCCF	No Common Cause Failures
NPV	Net Present Value [€]
OSS	Offshore Substation
OWPP	Offshore Wind Power Plants
RBD	Reliability Block Diagram
TEE	Thermoelectric Equivalent
TOT	Top Oil Temperature
WTG	Wind Turbine Generator

Parameters and constants

Δc_{oss}	change in OSS cost, [€]
ΔE_{curt}	change in curtailed energy, [MWh/yr]
ΔE_{loss}	change in energy losses, [MWh/yr]
$\Delta\vartheta_{or}$	rated TOT rise over ϑ_{amb}, [°C]
$\Delta\vartheta_{hr}$	rated HST rise over ϑ_{tot}, [°C]
λ	failure rate, [failure/year]
$\mu_{K,av}$	avg. windfarm availability, [%]
ν_{pu}	actual oil viscosity w.r.t. rated oil temperature, [pu]
ψ	random number generating function for WTG availability, [pu]
σ	standard deviation, [pu]
τ_0	thermal time constant - oil, [hour]
τ_h	thermal time constant - wdg, [hour]
τ_{WTG}	WTG availability duration, [hour]
ϑ_{amb}	ambient temperature, [°C]
$\vartheta_{hst,w}$	weighted average HST, [K]
ϑ_{hst}	hot-spot temperature (HST),[°C]
ϑ_{tot}	top-oil temperature (TOT), [°C]
A	pre-exponential factor, [1/hour]
c_{ossM}	weight dependent cost of OSS, [€/tonne]
C_{th}	thermal capacitance of transformer, [Wh/°C]
c_T	cost of transformer, [€]
c_w	strike price for windfarm, [€/MWh]
d_r	discount rate, [%]
e	empirically derived coefficient for transformer scaling
E_a	minimum activation energy to start the reaction (1.11×10^5), [kJ/mol]
E_{del}	energy delivered, [MWh/yr]
$K_{T,pu}$	transformer load current, [pu]
K_{WTG}	available WTGs in windfarm, [%]
L_{WF}	design lifetime of windfarm, [years]
M_T	mass of transformer, [tonne]
n_T	number of parallel transformers
$P_{loss,cu,T}$	transformer losses - load, [W]
$P_{loss,nl,T}$	transformer losses - no load, [W]
$P_{loss,T,pu}$	temperature dependent load losses of transformer, [pu]
P_{OSS}	power input at OSS, [W]
P_T	transformer rating, [W]
P_{WF}	maximum windfarm generation, [W]
R	ratio of transformer rated load losses to no-load losses, [pu]
r	repair rate, [repair/year]
R_g	ideal gas constant, [J/(mol.K)]
w	moisture content in the insulation paper, [pu]
x,y	empirically derived cooling coefficients for oil and winding
Z_T	representative transformer parameter in Table 2
$\mathbf{P}$	state transition matrix

Sets and indices:

base	base case
$i \in Y$	set of years
pu	per-unit value with rated value as base
$s \in S$	set of scenarios
$t \in \tau$	set of hours
$u \in U$	set of test-case designs

1. Introduction

Offshore wind energy has experienced exponential growth over the last decade, with cumulative global capacity reaching 23.1 GW in 2019. The strike price for offshore wind energy has driven down significantly from 195 €/MWh for the 402 MW Dudgeon windfarm completed in 2017 to 45 €/MWh for the 1200 MW Doggerbank Creyke Beck A to be completed in 2025 as per the latest CfD auction results [1]. This decrease in levelised cost of energy (LCOE) for offshore wind is facilitated by the intense price competition in the markets, which challenges the manufacturers and developers alike to optimize the entire value chain [2].

The electrical export systems for Offshore Wind Power Plants (OWPPs) are known to consist of not only components that are inherent bottlenecks like HV cables but also components that are commonly over-dimensioned like power transformers. The additional transformer capacity can be utilized during contingency conditions, but for OWPP applications that have an operation life between 25 and 30 years the transformers are still cautiously oversized [3]. This, when combined with the intermittent nature of the wind, can result in significant under-utilization of the transformer design lifetime (usually 40–45 years) [4]. Since the OWPP export transformers are the heaviest components located on the offshore substations, the optimal rating of these components can reduce the weight on offshore platforms significantly which can potentially drive down the LCOE for offshore wind even further.

Dynamic Thermal Rating (DTR) principle allows the transformers to be used beyond their nameplate ratings for given ambient temperature and load profile during the design process by setting a limit on maximum thermal capacity provided in IEEE C57.91 [5] and IEC 60076-7 [6] for both the normal cyclic and emergency loading conditions[7]. The recent breakthroughs in Thermo-Electric Equivalent (TEE) and aging models of transformers suggest that temporal development of Top Oil (TOT) and Hot Spot (HST) temperatures can be calculated efficiently [8,9]. This evaluation can be combined with monitoring of moisture and oxygen development for accurate assessment of transformer health in real-time [10–12]. The detrimental influence of transients (particularly cable switching and nearby faults) leading to transformer failure are of importance for transformer ageing [13]. However, the utilization of this information during the design phase is a challenging task because of limited research and practical experience in this field [14].

Due to the intermittent nature of the wind, annual capacity factor for OWPPs ranges between 38–46 % [1], which is also highly influenced by availability of wind turbines [15,16]. On the other hand, transformer outages due to maintenance or failures can result in additional thermal stress on the transformers still in operation [14,17]. It is possible to account for contingency situations by using a probabilistic approach based on Markov chain principle, which allows the simulation of

normal, abnormal and fail states [18] and by estimating failure rates based on risk functions [19]. Moreover, the overall cost and revenue optimization over the windfarm lifetime is crucial for such an approach because smaller transformers can result in energy curtailment and higher system losses [20].

Although optimal utilization of power transformers using DTR is a relatively unexplored concept, its application on transformers already installed in the transmission system [21,22] or in OWPPs [3,23] has been addressed in the literature. But DTR-based design of transformers during the planning phase of windfarms has not been touched upon, particularly because of the risks involved in determining transformer size that would ensure optimal system reliability and windfarm profitability. In this paper, a novel methodology is proposed for determining the rating of power transformers for cost optimization of offshore windfarm export system. The proposed framework utilizes DTR for transformer load optimization and ensures reliability of design by tracking lifetime utilization. The reliability aspect is further reinforced intuitively by simulating transformer probabilistic contingency situations for two unique design concepts suggested in this paper. The energy availability over the windfarm lifetime is optimized by weighing revenue loss due to energy loss and curtailment with upfront windfarm development and capital costs for different transformer designs.

The rest of the paper is based on the following structure. Section 2 starts off with a brief discussion on conventional design practices and importance of offshore windfarm transformers. This is followed by a detailed description of the individual blocks of the novel methodology proposed in this paper for reliability and economic optimization of OWPP transformers. The framework for transformer contingency and dynamic lifetime utilization analysis is also provided in this section. In Section 3, the test case windfarm export system for optimal transformer design is formulated and simulated worst-case contingency scenarios are illustrated. Moreover, the case studies of two design concepts for the windfarm transformers and relevant oxygen/moisture development are also elaborated in this section. Finally, the results of the test case are discussed in Section 4 and the paper is concluded in Section 5.

2. Background and methodology

This section takes a top-down approach to present the unique technique of defining the rating of offshore substation transformers based on dynamic rating and optimal lifetime utilization.

2.1. Power transformers and debottlenecking of OWPP export system

High Voltage AC based export systems for Offshore Wind Power Plants (OWPP), presented in Fig. 1, are connected to the onshore grid using long HV export cables. The number of substations needed to transmit the wind energy to the shore primarily depends on the length of the cable and the windfarm capacity, but the design regulations and the redundancy requirements of the local transmission system operator can also influence this number. The Offshore Substation (OSS), located close to the wind turbines, houses all the necessary HV equipment needed to collect the wind energy and to step-up the voltage for transmission through the export cables. Whereas before the connection of the HV export cables to the transmission grid on land, an intermediate onshore substation is usually needed. Some or all of the following components are part of these substations: HV transformers, shunt reactors, HV filters, dynamic compensators (incl. STATCOM, FACTS, SVC etc.), HV/MV switchgears, LV systems etc.

The offshore substation, like the one in Fig. 2, consists of the main power transformers also called OSS transformers, which are the heaviest components in the substation. Conventionally, these transformers are over-dimensioned for *n-1* contingency considerations, such that if one of the OSS transformers is not available, the rest should be able to supply uninterrupted power without the consideration of DTR. Whereas the capital investment associated with export cables drive the system designers to rate these cables to their thermal limits, which consequently makes the export cables the primary system bottlenecks. Therefore DTR is used to ensure optimal utilization of these components. On the other hand, due to the intermittent nature of wind and contingent over-dimensioning the additional capacity of transformers is rarely ever used which eliminates the need for employing DTR on OSS transformers designed using current practices. Hence in order to strive towards an optimal design of the export system, DTR should be taken into account for transformer design as well.

2.2. Method description of the proposed framework

The novel algorithm proposed in Fig. 3 provides the framework for optimal transformer rating for OWPP projects. The proposed methodology makes use of scenario generation principle to allow simulation of different randomly-chosen energy availability combinations. In the available data block, the historical site information including wind profile (speed and direction) and power curve for the chosen Wind Turbine Generator (WTG) model are used. These data along with ambient temperature profile are input to the reliability block which generates long-term scenarios of transformer loading while accounting for transformer and WTG contingency. The hourly load profile for OSS transformer is then used by the DTR block to calculate the thermal stress and determine transformer ageing based on this stress. Afterwards, the output block calculates the economic influence of energy losses and curtailment due to transformer size reduction. The Sections 2.3, 2.4 and 2.5 discuss the latter 3 blocks of the algorithm and the methodology behind each step extensively.

2.3. Reliability and availability considerations in scenario generation

The proposed methodology uses scenario generation to account for uncertainty in wind generation, variation in turbine availability and possible transformer contingency. In this paper, it is assumed that the availability of long-term site data can eliminate the need to address uncertainty in generation. But to address the influence of Wind Turbine Generators (WTGs) and export transformer outage, several reliability scenarios need to be simulated. Each of these scenarios will result in different thermal stress on the transformer. The scenario with the highest thermal stress causing worst case transformer ageing is to be used for the final design. It must be mentioned that this approach is probabilistic and the reliability of the final design would improve significantly, if sufficiently large number of scenarios are tested for.

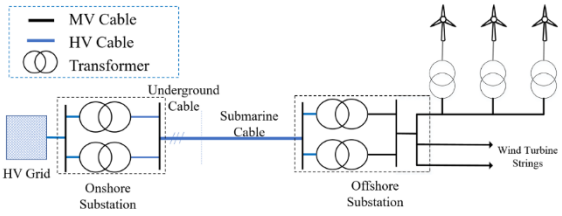

Fig. 1. Simplified layout for offshore windfarm export system.

Fig. 2. Offshore substation at Anholt windfarm.

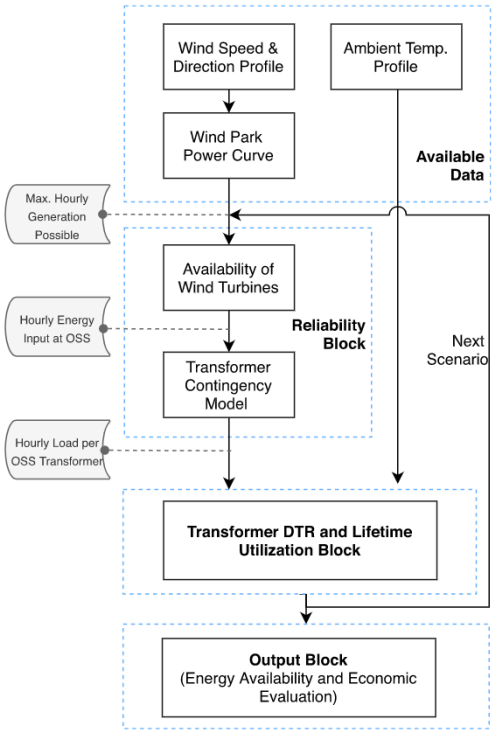

Fig. 3. Main algorithm for reliability and economic optimization of offshore windfarm transformers.

For offshore windfarms, system availability can be classified into two main categories: time and energy availability, each influencing the business case and system design differently. Time availability determines whether the system is connected to the grid connection point without necessarily being able to transmit the entire production capacity of the windfarm. Energy availability, on the other hand, depicts the ability of the export system to transmit the rated capacity of the offshore windfarm. Since time availability only determines the ability of the system to be connected to the grid at any given time, the actual business case is dependent on the amount of energy transmitted to the grid. Therefore, in this approach energy availability is used for dynamic rating based design of OSS transformers for achieving the most cost-effective transmission of generated energy to the onshore grid.

This paper splits energy availability into two design concepts: *n-1 contingent* and *non-contingent*. These two options are expected to be prevalent in OWPP export system design for future projects considering the trend in requirements in different markets across the globe. Considering the system of Fig. 1, the Reliability Block Diagrams (RBDs) for 100 % energy availability of these two design concepts with primary focus on offshore and onshore transformers are provided in Fig. 4. Irrespective of the number of parallel transformers in OSS, the RBDs will not change because the system will not be able to transmit 100 % energy (at rated windfarm production) to the shore in case of transformer failure(s) unless Dynamic Thermal Rating (DTR) based operation is considered [14].

2.3.1. Wind turbine availability

The mechanical and other stress on wind turbines result in frequent maintenance activities, which means that not all the WTGs will be available at all times [15]. Therefore it is important to understand the fact that even at ideal wind speeds, the windfarm production may not be 100%. On the other hand, the recently introduced power-boost function in the wind turbines makes it possible for offshore windfarms to produce beyond the rated capacity by resolving wake effect and other energy restricting phenomena at certain windspeeds [24].

These characteristics can be simulated and the percentage availability of WTGs in a windfarm K_{WTG} can be calculated by combining simple distributions [16]. The formulation in (1) uses two normally distributed functions ($\mathcal{N}_{act}$ and $\mathcal{N}_{out}$) to generate random numbers, the combination of which dictates the hourly windfarm generation or hourly energy input at OSS in Fig. 3. The first function generating 95% of the samples represents the general wind turbine availability, while the second function represents the remaining 5% outliers which allows incorporation of anomalies due to common-cause failures, natural events etc.

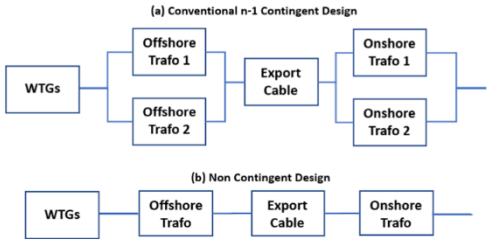

Fig. 4. Reliability block diagrams of simplified offshore windfarm export system of Fig. 1 for two different design concepts (irrespective of the number of transformers).

$$K_{WTG,s}(\tau_{WTG}) \sim \begin{matrix} \psi(0 \leqslant X(\tau_{WTG}) < 0.95) \cdot \mathcal{N}_{act,s}(\mu_{K,av}, \sigma^2_{act}) + \\ \psi(0.95 \leqslant X(\tau_{WTG}) \leqslant 1.0) \cdot \mathcal{N}_{out,s}(\mu_{K,av}, \sigma^2_{out}) \end{matrix} \quad (1)$$

s.t.

$$\{X \in \mathbb{R} | 0 \leqslant X \leqslant 1.0\}$$
$$\{\psi(z) = 1 | z = true\}$$
$$\{\psi(z) = 0 | z = false\}$$
$$K_{WTG,min} \leqslant \mathcal{N}_{act,s}(\mu_{K,av}, \sigma^2_{act}) \leqslant K_{WTG,max}$$
$$0 \leqslant \mathcal{N}_{out,s}(\mu_{K,av}, \sigma^2_{out}) \leqslant K_{WTG,max}$$
$$\sigma^2_{out} = 5\sigma^2_{act}$$

where X is a randomly generated real number between 0 and 1. The two normally distributed random variables ($\mathcal{N}_{act}$ and $\mathcal{N}_{out}$) are averaged around the mean availability of wind turbines $\mu_{K,av}$, but with varying standard deviations (σ_{act} and σ_{out}). The roll-over period τ_{WTG} defines the duration for which each availability is held (i.e. for how long a given number of WTGs will be available), which is influenced by wind turbine repair rate and other factors. The WTG availability figures in [15] can be reproduced by setting the variance of outliers σ^2_{out} considerably higher than the variance of actual windfarm availability σ^2_{act}, as shown in constraints for (1) [16]. It must be mentioned that both $\mathcal{N}_{act}$ and $\mathcal{N}_{out}$ are bound by maximum availability $K_{WTG,max}$ which can be higher than 100% to incorporate the power-boost feature. On the other hand the minimum general availability $K_{WTG,min}$ can be predefined based on operational and maintenance targets of the OWPP. As a result, the hourly energy input at OSS can be determined using (2), where P_{WF} represents maximum hourly generation possible by the windfarm for the given windspeed profile.

$$\begin{matrix} P_{OSS,s}(t) & = K_{WTG,s}(\tau_{WTG}) \cdot P_{WF}(t) \\ \text{s.t.} & t \leqslant \tau_{WTG} \end{matrix} \quad (2)$$

2.3.2. Contingency of OSS transformers

For the proposed methodology, the load on individual transformers will have to be scaled as the number of transformers available at a given time changes. At a given instant, each transformer can either be available for operation (UP state) or not due to failure, maintenance etc (DOWN state). The phenomena of transition between these states is shown in Fig. 5. In this paper, the transformer failure and repair simulations are performed using Discrete Time Markov Chain (DTMC) model, which takes a probabilistic determination approach for transition of a system between states [19,20].

For the state transition matrix **P** in Fig. 5, the diagonal elements represent the probability of staying in the respective states during time-step Δt. While the non diagonal elements in each row represent the probability of jumping from that state to the respective state of the column. For constant failure and repair rates λ and r, the probability that a component will fail within time-step Δt is approximately $\lambda\Delta t$. While its probability of returning from a failed state to normal state within the time step is $r\Delta t$ [18].

For a system with n_T parallel transformers, the total Markov states will be $n_s = 2^{n_T}$ if Common Cause Failures (CCF) are considered and $n_s = n_T + 1$ for No Common Cause Failures (NCCF). For simplification of design, the paper further classifies these Markov states into Normal, Abnormal and Fail conditions, such that transformer load stays within the design capacity for normal state only.

Offshore developers tend to use two different design concepts for transformers: n-1 contingent and non-contingent designs. The former approach is more conservative as total transformation capacity is considerably more than OWPP size. Therefore, n-1 contingent design would behave normally (load ⩽rated load) even when one transformer is out of operation; where as for the non-contingent design, normal state would only be possible when all the transformers are available. The fail state will only occur when all the transformers are simultaneously unavailable, while all the remaining states would classify as abnormal. This is further illustrated in Fig. 6 for NCCF considerations, where the number of states for 3 parallel transformer system: 3UP (all transformers in operation), 2UP (one transformer failure), 1UP (two transformers failure) and 0UP (all transformers failure) are classified into normal, abnormal and fail state types for the two design concepts.

The discussion so far has been summarized in Table 1 for a general system with n_T parallel transformers for both NCCF and CCF considerations. It is noteworthy that the total number of normal states are generally higher for n-1 contingent design as compared to non-contingent one. Furthermore, the importance of using Dynamic Thermal Rating (DTR) for maximizing the availability of energy or energy transferred to the shore particularly for the abnormal state is also highlighted in Table 1. Lastly, depending on the system state, the transformer contingency block in Fig. 3 scales the individual transformer load as per windfarm production for DTR case [7], which is elaborated further in Section 3.3.

2.4. Transformer DTR and lifetime utilization

In order to ensure reliable operation of power transformers over the course of their lifetime, it is important to determine their thermal performance over the period [14]. This can be done by determining two key parameters: Top Oil Temperature (TOT) and Hot Spot Temperature (HST). Moreover, the influence of oxygen and moisture on ageing of paper insulation needs to be tracked as well. It is important to mention that transient stresses can often lead to premature failure of transformers, which is of particular interest in the offshore environment [13]. However, since the size optimization of transformer directly influences the thermal stress and remaining design parameters are left to be untouched, this paper assumes the transformer to be able to withstand these transients over OWPP lifetime.

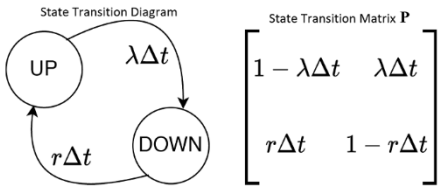

Fig. 5. Illustration of state classification for a 3 parallel transformers system with NCCF considerations for both *n-1 contingent* and *non-contingent* design concepts.

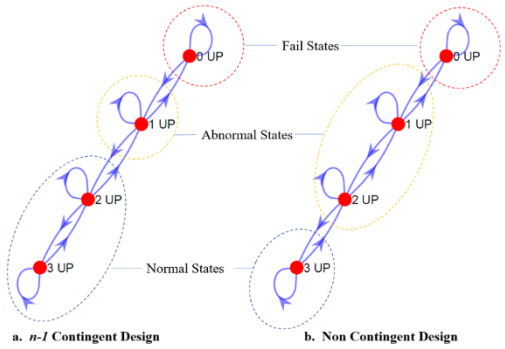

Fig. 6. Illustration of state classification for a 3 parallel transformers system with NCCF considerations for both *n-1 contingent* and *non-contingent* design concepts.

In Fig. 7, the DTR and lifetime utilization block from Fig. 3 is expanded. There are two sub-blocks, the steps in which are repeated for each scenario and each transformer size under consideration. The first sub-block computes the temporal evolution of critical transformer temperatures (TOT and HST) and curtails the transformer load when these temperatures cross the predefined limits. The second sub-block determines transformer's Loss of Life (LL) over the windfarm lifetime for the calculated HST and predefined oxygen and moisture conditions using Degree of Polymerization (DP). It should be mentioned that the influence of varying transformer size and winding temperature on load and no load losses are also considered. The models used for thermal and ageing assessment of transformers are explained in detail in the sub-Sections 2.4.1 and 2.4.2.

2.4.1. Thermal assessment of transformers using Thermoelectric Equivalent (TEE) models

The estimation of critical transformer temperatures can either be done by using state-of-the-art Thermoelectric Equivalent (TEE) models or by using computational fluid dynamics based and thermohydraulic network based models which are more complex to develop and require additional design information about the transformer [25].

The TEE models, also known as empirical models because of their experiential nature, provided in the international loading guides IEEE C57.91 [5] and IEC 60076-7 [6] are simpler to implement and accepted across the industry. However, the models presented in [8,9] are found to perform better for low ambient temperatures and varying load conditions by accounting for temperature dependent oil viscosity variation and load losses. This property makes them more adequate for offshore windfarm transformer application [3].

The top-oil and hot-spot temperatures can be determined using Eqs. (3) and (4) from [9]. The structure of these equations is similar to the models presented in IEEE C57.91 but the placement of transformer cooling mode coefficients and oil viscosity variation parameter in the models is the key difference [3].

$$\tau_0 \frac{d\vartheta_{tot}}{dt} = \Delta\vartheta_{or}\left(\frac{K_{T,pu}(t)^2 R + 1}{R+1}\right) - \left(\frac{\vartheta_{tot}(t) - \vartheta_{amb}(t)}{\left[\nu_{pu}(t)\Delta\vartheta_{or}\right]^{1-x}}\right)^{1/x} \tag{3}$$

$$\tau_h \frac{d\vartheta_{hst}}{dt} = \Delta\vartheta_{hr} K_{pu}(t)^2 P_{loss,T,pu}(\vartheta_{hst}) - \left(\frac{\vartheta_{hst}(t) - \vartheta_{tot}(t)}{\left[\nu_{pu}(t)\Delta\vartheta_{hr}\right]^{1-y}}\right)^{1/y} \tag{4}$$

$$\tau_0 = C_{th}\left(\frac{\Delta\vartheta_{or}}{P_{loss,T}}\right) \tag{5}$$

where ϑ_{tot} and ϑ_{hst} represent the calculated TOT and HST respectively, expressed in °C. $K_{T,pu}$ is the transformer load current in p.u. with rated load current as base; R is the ratio of load losses to no-load losses at rated load; $\Delta\vartheta_{or}$ is the TOT rise over ambient temperature ϑ_{amb} at rated load

Table 1
Classification of Markov states and design concepts.

State Class	No. of States n_s in Considered Design Concepts				Energy Availability		Transformer Load Scaling Factor
	$n-1$ Contingent Design		Non Contingent Design				
	CCF	NCCF	CCF	NCCF	w/o DTR	DTR	(DTR)
Normal	$1+n_T$	2	1	1	Full *	Full	Rated (≤ 1)
Abnormal	$2^{n_T}-(n_T+2)$	$(n_T+1)-3$	$2^{n_T}-2$	$(n_T+1)-2$	Partial	Full °	Increased ($\geqslant 1$)
Fail	1	1	1	1	Nil	Nil	No Load (0)

CCF - Considering common cause failures and limited repair resources
NCCF - Not considering common cause failures and repair resources are not limited
* Full energy available unless curtailment needed due to extreme ambient conditions or thermal limitations.

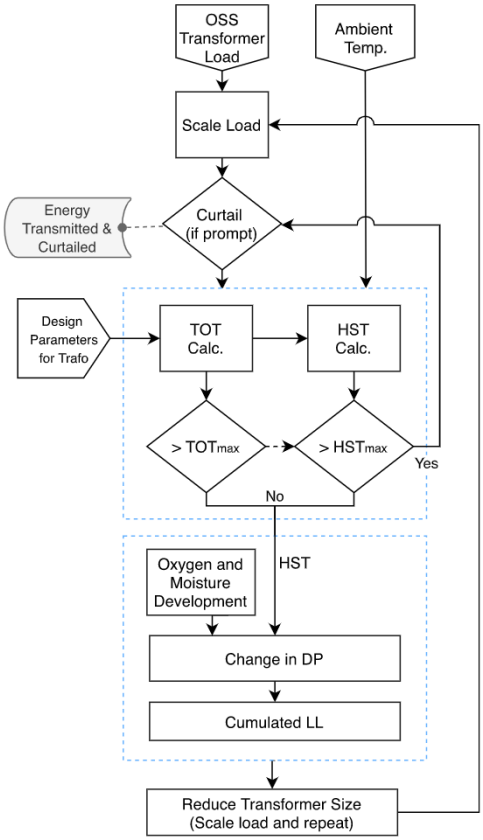

Fig. 7. Transformer DTR and lifetime utilization block.

both expressed in °C, while $\Delta\vartheta_{hr}$ is the rated HST rise over TOT for rated load of 1 pu. The thermal time constant for oil τ_0 (hour), dependent on rated TOT rise over ambient temperature $\Delta\vartheta_{or}$, total transformer losses at rated load $P_{loss,T}$ (Watt) and thermal capacity of the oil C_{th} (Wh/kg °C) is performed using (5).

The time-varying, temperature-dependent oil viscosity ν_{pu} is the ratio between the actual oil viscosity ν_{oil} at time t and oil viscosity at rated TOT rise ν_{or}, as mentioned in (6). Similarly, $P_{loss,T,pu}(\vartheta_{hst})$ presents the dependence of load losses on temperature, which are represented in pu with $P_{loss,T}$ as base and has been illustrated in [9].

$$\nu_{pu}(t)=\frac{\nu_{oil}(t)}{\nu_{or}}=e^{\left(\frac{2797.3}{\vartheta_{tot}(t)+273}-\frac{2797.3}{\vartheta_{amb}(t)+\Delta\vartheta_{or}+273}\right)} \tag{6}$$

The transformer cooling modes determine the values of the constants x and y which are derived empirically. The heat flow is non-linearly dependent on temperature difference which influences the convective cooling process. Therefore the transformer cooling mode (free or forced convection) defines the change in temperature gradient for transformer oil and winding [26]. The first-order differential equations of (3) and (4) can be solved using Backward Euler approximation by assuming cold-start for transformer and initiating ϑ_{tot} and ϑ_{hst} to be same as ϑ_{amb}. The initialization has minimum influence on long-term estimation over OWPP lifetime, as the solution quickly reaches stability and the influence of initial error are minimized as per Lyapunov stability principle [27].

2.4.2. Thermal life expectancy of insulation

For risk-based estimation of failure rates, the reliability of the proposed methodology is ensured by tracking the aging of insulation paper over its lifetime [19]. Solid insulation is generally considered to be the primary component that defines the transformer's lifetime, as it is more sensitive to high temperatures as compared to other components close to the HST location. Moreover, the difficulty to replace the paper and pressboard after a failure and the associated system downtime makes the ageing analysis of the commonly used cellulose-based insulation crucial for defining the transformer's end-of-life [28].

The heat transfer from the hottest spot of the winding serves as catalyst for chemical reactions, which accelerates the aging of insulation paper. As the cellulose ages thermally in an operating transformer, three mechanisms contribute to its degradation: Hydrolysis, Oxidation and Pyrolysis. Whereas, the agents responsible for the respective mechanisms are residual moisture content in paper, oxygen content in oil, and heat at HST location.

The property of the cellulose-based solid insulation paper that is widely accepted to indicate its integrity is the tensile strength measured via Degree of Polymerization (DP) estimation [12]. The variation in DP of paper insulation can be described by reformulating the Arrhenius reaction rate theory in terms of a first order process:

$$\frac{1}{DP(t)}-\frac{1}{DP_0}=Ae^{\frac{E_a}{R_g[\vartheta_{hst}(t)+273]}}t \tag{7}$$

$DP(t)$ and DP_0 represent the DP values at the end and in the beginning of the examined time frame respectively. E_a is the minimum activation energy to start the reaction, the value of which is fixed to 1.11×10^5 kJ/mol based on the analysis in [11,10]; R_g is the ideal gas constant (8.314 J/(mol K)). The pre-exponential factor A (in 1/hour) is dependent on moisture and oxygen contents, and can be determined using either of the approaches proposed in [10,29].

This formulation can be used to enumerate the change in DP after each interval. But in order to determine the effect of oxygen and moisture variation over the transformer life, it is important to use average representative values of HST over longer periods (days, months, years etc.) instead of instantaneous values. However, using numerical average of HST will be inappropriate because of the nonlinear relation in (7). Therefore, it is proposed to use the weighted average HST $\vartheta_{hst,w}$ (Kelvin) which results in similar aging over the given time period by incorporating the Arrhenius reaction factor $e^{\frac{E_a}{R_g[\vartheta_{hst}(t)+273]}}$ as the varying HST would. This is shown in (8), where i represents the number of

instantaneous intervals with constant HST over the length of selected long periods.

In order to assess the transformer's expected lifetime for the given loading, the industry-wide accepted end-of-life criterion is used [7]. The criterion suggests that a newly commissioned transformer has a DP value of 1000 when put into operation. Whereas when the DP value decreases to 200, at which its retained tensile strength falls to 20%, the transformer is said to have reached its end-of-life [5]. Hence, for the given load condition, the percentage loss-of-life (*LL*) of the transformer during the time-period t_i is calculated using (9).

$$\vartheta_{hst,w} = \frac{1}{\frac{R_g}{E_a} ln \frac{\sum_1^i e^{\frac{E_a}{R_g[\vartheta_{hst}(i)+273]}}}{i}} \text{ [K]} \tag{8}$$

$$LL_i = \frac{t_i}{\frac{1}{1000}\frac{1}{A} e^{\frac{E_a}{R_g \vartheta_{hst,w}}}} \times 100 \text{ [\%]} \tag{9}$$

2.5. Economic evaluation

The overall economic influence of the novel problem proposed in this paper can be evaluated by assessing the individual cost impacts of using smaller OSS transformers. Two major aspects are considered in this paper: capital expenses in the year 0 and revenue over the OWPP lifetime which accounts for energy curtailment due to DTR [20] The minor influences on costs related to operation, maintenance, installation etc. are not considered.

Variation of transformer cost, mass and losses can be empirically derived by relating the transformer rating $P_{T,u}$ with the base transformer size $P_{T,base}$ using (10) and respective scaling exponent *e* from Table 2 [30], such that *Z* is replaced by the relevant parameter. The transformer scaling relation has been derived by fixing four parameters including frequency, basic insulation level, current density and magnetic flux density, while varying only the core dimensions (cross-section and window area for windings) with transformer rating.

$$\Delta Z_{T,u} = Z_{T,base}\left[1 - \left(\frac{P_{T,u}}{P_{T,base}}\right)^e\right] \tag{10}$$

The business case assessment of transformer size optimization is done by calculating the variation in Net Present Value (NPV), as shown in (12).

$$NPV_u = NPV_{base} + \Delta NPV_u \tag{11}$$

$$\Delta NPV_u = \Delta c_{T,u} + \Delta c_{oss,u} - \sum_{i=1}^{L_{wf}} c_{w,i}\left(\frac{\Delta E_{curt,i,u} + \Delta E_{loss,i,u}}{(1+d_r)^i}\right) \tag{12}$$

ΔNPV_u determines the change in Net Present Value (€) between the base test case and reduced transformer size test case *u*. Hence positive ΔNPV_u would reflect a good business case of using a smaller transformer over the windfarm lifetime, while negative and zero values represent poor and neutral business cases respectively. Therefore, in this algorithm the reduction in transformer size is considered to have influences on three major costs:

- Reduction in cost of transformer $\Delta c_{T,u}$ (€) using (10) and scaling exponent *e* from Table 2, such that Z_T is replaced by transformer cost c_T.

Table 2
Scaling exponents for (10) for oil-filled HV power transformers [30]

Symbol for Z_T	Transformer Parameter	Value of Exponent *e*
M_T	Mass	3/4
c_T	Cost	3/4
$P_{loss,cu,T}$	Load loss (rated)	4/5
$P_{loss,nl,T}$	No-load loss (rated)	4/5

- Reduction in cost of OSS $\Delta c_{oss,u}$ (€). This cost is directly influenced by reduction in transformer weight and footprint. Offshore substation foundation contribute substantially to the overall OSS cost and it is known to depend directly upon the offshore platform's weight. Since transformers are the heaviest components on the platform, $\Delta c_{oss,u}$ can directly be related to transformer weight and footprint reduction. Although their relation with the amount of steel is complicated to derive, experience suggests that a unit change in transformer weight is complemented by a unit change in platform steel weight reduction as well. Hence, the overall OSS cost reduction $\Delta c_{oss,u}$ (€) can be estimated using (13), where c_{ossM} is weight dependent cost of OSS (€/tonne) and ΔM_T is determined using (10) and Table 2.

$$\Delta c_{oss,u} \sim 2 c_{ossM}\left(\Delta M_{T,u}\right) \tag{13}$$

- Loss in revenue due to increased energy curtailment and transformer losses over windfarm lifetime L_{wf} (*years*). As compared to the base case, the energy curtailment and transformer energy losses in year *i* are expected to increase by $\Delta E_{curt,i,u}$ and $\Delta E_{loss,i,u}$ (MWh/year) respectively for the test case *u*. Both these energies are obtained as outputs of the proposed algorithm, but the transformer losses need to be scaled. Therefore the no load losses $P_{loss,nl,T}$ and copper losses $P_{loss,cu,T}$ are scaled with respect to the base size using (10) and Table 2. Furthermore c_w represents the price of energy to be sold from the windfarm (€/MWh), while d_r is the discount rate (%) in (12).

3. Case study and problem formulation

3.1. Test case windfarm export system

In order to assess the credibility of the proposed methodology, the test OWPP export system presented in Fig. 8 is used. The 1200 MW offshore test windfarm located in the North Sea, approximately 50 km off the coast of UK, transmits the generated energy to the shore using four 33/220 kV transformers and two 220 kV export cables. For this case study, the HV cables and the electrical equipment other than transformers in the offshore substation are deliberately over-dimensioned to avoid bottlenecks during contingency simulations. For the two design concepts established in this study, two different transformers are used. The parameters relevant for thermal assessment of these transformers are provided in Table 3.

For economic evaluation, the discussion in [31] for a 1.2 GW offshore windfarm is followed and the available cost functions are updated for inflation and currency conversion. The two OSS will cost 86.4 M€, each weighing 1200 tonnes approximately. Considering 1:1 ratio between fixed costs and weight dependent foundation costs, c_{ossM} is estimated to be 18000 €/tonne $\left(\frac{86.4}{2}\cdot\frac{1}{1200}\cdot\frac{1}{2}\right)$. The discount rate is set to 6.75% [32], and the c_w is fixed to 44.99 €/MWh over the OWPP lifetime, which is similar to the strike price of the 1.2 GW Doggerbank Creyke Beck A as per the latest CfD auction results [1].

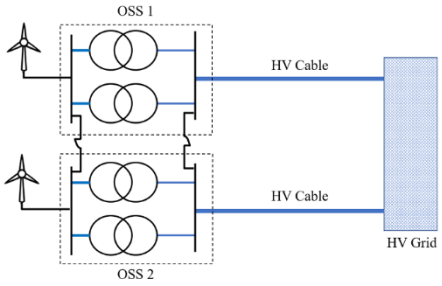

Fig. 8. Test case offshore windfarm export system.

Table 3
Transformer thermal parameters for base size [9,22]

Parameters		Design Concept	
Symbol	Unit	*n-1* Contingent	Non Contingent
$P_{T,base}$	MVA	400	300
$P_{loss,cu,T}$	kW	580.6	411.8
$P_{loss,nl,T}$	kW	111.6	74.7
$\Delta\vartheta_{or}/\Delta\vartheta_{hr}$	°C	40.2/21.1	38.3/20.3
C_{th}	kWh/K	80.2	59.6
τ_h	min	6.6	7
$M_{T,base}$ [30]	tonne	402	297
$c_{T,base}$ [30]	M€	2.7	2.1

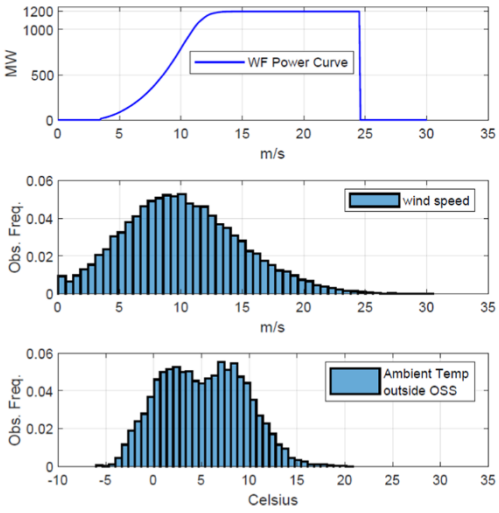

Fig. 9. Available data for the 1.2 GW MW test case windfarm in the North Sea. OWPP power curve, normalized histograms for wind speed [33] and ambient temperature profiles outside OSS [34] for 15 years.

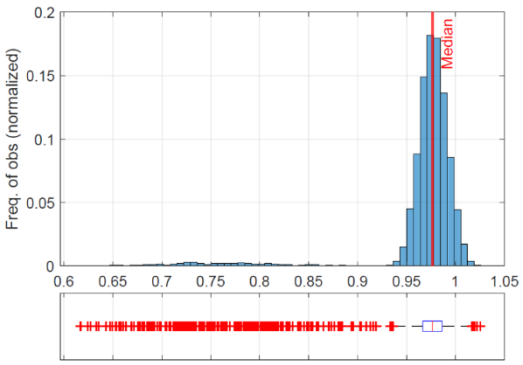

Fig. 10. Availability of percentage of wind turbines over the 30-year design lifetime for one of the simulated scenarios for the test case windfarm.

$$\mathbf{P} = \begin{bmatrix} 1-4\lambda(\Delta t) & 4\lambda(\Delta t) & 0 & 0 & 0 \\ r(\Delta t) & 1-(r+3\lambda)(\Delta t) & 3\lambda(\Delta t) & 0 & 0 \\ 0 & 2r(\Delta t) & 1-(2r+2\lambda)(\Delta t) & 2\lambda(\Delta t) & 0 \\ 0 & 0 & 3r(\Delta t) & 1-(3r+\lambda)(\Delta t) & \lambda(\Delta t) \\ 0 & 0 & 0 & 4r(\Delta t) & 1-4r(\Delta t) \end{bmatrix} \tag{14}$$

15 years of historic hourly wind speed data for the test case windfarm has been used in this study [33]. This is further complemented by the 15-year hourly ambient temperature data for the OSS available at [34]. The influence of varying ϑ_{amb} on OSS's internal temperature that the transformers will endure is simulated using the approach prescribed in [35]. The relevant preprocessed data has been plotted in Fig. 9 along with the power curve for the test windfarm. It is important to note that the design lifetime of the test windfarm is 30 years, therefore it is assumed that the data will repeat itself after the 15 year duration.

3.2. Considerations for reliability evaluation

The WTG availability over the 30 year design lifetime of the test case windfarm is defined using (1). The average availability μ_{av} is set to 96% based on practical experience reported in [36], while the maximum availability $\mu_{av,max}$ is set to 105% to account for power-boost function in WTGs [24]. The number of available WTGs follow a day-to-day turnover hence each day is treated to have an independently drawn random number of WTGs in service ($\tau_{WTG} = 24$ h) [16]. The resulting distribution for one of the simulated scenarios is shown in Fig. 10.

For transformer contingency, the reliability survey from [17] has been used. For 220 kV large offshore transformers (>100 MVA), the Mean Time To Failure (MTTF) is approximately 25 years, with average repair time of 73 days (repair rate $r = 5$ repairs/year). However, the increased loading due to DTR can lead to frequent transformer down-time (failure and maintenance), which is why this paper ensures reliability of design by considering conservative MTTF of 10 years (failure rate $\lambda = 0.1$ fail/year) [20]. Referring to Table 1, for the given case of 4 parallel transformers for NCCF considerations with unrestricted repair resources, the system will have 5 possible states as specified in the state transition matrix **P** in (14) where $\Delta t = 1$ hour (1/8760 years). The transition probability for each state is provided in Fig. 11 for both the design concepts. It is important to note that due to low failure and repair rates, the probability of transition between states is also low for the given test case.

Finally, the reliability of design is ensured by simulating multiple scenarios (Section 3.4), and quantifying the following reliability indices: Transformer LL (Section 4.2), Energy delivered E_{del} and NPV for cost reliability benefits (Section 4.3).

3.3. Test case classification

The proposed methodology is unique in its adaptability for different design and operation practices of the industry. This is demonstrated by considering the following test case classifications.

3.3.1. System design concepts

The two design concepts of either accounting for contingency during transformer design or completely relying on DTR during transformer contingency will be considerably prevalent in the offshore windfarm industry. Therefore both these design approaches are tested and the respective influence on transformer load at different states of transformer availability is provided in Table 4. The need for energy curtailment and transformer losses is also shown.

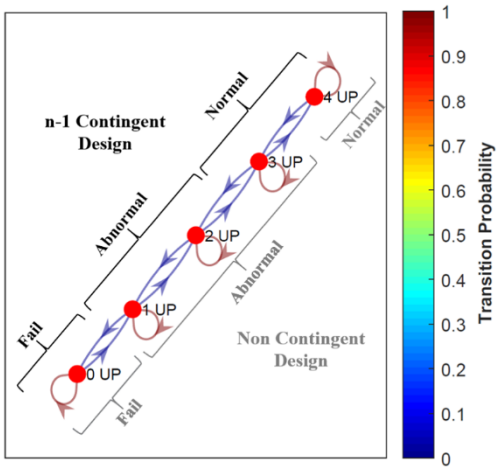

Fig. 11. State transition probability and state classification for n-1 and non contingent design concepts for the four-transformer test case.

3.3.2. Oxygen and moisture variation

Besides examining the influence of varying HST, the acceleration of transformer insulation aging due to moisture and oxygen is assessed for three different scenarios identified in Table 5: Conservative, High moisture development in paper, High oxygen ingress in oil. This is performed not only to ensure the reliability of this analysis but also to generalize its applicability to transformers with varying manufacturing quality and operating conditions.

3.4. Scenario generation and simulation results

Cost and design optimization of offshore windfarms is an iterative process because of the associated uncertainty. In the proposed methodology this uncertainty is resolved by repeating the calculation for multiple scenarios. For the given test case, 100 scenarios have been generated and optimal transformer size is determined based on the worst scenario. A dedicated test machine (i7-9850H 2.6 GHz with 6 cores, 64 GB RAM and 64-bit Windows 10 OS) took 5.5 h to complete the end-to-end simulations. The differential equations were solved using Backward Euler approximation in Matlab. It is recommended to generate even more scenarios to ensure reliability of design.

In Fig. 12, 10 worst-case scenarios out of the simulated 100 scenarios are provided. The box-plots for the 15 year time series for wind turbine availability, power entering the OSS (windfarm generation) and transformer load for the two design concepts disclose that two transformers failed simultaneously at some point for scenarios 6 and 7 only. Scenario 7 resulted in highest thermal stress and highest ageing acceleration, which is why from this point onward this paper presents results for this scenario only.

Table 5
Development of moisture in paper and oxygen in oil over 30 years for the 3 examined scenarios

Scenario	Moisture (%)		Oxygen (ppm)	
	Initial	Final	Initial	Final
Conservative	0.5	3	2000	7000
High Moisture	2	5	2000	7000
High Oxygen	0.5	3	20,000	40,000

The simulation of transformer states over the observed duration for scenario 7 is provided in Fig. 13. It can be observed that the two-transformer-failure state (2UP) is reached close to Year 8, but the state 1UP occurs multiple times over the 15-year duration. Referring to Fig. 14, the n-1 contingent design will mostly be in Normal Load state (⩽rated load) over the course of first 15 years except for a small duration Year in 8. Where as for the Non Contingent Design, the probability of abnormal load state is higher and is exhibited frequently over the observed simulated duration. This will definitely influence the difference in optimal rating of transformers for the two design concepts.

4. Results and discussion

4.1. Thermal assessment during critical periods

Out of the two design concepts, the base n-1 contingent design results in zero energy curtailment during the worst case scenario of 2 simultaneous transformer failures (n-2 contingency) in year 8 as shown in Fig. 15. But some curtailment is observed if the transformer size is reduced to the optimal rating because HST has to be limited to the 140 C limit [5] [6]. On the other hand, Fig. 16 reveals that the non-contingent design concept results in some curtailment for both the base and optimal ratings during n-2 contingency situation.

For a less thermally stressful period of 1 transformer failure in year 13, shown in Fig. 17, neither of the designs violate the thermal limits for HST and TOT for the base size. However minor curtailment will be needed for optimally rated transformer for the non-contingent design. The HST distribution for the entire windfarm lifetime in Fig. 18 for n-1 contingent design reveals that as the transformer size decreases HST tends to get closer to the recommended thermal limits but it still operates at low HST values for a significant portion of its lifetime.

4.2. Lifetime assessment for size optimization

The lifetime utilization of transformers over the 30-year design lifetime shown in Fig. 19 reveals that highest reduction in DP is observed

Table 4
Design concepts and their influence on transformer load and power delivered for each state

n-1 Contingent Design Concept				Non-Contingent Design Concept			
State		Load Scaling Factor	Total Power Curtailment and Losses	State		Load Scaling Factor	Total Power Curtailment and Losses
Name	Description			Name	Description		
4 UP	Low load	0.75	$P_{curt} = 0$ $P_{loss} < P_{loss,r}$	4 UP	Rated load	1.0	$P_{curt} = 0$ $P_{loss} \leqslant P_{loss,r}$
3 UP	n-1 contingency (rated load)	1.0	$P_{curt} = 0$ $P_{loss} \leqslant P_{loss,r}$	3 UP	n-1 contingency (high load)	1.33	P_{curt} and P_{loss} calc. by simulation
2 UP	2 transformers share total load	1.5	P_{curt} and P_{loss} calc. by simulation	2 UP	2 transformers share total load	2.0	P_{curt} and P_{loss} calc. by simulation
1 UP	1 transformer supplies total load	3.0	P_{curt} and P_{loss} calc. by simulation	1 UP	1 transformer supplies total load	4.0	P_{curt} and P_{loss} calc. by simulation
0 UP	All transformers offload	0	$P_{curt} = P_{gen}$ $P_{loss} = 0$	0 UP	All transformers offload	0	$P_{curt} = P_{gen}$ $P_{loss} = 0$

Fig. 12. 10 worst-case scenarios out of 100 scenarios simulated over 15 years showing wind turbine availability, power entering OSS and transformer load for the two design concepts.

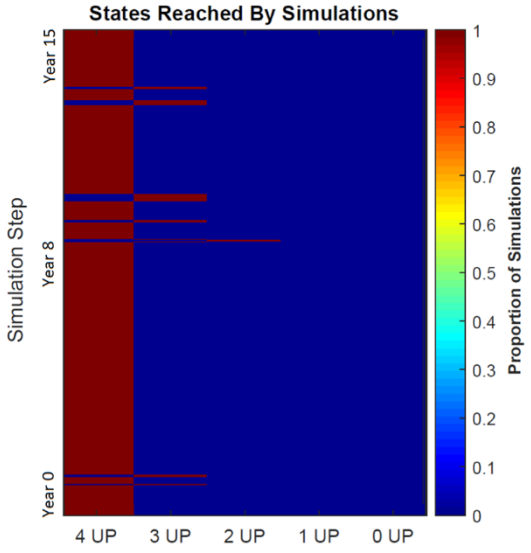

Fig. 13. States reached during DTMC simulations for worst-case scenario 7 in Fig. 12.

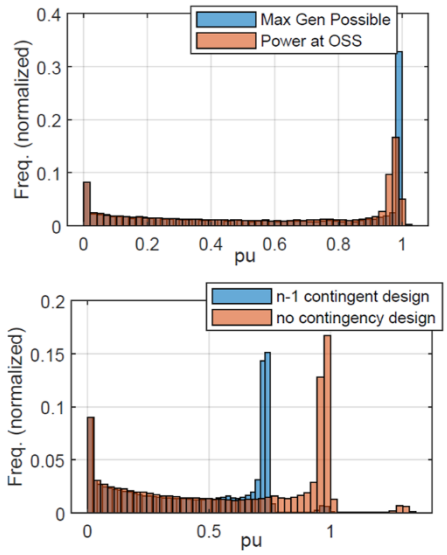

Fig. 14. Histograms for power at different stages for scenario 7. Top: OWPP generation (pu) considering 100% and varying WTG availability. Bottom: Transformer loading in pu for the two design concepts.

during the two n-2 contingency situations because of high HST. But as the transformer size is reduced, even one transformer failure can be thermally stressful for the transformers resulting in accelerated ageing. The influence of transformer size reduction on weighted HST and lifetime utilization is provided in Fig. 20 for the two design concepts. It is perceivable that for the n-1 contingent design, transformer size can be reduced to 70% of its base design to outlast the windfarm design lifetime. Whereas, for the non-contingent design, this reduction can only be to 90%.

4.3. Transformer rating for economic optimization

It is important to note that even though a smaller transformer can match the lifetime of the windfarm, it might still not be optimal for the overall business case. This is because smaller transformers will result in higher curtailment during contingency situations and higher losses due to high temperatures. This is verified in Fig. 21 for the two design concepts in which energy delivered $E_{del} = \sum_{i=1}^{L_{wf}} \sum_{t=1}^{8760} \left(P_{gen,t,i} - P_{loss,t,i} - P_{curt,t,i}\right)$. The overall efficiency of power transmission reduces by 0.25 % for the n-1 contingent design if the transformer size is reduced to 70 percent of the base rating.

The business case for the two design concepts has been assessed by calculating the change in NPV as compared to base transformer size using (12). The results in Fig. 22 for the worst case scenario suggest that the n-1 contingent design concept can improve the NPV by up to 5 M€ for the given test case of 1200 MW windfarm with 4 transformers, if all the OSS transformers' rating are reduced to 85% of their original capacity. For the non-contingent concept, the extent of this frugality is significantly lower but even in this case, transformer size of 0.9 pu will result in the best business case. The average cost reduction for the 100 scenarios is 7.6 M€ at 0.75 size factor for the n-1 contingent design concept and 1.5 M€ at 0.85 size factor for the non contingent design concept.

4.4. Influence of oxygen and moisture variation

It is understood that the impact of oxygen content in oil on insulation aging is much more severe as compared to moisture content in paper. This characteristic is clearly demonstrated in Fig. 23, where the

Fig. 15. Assessment of *n-1 contingent* design during n-2 contingency. Top: transformer load and power curtailment (base and optimal rating). Middle: thermal performance for base transformer rating. Bottom: thermal performance for optimal transformer rating.

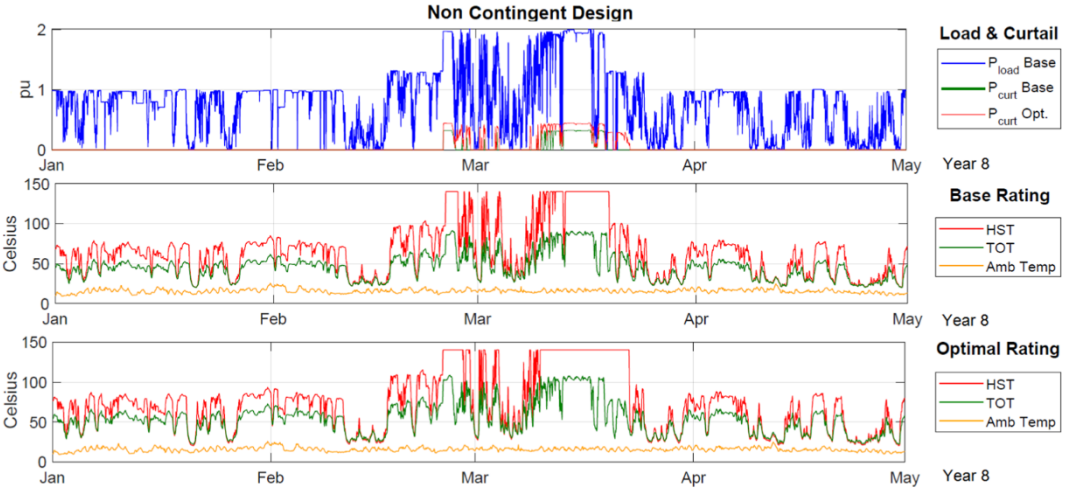

Fig. 16. Assessment of *non-contingent* design during n-2 contingency. Top: transformer load and power curtailment (base and optimal rating). Middle: thermal performance for base transformer rating. Bottom: thermal performance for optimal transformer rating.

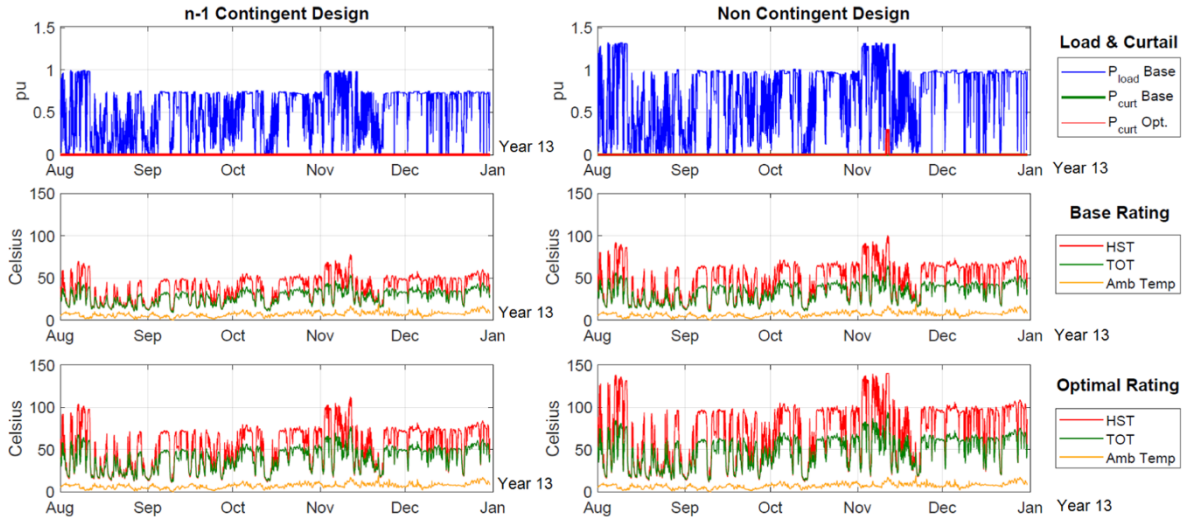

Fig. 17. Assessment of the two design concepts during n-2 contingency. Top: transformer load and power curtailment (base and optimal rating). Middle: thermal performance for base transformer rating. Bottom: thermal performance for optimal transformer rating.

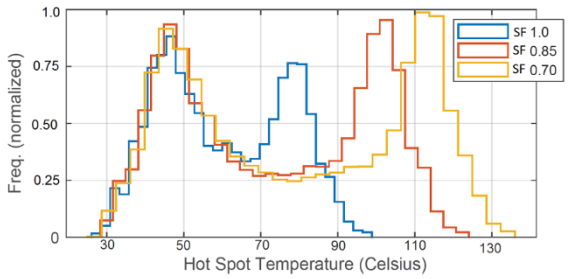

Fig. 18. 30-year HST distribution for n-1 contingent design concept for different transformer ratings.

expected lifetime of transformer for the n-1 contingent design concept is assessed for gradual reduction in transformer rating for worst-case scenario number 7. Under conservative moisture and oxygen development test case, the conventionally sized transformer would outlast the windfarm lifetime of 30 years considerably. A similar behavior is observed for high-moisture test case, but the drop in expected lifetime is much more abrupt for both the high-moisture and high-oxygen test cases which represent uncharacteristically high values of moisture and oxygen respectively. For optimal sizing, transformers can potentially be derated to size factors of 0.92 and 0.97 for these respective test cases. It must be mentioned that for the conservative test case, this potential reduction was up to 0.70 pu size factor.

5. Conclusion

This paper has proposed a novel methodological approach for cost optimization of Offshore Wind Power Plant (OWPP) export system by utilizing Dynamic Thermal Rating (DTR) based transformer design. The analysis confirms that the size of OWPP transformers can be reduced significantly to optimize the business case over windfarm lifetime without compromising the reliability of operation.

The algorithm utilizes the site assessment data to determine windfarm energy generation over the OWPP lifetime. Afterwards, multiple scenarios are generated to determine the time-varying load on individual transformers which are influenced by two important factors: availability of wind turbines and contingency of transformers. Transformer availability is uniquely addressed by utilizing the probabilistic approach of system's transitions between normal, abnormal and fail states, which is based on discrete time Markov chain models. This statistical approach of generating multiple scenarios and choosing the worst case condition to design OSS transformers ensures reliability of design under the given system requirements. Finally, critical transformer temperatures including top-oil and hot-spot temperatures are calculated using state-of-the-art thermal models, while degree of polymerization based technique is used to track transformer lifetime utilization for different oxygen and moisture developments. Hence the main agents responsible for the chemical aging of the transformer insulation paper including water, oxygen and heat are accurately addressed. It is stressed that transformer design optimization based on this methodology should be followed by an intensive monitoring of winding temperature and transformer oil properties over the operation life.

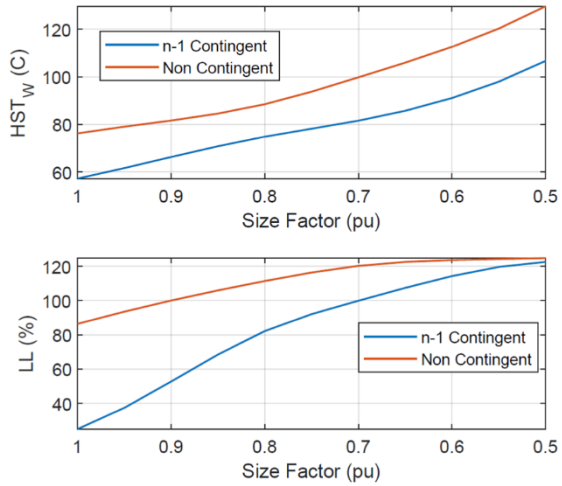

Fig. 20. Influence of transformer size reduction on weighted HST average ($\vartheta_{hst,w}$) and transformer utilized lifetime after 30 years of operation for the two design concepts and worst case scenario.

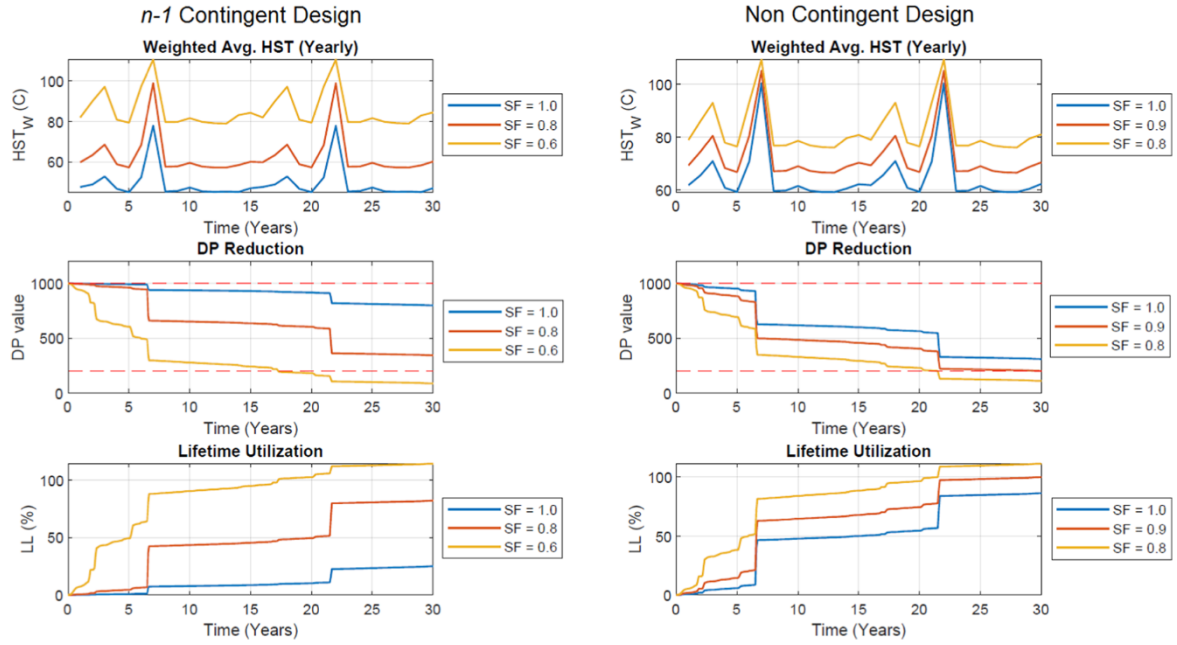

Fig. 19. Lifetime assessment of the two transformer designs for the chosen worst case scenario. Lifetime utilization is calculated based on decrement in degree of polymerization for conservative oxygen and moisture development.

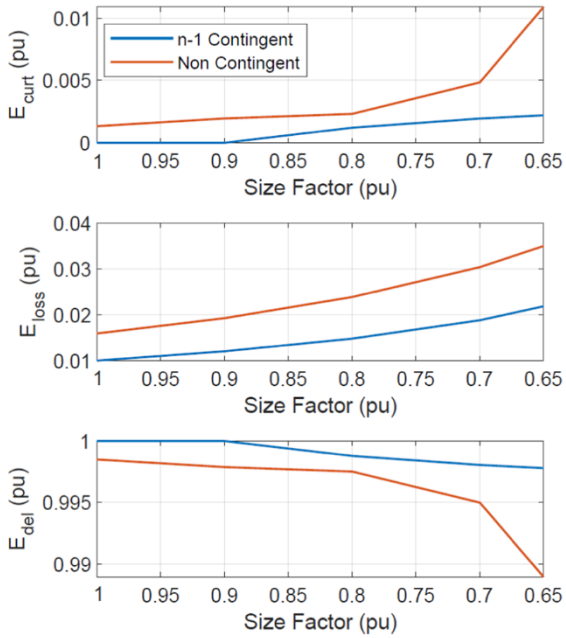

Fig. 21. Influence of transformer size reduction on energy curtailment, losses and energy delivered over windfarm lifetime for the two design concepts and worst case scenario. All the quantities are in pu with values for the conventional n-1 contingent design concept transformer size (400 MVA) as base.

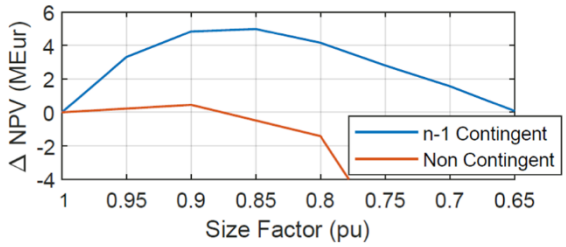

Fig. 22. Influence of transformer size reduction on the NPV for the two design concepts for the worst case scenario.

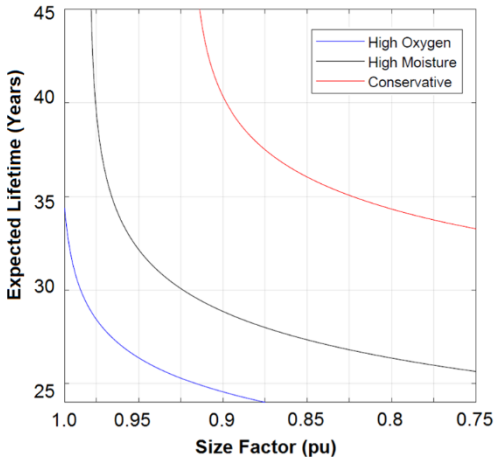

Fig. 23. Influence of transformer size reduction on expected transformer lifetime for n-1 contingent design concept and selected scenario. The 3 test cases (conservative, high moisture, high oxygen) are presented.

Fifteen years of site assessment data for a 1200 MW test case windfarm with four 33/220 kV transformers have been used. For the two design concepts including *n-1 contingent* and *non-contingent* approach, transformers are found to be abnormally loaded more often for the latter option which also results in higher energy curtailment and losses due to higher thermal stress. Results indicate that for the test case windfarm, the transformers can potentially be rated to 70% of the base size for the *n-1 contingent* design and up to 90% for the *non-contingent* design concept even for the worst-case scenario under conservative assumptions for transformer oxygen and moisture development. High oxygen test case is found to be more hazardous to the health of paper insulation than high moisture, both of which represent unconventionally poor manufacturing quality.

For economic optimization, the costs are weighed to year 0 by calculating the major upfront costs for transformer and OSS foundation, and by assessing the change in windfarm yearly revenue due to yearly energy curtailment and losses over the OWPP lifetime as a result of smaller transformers. The windfarm business case improves significantly as the transformer size is optimized and can potentially lead to multi-million Euros profit for both the design concepts. Such an approach for OSS transformer design can lead to further reduction of the cost of energy for offshore windfarms, facilitating the integration of OWPP in the grid.

CRediT authorship contribution statement

Syed Hamza Hasan Kazmi: Conceptualization, Methodology, Software, Formal analysis, Visualization, Writing - original draft. **Tor Laneryd:** Data curation, Methodology, Writing - review & editing. **Konstantinos Giannikas:** Validation, Investigation, Visualization, Writing - review & editing. **Søren Frost Ahrenfeldt:** Validation, Resources, Project administration. **Troels Stybe Sørensen:** Supervision, Writing - review & editing, Project administration. **Thomas Herskind Olesen:** Resources, Validation, Supervision, Writing - review & editing. **Joachim Holbøll:** Conceptualization, Validation, Supervision, Project administration, Writing - review & editing.

Declaration of Competing Interest

The authors declare that they have no known competing financial interests or personal relationships that could have appeared to influence the work reported in this paper.

Acknowledgement

Authors would like to thank Innovation Fund Denmark for project sponsorship. The cooperation of Bent Juhl Madsen from Radius Elnet is highly appreciated. The OPTIMUM framework project collaboration between DTU, Energinet and Ørsted oversees this work.

Appendix A. Supplementary material

Supplementary data associated with this article can be found, in the online version, at https://doi.org/10.1016/j.ijepes.2020.106684.

References

[1] Walsh C, Ramírez L, Fraile D. Offshore wind in europe – key trends and statistics 2019 (wind europe), https://windeurope.org/wp-content/uploads/files/about-wind/statistics/WindEurope-Annual-Offshore-Statistics-2019.pdf (Feb 2020).
[2] Navigant. Connecting offshore wind farms- a comparison of offshore electricity grid development models in northwest europe, https://guidehouse.com/-/media/www/site/downloads/energy/2019/2019-navigant-comparison-offshore-grid-development.pdf (July 2019).
[3] Kazmi S, Holbøll J, Olesen T, Sørensen T. Dynamic thermoelectric modelling of oil-filled power transformers for optimization of offshore windfarm export systems. In: Proceedings of CIGRE Aalborg 2019 international symposium, CIGRE (International Council on Large Electric Systems); 2019.
[4] Viafora N, Kazmi S, Olesen T, Sørensen T, Holbøll J. Load dispatch optimization using dynamic rating and optimal lifetime utilization of transformers. In: Proceedings of IEEE PES Powertech 2019, IEEE PES, Milan, Italy; 2019. doi: 10.1109/PTC.2019.8811002.

[5] IEEE guide for loading mineral-oil-immersed transformers and step-voltage regulators – redline, IEEE Std C57.91-2011 (Revision of IEEE Std C57.91-1995) – Redline; 2011. p. 1–172.
[6] IEC, IEC 60076–7 power transformers: Loading guide for oil-immersed power transformers; 2018.
[7] Ruosong X, Xiang Y, Xie K. Power system reliability evaluation incorporating dynamic thermal rating and network topology optimization. IEEE Trans Power Syst 2018;33(6):6000–12.
[8] Susa D, Nordman H. IEC 60076–7 loading guide for thermal model constants estimation. Int Trans Electrical Energy Syst 2013;23(7):946–60.
[9] Susa D, Lehtonen M. Dynamic thermal modeling of power transformers: further development-part I. IEEE Trans Power Delivery 2006;21(4):1961–70.
[10] Martin D, Cui Y, Ekanayake C, Saha T. An updated model to determine the life remaining of transformer insulation. IEEE Trans Power Delivery 2015;30(1):395–403.
[11] Lundgaard L, Hansen W, Linhjell D, Painter T. Aging of oil-impregnated paper in power transformers. IEEE Trans Power Delivery 2004;19(1):230–9.
[12] W.G. D1.53, Ageing of liquid impregnated cellulose for power transformers, CIGRE TB 2018; 94.
[13] McBride J, Melle T, Lopez-Fernandez X, et al. Investigation of the interaction between substation transients and transformers in HV and EHV applications. IEEE Trans Power Delivery 2020. 10.1109/TPWRD.2020.3014595.
[14] Zhou D, Wang Z, Li C. Data requisites for transformer statistical lifetime modelling–part i: Aging-related failures. IEEE Trans Power Delivery 2013;28(3):1750–7.
[15] C.O.W. Energy, System performance, availability and reliability trend analysis - portfolio review; 2019, https://ore.catapult.org.uk/stories/system-performance-availability-and-reliability-trend-analysis-sparta/.
[16] Viera R, Sanz-Bobi M. Failure risk indicators for a maintenance model based on observable life of industrial components with an application to wind turbines. IEEE Trans Reliab 2015;62(3):569–82.
[17] W.G. A2.37, Transformer reliability survey, CIGRE Technical Brochure 2015; 122.
[18] Yong W, Han X. Power system operational reliability equivalent modeling and analysis based on the markov chain. In: Proceedings of 2012 IEEE International Conference on Power System Technology (POWERCON), IEEE, Auckland, New Zealand, 2012. doi:10.1109/PowerCon.2012.6401316.
[19] Jurgensen J, Nordstrom L, Hilber P. Estimation of individual failure rates for power system components based on risk functions. IEEE Trans Power Delivery 2019;34(4):1599–607.
[20] Teh J, Cotton I. Reliability impact of dynamic thermal rating system in wind power integrated network. IEEE Trans Reliab 2016;65(2):1081–9.
[21] Rocha OD, Morozovska K, Laneryd T, Ivarssonc O, Ahlrotc C, Hilbera P. Dynamic rating assists cost-effective expansion of wind farms by utilizing the hidden capacity of transformers. Electrical Power Energy Syst 2020;123. https://doi.org/10.1016/j.ijepes.2020.106188.
[22] Viafora N, Morozovska K, Kazmi SHH, Laneryd T, Holbøll PHJ. Day-ahead dispatch optimization with dynamic thermal rating of transformers and overhead lines. Electric Power Syst Res 2019;171:194–208. https://doi.org/10.1016/j.epsr.2019.02.026.
[23] Kazmi S, Holbøll J, Olesen T, Sørensen T. Dynamic thermoelectric modelling of oil-filled transformers for optimized integration of wind power in distribution networks, in. In: Proceedings of 25th international conference on electricity distribution, Cired; 2019.
[24] Gamesa S. Energy thrust. energy output upgrade for wind turbines. 2019. https://www.siemensgamesa.com/products-and-services/service-wind/energy-thrust.
[25] Kazmi S, Holbøll J, Olesen T, Sørensen T. Thermoelectric modelling and optimization of offshore windfarm export systems - state of the art. In: Proceedings of 2019 global power, energy and communication conference, IEEE, Cappadocia, Turkey; 2019. p. 331–6. https://doi.org/10.1109/GPECOM.2019.8778513.
[26] Oluwaseun A, Tyalvsky D. Acceptability of three transformer hottest-spot temperature models. IEEE Trans Power Delivery 2012;27(1):13–22.
[27] Teschl G. Ordinary differential equations and dynamical systems. Providence, USA: American Mathematical Society; 2012. Ed: 140.
[28] Lelekakis N, Wijaya J, Martin D, Saha T, Susa D, Krause C. Aging rate of grade 3 presspaper insulation used in power transformers. IEEE Trans Dielectr Electr Insul 2014;21(5):2355–62.
[29] Lelekakis N, Martin D, Wijaya J. Ageing rate of paper insulation used in power transformers part 1: Oil/paper system with low oxygen concentration. IEEE Trans Dielectr Electr Insul 2012;19(6):1999–2008.
[30] DOE, Us department of energy – energy conservation program: Energy conservation standards for distribution transformers, https://www1.eere.energy.gov/buildings/appliance_standards/pdfs/dt_final_rule.pdf (June 2019).
[31] B. Associates, Guide to an offshore wind farm (updated) – the crown estate and ore catapult, https://ore.catapult.org.uk/app/uploads/2019/04/BVGA-5238-Guide-r2.pdf (April 2019).
[32] G. Thornton, Clean energy pipeline – renewable energy discount rate survey results; 2017. http://www.cleanenergypipeline.com/Resources/CE/ResearchReports/ (Jan 2018).
[33] MO, Wind speed and direction – england north sea – met office uk, https://www.metoffice.gov.uk/research/climate/maps-and-data/uk-and-regional-series (2020).
[34] MOI, Mercator ocean international – ambient temperature – european north west shelf seas, https://resources.marine.copernicus.eu/ (2020).
[35] Elovaara J, Klepac A. Impact of Ambient Conditions on Substations, no. 2018:37 in TRITA-EECS-AVL, Springer, Cham; 2019, QC 20180423.
[36] Henderson A, Baldock N, Aristi I, Newton C. Low-hanging fruit for reducing the cost of energy: Optimising the electrical export capacity. In: Proceedings of EWEA offshore wind 2015, EWEA; 2015.

[Pub. J2]

S. H. H. Kazmi, N. Viafora, B. C. Pal, T. S. Sørensen, T. H. Olesen and J. Holbøll, **"Offshore Windfarm Design Optimization using Dynamic Rating for Transmission Components"**, (Dec, 2020) submitted to *IEEE Transactions on Power Systems*

The submitted version of the paper is attached.

Offshore Windfarm Design Optimization using Dynamic Rating for Transmission Components

Syed Hamza H. Kazmi, *Student Member, IEEE,* Nicola Viafora, *Student Member, IEEE,* Troels S. Sørensen, Thomas H. Olesen, *Member, IEEE*, Bikash C. Pal, *Fellow, IEEE*, Joachim Holbøll, *Sr. Member, IEEE*

***Abstract*—The foreseen development of large-scale Offshore Windfarms (OWFs) further from the shore dictates that the OWF transmission system must be optimally designed based on Dynamic Thermal Rating (DTR) in order to fully utilize the intermittent nature of the wind and to keep the offshore wind cost-competitive. In this paper, a comprehensive, DTR-based, two-stage stochastic model is presented, which has been developed for investment decision support for OWF size and HVAC transmission systems. Complex DTR models for all the critical HV components are made fit for the mixed-integer linear programming problem, while accounting for the stochasticity in wind generation and component availability. The main decisions incorporate the discrete size of OWFs, HV subsea export cable cross-sections and ratings for transformers and shunt reactors. For validation, an actual testcase OWF off the east coast of UK has been used. Results indicate that DTR-based iterative design of OWF and its transmission components can significantly improve the business case, even though transmission efficiency and energy delivered are not maximum for the optimal design case.**

***Index Terms*—Dynamic thermal rating, offshore windfarms, stochastic design optimization, HVAC transmission, reliability.**

NOMENCLATURE

A. Sets (Indices) and Components (Superscipts)

$j \in \mathcal{J}$	Set of tangent lines for losses approximation
$k \in \mathcal{K}$	Set of candidate design cases (Opt. case: k_{opt})
$l \in \mathcal{L}$	Set of tangent lines for ageing approximation
$s \in \mathcal{S}$	Set of scenarios
$t \in \mathcal{T}$	Set of hours in each year
$y \in \mathcal{Y}$	Set of years in windfarm lifetime Π^{WF} [yr]
base, opt	Base and optimal design cases
tur	Wind Turbines (WTs)
c	Cables and circuits
trf	Transformers
SR	Shunt Reactors

B. Parameters and Inputs

a_k, b_k	Thermal coefficients for cables and transformers
$A^{\text{w}}_{t,s}$ $A^{\text{c}}_{t,s}$	OWF & transmission circuit availability
c_k	Cost of components [€/unit, €/km, €/tonne]
$C_{x,k}$ C_{soil}	Thermal capacitance for cable & soil [J/m°C]
g_k	Cost coefficients for cables
$I^{\text{c}}_{Q\ k}$	Reactive component of cable current [A]
L^{c}	Length of subsea export cable [m]
m_k	Mass of relevant components [tonne]
n	Number of components
$p_{j,l}$ $q_{j,l}$	slope and intercepts for linear approx.
$P^{\text{w}}_{t,s}$	OWF power generation [pu]
r_k	Resistance of components at temp. limits [Ω]
S_k	Rated power of components [MVA, MW, MVAr]
$T_{x,k}$ T_{soil}	Thermal resistance for cable & soil [m°C/W]
$W_{d,k} W_{nl,k}$	Dielectric & noload loss in cables & trafos [W]
i	Discount rate for NPV calculation [pu]
γ	Power purchase agreement price [€/MWh]
Λ, Υ	Failure & repair rates for components [hr^{-1}]
λ^{c}_s λ^{c}_a	Loss factors for cable screen and armouring [pu]
$\vartheta^{\text{amb}}_{t,s}$ $\vartheta^{\text{sea}}_{t,s}$	Ambient and seabed temperatures [°C]

C. Decision variables

C_0	Investment costs $= f\left(n^{\text{tur}}, C^{\text{fix}}, C^{\text{exp}}_k\right)$ [M€]
$I_{t,s}$ $I_{P\ t,s}$	Component load current apparent and active [A]
n^{tur}	Number of wind turbines
$P^{\text{gen}}_{t,s}$	Hourly power generated by the OWF [MW]
$P^{\text{cut}}_{t,s}$ $P^{\text{inj}}_{t,s}$	Hourly power curtailed & injected to grid [MW]
R_s	Total revenue over OWF lifetime [M€]
$W_{t,s}$	Losses in components [W]
$\vartheta^{\text{serv}}_{t,s}$ $\vartheta^{\text{cond}}_{t,s}$	Cable serving & cond. temp. rise over ϑ^{sea} [°C]
$\vartheta^{\text{top}}_{t,s}$ $\vartheta^{\text{hst}}_{t,s}$	Transformer top oil & hot spot temp. [°C]
$\lambda_{y,s}$	Transformer loss of life - yearly (LL) [hr]

I. INTRODUCTION

The growth in offshore wind has been expedited exponentially by decreasing the Levelised Cost Of Energy (LCOE) from 180 to less than $40\frac{€}{\text{MWh}}$ over the last decade [1]. This has resulted in intense price competition in the markets and has prompted developers and manufacturers alike to optimize the entire value chain [2]. The electrical infrastructure for Offshore Wind Farms (OWFs) usually consist of two systems: the collection system interconnecting Wind Turbines (WTs) with Offshore Substations (OSSs) and the HV transmission system responsible for energy transfer from OSS to the onshore station. Conventionally, the number of WTs and ratings of HV transmission components are coupled iteratively during the OWF design phase [3]. With the development of large-scale OWFs further from the shore, the potential to optimize the transmission components escalates as well. Utilization of Dynamic Thermal Rating (DTR) for the dimensioning of these components and optimization of the OWF size based on this design can drive down the LCOE further.

Over the years, several publications [3]–[14] have been presented for OWF design optimization addressing the electrical infrastructure's efficiency and costs related to investment and operation. A vast majority of these publications focus on layout and array cable routing optimization for the collection

system alone [4]–[8], whereas only a handful of research has been done on transmission system with most publications focused only on the HVAC submarine cables optimization without DTR [3], [9]–[11] and with DTR [12]–[14]. The potential of cost reduction by optimization of remaining components [15] and by employing DTR on the entire system altogether is completely unexplored [16], [17].

In contrast to Static Thermal Rating (STR), accurate and computationally efficient thermal models are needed for DTR-based design. Empirically derived Thermo-Electric Equivalent (TEE) models fit this profile to a large extent. For oil-filled components, the first-order differential models from [18], [19] can be made fit for linear estimation [16], [20] for intermittent dynamic offshore wind generation [15]. Contrarily, single-core equivalent TEE models for three-core HVAC subsea cables in [21]–[23] are complicated to design [24], but can be transformed to account for effective losses in long cables [25], [26] and backfill soil's thermal parameter variation [27].

OWF transmission system's contingency and reliability assessment is a critical step during the design phase owing to longer repair times and increasing capacity factors [5], [17]. The stochastic nature of system's availability can be addressed by using probability-based methods relying on analytical techniques [28] or Monte Carlo simulations [5], [10], [29]. The computational stress of these techniques for design optimization is a challenge that needs to be resolved.

In this paper, a comprehensive model for investment decision support for OWF size and HVAC-based transmission system design is proposed. This two-stage stochastic model uses DTR for optimal utilization of HV components over the windfarm lifetime and has three fundamental characteristics: business case assessment (incl. investment cost and weighted revenue loss due to energy not served), reliability of operation and transmission efficiency. Besides the investment decision parameters, the model determines the optimal OWF size and optimal design case incl. ratings of subsea export cables, power transformers and shunt reactors. The main contributions of this work include: a) Development and validation of a simplified TEE model for subsea cables which is fit for linear optimization. b) Employment of linearized dynamic lifetime utilization of transformer for OWF design. c) Inclusion of contingency scenarios for OWF export system based on *Monte Carlo* simulations. d) Proposal of a two-stage stochastic model for business-case optimization of OWF design by using DTR on the entire HV transmission network accounting for load-dependent losses, curtailment and reliability over OWF lifetime. e) Finally, new research direction in DTR-based transmission system optimization of OWFs.

Remaining paper is structured as follows. Overview of the methodology is given in Sec. II, followed by presentation and validation of DTR models for the relevant transmission components in Sec. III. The novelty of the proposed optimization methodology is elaborated in detail in Sec. IV. Sec. V presents the test case OWF, its design cases and economic assumptions, while the relevance of the proposed problem is demonstrated in Sec. VI. Finally, the paper is concluded in Sec. VII.

II. Overview of the Proposed Framework

The novel methodology proposed in this paper follows four basic steps, as shown in Fig. 1. The first two steps generate inputs for the optimization problem. First of all, depending on windfarm topology and other predefined factors, a number of potential design cases $\mathcal{K}$ with unique combinations of transformer and cable ratings are preselected. Therefore, component costs, ratings and thermal parameters for each design case are readily available for the optimization framework. Secondly, in order to ensure the reliability of design, stochasticity of wind speed and temporal availability of WTs and transmission system is accounted for through scenario generation. A set of $\mathcal{S}$ scenarios for hourly wind power generation profile [pu] over windfarm lifetime are generated by performing ARIMA-based trend analysis of long-term historic site data (incl. windspeed and direction profiles). Possible failures and contingency conditions are also pre-simulated in this step which are based on component reliability indices.

In step 3, for each design case the optimization problem maximizes the business case over OWF lifetime and determines the respective optimal number of wind turbines n^{tur}. The two-level problem deals with operational scenarios and hourly constraints (incl. component loading, temperatures, ageing, losses and possible curtailment) at the lower level; whereas, the upper level manages yearly energy injection and component lifetime utilization over the windfarm lifetime. Finally, the component ratings and optimal n^{tur} for the best design case k_{opt} resulting in maximum NPV are chosen in step 4.

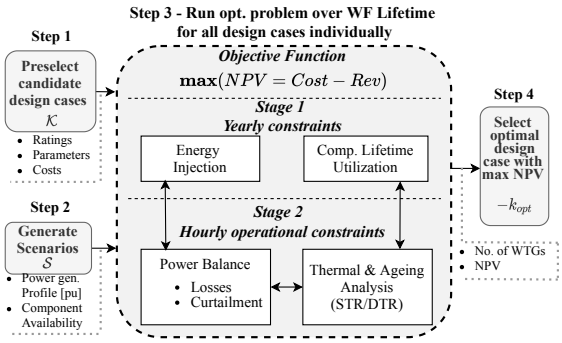

Fig. 1. Proposed framework for the novel optimization strategy

III. Dynamic Rating Models of HV Components

As shown in Fig. 2, the HVAC OWF export system is equipped with n^{c} interlinked parallel circuits consisting of 3-core subsea cables, two parallel transformers in the OSS, with optional shunt reactors in the middle for long cables.

A. Cable Thermal Modeling

As per existing industrial practices, the conductor temperature is limited to 90 °C for XLPE insulated cables to ensure acceptably low rate of thermal ageing over their lifetime [13]. Therefore estimation of conductor temperature is critical for optimal utilization of HV Cables. The complex TEE model presented in Fig. 3 can be used to calculate the temperature

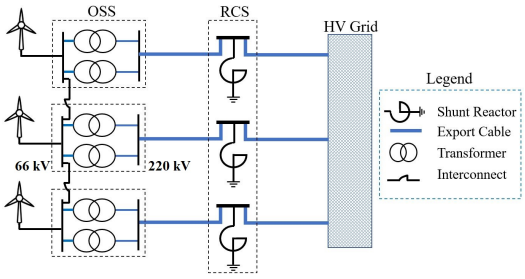

Fig. 2. Typical layout for a large OWF HV export system with three circuits

rise over seabed temperature for cable conductor and serving represented by ϑ^{cond} and ϑ^{serv} respectively [21] [22]. The distributed 3-phase dielectric losses W_d^{c} [W/m] are treated as constants as they depend upon voltage, cable construction and design properties. The remaining sources of heat generation in cables W^{cond} (Ohmic conductor losses = $3I^{\text{c}^2} r'^{\text{c}}_{ac}$ [W/m]), W^s (screen losses) and W^a (armor losses) are load dependent and time variant, where I^{c} represents cable load current [A] and r'^{c}_{ac} represents conductor AC resistance [Ω/m] accounting for skin and proximity effects [25]. W_s and W_a are calculated by scaling the conductor losses W^{cond} with factors λ_s^{c} and λ_a^{c} which are cable construction dependent and can be treated as constants in this study. The thermal resistances T_1, T_2 and T_3 [m°C/W] and capacitances [J/m°C] are treated as constants. This model has potential shortcomings for 3-core cables in offshore windfarm applications due to single core equivalency assumptions [23] and negligence of cyclic load influence on thermal properties of the back-fill material [27]. But the compromise between computational speed and accuracy makes it ideal for this methodology [13] [22].

In order to make the TEE model fit for optimization, a simplified model is proposed in this paper. The simplified model shown in Fig. 3 (bottom) uses lumped-parameter approach to merge the losses, thermal capacitances and thermal resistances for conductor, insulation, serving etc. The total losses $W^{\text{tot c}}$ are simply the sum of all the losses per length referred to the conductor, calculated using (1); whereas the remaining lumped parameters T_x and C_x are obtained by training the simplified model over synthetic data for each cable type and fitting

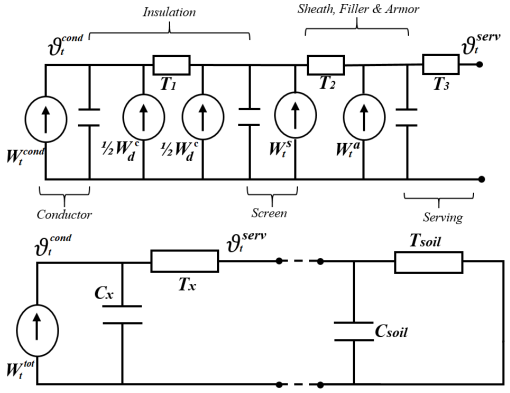

Fig. 3. Single core equivalent TEE models for 3-core subsea cables. Top: Complex model [21] [22], Bottom: Simplified lumped model including soil.

the parameters for optimal approximation [24]. The temporal development of ϑ^{serv} and ϑ^{cond} representing temperature rise over ambient seabed temperature for cable conductor and serving respectively can be calculated using (2) and (3).

$$W_t^{\text{tot c}} = W_d^{\text{c}} + 3(1 + \lambda_a^{\text{c}} + \lambda_s^{\text{c}}) I_t^{\text{c}^2} r'^{\text{c}}_{ac} \tag{1}$$

$$\tau'_x \frac{d\vartheta_t^{\text{serv}}}{dt} = \frac{T_{soil}}{T_x + T_{soil}} \vartheta_t^{\text{cond}} - \vartheta_t^{\text{serv}} \tag{2}$$

$$\tau_x \frac{d\vartheta_t^{\text{cond}}}{dt} = T_x W_t^{\text{tot}} + \vartheta_t^{\text{serv}} - \vartheta_t^{\text{cond}} \tag{3}$$

where the time constants in seconds are determined as: $\tau_x = T_x C_x$ and $\tau'_x = \frac{T_x T_{soil}}{T_x + T_{soil}} C_{soil}$. The thermal resistance T_{soil} and capacitance C_{soil} for soil are to be made available beforehand. The lumped-parameter model is inherently conservative for conductor temperature estimation than the complex TEE model, because the losses are collectively referred to the conductor. The cautiousness is further ensured by using conductor resistance r'^{c}_{ac} values at 90 °C. After applying Backward Euler approximation with fixed time step Δt, the temperatures can be estimated using (4) and (5):

$$\vartheta_t^{\text{serv}} = a_1 \vartheta_{t-1}^{\text{serv}} + a_2 \vartheta_t^{\text{cond}} \tag{4}$$

$$\vartheta_t^{\text{cond}} = \frac{1}{a_3} \left[a_4 \vartheta_{t-1}^{\text{cond}} + a_5 \vartheta_{t-1}^{\text{serv}} + a_6 W_t^{\text{tot c}} \right] \tag{5}$$

where the thermal coefficients a are calculated as:

$$a_1 = \frac{\tau'_x}{\tau'_x + \Delta t}, \qquad a_2 = \frac{T_{soil}}{T_x + T_{soil}} \left(\frac{\Delta t}{\tau'_x + \Delta t} \right) \tag{6}$$
$$a_3 = \frac{1}{1 - a_2 \frac{\Delta t}{\tau_x + \Delta t}}, \quad a_4 = a_3 \frac{\tau_x}{\tau_x + \Delta t}$$
$$a_5 = a_1 a_3 \frac{\Delta t}{\tau_x + \Delta t}, \quad a_6 = a_3 T_x \frac{\Delta t}{\tau_x + \Delta t}$$

In Fig. 4, the performance of the proposed TEE model based on the simplified lumped-parameter approach is compared to the complex TEE model. Two XLPE insulated cables with Copper conductor 800 mm^2 and 1200 mm^2 are subjected to similar cyclic loads scaled to the maximum current carrying capacities of the respective cables. The simplified model is observed to be more conservative than the complex one, and the accuracy of estimation is found to be acceptable for the lumped-parameter approach. These tests have been carried out for a variety of Aluminum and Copper conductor cables for varying sizes with similar results.

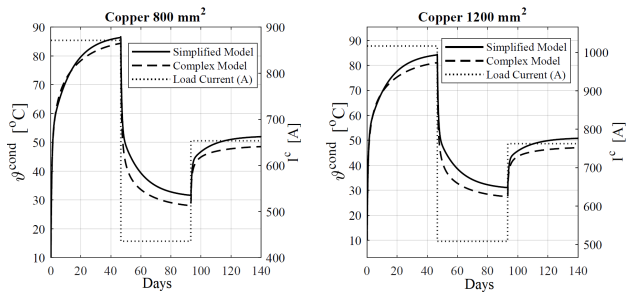

Fig. 4. Comparison of simplified and complex TEE models for conductor temperature estimation using 220 kV subsea, XLPE-insulated, Copper cables under cyclic load current I^{c} as test cases. Left: 800 mm^2, Right: 1200 mm^2

B. Transformer Thermal and Lifetime Modeling

The rating of transformers is optimized by not only accounting for thermal dynamics, but also the ageing rate of transformer insulation. The critical Top Oil Temperature (TOT) and Hot Spot Temperature (HST) are estimated using the linearized version of the non-linear differential equations from the industry-wide accepted IEEE C57.91 models [18] for hourly load and forced cooling conditions [20], as shown in (7) and (8). These simplifications keep the optimization problem convex without loss of accuracy [16].

$$\vartheta_t^{\text{top}} = b_1 \left(\frac{I_t^{\text{trf}}}{I_{rated}^{\text{trf}}} \right)^2 + b_2 \vartheta_t^{\text{amb}} + b_3 \vartheta_{t-1}^{\text{top}} + b_4 \tag{7}$$

$$\vartheta_t^{\text{hst}} = \vartheta_t^{\text{top}} + \vartheta_{\text{hr}} \left(\frac{I_t^{\text{trf}}}{I_{rated}^{\text{trf}}} \right)^2 \tag{8}$$

where ϑ^{amb}, ϑ^{top} and ϑ^{hst} represent ambient temperature, TOT and HST respectively in °C. Both the temperatures are dependent on per-unit transformer load calculated using rated and real-time HV side currents I_{rated}^{trf} and I^{trf} [A] respectively, while ϑ_{hr} [°C] is the rated HST rise over TOT for rated load and coefficients b are constants depending on transformer construction [16] [20]. For optimal utilization of the transformer, the lifetime model based on Arrhenius reaction rate theory is used to track the transformer loss of life over the windfarm lifetime [19], as shown in (9). In this formulation, λ_τ represents the cumulative Loss-of-Life LL [hours] in time duration τ [hours] using the development of hot-spot temperature ϑ^{hst}.

$$\lambda_\tau = \int_0^\tau \Delta\lambda_t \, dt = \int_0^\tau e^{\left(\frac{15000}{373} - \frac{15000}{\vartheta_t^{\text{hst}} + 273} \right)} dt \tag{9}$$

C. Shunt Reactor Modeling

Offshore windfarms located > 80 km off the sea coast may require additional reactive compensation to ensure effective transmission if HVAC transmission is used. So even though, 50 % of this compensation is performed at the two ends of the cable in the OSS and Onshore Substation (OnSS), an additional substation might be needed near the midpoint of the offshore cable section called Reactive Compensation Station (RCS), as shown in Fig. 2. Each cable design case $k \in \mathcal{K}$ will influence the rating of 3-phase shunt reactors placed in RCS as it is dependent on cable charging current. This is shown in (10) and (11) for the assumption of uniform compensation from each end and stable voltage operation.

$$I_{\text{Q}}^{\text{c}} = \frac{1}{4} \left(2\pi f Q'^{\,\text{c}} L^{\text{c}} \frac{V_{ll}}{\sqrt{3}} \right) \times 10^3 \tag{10}$$

$$S^{\text{SR}} = 2 \left(\sqrt{3} V_{ll} I_{\text{Q}}^{\text{c}} \right) \tag{11}$$

where I_{Q}^{c} is the peak charging current at the OSS, OnSS and RCS ends of the export cable [A] and $Q'^{\,\text{c}}$ is the capacitance [μ F/m], both of which vary with cable design case k. V_{ll} and f are transmission system voltage [kV] and frequency [Hz]; L^{c} is the length of the export cable [m] and S^{SR} represents the rating of RCS shunt reactor [kVA].

D. Power Losses Approximation

For export cables, losses for the whole cable are simply evaluated as $W^{\text{c}} = W^{\text{tot c}} L^{\text{c}}$. But cable current I^{c} varies not only with load (I_{P}^{c}) but also along the cable length due to charging. As discussed earlier, the charging current peaks only at the OSS, OnSS and RCS ends of the cable. This peak current I_{Q}^{c} can result in overestimation of losses by up to 100% [25], which is corrected using the approximation 2 from [26]. This is shown in (12) where r^{c} is the total resistance of the export cable calculated conservatively at 90 °C using (13).

$$W_t^{\text{c}} = 3r^{\text{c}} \left(I_{\text{P}\,t}^{\text{c}^2} + \frac{1}{2} I_{\text{Q}}^{\text{c}^2} \right) + W_d^{\text{c}} L^{\text{c}} \tag{12}$$

$$r^{\text{c}} = (1 + \lambda_a^{\text{c}} + \lambda_s^{\text{c}}) r'^{\,\text{c}}_{ac} L^{\text{c}} \tag{13}$$

Similarly for OSS transformers, losses can be calculated using (14), where I^{trf} refers to HV side current [A]. The total winding resistance r^{trf} [Ω] is referred to the HV side and W_{nl}^{trf} represent constant no load losses [W], both of which can be readily available for each design case during OWF design phase. For conservatism, constant r^{trf} values are used at 110 °C.

$$W_t^{\text{trf}} = 3r^{\text{trf}} I_t^{\text{trf}^2} + W_{nl}^{\text{trf}} \tag{14}$$

IV. Proposed Methodology

The objective of the proposed problem is to maximise the expected net present value of the wind farm by considering the underlying uncertainty in the wind availability and the dynamic thermal behavior of HV components.

A. Scenario Generation

For each scenario s in $\mathcal{S}$, time series of wind power production P^{w} is simulated using the methodology in [30] based on ARIMA models. This approach accounts for the double-bounded nature of wind power time series by introducing a limiter that prevents the simulated power to exceed the nominal values [13]. This methodology is complemented in this paper by considering a time series of WT availability A^{w} [17] and number of available export circuits A^c at every instant, calculated using reliability indices Mean Time To Failure (MTTF) and Mean Time To Repair (MTTR).

For an OWF export system equipped with n^{c} parallel radial circuits, the load is equally divided between all circuits under normal operation state. During contingency, the number of available circuits (A^{c}) reduce and the load has to be scaled accordingly to ensure maximum transmission. In this formulation, a Discrete Time Markov Chain (DTMC) model is used for contingency simulation, which dictates the transition between one system state to another by taking a probabilistic determination approach [28].

In Fig. 5, the state transition diagram is provided for the OWF export system without consideration of common cause failures. The system can have $n^{\text{c}} + 1$ possible states in total, and the number of available circuits A^{c} in each state can range from n^{c} (normal operation) to 0 (all parallel circuits failure). For constant failure and repair rates Λ (1/MTTF) and Υ (1/MTTR), the probability that a component will fail

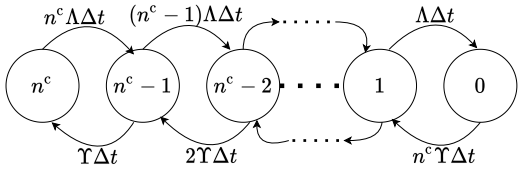

Fig. 5. DTMC state transition diagram for a system with n^{c} parallel radial circuits. Each circle represents a state, values inside the circle present the number of available circuits A^{c} in the respective state; while arrows represent transition probability in each simulation step.

within time-step Δt is determined using the factor $\Lambda\Delta t$; while the probability of repair of a failed equipment in this period is governed by $\Upsilon\Delta t$. Reliability indices Λ and Υ of the circuit [1/hr] are obtained by using the individual values for subsea cables, transformers and shunt reactors connected in series, as shown in (15) and (16) [31]. Even with two parallel transformers per circuit, redundancy is not assumed in order to add conservatism in design.

$$\Lambda = \Lambda^{\mathrm{c}} + \Lambda^{\mathrm{trf}} + \Lambda^{\mathrm{SR}} \tag{15}$$

$$\Upsilon = \Upsilon^{\mathrm{c}} + \Upsilon^{\mathrm{trf}} + \Upsilon^{\mathrm{SR}} \tag{16}$$

B. Problem formulation

The methodology is formulated as a two-stage stochastic problem, where the first stage considers the investment decision, i.e., the optimal number of wind turbines for a given design case, and the second stage models each scenario in an hourly operational time-frame indexed with t. The objective function includes a cost term C_0, depending on the design case under consideration, and a revenue term R_s with an associated probability π_s, which depends on the energy sold to the grid in each scenario s. The problem is compactly formulated as:

$$\max_{\Xi} \quad \left(-C_0 + \sum_{s\in\mathcal{S}} \pi_s R_s\right) \tag{17a}$$

$$\begin{aligned}
\text{s.t.} \quad & (21), && \text{Wind farm size}, && \\
& (22)-(23), && \text{Power Balance}, && \forall s, \forall t \\
& (25)-(28), && \text{Load \& Losses approx.}, && \forall s, \forall t, \forall j \\
& (35)-(37), && \text{Thermal dynamics}, && \forall s, \forall t \\
& (38)-(39), && \text{Aging dynamics}, && \forall s, \forall t, \forall y
\end{aligned}$$

where Ξ is the list of decision variables which are described together with the associated constraints in the following.

1) Objective Function: The first term in the objective function models the initial investment cost of the windfarm. The formulation in (18) considers three elements: cost of turbines, cost of HV export system C^{exp} depending on preselected design case k and fixed costs C^{fix} which are not influenced by minor changes in OWF size and transmission system.

$$C_0 = n^{\mathrm{tur}} c^{\mathrm{tur}} + C_k^{\mathrm{exp}} + C^{\mathrm{fix}} \tag{18}$$

$$\begin{aligned} C_k^{\mathrm{exp}} = {} & n^{\mathrm{c}} L^{\mathrm{c}} c_k^{\mathrm{c}} + n^{\mathrm{trf}} c_k^{\mathrm{trf}} + n^{\mathrm{SR}} c_k^{\mathrm{SR}} + \\ & 2c^{\mathrm{oss}} \left(n^{\mathrm{trf}} m_k^{\mathrm{trf}} + n^{\mathrm{SR}} m_k^{\mathrm{SR}}\right) \end{aligned} \tag{19}$$

where the integer values n represent number of turbines (tur), cables (c), transformers (trf) and shunt reactors (SR); c represents cost functions for each component in €, except cable costs c^{c} [€/km] and weight dependent costs of OSS/RCS c^{oss} [€/tonne] which are linked with transmission system length L^{c} and component masses m [tonnes] respectively. Consequently the influence of varying oil-filled components rating on foundation costs of substations are also accounted for. The sole decision variable in C_0 is the number of turbines n^{tur}, which sets the size of the wind farm and affects the power flow on the export system in the operational frame-work. The revenue stream in each scenario is modelled with R_s, which considers yearly values depending on yearly injected energy $\sum P^{\mathrm{inj}}$

$$R_s = \sum_{y\in\mathcal{Y}} \frac{\gamma}{(1+i)^y} \sum_{t\in\mathcal{T}} P_{t,s}^{\mathrm{inj}} \tag{20}$$

where i is the discount factor, γ is the price at which energy is sold [€/MWh] and $P_{t,s}^{\mathrm{inj}}$ is the power [MW] injected in each hour for each scenario. The approach in the proposed methodology assumes that yearly revenues generated from selling the energy to the grid are repeated every year.

2) Wind Farm Size: The size of the wind farm for each design case is limited by the first-stage decision variable n^{tur} with constraint in (21), where $\underline{n^{\mathrm{tur}}}$ and $\overline{n^{\mathrm{tur}}}$ model min and max number of turbines that can be installed, respectively.

$$\underline{n^{\mathrm{tur}}} \le n^{\mathrm{tur}} \le \overline{n^{\mathrm{tur}}} \tag{21}$$

3) Power Balance: For each operational hour, contingencies in (22) - (23) ensure power balance in the system, while (24) determines the generated power for each scenario of WT availability A^{w} [pu] and OWF generation profile P^{w} [pu].

$$P_{t,s}^{\mathrm{gen}} - P_{t,s}^{\mathrm{cut}} - A_{t,s}^{\mathrm{c}} \left(W_{t,s}^{\mathrm{c}} - 2W_{t,s}^{\mathrm{trf}} - W^{\mathrm{SR}}\right) - P_{t,s}^{\mathrm{inj}} = 0 \tag{22}$$

$$0 \le P_{t,s}^{\mathrm{cut}} \le P_{t,s}^{\mathrm{gen}} \tag{23}$$

$$P_{t,s}^{\mathrm{gen}} = A_{t,s}^{\mathrm{w}} P_{t,s}^{\mathrm{w}} S^{\mathrm{tur}} n^{\mathrm{tur}} \tag{24}$$

where P^{gen}, P^{cut} and P^{inj} represent hourly generated, curtailed and injected powers [MW], while W identifies load-dependent hourly MW losses in each component. The rating of WT S^{tur} [MW] and hourly availability of circuits A^{c} [pu] are predefined during pre-design and scenario generation phases respectively.

4) Component Load and Losses Approximation: The hourly load current for cables I^{c} and transformers HV side I^{trf} in [A] are determined using (25)-(26), where V_{ll} is the line-to-line transmission system voltage, while S_{rated}^{trf} and I_{rated}^{trf} represent transformer MVA rating and rated HV-side current [A] respectively. The currents are not constrained in this formulation for DTR operation.

$$I_{\mathrm{P}\,t,s}^{\mathrm{c}} = \frac{1}{A_{t,s}^{\mathrm{c}}} \frac{(P_{t,s}^{\mathrm{gen}} - P_{t,s}^{\mathrm{cut}})}{\sqrt{3}V_{ll}} \tag{25}$$

$$I_{t,s}^{\mathrm{trf}} = \frac{1}{2A_{t,s}^{\mathrm{c}}} \frac{(P_{t,s}^{\mathrm{gen}} - P_{t,s}^{\mathrm{cut}})}{S_{rated}^{\mathrm{trf}}} I_{rated}^{\mathrm{trf}} \tag{26}$$

Referring to (12) and (14), component losses are modelled with piece-wise linear approximation method after expressing the currents I^{c} and I^{trf} as sets of j linear inequality constraints

with slope p and intercept q in (27)-(30), as shown in Fig. 6. The intercept term q_j also accounts for no-load losses.

$$W^{\mathrm{c}}_{t,s} \geq p^{\mathrm{c}}_j I^{\mathrm{c}}_{\mathrm{P}\,t,s} + q^{\mathrm{c}}_j \tag{27}$$
$$W^{\mathrm{trf}}_{t,s} \geq p^{\mathrm{trf}}_j I^{\mathrm{trf}}_{t,s} + q^{\mathrm{trf}}_j \tag{28}$$
$$q^{\mathrm{c}}_j = q^{\mathrm{c}}_{j0} + \frac{3}{2} I^{\mathrm{c}^2}_Q r^{\mathrm{c}} + W^{\mathrm{c}}_d L^{\mathrm{c}} \tag{29}$$
$$q^{\mathrm{trf}}_j = q^{\mathrm{trf}}_{j0} + W^{\mathrm{trf}}_{nl} \tag{30}$$

5) Thermal Dynamics: Reformulation of (4)-(5), gives temporal development of cable conductor temperature rise in (31)-(32); while (7)-(8) are combined with (14) to determine transformer critical temperatures linearly in (33)-(34). The limits on these quantities are enforced with the set of constraints in (35)-(37), where ϑ^{sea} is the nominal sea-bed temperature. $\overline{\vartheta^{\mathrm{c}}}$ is conservatively limited to 90 °C, while incautious emergency loading limits of 115 and 140 °C are used for transformer $\overline{\vartheta^{\mathrm{top}}}$ and $\overline{\vartheta^{\mathrm{hst}}}$ respectively [18].

$$\vartheta^{\mathrm{serv}}_{t,s} = a_1 \vartheta^{\mathrm{serv}}_{t-1,s} + a_2 \vartheta^{\mathrm{c}}_{t,s} \tag{31}$$
$$\vartheta^{\mathrm{c}}_{t,s} = \frac{1}{a_3}\left(a_4 \vartheta^{\mathrm{c}}_{t-1,s} + a_5 \vartheta^{\mathrm{serv}}_{t-1,s} + \frac{a_6}{L^{\mathrm{c}}} W^{\mathrm{c}}_{t,s}\right) \tag{32}$$
$$\vartheta^{\mathrm{top}}_{t,s} = b_1\left(\frac{W^{\mathrm{trf}}_{t,s} - W^{\mathrm{trf}}_{nl}}{3 r^{\mathrm{trf}} I^{\mathrm{trf}^2}_{rated}}\right) + b_2 \vartheta^{\mathrm{amb}}_{t,s} + b_3 \vartheta^{\mathrm{top}}_{t-1,s} + b_4 \tag{33}$$
$$\vartheta^{\mathrm{hst}}_{t,s} = \vartheta^{\mathrm{top}}_{t,s} + \vartheta_{\mathrm{hr}}\left(\frac{W^{\mathrm{trf}}_{t,s} - W^{\mathrm{trf}}_{nl}}{3 r^{\mathrm{trf}} I^{\mathrm{trf}^2}_{rated}}\right) \tag{34}$$
$$\vartheta^{\mathrm{c}}_{t,s} \leq \overline{\vartheta^{\mathrm{c}}} - \vartheta^{\mathrm{sea}}_{t,s} \tag{35}$$
$$\vartheta^{\mathrm{top}}_{t,s} \leq \overline{\vartheta^{\mathrm{top}}} \tag{36}$$
$$\vartheta^{\mathrm{hst}}_{t,s} \leq \overline{\vartheta^{\mathrm{hst}}} \tag{37}$$

6) Aging Dynamics: The reliability of transformer design is further ensured by limiting its lifetime utilization. To keep the optimization problem convex, the exponential function in (9) is linearized piece-wise in (38), as shown in Fig. 6. The cumulative yearly LL is limited to $\overline{\lambda} = 8760 \times 17.12/\Pi^{\mathrm{WF}}$, where Π^{WF} is the OWF design lifetime [yr] and 17.12 is the rated transformer life in years at constant $\vartheta^{\mathrm{hst}}_{rated}$ as per [18].

$$\Delta\lambda_{t,s} \geq p_l \vartheta^{\mathrm{hst}}_{t,s} + q_l \tag{38}$$
$$\lambda_{y,s} = \sum_{t \in \mathcal{T}} \Delta\lambda_{t,s} \leq \overline{\lambda} \tag{39}$$

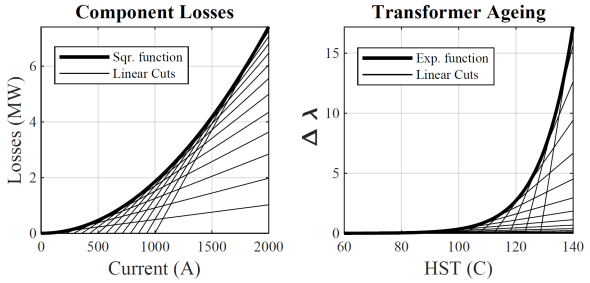

Fig. 6. Piecewise approximation of non-linear functions. Left: Square function for losses with $\mathcal{J} = 15$ cuts for 100 km long 1600 mm^2 Cu cable. Right: Exponential function for transformer life with $\mathcal{L} = 30$ cuts

V. Test Case OWF Transmission system

An actual windfarm off the east coast of UK has been used as inspiration. The test case OWF export system consists of three interlinked parallel circuits, like the one in Fig. 2. Each circuit comprises of 2 parallel 66/220 kV transformers ($n^{\mathrm{trf}} = 6$) and one 100 km long 3-core XLPE subsea cable with Copper conductor ($n^{\mathrm{c}} = 3$). Reactive compensation is performed at the mid-point of the cable by three 3-phase shunt reactors ($n^{\mathrm{SR}} = 3$). In total, there are three OSS and one RCS, while the design lifetime (Π^{WF}) of 30 years is considered. A total of $\mathcal{S} = 30$ scenarios of P^{w}, WT availability A^{w} and number of available export circuits A^{c}_t are simulated for duration of $\mathcal{T} = 8760$ hr (1 year) each.

For benchmarking, the optimization algorithm has been run with STR and compared with the results for DTR to assess the improvement in business case due to dynamic rating. For base test case with STR, called Base$_{\mathrm{STR}}$, constraints for OWF Size (21), Thermal and Ageing Dynamics (35)-(39) are not relevant. Instead the windfarm is rated at 1197 MW ($n^{\mathrm{tur}}_{base} = 171$, $S^{\mathrm{tur}} = 7$ MW) with 250 MVA OSS transformers and 1600 mm^2 cables and the load I in (25)-(26) are constrained to 1 pu. For all the DTR test cases, n^{tur} is limited between 143 and 200; where as the pre-selection of candidate designs considering the network configuration, base OWF size and manufacturer availability is performed. There are 5 transformer and 4 cable sizes that are found to be appropriate, as shown in Table I. Therefore, 20 candidate design cases $\mathcal{K}$ = {Trafo [MVA], Cable [mm^2]} are considered: {T250, C1600}, {T250, C1400}... {T150, C1000}. All the parameters necessary for test case simulation, with the exception of thermal coefficients, are provided in Table I.

TABLE I
Shortlisted Component Sizes for Candidate Design Cases

Component	Parameter		Design Cases				
Transformer	S^{trf}_{rated}	[MVA]	**250**	**225**	**200**	**175**	**150**
	r^{trf} at 110C	[Ω]	1.64	2.49	2.98	3.65	4.12
	W^{trf}_{nl}	[kW]	74.14	67.33	61.42	55.63	49.18
Cable	Cond. Size	[mm^2]	**1600**	**1400**	**1200**	**1000**	-
	S^{c}_{rated} (STR)	[MVA]	417	404	387	370	-
	I^{c}_{rated} (STR)	[A]	1095	1060	1016.5	971	-
	r^{c}_{ac} at 90C	[$\mu\Omega$/m]	16.02	17.31	19.11	21.18	-
	Q^{c}	[μF/km]	0.214	0.201	0.190	0.178	-
Shunt Reactor	S^{SR}_{rated}	[MVAr]	**165**	**152**	**143**	**135**	-

As per the latest auction results, discount rate $i = 6.75\%$ and $\gamma = 44.9$ [€/MWh] are used similar to the strike price of the 1.2 GW Doggerbank Creyke Beck A [1]. For all the design cases, the cost and mass of oil-filled components can be empirically derived using (40) [15], such that Z is replaced by the relevant parameter (c or m). Similarly for XLPE insulated subsea cables with Cu conductor, the cost can be calculated using (41), where coefficients g_1, g_2 and g_3 are dependent on nominal voltage of the cable [4]. Remaining cost parameters incl. c^{tur}, c^{oss} and C^{fix} are obtained from [32].

$$Z^{\mathrm{trf,SR}}_k = Z_{base}\left(\frac{S^{\mathrm{trf,SR}}_{rated,k}}{S^{\mathrm{trf,SR}}_{base}}\right)^{3/4} \tag{40}$$
$$c^{\mathrm{c}}_k = L^c\left(g_1 + g_2\ e^{g_3 I^{c^2}_{rated,k}}\right) \tag{41}$$

VI. Results and Discussion

A. Economic Analysis

In order to benchmark the results, design case {T250, C1600} from Table I with STR (Base_{STR}) is used for reference. The optimization problem is then solved separately for all the 20 design cases in $\mathcal{K}$ with DTR. In Fig. 7, the optimal number of wind turbines n^{tur} and the change in optimal NPV for each design case with respect to Base_{STR} are provided. For the test case windfarm, the business case has significantly improved by the mere application of DTR. For design case {T250, C1600} with DTR (Base_{DTR}), NPV increases by 327 M€ by installing 200 turbines compared to 171 for Base_{STR} case and by reducing power curtailment during contingency, as shown by efficiency of design (η) in Table II.

The highest NPV increase is observed for the {T200, C1400} design case (Optimal), which is 51 M€ higher than (Base_{DTR}) and employs 191 turbines. Referring to η in Table II, the Optimal case results in slightly higher curtailment than (Base_{DTR}) during contingency, but the savings in initial investment outweigh the revenue losses, which also results in lowest LCOE [$\frac{€}{\text{MWh}}$] for the Optimal case. Similarly, the OSS transformer is severely underutilized by the end of windfarm lifetime for the two Base cases, as compared to the transformer lifetime utilization LL [%] for the Optimal case.

B. Dynamic Rating and Component Utilization

DTR allows ϑ^{hst} to be limited to emergency cyclic limits of 140 °C [18] and ϑ^{c} to 90 °C [21]. The histograms provided in Fig. 8 for the Base {T250, C1600} and Optimal {T200, C1400} cases suggest that both the transformers and the cables operate close to the respective thermal limits more often for the Optimal case. Furthermore, for the scenario with simulated contingency, the thermal stress is higher for both the Base and Optimal cases because component utilization is stretched to the limits to ensure maximum energy transfer during contingency.

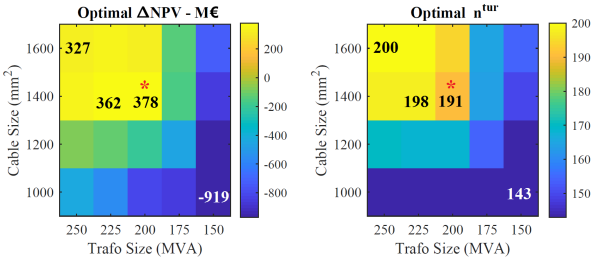

Fig. 7. Results of the opt. problem for all the design cases in $\mathcal{K}$. Change in optimal NPV (ΔNPV) is provided with respect to Base_{STR} for each case

TABLE II
Economic and Efficiency Result Parameters

Parameter			Design Case		
Label	Unit	Formula	Base_{STR}	Base_{DTR}	Optimal
LCOE	[$\frac{€}{\text{MWh}}$]	$\frac{C_o(1+i)^y}{\sum_{y\in\mathcal{Y}}\pi_s\sum_{s\in\mathcal{S}}\sum_{t\in\mathcal{T}}P^{\text{inj}}_{t,s}}$	32.62	30.45	29.56
η	[%]	$\frac{\sum_{y\in\mathcal{Y}}\sum_{s\in\mathcal{S}}\sum_{t\in\mathcal{T}}P^{\text{inj}}_{t,s}}{\sum_{y\in\mathcal{Y}}\sum_{s\in\mathcal{S}}\sum_{t\in\mathcal{T}}P^{\text{gen}}_{t,s}}$	97.15	98.61	98.13
LL	[%]	$\frac{\sum_{y\in\mathcal{Y}}\pi_s\sum_{s\in\mathcal{S}}\lambda_{y,s}}{8760\,\Pi^{\text{WF}}}$	1.25	3.5	62

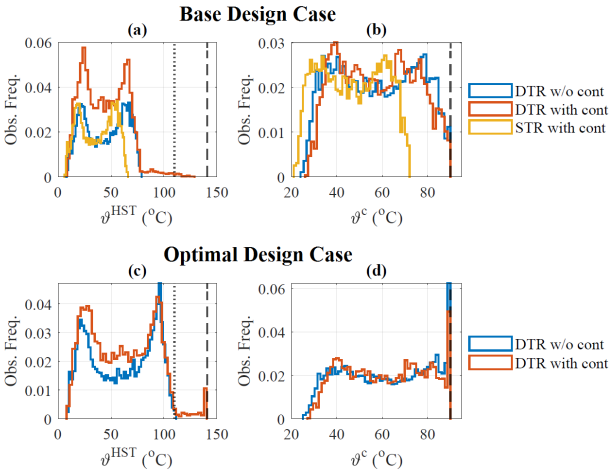

Fig. 8. Histograms for transformer HST ϑ^{hst} and cable conductor temperature ϑ^{c} (incl. seabed temp. ϑ^{sea}) for two scenarios in $\mathcal{S}$ (with & without contingency) for Base{T250, C1600} & Opt.{T200, C1400} cases

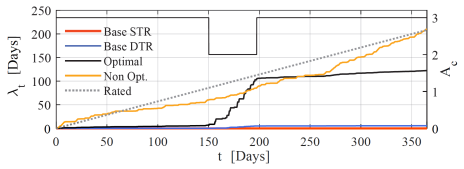

Fig. 9. System availability A^{c} and transformer loss-of-life LL (days) for scenario with contingency.

In Fig. 9, the optimal transformer loss-of-life LL for one of the simulated scenarios in $\mathcal{S}$ with contingency are provided for different design cases in $\mathcal{K}$. As the available circuits A^{c} reduce to 2 around the 150$^{\text{th}}$ day, the additional thermal stress due to increased loading results in higher LL. This is most significant for the Optimal case, while minor for Base_{DTR}. The Non-Optimal case of {T175, C1600} results in optimal LL in this scenario as it is closest to the rated value by the year-end, but doesn't provide the best business case.

C. Power Balance and Component Load during Contingency

For the scenario discussed above, the cable load current and power curtailment are provided in Fig. 10. As A^{c} reduces to 2, I^{c} goes beyond the rated 1 pu value regularly for the Base_{DTR} and Optimal cases, while power needs to be curtailed for the Base_{STR} case. Around the 155-day mark, some curtailment is also needed for the Optimal and Base_{DTR} cases because ϑ^{c} and ϑ^{hst} reach their respective limits, as shown in Fig. 11.

VII. Conclusion

A comprehensive, Dynamic Thermal Rating (DTR) based, two-stage stochastic model has been put forward in this paper, which can be used as investment decision support for OWF design and HVAC-based transmission system optimization. The two-stage problem resolves investment decision by defining optimal windfarm size in the first stage and DTR-based

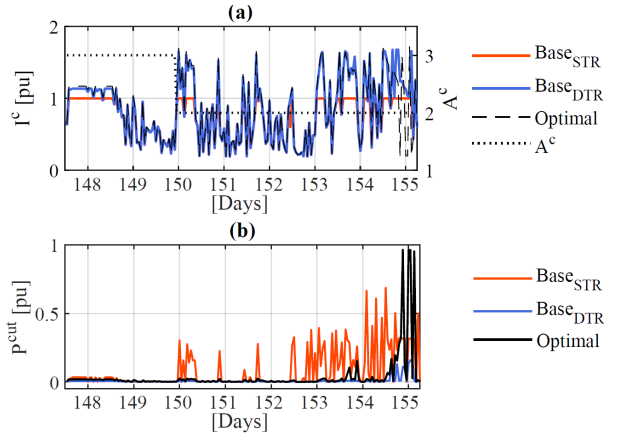

Fig. 10. Scenario with contingency. Top: system availability A^{c} and load current I^{c}. Bottom: curtailed power $\mathrm{P}^{\mathrm{cut}}$ [pu] with $\mathrm{P}^{\mathrm{gen}}$ as base.

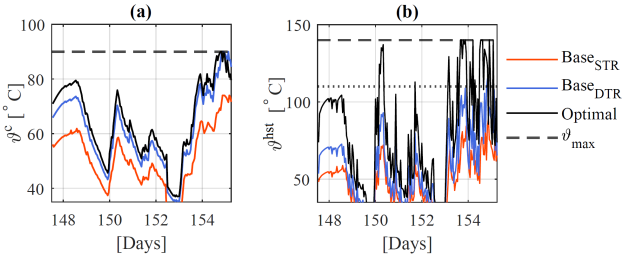

Fig. 11. Transformer HST ϑ^{hst} and cable conductor temperature ϑ^{c} (incl. seabed temp. ϑ^{sea}) in contingency scenario for Base{T250, C1600} & Opt.{T200, C1400} cases. Respective thermal limits are also mentioned.

component ratings with the inclusion of scenarios of stochasticity in wind generation and transmission system reliability in the second stage. The proposed lumped TEE model for HV subsea cables is proven to be fit for linear optimization with acceptable accuracy. The application of the proposed methodology on an actual test case windfarm indicates that mere application of DTR during operation increases the business case significantly which is further improved by DTR-based design. This engineering model can be used as a decision tool for design optimization and planning of large OWFs and their transmission systems, as it is generic enough to be expanded to different topologies of HVAC-based OWF transmission.

REFERENCES

[1] C. Walsh and D. Fraile, "Offshore wind in europe - key trends and statistics 2019 (wind europe)," https://windeurope.org/, Feb 2020.

[2] P. Hou, J. Zhu, G. Yang, and Z. Chen, "A review of offshore wind farm layout optimization & electrical system design methods," *Jour. of Modern Power Systems & Clean Energy*, vol. 7, pp. 975–986, 2019.

[3] H. Park and R. Baldick, "Transmission planning under uncertainties of wind and load: Sequential approximation approach," *IEEE Trans. on Power Systems*, vol. 28, no. 3, pp. 2395–2402, Aug 2013.

[4] J. Pérez-Rúa, M. Stolpe, K. Das, and N. A. Cutululis, "Global optimization of offshore wind farm collection systems," *IEEE Trans. on Power Systems*, vol. 35, no. 3, pp. 2256–2267, May 2020.

[5] M. Banzo and A. Ramos, "Stochastic optimization model for electric power system planning of offshore wind farms," *IEEE Trans. on Power Systems*, vol. 26, no. 3, pp. 1338–1348, Aug 2011.

[6] S. Wei, L. Zhang, Y. Xu, and F. Li, "Hierarchical optimization for the double-sided ring structure of the collector system planning of large offshore wind farms," *IEEE Trans. on Sustainable Energy*, vol. 3, no. 8, pp. 1029–1039, Jul 2017.

[7] J. Gonzalez, M. Payan, and J. Santos, "A new and efficient method for optimal design of large offshore wind power plants," *IEEE Trans. on Power Systems*, vol. 28, no. 3, pp. 3075–3084, Aug 2013.

[8] H. Ergun, D. V. Hertem, and R. Belmans, "Transmission system topology optimization for large-scale offshore wind integration," *IEEE Trans. on Sustainable Energy*, vol. 3, no. 4, pp. 908–917, Oct 2012.

[9] M. Sedighi, M. Moradzadeh, and M. Fahrioglu, "Simultaneous optimization of electrical interconnection configuration and cable sizing in offshore wind farms," *Jour. of Modern Power Systems & Clean Energy*, vol. 6, pp. 749–762, 2018.

[10] H. Park, R. Baldick, and D. Morton, "A stochastic transmission planning model with dependent load and wind forecasts," *IEEE Trans. on Power Systems*, vol. 30, no. 6, pp. 3003–3011, Jan 2015.

[11] A. Cerveira, A. Sousa, and J. Baptista, "Optimal cable design of wind farms: The infrastructure and losses cost minimization case," *IEEE Trans. on Power Systems*, vol. 31, no. 6, pp. 4319–4329, Nov 2016.

[12] J. Pérez-Rúa, K. Das, and N. A. Cutululis, "Optimum sizing of offshore wind farm export cables," *International Journal of Electrical Power & Energy Systems*, vol. 113, pp. 982–990, Dec 2019.

[13] S. Catmull, R. D. Chippendale, and J. A. Pilgrim, "Cyclic load profiles for offshore wind farm cable rating," *IEEE Trans. on Power Delivery*, vol. 31, no. 3, pp. 1242–1250, June 2016.

[14] M. A. H. Colin and J. A. Pilgrim, "Offshore cable optimization by probabilistic thermal risk estimation," in *IEEE International Conference on Probabilistic Methods Applied to Power Systems*, USA, 2018.

[15] S. H. Kazmi, T. Laneryd, and J. Holboll, "Cost optimized dynamic design of offshore windfarm transformers with reliability and contingency considerations," *Int. Journal of Electrical Power & Energy Systems*, vol. Provisionally Accepted, 2020.

[16] N. Viafora, K. Morozovska, and S. H. Kazmi *et al*, "Day-ahead dispatch optimization with dynamic thermal rating of transformers and overhead lines," *Electric Power Systems Research*, vol. 171, pp. 194–208, 2019.

[17] J. Teh and I. Cotton, "Reliability impact of dynamic thermal rating system in wind power integrated network," *IEEE Trans. on Reliability*, vol. 65, no. 2, pp. 1081–1089, 2016.

[18] *Guide for Loading Mineral-Oil-Immersed Transformers and Step-Voltage Regulators - Redline*, IEEE C57.91-2011 Std., Mar 2011.

[19] *Loading guide for oil-immersed power trafos*, IEC 60076-7 Std., 2018.

[20] N. Viafora, S. Kazmi, T. Olesen, T. Sørensen, and J. Holbøll, "Load dispatch optimization using dynamic rating and optimal lifetime utilization of transformers," in *Proceedings of IEEE PES Powertech*, Italy, 2019.

[21] *Calculation of the Cyclic and Emergency Current Rating of Cables. Part 2: Cyclic Rating of Cables Greater Than 18/30 (36) kV and Emergency Ratings for Cables of all Voltages*, IEC60853-2 Std., AD:2008.

[22] R. Olsen, G. Anders, J. Holboll, and U. S. Gudmundsdottir, "Modelling of dynamic transmission cable temperature considering soil-specific heat, thermal resistivity and precipitation," *IEEE Transactions on Power Delivery*, vol. 28, no. 3, pp. 1909–1917, July 2013.

[23] D. Chatzipetros and J. A. Pilgrim, "Review of the accuracy of single core equivalent thermal model for offshore wind farm cables," *IEEE Trans. on Power Delivery*, vol. 33, no. 4, pp. 1913–1921, August 2018.

[24] S. Kazmi, T. Olesen, and J. Holbøll, "Machine learning based temperature forecast for offshore windfarm export cables," in *CIGRE SC B1 (Insulated Cables For Future Power Systems)*. Paris: CIGRE, 2020.

[25] A. Madariaga, J. Martın, and O. A. Lara, "Effective assessment of electric power losses in three-core xlpe cables," *IEEE Trans. on Power Systems*, vol. 28, no. 4, pp. 4488–4495, Nov 2013.

[26] H. Brakelmann, "Loss determination for long three-phase high-voltage submarine cables," *Eur. Trans. Elect. Power*, vol. 13, no. 3, pp. 193–197, Nov 2003.

[27] O. Gouda, G. F. Osman, W. A. Salem, and S. H. Arafa, "Cyclic loading of underground cables including the variations of backfill soil thermal resistivity and specific heat with temperature variation," *IEEE Trans. on Power Delivery*, vol. 33, no. 6, pp. 1242–1250, Jan 2019.

[28] R. Billinton and R. N. Allan, *Reliability Evaluation of Engineering Systems: Concepts and Techniques*. New York, USA: Plenum, 1992.

[29] Y.-K. Wu, P. E. Su, Y.-S. Su, and W. S. Tan, "Economics and reliability-based design for an offshore wind farm," *IEEE Trans. on Industry Applications*, vol. 53, no. 6, pp. 5139–5149, Jan 2018.

[30] P. Chen, T. Pedersen, and B. Bak-jensen, "Arima-based time series model of stochastic wind power generation," *IEEE Trans. on Power Systems*, vol. 25, pp. 667–676, 2010.

[31] J. Jurgensen, L. Nordstrom, and P. Hilber, "Estimation of individual failure rates for power system components based on risk functions," *IEEE Trans. on Power Delivery*, vol. 34, no. 4, pp. 1599–1607, 2019.

[32] BVG, "Guide to an offshore wind farm (updated)," https://ore.catapult.org.uk/app/uploads/2019/04/BVGA-5238-Guide-r2.pdf, April 2019.

[Pub. C1]

S. H. H.Kazmi, T. H. Olesen, T. S. Sørensen and J. Holbøll, **"Thermoelectric Modelling and Optimization of Offshore Windfarm Export Systems - State of the Art"**, *IEEE Global Power, Energy and Communication Conference (GPECOM)*, Nevsehir, Turkey, July 2019.

The published version of the paper is attached.

Thermoelectric Modelling and Optimization of Offshore Windfarm Export Systems - State of the Art

Syed Hamza Hasan Kazmi
Electrical Systems
Ørsted Offshore
Gentofte, Denmark
syeka@orsted.dk

Joachim Holbøll
Dept. of Electrical Engg.
Tech. University Denmark
Lyngby, Denmark
jh@elektro.dtu.dk

Thomas Herskind Olesen
Electrical Systems
Ørsted Offshore
Fredericia, Denmark
thole@orsted.dk

Troels Stybe Sørensen
Electrical Systems
Ørsted Offshore
Gentofte, Denmark
troso@orsted.dk

***Abstract*— With recent developments and cost reduction, offshore windfarms are set to lead the energy markets of the west by 2030. This development can further be accelerated if the wind intensive periods can be utilized efficiently by optimizing the limited network capacity and if the energy output is increased during contingency outages. Therefore, dynamic rating operation of components that are primary system bottlenecks becomes crucial. This paper identifies potential bottlenecks in offshore windfarm export systems and provides an extensive state-of-the-art review of dynamic thermoelectric models which are applicable for real-time loadability assessment of the identified components. The loadability of these components is directly dependent on their thermal state, which is evaluated based on analytical solutions of the dynamic thermoelectric model, including the complicated heat transfer and temperature development phenomena in the identified components. Moreover, potential risks of using these models for offshore windfarm applications are also identified.**

Keywords— Dynamic thermal rating, cable, thermoelectric modelling, offshore windfarm, renewable integration, transformer

I. INTRODUCTION

Wind energy is a major contributor to the annual electricity generation in Denmark [1] and it is projected to increase even further by 2030 [2] in order to keep up with the targets defined by the Danish Government's 'Energy Agreement' of 2018 [3]. A sizable portion of this increment is bound to be delivered by Offshore Wind Power Plants (OWPPs). But bottlenecks in OWPPs export systems and the system improvement costs related to resolving these bottlenecks are major barriers to this prognosis [4], [5].

Some bottlenecks can be removed and the unused potential of some of the major components of OWPP export systems can be exploited by switching to Dynamic Thermal Rating (DTR) instead of using static rating based on conservative assumptions including continuous full load, high solar radiation, and fixed ambient temperatures [6]. The majority of publications on DTR so far have focused on overhead lines (OHLs), including extensive thermal modeling, inclusion of weather forecasts [7], [8] and innovative real-time sag measurement [9] to effectively increase the dynamic rating based operation. However, OHLs do not play such an influential role in the debottlenecking of offshore windfarms.

Therefore, the attention must shift to all the remaining components which include transformers, subsea and underground cables, shunt reactors, HV filters, compensators, MV/HV switchgears, CTs, VTs, Circuit Breakers etc. These components can be prioritized based on their impacts on system's loadability and bottlenecks. Utilization of real-time monitoring techniques can contribute to raise the possible loading of some of these components above the static limit 99% of the time. Similarly, a handful of publications claim that the conservative static limits can be exceeded by 30% of the limit about 90% of the time using the DTR principle [10].

The characteristic loadability of underground cables is typically based on the international standard IEC 60287 [11] and the cyclic ampacity is based on IEC 60853 [12] along with certain recent CIGRE publications discussing the optimization of these standard models using Distributed Temperature Sensing (DTS) and Real Time Thermal Rating [10], [13]. This provides sufficient information for HV cables, but little to no work has been done for rest of the identified components.

The dynamic loading guides for power transformers disseminated by IEEE [14] and IEC [15] have evolved since the early 1990's and these guides are still subjects of development, whereas the CIGRE Brochure 659 [16] provides an extensive overview on the topic. The integration of distributed generation in existing electrical infrastructure has shifted the focus towards short term dynamic rating of transformers as well, which can be used for OWPP export system optimization and debottlenecking [17], [18].

The measurement of critical temperatures variation with load in HV/MV cables and oil-filled transformers using fibre-optic sensors like DTS is often costly and even unavailable. Moreover, these solutions are not perfect for real-world applications because the sensors may not be able to locate hotspots or may not determine the exact conductor or winding temperature. Therefore, dynamic thermal estimation of these components is performed using thermal modeling techniques, predominantly based either on the Finite Element Method (FEM) and Computational Fluid Dynamic (CFD) [16], [19] or on Thermoelectric Equivalent (TEE) circuits representing the heat flow equations using the thermoelectric analogy [20]. The accuracy of CFD and FEE modelling is higher than the latter approach and these can also allow determination of complete temperature distribution under the assumption that all thermal parameters are known. But the advantages offered by TEE models like the simplicity of design, easy availability of input parameters, minimal computational requirements and the adaptability for components with different construction and design features make the TEE modelling technique an ideal tool for optimized dynamic operation [11], [21].

This paper reviews the state-of-the-art for thermoelectric modelling and dynamic rating of two major components of the OWPP export system: HV/MV cables and transformers. The potential issues and risks involved in using the prominent methods for dynamic modeling of these components in windfarm applications are also discussed. The remaining paper is organized as follows: Initially, section 2 unfolds the simplified transmission system for OWPPs and identifies the critical components that cause constrictions in the system. Later, sections 3 and 4 present state-of-the-art for dynamic thermoelectric modeling of transformers and cables respectively. The state-of-the-art includes a review of recommended loading guides by IEC, IEEE and CIGRE, along with some prominent publications discussing conventional and advanced models.

978-1-5386-8086-5/19/$31.00 ©2019 IEEE

II. Optimization of OWPP Export Systems

The Offshore Wind Power Plant (OWPP) export system based on HVAC technology, as identified in Fig.1, has an offshore substation close to the wind turbines and an onshore substation on land which serves as an interface between the export system and the transmission grid. Whereas the number of reactor substations depends upon the windfarm's distance from the shore. This system consists of a number of HV components ranging from HV/MV cables and transformers to Shunt Reactors, HV filters, Gas Insulated Switchgears (GIS) and compensators (incl. STATCOM, FACTS, SVC etc.).

The long export cables (underground and subsea) are used rather conservatively because of the associated capital investment and are known to be the primary bottlenecks in this system. On the other hand, the system bottleneck can often move to the main transformers during contingency or planned/unplanned maintenance. Moreover, both these components are often over-dimensioned and consequently underutilized [22]. Therefore, optimized utilization of these 2 components using dynamic rating beyond their design limits for certain periods becomes crucial for optimization of OWPP export system. Publications discussing the utilization of unused potential of components including reactors, HV filters and GIS are rare, primarily because this is seldom a problem in today's system. Based on this analysis, this paper focuses only on thermal estimation of transformers and cables for offshore windfarm transmission systems.

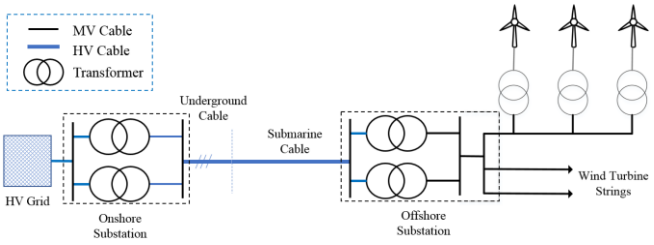

Fig. 1. Simplified layout for offshore windfarm export system

III. Thermoelectric Modelling of Transformers

The loading capability of a transformer is directly dependent on its Hot Spot (HST) and Top Oil (TOT) temperatures [14], [23]-[24]. In order to optimize the electrical export systems of offshore windfarms with transformers as one of the bottlenecks, real-time estimation of HST and TOT to calculate their dynamic loadability is a cost-effective solution. However, the estimation of these temperatures in oil-filled transformers is difficult as compared to cables because of the complicated heat transfer phenomenon [25].

The Thermoelectric Equivalent (TEE) methodology uses the analogy between principles of thermodynamics and charge/discharge mechanism of the RC-circuit, which makes it easier to grasp for electrical engineers [26]. The structures of almost all the differential equations-based TEE models discussed in this paper are directly or indirectly inspired by the circuit of Fig. 2 based on (1), which was originally coined in [27], [28] for temperature development in electrical machines and is also known as the Exponential Law.

$$q = C_{th}\frac{d\theta'}{dt} + \frac{\theta' - \theta}{R_{th}} \qquad (1)$$

Here q represents the heat generated by losses (analogous to current), $\theta' - \theta$ is the temperature difference (analogous to voltage), while C_{th} and R_{th} are the thermal capacitance and thermal resistance (analogous to electrical capacitance and resistance) and t represents the time. The TEE circuit of Fig. 2 can be used to estimate both the TOT and HST for transformers by substituting the relevant variables with the parameters of Table I, as originally suggested by *Swift* in [26]. Where q_{fe} and q_{wdg} represent iron and winding copper losses; ϑ_{tot} , ϑ_{hst} and ϑ_{amb} are the top-oil, hot-spot and ambient temperatures respectively; $R_{th\ oil\text{-}air}$ and $R_{th\ wdg\text{-}oil}$ are non-linear oil-to-air and winding-to-oil thermal resistances; $C_{th\ oil}$ and $C_{th\ wdg}$ represent the thermal capacitance for oil and winding.

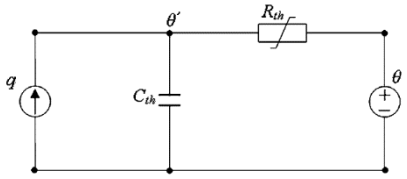

Fig. 2. Generic thermoelectric equivalence circuit for transformer temperature estimation (Hot-Spot and Top-Oil) [26]

TABLE I. Parameters for TOT and HST Estimation (Fig. 2)

Variable	TOT	HST
q	$q_{fe} + q_{wdg}$	q_{wdg}
θ'	ϑ_{tot}	ϑ_{hst}
R_{th}	$R_{th\ oil\text{-}air}$	$R_{th\ wdg\text{-}oil}$
C_{th}	$C_{th\ oil}$	$C_{th\ wdg}$
θ	ϑ_{amb}	ϑ_{tot}

A. Historical Development of Transformer TEE Models

The TEE models presented in renowned loading guides by IEC and IEEE have certain limitations. Therefore, over the years numerous publications can be found offering simplifications, clarifications and recommendations for improvement of these guides. Some of the prominent ones along with the international loading guides are mentioned.

1) IEEE C57.91 Loading Guide [14], [29]–[31]:

The industry-wide accepted loading guides of IEEE [14], [29]-[31] have evolved significantly over the last 3 decades. These guides utilize the exponential law of (1) or its approximation to calculate the final TOT and HST rise. The ultimate temperature rise is estimated using the principle that the generated heat q is dissipated through conduction, convection and radiation. Whereas, the Poisseulle's law of flow is applicable with the assumption that there is minimal turbulence in the oil ducts, as suggested by Montsinger in [32]. Consequently, the impact of transformer cooling modes is considered. A number of publications prove that these models perform inadequately for low ϑ_{amb}, and the calculated temperature rise is vulnerable to transients and load changes, which is extremely important for windfarm applications because of wind energy's intermittent nature [33]-[35].

2) IEC Loading Guides [15], [20], [23]:

The former IEC loading guide 60354 [15] and its improvements 60076 [23]-[24] propose 2 different methods: differential and exponential. The former is the same as IEEE C57.91; while the latter, exponential-based, is only suitable for step-load change and is dependent on arbitrarily obtained parameters. This uncertainty is resolved by a number of publications discussing extension, parameter estimation and experimental elaboration for the exponential model of IEC 60076-7 [36]-[38]. However, the dependence of this model on transformer construction-specific parameters obtainable

only through prolonged heat-run tests makes it impractical for widescale OWPP optimization.

3) Swift et al. [26], [39] (2001):

The simplified description of the thermal-electrical analogy based on the convective heat transfer and its application to determine a transformer's HST and TOT are discussed in this model. Like the differential models of loading guides, it is essentially based on Fig. 2, i.e. it assumes the conditions for *lumped capacitance*, but it distinctively introduces two different circuits for heat transfer: winding-to-oil and oil-to-air. The impact of cooling mode is also addressed differently. The reasons for its limited accuracy are addressed in [40] and [41].

4) Susa et al. [33]-[34], [42]-[43] (2013)

The time delay between TOT and HST rise, as measured and quantified in [25], results in HST which is higher than the one calculated by IEC loading guides. The model in [33] builds upon the discussion of *Swift's* model and incorporates the impact of temperature change on the thermal characteristics of transformer oil in TOT and HST calculations, thereby increasing the accuracy of calculations during transient states. The model focuses on the non-linearity of the thermal resistance and primarily includes oil viscosity changes and loss variations with temperature, and it is further improved in [34] and [42].

5) Djamali [17], [18] (2017)

The model calculates the TOT for indoor distribution transformers and extends the findings of Swift and Susa by further addressing the heat transfer due to conduction, radiation and ventilation in the transformer room. Therefore, the transformer's loadability can be estimated using the room's ventilation temperature. Transformers in offshore platforms can be placed indoors with controlled temperature, therefore the analysis seems practically viable.

6) Josue [44] (2012)

Like Susa, this model modifies the IEC 60076-7 loading guides by investigating the variation of transformer oil viscosity with temperature, along with the dependence of winding losses on temperature. The oil temperature is equated to the HST to determine the change in its viscosity and simulate the extreme condition.

7) Miscellaneous Models

Besides the models mentioned above, there are many models that suggest improvements to the loading guides. For example, [45] investigates the influence of weather conditions (including wind speed and solar radiation) on transformer's TOT, [37] extends these models for smaller transformers, while [38] assesses a transformer's overload capability by estimating standardized error in TOT calculation but uses the design information of the transformer to estimate the heat transfer modes in it. On the other hand, [46] offers a unique perspective of identifying the sources of errors in dynamic modeling of transformers.

8) Machine Learning based Models

With the increasing computing capacity, the use of machine learning to effectively calculate the TOT and HST of transformers has also been discussed from time and again. Tang *et al.* in [47], [48] take the inspiration from artificial neural networks to use a genetic algorithm for identification of global solutions to estimate thermal parameters R_{th} and C_{th}. The model also incorporates the impact of cooler states (on/off) prior to parameter estimation. Similarly, [49] uses the same approach for cast-resin dry-type transformers. Other methods range from neural networks [50] to neuro-fuzzy ones [51]. Moreover, the practicality of using evolving fuzzy networks is also evaluated [52]. However, the application of such models would require ample training data, which is unfortunately not readily available in today's power systems.

B. Structural Evaluation of Selected Models

The evaluation of TOT and HST estimation for 3 main differential equations-based TEE models is performed. The loading guides models, originally presented as exponential solutions in [24], [29], are converted into the respective differential equations to maintain structural homogeneity.

1) Loading Guides IEC and IEEE [24], [29]

$$\tau_0 \frac{d\vartheta_{tot}}{dt} = \Delta\vartheta_{or}\left(\frac{K(t)^2 R + 1}{R + 1}\right)^n - [\vartheta_{tot}(t) - \vartheta_{amb}(t)] \quad (2)$$

$$\tau_h \frac{d\vartheta_{hst}}{dt} = \Delta\vartheta_{hr} K(t)^{2m} - [\vartheta_{hst}(t) - \vartheta_{tot}(t)] \quad (3)$$

2) Swift et al. [26], [39]

$$\tau_0 \frac{d\vartheta_{tot}}{dt} = \Delta\vartheta_{or}^{\frac{1}{n}}\left(\frac{K(t)^2 R + 1}{R + 1}\right) - [\vartheta_{tot}(t) - \vartheta_{amb}(t)]^{\frac{1}{n}} \quad (4)$$

$$\tau_h \frac{d\vartheta_{hst}}{dt} = \Delta\vartheta_{hr}^{\frac{1}{m}} K(t)^2 - [\vartheta_{hst}(t) - \vartheta_{tot}(t)]^{\frac{1}{m}} \quad (5)$$

3) Susa et al. [33], [34]

$$\tau_0 \frac{d\vartheta_{tot}}{dt} = \Delta\vartheta_{or}\left(\frac{K(t)^2 R + 1}{R + 1}\right) - \left(\frac{\vartheta_{tot}(t) - \vartheta_{amb}(t)}{[\mu_{pu}(t)\,\Delta\vartheta_{hr}]^{1-n'}}\right)^{1/n'} \quad (6)$$

$$\tau_h \frac{d\vartheta_{hst}}{dt} = \Delta\vartheta_{hr} K(t)^2 P_{pu}(\vartheta_{hst}) - \left(\frac{\vartheta_{hst}(t) - \vartheta_{tot}(t)}{[\mu_{pu}(t)\,\Delta\vartheta_{hr}]^{1-m'}}\right)^{1/m'} \quad (7)$$

Where ϑ_{amb} is the ambient temperature (°C); K is the transformer load current in p.u. with rated load current as base; ϑ_{tot} and ϑ_{hst} are the calculated Top Oil and Hot Spot Temperatures respectively, expressed in °C; R is the ratio of load losses to no-load losses at rated load; $\Delta\vartheta_{or}$ is the TOT rise over ambient temperature ϑ_{amb} at rated load (°C), while $\Delta\vartheta_{hr}$ is the rated HST rise over TOT for rated load of 1 pu. The estimation of μ_{pu} (temperature dependent oil viscosity in pu) and $P_{pu}(\vartheta_{hst})$ (variation of load losses with HST in pu) can be performed using [33], [34]. The empirically derived exponents *n, m, n'* and *m'* have been extensively researched for almost a century and the values vary with the transformer cooling mode (i.e. ONAN, ONAF etc.), the mass distribution of transformer components [30] and oil flow type (i.e. the presence or absence of turbulence in oil flow) [25], the values for which are provided in Table II [24], [34].

The thermal time constants for oil τ_0 and winding τ_h are usually obtained using the heat run test, but τ_0 can also be estimated using slightly differing methods. The IEEE guides [29], [30] use manufacturer-defined rated losses and $\Delta\vartheta_{or}$ for ODAF cooling *(n, m = 1)* but require additional manipulation for *(n < 1)*. Similarly, IEC 60076-2 [20] uses real-time load-dependent temperature rise, while IEC 60076-7 [24] recommends using the average oil temperature rise instead. It

must also be mentioned that IEC 60076-7 recommends the use of a correction factor (<1) for oil time constants to compensate for the mismatch between the time constants for top oil and average oil in ONAN and ONAF transformers, as scrutinized by Nordman *et al*. in [25]. All of these techniques require detail information regarding the mass and material of different transformer components (winding, oil, core etc.).

Referring to (2) – (7), it can be concluded that the basic structure of the 3 selected models is similar. The first-order non-linear differential equations have 3 basic terms: Rate of temperature change on the left-hand side, Heating-term which is dependent on load losses and Cooling-term which is dependent on relevant temperature difference. The inclusion of oil viscosity in Susa (6)-(7) is accurately reflected in the cooling-term. The major difference in the 3 models is the location of empirical constants. The models from loading guides (2)-(3) and Swift (4)-(5) distinctively place these constants on the heat-in term, while the Susa model does otherwise, which appears to be thermodynamically accurate.

TABLE II. EMPIRICAL CONSTANTS FOR IEEE [29], SWIFT [26] AND SUSA [34] MODELS

Transformer Cooling Mode	IEEE C57.91		Susa et al. [a]	
	n	*m*	*n′*	*m′*
Oil Natural Air Natural (ONAN)	0.8	0.8	0.8	0.67
Oil Natural Air Forced (ONAF)	0.9	0.8	0.83	0.67
Oil Forced Air Forced (OFAF)	0.9	0.8	0.83	0.67
Oil Directed Air Forced (ODAF)	1.0	1.0	0.83	0.67

[a] *Values for onload condition (circulating oil) with external cooling are provided*

C. Discussion regarding DTR of Transformers in OWPP

The models presented earlier have some inherent limitations for OWPP application. IEEE and IEC loading guides have accuracy limitations, Swift models perform inadequately when forced convection is used for cooling, whereas the complexity of the other methods make them less suitable for real-time dynamic rating applications.

The various sources for harmonics amplification in OWPPs including long HVAC cables, power electronic converters etc. [53] can increase the lifetime reduction phenomena in transformers for rated load. Therefore because of increased losses, load reduction becomes necessary [29], [54]. Hence, the incorporation of these losses in transformer DTR modelling is compulsory for accurate HST and TOT determination. Similarly, the transformer oil viscosity can vary significantly with temperature and this variation depends on the type of oil used and the variation is maximum for low ambient temperatures, which is common in OWPP applications [55]. The development of TOT and HST is therefore influenced by the type of transformer oil because viscosity affects the flow patterns and convective cooling.

IV. CABLES LOADABILITY & THERMOELECTRIC MODELLING

As already discussed, cables used to transmit energy from offshore substations to the onshore ones are known to be the primary bottlenecks in OWPP export systems. This is true primarily because the associated capital costs restrict the potential provision of multiple subsea cables. Therefore, optimized loadability of cables is extremely important for a good business case. Only HVAC cables are discussed here.

A. Determination of HV/MV Cables Loadability for OWPP

Like the remaining HV electrical components, the temperature of the insulating material defines the loadability of power cables [11]. Several cable manufactures propose 90 ^{o}C to be the upper limit for the conductor temperature for Cross-Linked Poly-Ethylene (XLPE) insulated cables for cyclic load, in order to prevent the dielectric and mechanical strength of the cables from deterioration and to preserve cables' life [12]. The dependence of XLPE cables' properties on temperature and the impacts of thermal ageing have been critically investigated since the introduction of these cables more than 4 decades ago. These properties include thermal resistivity, specific heat, electrical breakdown strength under AC and impulse voltages, tensile strength, electrical resistivity, permittivity (dielectric strength) and loss factor (tan delta) [56]-[58]. The investigation results are documented in some prominent publications [59 – 63].

The loadability of cables can either be defined for a permanent period (until end of life) called steady load (IEC 60287) or for shorter duration called dynamic load. In both cases, the physical limitations of the cables are never violated. Dynamic loading (IEC 60853) ensures optimal utilization of cables and can usually be of two types: cyclic (daily load cycles) or emergency (short durations) [12], [63]-[64]. Even though, these loading limits are extremely useful in OWPP applications owing to wind energy's intermittent nature, these are not readily used because of reasons already discussed.

B. Dynamic Thermoelectric Modelling of HV/MV Cables

As mentioned earlier, determination of OWPP cable HST for real-time DTR application is practically feasible only if appropriate thermoelectric models capable of performing online calculations of cable core or insulation temperature are used [65], which is not possible using IEC 60287 and 60853. An extensive literature review reveals that the major thermal models can be divided into three categories: FEM-based, Laplace transformation-based and Differential equation-based models, out of which only the last 2 models qualify as thermoelectric ones. It must also be mentioned that the exact implications of these methods are not documented well enough, essentially because different manufacturers and consultants employ these models in commercially available software such as [66]-[70]. Keeping the discussion aligned with Section 3, this section focuses particularly on Laplace and differential-based models.

1) Laplace-based Models

Laplace transformation-based methods (IEC 60853) utilize the exponential integrals to determine conductor temperature development during load change [58], [63]. The models proposed in [57], [71] use exponential integrals to evaluate the dynamic thermal response and take into account all external parameters (known and unknown) to accurately determine the cable's loadability.

2) Differential Equation based Models

The models are also based on Fig. 2 [27] and follow the same principle as TEE modeling of transformers discussed in previous section. These models are established by dividing the subcomponents of cables (conductors, insulator, screens etc.) into thermal zones with respective thermal capacitance and resistance, which is essential when analysis is not based on exponential integrals and attainment factors [72]. Moreover, the ambient conditions and variation of thermal parameters of soil (or other medium) with temperature are also considered.

The steady-state thermoelectric model of Fig. 3 for subsea cables, extracted from [11], [71] takes into account armor losses, which are crucial for subsea cables, but it is based on

some simplified assumptions. The heat losses are represented by W (W/m), each node represents a temperature θ, while T and C are the thermal resistances and capacitances respectively. The subscripts definitions are critical: *c, d, s* and *a* represent the conductor, dielectric (insulation), screen and armor respectively. While 1, 2 and 3 are used to define the thermal parameters of dielectric, armor and surroundings respectively. The conductor temperature (θ_C) calculated using this model is given by (8). The sheath losses W_s and armor losses W_a can be calculated using the conductor losses W_c as $\lambda_1 W_c$ and $\lambda_2 W_c$ respectively. Where, sheath and armor loss factors λ_1 and λ_2 can either be obtained according to IEC 60287 [11] or as per improvements in [71].

$$\frac{d\theta_C}{dt} = \frac{1}{C_1}\left(W_C + \frac{1}{2}W_d - \frac{\Delta\theta_C - \Delta\theta_S}{T_1}\right) \tag{8}$$

Equivalent to transformer TEE models, $\Delta\theta_S$ in (8) is found using a similar equation. Some publications [73]-[74] claim improved performance and accuracy by combining the differential models for a cable's internal parameterization and Fourier models for external. According to [75], machine learning and genetic algorithms are also suitable for the differential approach. Moreover, the cable surroundings are divided into multiple loops for increased accuracy, but this approach can be computationally expensive.

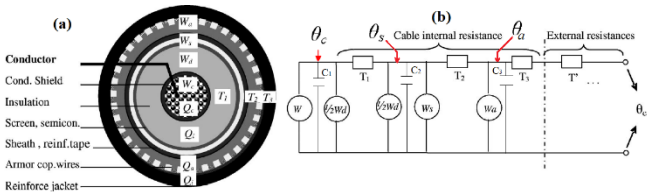

Fig. 3. Single Core Cable Layout. (a) Cross-section. (b) Thermal network for dynamic rating operation [52]

C. Discussion regarding DTR of Cables in OWPP

The information of ambient conditions including temperature, thermal properties etc. of the cable's surrounding material (soil, water etc.) is used as inherent input to almost all the models discussed earlier, which makes it extremely critical [57], [71]. This information is either estimated, measured or both. Temperature measurements along cables are performed using PT100 sensors, thermocouples or optical-fibres. But the length of offshore cables for OWPPs result in precision issues which may consequently miss the possible hotspot development [74]. Moreover, there can be inherent hot-spots in OWPP cable installations (E.g. J-tubes and landfills), which cause major bottlenecks. Also, the cable length creates significant complications (including harmonics) which must be accounted for in the thermoelectric models [75]. A number of advanced measurement and monitoring methods can be used to improve these models. These methods include Time-Domain Reflectometers, Distributed Temperature Sensing (DTS), Line Resonance Analysis (LIRA) and Distributed Acoustic Sensing (DAS).

V. Conclusion

A comprehensive study has been conducted on transmission system optimization for offshore windfarms. Transformers and cables are identified as the potential bottlenecks in the windfarm export system. The relevant thermoelectric modeling techniques proposed over the last few decades, which can be used to overcome the congestion challenges in the network based on dynamic thermal estimation have been mentioned. Some of these techniques are primarily based on industry-wide accepted IEEE and IEC loading guides. But the limitations of these models have been extensively worked out in several recent publications suggesting model improvements. All these techniques have been thoroughly reviewed in this paper and the potential risks for offshore windfarm applications have also been identified.

Acknowledgment

Authors would like to thank Innovation Fund Denmark and Ørsted Offshore A/S for supporting the work. The OPTIMUM framework project collaboration between DTU, Energinet.dk and Ørsted oversees this work.

References

[1] Environmental Report 2017 – 'Environmental report for Danish electricity and CHP for 2016 status year,' Energinet.dk

[2] 'Denmark's Energy and Climate Outlook 2017' *Danish Energy Agency*, March 2017

[3] 'Energy Agreement: Danish Climate Policy Plan Towards a Low Carbon Society', *Danish Government*, 2018,

[4] S. Abbott, S. Abdelkader 'Experimental Validation & Comparison of IEEE, CIGRE Dynamic Line Models', *IEEE - Universities Power Engineering Conference,* 2010 45th International, Wales, Dec 2010

[5] W. Winter, K. Elkington 'Pushing the Limits: Europe's New Grid: Innovative Tools to Combat Transmission Bottlenecks & Reduced Inertia', *IEEE Power Energy Magazine*, Vol 13, Dec 2014, pp 60-74

[6] N. Alguacil, M. H. Banakar and F. D. Galiana, "Electrothermal coordination part II: case studies," *IEEE Transactions on Power Systems*, vol. 20, no. 4, pp. 1738-1745, Nov. 2005

[7] CIGRE WG B2.43, "Guide for thermal rating calculations of overhead lines", *Technical Brochure 601*, Paris, France 2014

[8] IEEE Standard 738, "IEEE Standard for calculating the current-temperature relationship of bare overhead conductors", *IEEE Standard Association*, Washington, U.S.A 2014

[9] S. M. Mahajan, U. M. Singareddy, 'A Real-Time Conductor Sag Measurement System Using a Differential GPS', *IEEE Transactions on Power Delivery, Vol. 27 Issue: 2, Apr 2012, pp 475 - 480*

[10] CIGRE WG B1.45, 'Thermal Monitoring of Cable Circuits and Grid Operators' Use of Dynamic Rating Systems', *CIGRE 2016*

[11] IEC, 60287- 1-1. electric cables - calculation of the current rating (100 % load factor) and losses - general," *IEC, Tech. Rep*., 2006

[12] IEC 60853-1. calculation of cyclic, emergency current rating of cables up to and including 18/30 (36) kv,' *IEC, Tech. Rep.,* 1985.

[13] CIGRE WG B1.02, 'Optimization of Power Transmission Capability of Underground Cable Systems Using Thermal Monitoring' *Technical brochure 247*, Paris, France, Apr 2004

[14] 'IEEE C57.91: IEEE Guide for Oil-Immersed Transformers', 2004

[15] 'IEC 60354- Loading Guide for Oil-Immersed Transformers', 1991

[16] Lapworth, J., Picher, P., Channet, J., et al.: 'Transformer thermal modelling'. *Technical report, Cigre* Working Group A2.38, 2016

[17] M. Djamali, S. Tenbohlen, 'Real-Time Evaluation of the Dynamic Loading Capability of Indoor Distribution Transformers,' *IEEE Transactions on Power Delivery* Vol. 33, Jun 2018, pp 1134 - 1142

[18] M. Djamali and S. Tenbohlen, "Assessment of the dynamic overload capability of distribution transformers," in the *19th International Symposium on High Voltage Engineering (ISH),* 2015.

[19] H. Li, 'Assessment of underground cable ratings based on distributed temperature sensing,' *IEEE Transactions on Power Delivery*, vol. 21, no. 4, pp. 1763-1769, 2006.

[20] IEC 60076-2: Power Transformers-Temperature rise', April 1993

[21] M. Djamali, S. Tenbohlen, 'Hundred years of experience in the dynamic thermal modelling of power transformers,' *IET Gener. Transm. Distrib., 2017,* Vol. 11 Iss. 11, pp. 2731-2739

[22] M. H. Banakar, N. Alguacil and F. D. Galiana, 'Electrothermal coordination I: theory and implementation schemes,' *IEEE Transactions on Power Systems*, vol. 20 pp. 798-805, May 2005.

[23] IEC, 'IEC 60076-7:2018 power transformers - part 7: Loading guide for oil-immersed power transformers', vol. 60076, no. 7, 2018.

[24] IEC, "IEC 60076-7:2005 power transformers - part 7: Loading guide for oil-immersed power transformers," vol. 60076, no. 7, 2005.

[25] Nordman, H., Rafsback, N., Susa, D.: 'Temperature responses to step changes in the load current of power transformers', *IEEE Trans. Power Deliv*., 2003, 18, (1), pp. 107–112

[26] G. Swift, T. S. Molinski, 'A fundamental approach to transformer thermal modeling. Part I: Theory and equivalent circuit', *IEEE Trans. Power Del.*, vol. 16, no. 2, pp. 171–175, Apr.2001.

[27] Goldschmidt, R.: 'Temperature curves and the rating of electrical machinery', *J. Inst. Electr. Eng*., 1905, 34, (172), pp. 660–691

[28] Montsinger, V.M.: 'Effect of load factor on operation of power transformers', Trans. Electr. Eng., 1940, 59, (11), pp. 632–636

[29] IEEE Std C57.91-2011: IEEE Guide for Loading Mineral-Oil-Immersed Transformers and Step-Voltage Regulators', Dec 2011

[30] 'IEEE guide for loading mineral oil immersed overhead and padmounted distribution transformers rated 500 kVA and less with 65 C or 55 C average winding rise', 1981

[31] IEEE Std C57.91-1995: IEEE Guide for Loading Mineral-Oil-Immersed Transformers and Step-Voltage Regulators', Dec 1995

[32] Montsinger, V.M., Cooney, W.H.: 'Temperature rise of stationary electrical apparatus as influenced by radiation, convection and altitude', *Am. Inst. Electr. Eng.,* 1924, 43, (9), pp. 803–812

[33] D. Susa, M. Lehtonen, and H. Nordman, 'Dynamic thermal modeling of power transformers', *IEEE Trans. Power Del.*, vol. 20, no. 1, pp.197–204, Jan. 2005.

[34] D.Susa, M. Lehtonen 'Dynamic Thermal Modeling of Power Transformers: Further Development—Part I' *IEEE transactions on power delivery*, vol. 21, no. 4, October 2006, pp 1961 - 1970

[35] S. H. H. Kazmi, J. Holbøll, T. H.Olesen, T. S. Sørensen, 'Dynamic Thermoelectric Modelling of Oil-filled Power Transformers for Optimization of Offshore Windfarm Export Systems,' *CIGRE Symposium Aalborg*, 2019, in press

[36] D. Susa, H. Nordman, 'IEC 60076–7 loading guide thermal model constants estimation' *Int. Trans. Electr. Energ. Syst*. 2013; 946–960

[37] B. Das, T. Jalal 'Comparison & Extension of IEC Thermal Models for Dynamic Rating of Distribution Transformers' *POWERCON IEEE International Conference Power System Tech*, 2016

[38] M. Djamali, S. Tenbohlen, 'Malfunction Detection of the Cooling System in Air-Forced Power Transformers Using Online Thermal Monitoring' *IEEE transactions on power delivery*, v. 32, no. 2, 2017

[39] G. Swift, T. Molinski, R. Bray, 'A fundamental approach to transformer thermal modeling. Part II: Field verification', *IEEE Trans. Power Del.*, vol. 16, no. 2, pp. 176–180, Apr. 2001.

[40] O. Amoda, D. J. Tylavsky, G. A. McCUlla, 'Acceptability of Three Transformer Hottest-Spot Temperature Models', *IEEE Transactions on Power Delivery*, vol. 27, pp. 013-022, Jan 2012

[41] Jauregui-Rivera, L., Tylavsky, D.: 'Acceptability of four transformer top-oil thermal models. Part i: Defining metrics', *IEEE Trans. Power Deliv*., 2008,23, (2), pp. 860–865

[42] D.Susa, M. Lehtonen 'Dynamic Thermal Modeling of Power Transformers: Further Development—Part II' IEEE transactions on power delivery, vol. 21, no. 4, October 2006, pp 1971 - 1980

[43] D. Susa, M. Lehtonen, and H. Nordman, 'Dynamic thermal modeling of distribution transformers', *IEEE Trans. Power Del.*, vol. 20, no. 3, pp. 1919–1929, Jul. 2005.

[44] F. Josue, R. Saers, 'Transformer Hot-Spot Temperature Estimation for short-time dynamic loading' *IEEE International Conference on Condition Monitoring and Diagnosis*, 23-27 Sept. 2012

[45] I. Arifianto, R. Saers, 'Investigation of transformer top-oil temperature considering external factors,' *IEEE International Conf. on Condition Monitoring and Diagnosis*, Sept 2012, pp 198 - 201

[46] D. J. Tylavsky, Q. He, 'Sources of Error in Substation Distribution Transformer Dynamic Thermal Modeling' *IEEE transactions on power delivery*, vol. 15, no. 1, Jan 2000, pp. 178 - 185

[47] W.H. Tang, Q.H. Wu, 'Equivalent heat circuit-based power transformer thermal model' *IEE Proc-Electr. Powr Appl.,* Vol. 149, March 2002, pp 87 - 92

[48] W.H. Tang, Q.H. Wu, 'A Simplified Transformer Thermal Model Based on Thermal-Electric Analogy,' *IEEE transactions on power delivery*, vol. 19, July 2004, pp 1112 - 1119

[49] D. Azizian, M. Bigdeli, 'A Dynamic Thermal Based Reliability Model of Cast-Resin Dry-Type Transformers' *International Conference on Power System Technology*, 2010

[50] He, Q., Si, J., Tylavsky, D.: 'Prediction of TOT for transformers using ANN', *IEEE Trans. Power Deliv.*, 2000, pp. 1205–1511

[51] Hell, M., Costa, P.J., 'Participatory learning in powertransformers thermal modeling', *IEEE Trans. Power Deliv*., 2008, pp.2058–2067

[52] Souza, L.M., Lemos, A.P., Caminhas, W.M., et al.: 'Thermal modeling of power transformers using evolving fuzzy systems', *Eng. Appl. Artif. Intell.,* 2012, 25, (5), pp. 980–988

[53] L. H. Kocewiak, S. K. Chaudhary, Bo Hesselbæk, "Harmonic Mitigation methods in Large Offshore WPPs," *12th Wind Integration Workshop*, 2013, pp 443–448

[54] 'IEEE std C57.110 Recommended Practice for Establishing Liquid-Filled and Dry-Type Power and Distribution Transformer Capability When Supplying Nonsinusoidal Load Currents', Mar 2008

[55] Al-Amin H., O'Brien J., Lashbrook M.: 'Synthetic ester transformer fluid: a total solution to windpark transformer technology', Renew. Energy, 2013, 49, pp. 33–38

[56] Olsen, R. S., Holbøll, J., & Guðmundsdottir, U. S. (2013). 'Dynamic Loadability of Cable Based Transmission Grids. Technical University of Denmark, Department of Electrical Engineering'

[57] G. Anders, A. Napieralski, 'Advanced modeling techniques for dynamic feeder rating systems," *IEEE Transactions on Industry Applicaitons*, vol. 39, no. 3, pp. 619-626, 2003.

[58] R. J. Millar, 'A comprehensive approach to real time power cable temperature prediction and rating in thermally unstable environments' PhD Dissertation, Helsinki University of Technology, Finland, 2006

[59] X. Qi and S. Boggs, 'Thermal and mechanical properties of epr and xlpe cable compounds,' *IEEE Electrical Insulation Magazine*, vol. 22, no. 3, pp. 24, May/June 2006.

[60] R. Eichhorn, 'A critical comparison of xlpe epr for use as electrical insulation on underground power cables,' *IEEE Transactions on Electrical Insulation*, vol. EI-16, no. 6, pp. 469-482, Dec 1981.

[61] C. Green, A. Vaughan, G. Stevens, 'On the temperature dependence of electrical and mechanical properties of recyclable cable insulation materials based upon polyethylene blends,' *Conference on Electrical Insulation and Dielectric Phenomena,* 2011, pp. 36-39

[62] M. Nedjar, 'Thermal aging on the electrical properties of crosslinked polyethylene," *Journal of Applied Polymer Science*, vol.111, pp. 1985-1990, Oct 2009.

[63] IEC 60853-2. calculation of the cyclic and emergency current rating of cables - greater than 18/30 (36) kv' - IEC, Tech. Rep., 1989.

[64] IEC 60853-2:2017 - Calculation of the cyclic and emergency current rating of cables. Part 2: greater than 18/30 (36) kV

[65] B.J. Grotenhuis, J.E. Jaspers, 'Increasing the capacity of cable systems using cable asset management based on thermal and mechanical properties' *16th International Conference and Exhibition on Electricity Distribution*, 2001

[66] ABB,Network manager scada dms,ABB, Sweden,Tech. Rep., 0215,

[67] Cymcap, December 2017.

[68] Siemens Energy, November 2018

[69] Areva T&D, 'e-terraplatform - the power to adapt!' 2005.

[70] De Wild, F. Meijer, and E. Geerts, 'Extracting more value from intelligent cable systems', August 2004, *Transmission and Distribution World*, pp. 22-27

[71] G. J. Anders, H. Brakelmann, 'Improvement in cable rating calculations by consideration of dependence of losses on temp," *IEEE Transactions on Power Delivery*, vol. 19, pp. 919-925, 2004.

[72] R. Olsen, J. Holboll, and U. Gudmundsdottir, 'Dynamic temperature estimation and real-time emergency rating of transmission cables,' in *IEEE Power & Energy Society General Meeting*. IEEE, July 2012.

[73] S.-H. Huang, W.-J. Lee, and M.-T. Kuo, 'An online dynamic cable rating system for an industrial power plant in the restructured electric market,' *IEEE Transactions in Industry Applications*, vol. 43, no. 6, pp. 1449-1458, 2007.

[74] T. Igi, H. Komeda, and S. Mashio, 'Study of the dynamic rating of a 138kv xlpe cable system by optical fiber monitoring," in *8th International Conference on Insulated Power Cables*, 2011

[75] M. Sakata and S. Iwamoto, 'Genetic algorithm based real-time rating for short-time thermal capacity of duct installed power cables,' *International Conference on Intelligent Systems Applications to Power Systems*, ISAP, 1996, pp. 85-90.

[Pub. C2]

S. H. H.Kazmi, T. H. Olesen, T. S. Sørensen and J. Holbøll, **"Dynamic Thermoelectric Modelling of Oil-Filled Transformers for Optimized Integration of Wind Power in Distribution Networks"**, Paper 1744, *25th International Conference on Electricity Distribution (CIRED)*, Madrid, Spain, June 2019.

The published version of the paper is attached.

DYNAMIC THERMOELECTRIC MODELLING OF OIL-FILLED TRANSFORMERS FOR OPTIMIZED INTEGRATION OF WIND POWER IN DISTRIBUTION NETWORKS

Syed Hamza Hasan KAZMI
Ørsted Offshore Wind
Denmark
syeka@orsted.dk

Joachim HOLBØLL
Technical University of Denmark
jh@elektro.dtu.dk

Thomas Herskind OLESEN
Ørsted Offshore Wind
Denmark
thole@orsted.dk

Troels Stybe SØRENSEN
Ørsted Offshore Wind
Denmark
troso@orsted.dk

ABSTRACT

Oil-filled power transformers are some of the most critical components in the distribution network. The grid upgrade cost along with congestion challenges associated with rapid increase in onshore wind energy integration in the distribution system can partly be resolved by dynamic loading of transformers. Distribution transformers can be dynamically rated if the temperatures, especially Top-Oil (TOT) and Hot-Spot (HST) temperatures, are accurately determined. This paper presents industry's well-proven and established differential equations-based thermo-electric models for transformers. The models are validated, and the performances are compared with the measured temperatures for a 6.8 MVA wind turbine transformer. Moreover, the thermal lifetime utilization of the test transformer is calculated based on its loading and ambient conditions history for the year 2017, using the recommendations of international loading guides. The annual thermal variations and lifetime utilization of test distribution transformer are assessed for an increase in wind energy production in 2017. Based on this analysis, further wind energy integration is facilitated by deferring grid expansion costs related to transformers

I. INTRODUCTION

Wind energy is a major contributor to the annual electricity generation in Denmark and it is projected to increase even further by 2030 [1]. Windfarms on land have traditionally been connected to the power system through the distribution grids. The integration of wind energy in the distribution network is hindered by a number of challenges. Some of these challenges associated with grid congestion due to integration of this additional load in the existing grid can be resolved by dynamically rated operation of the components that are the usual bottlenecks in the system. Moreover, dynamic rating of these components can also improve the energy contribution during high-wind periods.

Oil-filled transformers are not only used widely across the distribution networks, but also large wind turbines have dedicated transformers in the nacelle or in the tower base. The extensive presence of this component in the network, the absence of winding temperature monitoring systems and the capital investment related to transformers make it relevant to consider dynamic rating of transformers in the distribution network [2]. In order to load the transformers beyond the nameplate rating without violating their transient and steady-state thermal limits, comprehensive information of the temperatures critical for their operation is required. The high cost of the temperature monitoring equipment though makes it necessary to estimate/calculate these temperatures for distribution transformers. This paper focuses on the thermoelectric modeling and estimation of Top-Oil (TOT) and Hot-Spot (HST) temperatures of oil-immersed distribution transformers.

The transformer loading guides IEEE C57.91 [3] and IEC 60076-7 [4] present thermal models based on differential or exponential based functions. These models are relatively simpler to formulate as compared to *more-accurate*, *non-linear*, *differential-equations-based* thermoelectric models of [5] [6] [7] [8], which provides the basis for their popularity, also in the distribution network applications [2] [9]. This publication provides the state-of-the-art for these models and compares the physics and structure behind the formulation of differential-based models of [3] [6] [7]. Moreover, the grave dependence of these models on transformer parameters obtained through heat-run tests is also discussed. The TOT calculated through these differential-based models are then validated with the measured TOT for a 6.8 MVA Wind Turbine Generator (WTG) transformer based on its actual load and ambient condition history for 2017. The validation results are then presented for two different week-long periods with considerably different ambient and load conditions in winter and summer. The calculation of HST is then performed using the more accurate model.

International loading guides [3] [4] discuss the impacts of varying HST on transformer paper insulation aging, critical for defining transformer lifetime. These guides also give out recommended thermal limits for TOT and HST for dynamic loading of distribution transformers. The present paper makes use of this analysis to assess the lifetime utilization of the test WTG transformer based on its loading history in 2017. Its annual utilization pattern is found to be noticeably similar to windfarm transformers or distribution transformers close to windfarms. Hence, the impacts of further wind energy integration on thermal aging of distribution transformers is tested by increasing the annual wind power injected in 2017 by 0 to 80% allowing identification of optimal transformer utilization.

The remaining paper is structured as follows. The relevant thermoelectric models are presented in Section II. Section III discusses the phenomena of thermal aging. Section IV provides the details for test transformer and presents the case study, while the results are discussed in Section V. Section VI concludes the paper.

II. THERMOELECTRIC MODELLING OF OIL-FILLED TRANSFORMERS

Oil-filled transformers can in principle be dynamically loaded if the Hot Spot Temperature (HST), which is critical for transformer operation, is accurately determined [10]. Since the physically available temperature in most cases is the Top Oil Temperature (TOT), both temperatures will be included in the model. Unfortunately, the complex heat transfer phenomenon for oil-filled transformers as compared to other power system components, which makes a correct temperature estimation challenging.

A number of thermal models based on differential equations have been proposed throughout the years to simulate the dynamic thermal response of transformers under varying load, ambient and operating conditions. The models discussed in this section are popular in the industry because the variations in TOT and HST are effectively and accurately determined, while the design process is not as arduous [11]. Computational Fluid Dynamics (CFD) based models are reportedly more accurate for HST and TOT estimation but the complexity of design, requirement of detailed transformer construction information and computational extravagance make these impractical for wide-scale application in the distribution network because from a utility point of view, many of these details might not be available [12].

The well-established thermoelectric models presented in loading guides ANSI/IEEE C57.91 [3] and IEC 60076-7 [4] are accepted throughout the industry. IEC 60076-7 [4] provides 2 alternate models for thermal estimation: exponential-equations-based which are suitable for step load change and differential-equations-based which can be applied to any arbitrary load and ambient temperature variations. The parameters that significantly influence the accuracy of these models are transformer specific and can only be determined using prolonged heat-run tests which makes them unfeasible for distribution system application [9]. Despite this fact, the estimation of model constants for dynamic rating of transformers in distribution networks using [4] have been actively explored [2] [9] [13].

This paper focusses on the following two models for dynamic thermal modeling of distribution transformers: IEEE Claus 7 [3] and Susa [6] [7].

IEEE Clause 7 Model (C57.91) [3]

The differential equations determining the development of transformer TOT and HST are provided in (1) and (2).

$$\tau_0 \frac{d\vartheta_{tot}}{dt} = \Delta\vartheta_{or}\left(\frac{K(t)^2 R + 1}{R + 1}\right)^n - [\vartheta_{tot}(t) - \vartheta_{amb}(t)] \quad (1)$$

$$\tau_h \frac{d\vartheta_{hst}}{dt} = \Delta\vartheta_{hr} K(t)^{2m} - [\vartheta_{hst}(t) - \vartheta_{tot}(t)] \quad (2)$$

$$\tau_0 = C_{th}\left(\frac{\Delta\vartheta_{or}}{P_T}\right) \quad (3)$$

where ϑ_{amb} is the ambient temperature (°C); K is the transformer load current in p.u. with rated load current as base; ϑ_{tot} and ϑ_{hst} are the calculated Top Oil and Hot Spot Temperatures respectively, expressed in °C; R is the ratio of load losses to no-load losses at rated load; $\Delta\vartheta_{or}$ is the TOT rise over ambient temperature ϑ_{amb} at rated load (°C), while $\Delta\vartheta_{hr}$ is the rated HST rise over TOT for rated load of 1 pu. The thermal time constants (hour) for oil τ_0 and winding τ_h are usually obtained using the heat run test, but τ_0 can also be accurately determined using (3). Where, P_T is total losses at rated load (MW); C_{th} is thermal capacity of the oil (MWh/K) which can be approximated using methods suggested in [3] and [8] that require detail information regarding the mass and material of different transformer components (winding, oil, core etc.).

The empirically derived exponents *n* and *m* vary with transformer cooling mode (ONAN, OFAF etc.). The non-linear dependence of heat flow on temperature difference varies the convective cooling process and is therefore dependent on the cooling mode which also influences the thermal resistance and oil viscosity [5]. The empirical values of these exponents for different cooling modes, as suggested in [3] are given in Table I.

Susa *et al.* Model [6] [7] [8]

This model builds upon the fundamental thermoelectric model concepts for transformers proposed by Swift *et al.* in [5] and introduces the impact of temporal variation of oil viscosity and load losses with respect to temperature. The TOT and HST evolution with respect to load and ambient conditions are governed by the following first-order, non-linear, multivariable, differential equations:

$$\tau_0 \frac{d\vartheta_{tot}}{dt} = \Delta\vartheta_{or}\left(\frac{K(t)^2 R + 1}{R + 1}\right) - \left(\frac{\vartheta_{tot}(t) - \vartheta_{amb}(t)}{[\mu_{pu}(t)\,\Delta\vartheta_{hr}]^{1-n'}}\right)^{1/n'} \quad (4)$$

$$\tau_h \frac{d\vartheta_{hst}}{dt} = \Delta\vartheta_{hr} K(t)^2 P_{pu}(\vartheta_{hst}) - \left(\frac{\vartheta_{hst}(t) - \vartheta_{tot}(t)}{[\mu_{pu}(t)\,\Delta\vartheta_{hr}]^{1-m'}}\right)^{1/m'} \quad (5)$$

Where all the symbols similar to IEEE C57.91 model represent the same quantities. The oil viscosity μ_{pu} in pu is time variant and temperature dependent as it is the ratio between actual oil viscosity μ_o at time *t* and oil viscosity at rated TOT rise μ_{or}, as mentioned in (6). The dependence of load losses on temperature is introduced by the term $P_{pu}(\vartheta_{hst})$, calculated using (7), which takes into account the temperature dependence of both the copper $P_{cu,pu}$ and eddy losses $P_{e,pu}$ expressed in pu with P_T as base. Finally, the empirical constants *n'* and *m'*, representing the oil circulation mechanism inside the tank and heat dissipation through free or forced convection, are similarly obtained as for the IEEE model and tabulated in Table I.

TABLE I - EMPIRICAL CONSTANTS FOR IEEE [3] AND SUSA [6] MODELS

Transformer Cooling Mode	IEEE C57.91		Susa et al. *	
	n	*m*	*n'*	*m'*
Oil Natural Air Natural (ONAN)	0.8	0.8	0.8	0.67
Oil Natural Air Forced (ONAF)	0.9	0.8	0.83	0.67
Oil Forced Air Forced (OFAF)	0.9	0.8	0.83	0.67
Oil Directed Air Forced (ODAF)	1.0	1.0	0.83	0.67

** values for onload condition (circulating oil) with external cooling are provided*

$$\mu_{pu}(t) = \frac{\mu_o(t)}{\mu_{or}} = e^{\left(\frac{2797.3}{\vartheta_{tot}(t)+273} - \frac{2797.3}{\vartheta_{amb}(t)+\Delta\vartheta_{or}+273}\right)} \quad (6)$$

$$P_{pu}(\vartheta_{hst}) = P_{cu,pu}\left(\frac{235 + \vartheta_{hst}(t)}{235 + \Delta\vartheta_{hr}}\right) + P_{e,pu}\left(\frac{235 + \Delta\vartheta_{hr}}{235 + \vartheta_{hst}(t)}\right) \quad (7)$$

Comparison of models

Both the thermal estimation models seem to follow a similar pattern (Change in Temperature = Heat In – Heat Out). Heat-in is driven by the time variant load (resulting in losses) while heat-out is driven by the relevant temperature difference. The introduction of temperature dependent oil viscosity in the Susa *et al.* model effectively addresses the temperature-variant convective cooling property of the oil, which is complemented by the presence of temperature dependent load losses. But the distinct difference between the two models is the position of empirical exponents. In the IEEE model, these exponents are located at the heat-in section of the equation, while Susa *et al.* model puts these on the heat-out expression which is thermodynamically more accurate. It is observed that both the models obtain similar forms if the constants are set to 1 but differ significant otherwise. The dependence of each of these models on parameters obtained through the heat-run test is considerable, which can result in poor performance if the appropriate protocols are not followed during the temperature-rise test.

III. THERMAL AGING & LIMITS FOR OIL-FILLED TRANSFORMERS

One of the key components defining the thermal lifetime of an oil-filled transformer is the lifetime of its paper insulation. The location of HST, typically at or close to the top winding paper insulation, is known to have maximum thermal stress. Therefore, a transformer's lifetime can be determined by tracking the HST which is crucial for its dynamic loading [10]. The loading guides ANSI/IEEE C57.91 [3] and IEC 60076-7 [4] utilize the Arrhenius reaction rate theory to determine thermal aging of the insulation. The aging acceleration factor F_{AA} determining the relative aging rate of the transformer insulation is given by (8), while (9) determines the transformer loss of life LOL.

$$F_{AA}(t) = e^{\left(\frac{15000}{\vartheta_{h,ar}+273} - \frac{15000}{\vartheta_{hst}(t)+273}\right)} \quad (8)$$

$$LOL(t) = \int_{t_0}^{t} F_{AA}(\tau)\, d\tau \quad (9)$$

The aging acceleration factor F_{AA} is unit-less and it not only depends upon the actual hot spot temperature (ϑ_{hst}) in °C but also on $\vartheta_{h,ar}$ which is HST for designed lifetime of the insulation. The value of $\vartheta_{h,ar}$ is 110 °C for thermally upgraded paper insulation and 98 °C for non-upgraded paper. LOL is the cumulative loss-of-life for the period between t_0 and t, whose unit depends on the period τ. LOL is expressed as days in this paper. It must be mentioned that the loss-of-life represents the aging of paper insulation only, which is the predominant aging phenomenon for transformers that have been in the field for < 20 years [14]. Other phenomena including residual moisture content in oil/paper, degradation products etc. and the respective aging impacts are not addressed in this paper.

The thermal limits for distribution transformers specified in [3] [4] for different dynamic loading periods are summarized in Table II. The acceleration in chemical reactions and formation of gas bubbles beyond HST of 140 °C can jeopardize the transformer dielectric strength [4]. Transformer manufacturers, however, recommend maximum continuous HST of 110 °C for thermally upgraded paper. Nevertheless, even this limit is hardly ever reached because of protection designs, favorable ambient conditions and conservative operation philosophies.

TABLE II - THERMAL LIMITS FOR DISTRIBUTION TRANSFORMERS [3] [4]

	Normal Cyclic Loading	**Emergency Loading** (long-term)	**Emergency Loading** (<30 min)
HST	120 °C	140 °C	140 °C
TOT	105 °C	115 °C	110 °C

IV. TRANSFORMER UTILIZATION & WIND ENERGY INTEGRATION - CASE STUDY

The performance of the IEEE C57.91 and Susa *et al.* thermoelectric models is evaluated by comparing the TOT calculated using these models with the measured TOT for 2 different weeks in 2017 with considerably different ambient conditions for a transformer unit with external cooling. The 6.8 MVA, 34 kV / 0.69 kV, Dyn11, OFAF cooled test transformer is a wind turbine transformer used to connect the Wind Turbine Generator (WTG) to the array cable system. The MVA and voltage ratings of the test transformer in supplement with the connection types and cooling methods allow the study to be suitable for distribution system transformers. HST is not used as a parameter for performance evaluation because of unavailability of HST measurements for test transformer.

Wind energy generation has 2 distinguished features: intermittent-pattern and low-dispatch-cost. Therefore, actual loading and temperature patterns along with

ambient condition history of the 6.8 MVA WTG transformer for the year 2017 with 10-minute sampling rate are used and the utilization of transformer over the year is evaluated. Windfarm transformers or distribution transformers close to windfarms would undoubtedly have a comparable loading pattern. The test case evaluates the impacts of increasing wind energy integration in the distribution network on transformer's health without changing its size, by assessing the paper insulation's loss-of-life in 1 year. These impacts are emulated by upscaling the actual wind energy production in 2017 over the range of 0 to 80%. Two critical parameters are used to assess these impacts on transformers: transformer lifetime utilization (LOL) at the end of the year and the probability of violating the Cyclic and Emergency loading limits of Table II for Hot Spot Temperature. The later parameter is evaluated using the term *'prob(HST_{max})'*, which calculates the probability of 2 possibilities: how frequently the HST limit of 140 °C is crossed and for how long the cyclic and emergency limits are continuously sustained. The resulting value ranges between 0 and 1, where 0 suggests that the considered limits are never violated throughout the year and 1 represents the contrary extreme condition.

V. RESULTS & DISCUSSION

Validation of Thermoelectric Models and Performance Evaluation

The validation of IEEE Clause 7 (1) and Susa *et al.* (4) TOT thermoelectric models is performed for the test transformer for weeks 04 and 30 in 2017. The results including transformer load, TOT, HST and ambient temperature are plotted in Figures 1 and 2. It is perceivable that the temporal evolution of measured TOT is much closer to the TOT calculated using Susa *et al.* model as compared to the IEEE model. Also, the TOT calculated using Susa model is almost always slightly higher than the measured one, thereby resulting in a conservative estimation which would prevent transformer damage during dynamic loading. The Susa model also results in conservative estimations for HST as compared to IEEE, which is crucial for safe dynamic loading operation. The performances of the TOT models are compared by calculating the respective accumulated error (%) for the entire year with respect to the measured TOT. As anticipated, the accumulated error of Susa *et al.* model for TOT is 30.76% less than that of the IEEE model, which is also expected for the HST model. Consequently, the Susa *et al.* model is used for rest of the analysis related to HST in this paper.

Thermal Utilization of WTG Transformer in 2017

The load and temperature distribution of the test transformer for 2017 has been provided in Figure 3, along with lifetime utilization of the transformer calculated using (9). The WTG transformer is found to be slightly over-dimensioned which is also usually the case for distribution transformers. Despite this, the transformer is often moderately loaded because of the intermittent nature of wind energy. Consequently, the TOT and HST distributions are also on the lower-side most of the time. As a result, the utilization of thermal lifetime for the test transformer is also well below its designed lifetime and thermally, the transformer loss-of-life is total of 13 days out of the 365-day period in 2017.

Increase in wind energy integration

The discussion so far has substantiated two attributes. Firstly, the test transformer exhibits similar utilization patterns as corresponding windfarm transformers or distribution transformers close to windfarms. Secondly, the traditional dimensioning criteria for wind energy transmission transformers results in significant under-utilization. Therefore, the impact of further wind energy integration on the utilization of the same transformer in 2017 is evaluated.

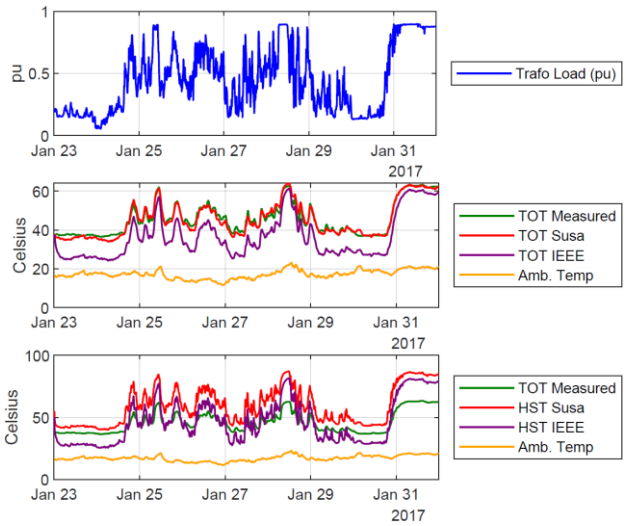

Figure 1 - Validation results for week 04 (Winter) - 2017

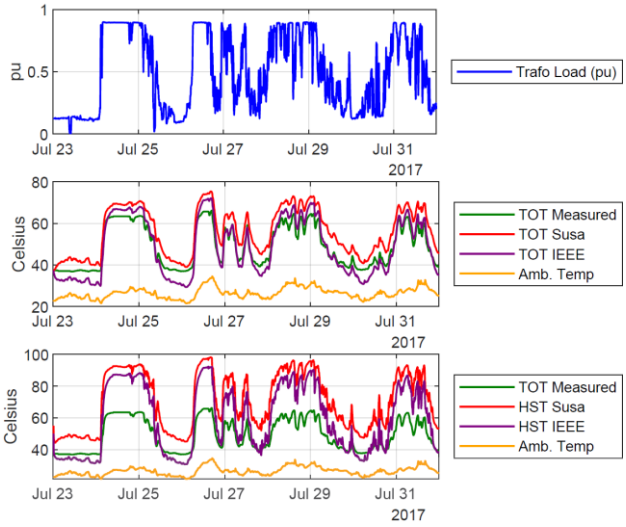

Figure 2 - Validation results for week 30 (Summer) - 2017

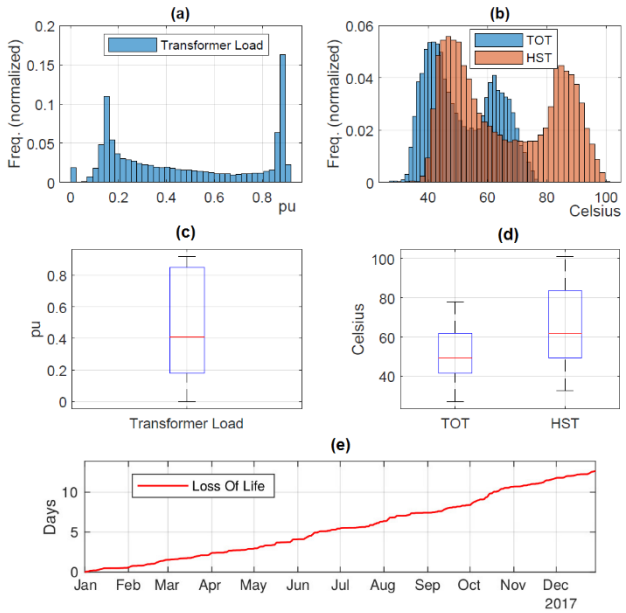

Figure 3 - Transformer utilization in 2017. (a, c) histogram and boxplot for load; (b, d) histogram and boxplot for Temperatures; (e) Calculated loss-of-life for test transformer insulation in 2017

Referring to Figure 4(a), annual lifetime utilization increases substantially beyond the designed lifetime of 1 pu for the test transformer, as the annual wind energy generation for the test WTG is increased by more than 50% in 2017, which is also verified for selected test cases in Figure 4(b). The HST starts violating the limits defined in Table II for annual wind generation increase of more than 45%, for which the expression *'1 - prob(HST_{max})'* reduces to a value less than 1. Hence, the thermal lifetime of the test transformer's paper insulation, under the given constraints, would have been optimally utilized in 2017, if the annual wind generation capacity of the test WTG had been scaled to 1.45 pu. Based on this analysis, further wind energy integration is facilitated by deferring grid expansion costs related to transformers.

VI. CONCLUSION

This paper presents the methods and results from dynamic thermal performance estimations. The industry's well-proven and established differential-equations-based thermoelectric models are presented and the physics behind the model formulation is compared. The validation process with the measured temperatures for a 6.8 MVA wind turbine transformer for the tested models proves the superiority of the Susa *et al.* model. The thermal lifetime utilization of the test transformer is calculated based on its loading and ambient conditions history for the year 2017, using the recommendations of IEC and IEEE loading guides. The annual thermal development and lifetime utilization of transformer suggests that the transformer can be optimally utilized by upscaling the wind energy production to 1.45 pu. Hence, grid expansion costs related to transformers can be deferred for further wind energy integration in the distribution network.

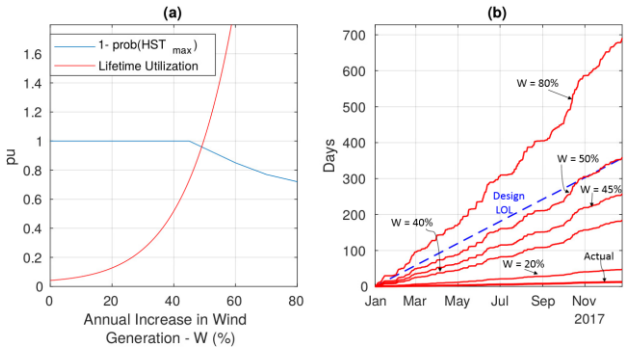

Figure 4 – Impacts of increase in wind energy integration on test transformer. (a) annual utilization in pu. (b) LOL for selected test cases. 'W' represents the upscaling of wind generation (%)

VII. ACKNOWLEDGEMENT

Authors would like to thank Peter Nielsen from Ørsted Offshore Wind A/S for his support, along with Innovation Fund Denmark and Ørsted for project sponsorship. The OPTIMUM framework project collaboration between DTU, Energinet.dk and Ørsted oversees this work.

REFERENCES

[1] 'Denmark's Energy and Climate Outlook 2017' *Danish Energy Agency*, March 2017

[2] B. Das, T. Jalal, 2016 'Comparison & Extension of IEC Thermal Models for Dynamic Rating of Distribution Transformers' *Proceedings of POWERCON IEEE Conference on Power Systems*, vol. 09, pp 1101-1108

[3] ANSI/IEEE, 2011, "IEEE guide for loading mineral-oil-immersed transformers and stepvoltage regulators," *IEEE Std. C57.91-2011 (Revision of IEEE Std. C57.91-1995)*, pp. 1–172, Mar 2011.

[4] IEC, 2005, "IEC 60076-7:2005 power transformers - part 7: Loading guide for oil-immersed power transformers" vol. 60076-7

[5] G. Swift, T. S. Molinski, 2001 "A fundamental approach to transformer thermal modeling. Part I: Theory and equivalent circuit," *IEEE Trans. Power Del.*, vol. 16, no. 2, pp. 171–175

[6] D. Susa, M. Lehtonen, and H. Nordman, 2005 "Dynamic thermal modeling of power transformers," *IEEE Trans. Power Del.*, vol. 20, no. 1, pp.197–204, Jan. 2005.

[7] D. Susa, M. Lehtonen, and H. Nordman, 2005, "Dynamic thermal modeling of distribution transformers," *IEEE Trans. Power Del.*, vol. 20, no. 3, pp. 1919–1929, Jul. 2005.

[8] D.Susa, M. Lehtonen, 2006, 'Dynamic Thermal Modeling of Power Transformers: Further Development—Part I' *IEEE trans. on power delivery*, vol. 21, no. 4, October 2006, pp 1971 - 1980

[9] L. Chittock, J. Yang, D. Strickland, 2016, 'Distribution network transformer thermal modelling parameter determination for dynamic rating applications' *Power Electronics, Machines and Drives (PEMD 2016), 8th IET International Conference*, vol. 08

[10] J. Rossenlind, 2013, "Lifetime modeling and management of transformers," *PhD Dissertation at KTH Stockholm.*

[11] M. Djamali, S. Tenbohlen, 2017 'Hundred years of experience in dynamic thermal modelling of power transformers,' *IET Generation. Transmission and Distribution conference*, 2017, Vol. 11 Iss. 11, pp. 2731-2739

[12] Lapworth, J., Picher, P., Channet, J., et al., 2016, 'Transformer thermal modelling'. *Technical report, Cigre Working Group A2.38*

[13] D. Susa, H. Nordman, 2013, 'IEC 60076–7 loading guide thermal model constants estimation' *Int. Trans. Electr. Energ. Syst*. 2013; 946–960

[14] P. Sen, S. Pansuwan, 2001 "Overloading and loss-of-life assessment guidelines of oil-cooled transformers", in: *Rural Electric Power Conference, IEEE, 2001.*

[Pub. C3]

S. H. H.Kazmi, T. H. Olesen, T. S. Sørensen and J. Holbøll, **"Dynamic Thermoelectric Modelling of Oil-filled Power Transformers for Optimization of Offshore Windfarm Export Systems"**, *CIGRE Symposium*, Aalborg, Denmark, June 2019.

The published version of the paper is attached.

Symposium Aalborg, Denmark
4th-7th June 2019

81 YM

Dynamic Thermoelectric Modelling of Oil-filled Power Transformers for Optimization of Offshore Windfarm Export Systems

Syed Hamza Hasan KAZMI *
Ørsted Offshore Wind
Denmark

Joachim HOLBØLL
Technical University of Denmark

Thomas Herskind OLESEN
Ørsted Offshore Wind
Denmark

Troels Stybe SØRENSEN
Ørsted Offshore Wind
Denmark

SUMMARY

Oil-filled power transformers are some of the most critical components of the electrical export system for Offshore Wind Power Plants (OWPPs). During contingency situations, dynamic loading of the export transformers becomes essential for debottlenecking and optimization of OWPPs, which is elaborated using a case study of Anholt offshore windfarm export system power transformers. Power transformers can be dynamically loaded if the temporal development of temperatures is known, especially Top-Oil (TOT) and Hot-Spot (HST) temperatures. Since the fibre-optic sensors for direct HST measurements are unavailable and the associated costs are high, these temperatures must be estimated using thermoelectric models based on differential-equations for real-time dynamic loading operation of transformers.

The renowned and industry-wide accepted thermal model of IEEE loading guide C57.91 is presented in this paper, along with the recently established but well proven model by Susa e*t al.* Both these models are validated using the instantaneous TOT measurements for one of the 140 MVA, 225kV/33 kV transformers in the Danish Anholt windfarm for the entire 2017 period. The model that is found to perform better is then used for HST calculation for the transformer and the thermal aging of its paper insulation is assessed based on its loading and ambient conditions history for 2017.

Furthermore, the thermal utilization and insulation loss-of-life *(LOL)* based on HST variation of the Anholt windfarm transformer is assessed for increased wind energy generation for 1 year. This is done by upscaling the actual instantaneous load of the test transformer for the entire period of 2017. The upscaling factor *'W'* is varied over the range of 1.0 to 1.6 pu with the actual instantaneous wind generation in 2017 at Anholt as base. The results are then used to provide insights into transformer dimensioning for offshore windfarm applications and to assess whether the transformer allows further wind energy integration in the existing export system for the Anholt offshore windfarm.

KEYWORDS

Power Transformers - Thermoelectric Modeling - Offshore Windfarms - Transformer Thermal Utilization - Hot Spot Temperature - Transformer Loss of Life - Thermal Aging.

*** syeka@orsted.dk**

1. INTRODUCTION

Offshore Wind Power Plants (OWPPs) contributed a sizeable portion of the annual wind energy generation in Denmark in 2017 [1], which is projected to increase even further over the next two decades. Similar trend is observed in the energy outlook of global leaders (including UK, USA, Germany etc.). However, the bottlenecks in OWPP export systems and the grid upgrade costs associated with the available solutions for these constraints are potential barriers to this projection [2]. Oil-filled power transformers are core components of the OWPP export systems and can result in system bottlenecks.

Direct Hot-Spot Temperature (HST) measurement of transformer winding using fibre-optic sensors has been investigated continually in recent times, but application of these methods for wide-scale thermal assessment of power transformers will only be possible in the distant future [3]. Therefore, estimation of transformer's extremely important operational parameters Top-Oil (TOT) and Hot-Spot (HST) temperatures under varying load and ambient conditions can either be performed using accurate but complex-to-design Computational Fluid Dynamics and Thermal Hydraulic Network based models [4], or by differential equations-based thermoelectric models [5] [6] [7] [8], which are simpler to design and offer sufficient accuracy. Moreover, these models can adequately perform real-time thermal evaluation, making them suitable for wide-scale dynamic loading applications [9].

In this paper one of the Anholt offshore windfarm export transformers is used as the test case. Instantaneous TOT measurements of the transformer for the entire 2017 are used for validation of the selected thermo-electric models. The actual load and ambient conditions history of the transformer for 2017 is used to assess the lifetime utilization of the paper insulation in this period. The moisture content of the test transformer insulation is found to be insignificant, therefore only the temperature and heat dependent aging of the transformer winding insulation is considered. Wind energy generation in 2017 for Anholt is then increased by an upscaling factor in the range of 1.0 to 1.6 pu to identify optimal transformer utilization and to provide insights into transformer dimensioning for offshore windfarms.

2. DEBOTTLENECKING AND OPTIMIZATION OF OWPP EXPORT SYSTEM USING CASE STUDY OF ANHOLT WINDFARM

Offshore Wind Power Plants (OWPP) are often connected to the onshore grid using long HV cables. Depending on the distance from the shore, the OWPP export system based on HVAC technology can consist of two or more substations. The offshore substation, like the one shown for Anholt windfarm in Fig. 1, is located close to the wind turbines and its primary function is to collect the generated wind energy and step-up the voltage for transmission through HV export cables. Whereas, the onshore substation serves as the interface between the export system and the transmission system grid on land. The need for reactor substations depends on the length of the HVAC export cable. These substations house some or all of the following components: HV transformers, shunt reactors, HV filters, dynamic compensators (incl. STATCOM, FACTS, SVC etc.), HV/MV switchgears, LV systems etc.

Figure 1 Offshore substation at Anholt windfarm [10]

High-voltage export cables are known to be the primary bottlenecks in the OWPP export system. Hence, the underutilized potential of the OWPP export system, identified by simplified layout in Fig. 2, can

often be made use of, by switching to Dynamic Thermal Rating (DTR) for the export cables. However, both in the cases of contingency and no contingency, this approach may result in other components with short thermal time constants becoming the bottlenecks. The thermal time constants in oil-filled transformers are relatively short as compared to export cables, which when combined with the capital investment related to transformer dimensioning in the OWPP export system makes these components ideal candidates for DTR.

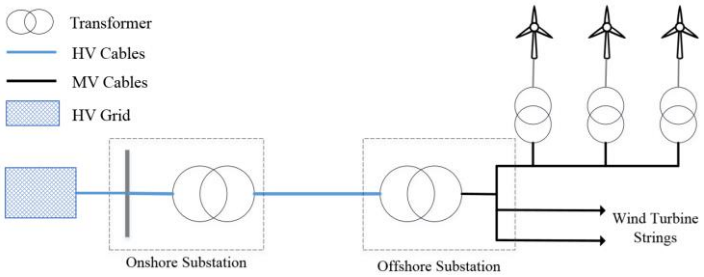

Figure 2. Simplified layout of offshore windfarm's electrical export system

The 400 MW Anholt windfarm in the Kattegat sea, as shown in Fig. 3a, is connected to the transmission system on land with a submarine cable making landfall at the city of Grenå in Jutland (Jylland), Denmark. The 111 wind turbines, each rated 3.6 MW, along with the 33kV array cable system were commissioned by Ørsted, while the export system of the windfarm including the offshore substation was commissioned by the Danish TSO Energinet.dk [10], as shown in Fig. 3b. The 3 export transformers in the offshore substation are rated at 140 MVA each, which brings the total transformer capacity of the export system to 420 MVA. Therefore, during transformer contingency or during planned/unplanned maintenance, dynamic rating of the export transformers seems to be a logical option. For that reason, one of these 140 MVA, 225/33 kV, YNd11, ONAN cooled transformers is used for test cases in this paper.

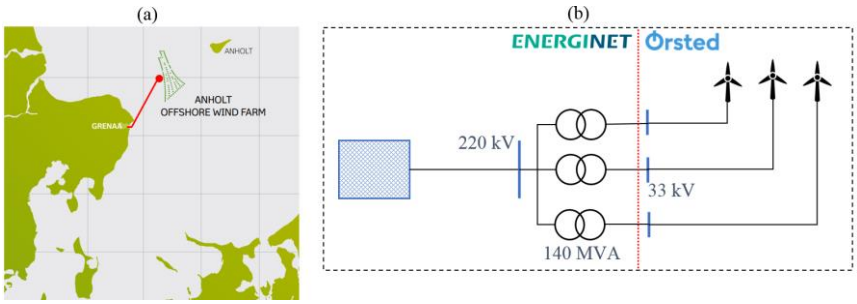

Figure 3 (a) : Location, wind turbine layout and connection for Anholt offshore windfarm [10].
(b) : Export System layout and ownership boundaries for Anholt windfarm

3. THERMOELECTRIC MODELS FOR OIL-FILLED POWER TRANSFORMERS AND VALIDATION FOR ANHOLT WINDFARM TEST CASE

The thermal performance of a power transformer is extremely important to determine because it influences both the operational reliability and the thermal lifetime of the transformer [11] [3]. The Hot-Spot (HST) and Top-Oil (TOT) temperatures can be approximated using differential-equations based thermoelectric models, despite the complex heat transfer phenomena in a transformer [12]. These models are simpler to design as compared to complex Computational Fluid Dynamics and Thermal Hydraulic Network based models [4]. Over the last few decades, a number of thermoelectric models have been proposed to emulate the impacts of varying load and ambient conditions on transformer TOT and HST. These models have been reviewed comprehensively in CIGRE Brochure 659 [13].

The differential-equation based thermoelectric models of international loading guides IEEE C57.91 [5] and IEC 60076-7 [6] are accepted throughout the industry. But these models are found to perform inadequately for low ambient temperature applications during continuously varying load conditions

[14]. In this paper, only the IEEE Clause 7 in C57.91 [5] and Susa *et al*. [7] [8] thermal models are discussed.

3.1 - IEEE Clause 7 Model [5]

According to the IEEE Loading Guide C57.91 (2011), the development of transformer TOT and HST can be determined using the differential equations of (1) and (2).

$$\tau_0 \frac{d\vartheta_{tot}}{dt} = \Delta\vartheta_{or}\left(\frac{K(t)^2 R + 1}{R + 1}\right)^n - [\vartheta_{tot}(t) - \vartheta_{amb}(t)] \quad (1)$$

$$\tau_h \frac{d\vartheta_{hst}}{dt} = \Delta\vartheta_{hr} K(t)^{2m} - [\vartheta_{hst}(t) - \vartheta_{tot}(t)] \quad (2)$$

where ϑ_{tot} and ϑ_{hst} represent the calculated Top Oil and Hot Spot Temperatures respectively, expressed in °C. *K* is the transformer load current in p.u. with rated load current as base; R is the ratio of load losses to no-load losses at rated load; $\Delta\vartheta_{or}$ is the TOT rise over ambient temperature ϑ_{amb} at rated load both expressed in °C, while $\Delta\vartheta_{hr}$ is the rated HST rise over TOT for rated load of 1 pu. The thermal time constants (in hour) for oil τ_0 and winding τ_h are usually obtained using the heat run test, but τ_0 can also be accurately determined using the approach explained in Section 3.3.

The empirically derived exponents *n* and *m* are representative of the transformer cooling mode (ONAN, OFAF etc.). The convective cooling process is varied by the non-linear dependence of heat flow on temperature difference. Therefore, the change in temperature gradients for transformer oil and winding are dependent on the cooling mode which also influences the thermal resistance and oil viscosity [15]. The empirical values of these exponents for different cooling modes, as suggested in [5] are provided in Table I.

3.2 - Susa *et al.* Model [7] [8]

The model proposed by Susa, Lehtonen and Nordman in [7] and further developed in [8] builds upon the fundamental thermoelectric model concepts for transformers proposed by Swift *et al.* in [15] based on the earlier learnings from Nordman [16]. This thermoelectric model introduces the impact of temporal variation of two quantities with respect to temperature: oil viscosity and load losses. The TOT and HST evolution with respect to load and ambient conditions are governed by the following first-order, non-linear, multivariable, differential equations:

$$\tau_0 \frac{d\vartheta_{tot}}{dt} = \Delta\vartheta_{or}\left(\frac{K(t)^2 R + 1}{R + 1}\right) - \left(\frac{\vartheta_{tot}(t) - \vartheta_{amb}(t)}{[\mu_{pu}(t)\,\Delta\vartheta_{hr}]^{1-n\prime}}\right)^{1/n\prime} \quad (3)$$

$$\tau_h \frac{d\vartheta_{hst}}{dt} = \Delta\vartheta_{hr} K(t)^2 P_{pu}(\vartheta_{hst}) - \left(\frac{\vartheta_{hst}(t) - \vartheta_{tot}(t)}{[\mu_{pu}(t)\,\Delta\vartheta_{hr}]^{1-m\prime}}\right)^{1/m\prime} \quad (4)$$

The structure of these equations is similar to the IEEE C57.91 models of (1) and (2). All the common symbols represent the same quantities. The oil viscosity μ_{pu} (pu) is the ratio between actual oil viscosity μ_o at time *t* and oil viscosity at rated TOT rise μ_{or}, as mentioned in (5). This ratio is time variant and temperature dependent, which is a distinctive attribute in the Susa *et al.* model. Similarly, $P_{pu}(\vartheta_{hst})$ presents the dependence of load losses on temperature, which are represented in pu with P_T as base and can be calculated using (6). The dependence of both the copper $P_{cu,pu}$ and eddy losses $P_{e,pu}$ on HST are taken into account in these calculations. The empirical constants in the Susa *et al.* model *n'* and *m'* represent the oil circulation mechanism inside the tank and heat dissipation through free or forced convection, and the respective values are tabulated in Table I.

$$\mu_{pu}(t) = \frac{\mu_o(t)}{\mu_{or}} = e^{\left(\frac{2797.3}{\vartheta_{tot}(t) + 273} - \frac{2797.3}{\vartheta_{amb}(t) + \Delta\vartheta_{or} + 273}\right)} \quad (5)$$

$$P_{pu}(\vartheta_{hst}) = P_{cu,pu}\left(\frac{235 + \vartheta_{hst}(t)}{235 + \Delta\vartheta_{hr}}\right) + P_{e,pu}\left(\frac{235 + \Delta\vartheta_{hr}}{235 + \vartheta_{hst}(t)}\right) \quad (6)$$

TABLE I - EMPIRICAL CONSTANTS FOR IEEE [5] AND SUSA [7] MODELS

Transformer Cooling Mode	IEEE C57.91		Susa et al. *	
	n	***m***	***n'***	***m'***
Oil Natural Air Natural (ONAN)	0.8	0.8	0.8	0.67
Oil Natural Air Forced (ONAF)	0.9	0.8	0.83	0.67
Oil Forced Air Forced (OFAF)	0.9	0.8	0.83	0.67
Oil Directed Air Forced (ODAF)	1.0	1.0	0.83	0.67

** values for onload condition (circulating oil) with external cooling are provided*

3.3 - Thermal Time Constant for Oil - τ_0

The thermal time constant for oil τ_0 can be calculated using (7)

$$\tau_0 = C_{th} \left(\frac{\Delta \vartheta_{or}}{P_T} \right) \tag{7}$$

$$C_{th} = C_{wdg}\, M_{wdg} + C_{fe}\, M_{fe} + C_{mp}\, M_{mp} + O_{oil}\, C_{oil}\, M_{oil} \approx 0.48\, M_{oil} \tag{8}$$

Which suggests that τ_0 (hour) is dependent on the rated TOT rise over ambient temperature - $\Delta \vartheta_{or}$, on total transformer losses at rated load P_T (W) and on the thermal capacity of the oil C_{th} (Wh/ ^{o}C). The thermal capacity of oil can either be approximated using the method suggested in [5], which requires detailed transformer information or by using the simplified empirical formulation of [7] that requires only the mass of the oil. Both these formulations are provided in (8). Where, M_{wdg}, M_{fe}, M_{mp} and M_{oil} represent the weights of windings, iron core, tank (metal parts) and oil respectively in kilograms. The remaining terms are explained and the relevant values are provided in Table II.

TABLE II - CONSTANTS FOR DETERMINING THERMAL TIME CONSTANT FOR OIL [5]

Symbol	***Description***	***Value***	***Unit***
C_{wdg}	*Specific Heat Capacity of Winding (Copper)*	*0.11*	*Wh/kg ^{o}C*
	Specific Heat Capacity of Winding (Aluminum)	*0.25*	*Wh/kg ^{o}C*
C_{fe}	*Specific Heat Capacity of Iron Core*	*0.13*	*Wh/kg ^{o}C*
C_{mp}	*Specific Heat Capacity of Tank and Metal Parts*	*0.13*	*Wh/kg ^{o}C*
C_{oil}	*Specific Heat Capacity of Oil*	*0.51*	*Wh/kg ^{o}C*
O_{oil}	*Correction factor for oil (ONAF, ONAN, OFAF)*	*0.86*	-
	Correction factor for oil (ODAF)	*1.0*	-

** Correction factors are based on the modeling performed in [8] and [16]*

3.4 - Comparison of models

The viscosity of transformer oil varies with temperature. This variation is extreme for temperatures lower than 10 ^{o}C and even though it is rather trivial for oil temperatures in the range of 40 to 100 ^{o}C, its variation is still most dominant in this temperature range when compared with the remaining physical properties of the oil including density, specific heat, thermal conductivity and expansion coefficients etc. [17]. Since the convective cooling capacity is directly dependent on viscosity, Susa rightly takes this into account for both the HST and TOT estimation, which is ignored by the IEEE C57.91 models. Similarly, the temperature dependence of load losses in the Susa *et al.* model increases the degree of accuracy to some extent. The thermoelectric models provided by IEEE in (1) and (2) and by Susa *et al.* in (3) and (4) are based on the following similar structure:

$$Temperature\ Change = f(Heat\ in) \quad - \quad f(Heat\ out)$$

The time varying load drives the Heat-In expression of the equation while the difference in relevant temperatures defines the Heat-Out process. Despite the similarity in structure, the convective cooling process is very different for the two models, which is due to the location of empirical constants. The empirically derived exponents *n* and *m* are placed with the load losses (Heat-In) in the IEEE model, while Susa *et al.* model puts these on the heat-out expression which is thermodynamically more accurate. It is observed that both the models obtain similar forms if the constants are set to 1 but differ significantly otherwise. Both these models depend heavily upon the transformer parameters that are obtained through heat-run tests. Therefore, the performance of both the models would be poor if appropriate protocols are not followed during the temperature-rise test or if any of the required parameters are not known.

Despite the limitations in accuracy of the IEEE Clause 7 model, it is widely used because of its simplified formulation. The model can be linearized easily allowing implementation of optimization algorithms for wide-scale dynamic rating application, a task that would be challenging with Susa *et al.* model.

3.5 – Validation Results for Anholt Export Transformer

The validation of Top Oil Temperature calculated using the IEEE C57.91 model of (1) and (2) and Susa *et al*. model of (3) and (4) is performed with the measured TOT for the 140 MVA export transformer for Anholt windfarm. The calculated TOT is based on the test transformer's recorded load and ambient temperature. Hot Spot temperatures are not used as the parameters for performance evaluation of these models because of unavailability of HST measurements for the test transformers. The validation results including transformer load, TOT, HST and ambient temperature are provided in Fig. 4 for the months of January and July in 2017 to emulate considerably different ambient conditions. It can be seen that the measured TOT is usually extremely close to the TOT calculated using Susa *et al.* model for both the test periods, with the green line often overlapping the red line. This accuracy is even more evident for low ambient temperatures of January as compared to the temperatures predicted by IEEE model, which is because of the correct approximation of oil viscosity variation with ambient temperature in the Susa model. During low load periods, the TOT calculated using Susa model remains slightly higher than the measured TOT. Therefore, transformer damage can be prevented due to conservative estimation during possible dynamic loading operation. The TOT calculated using IEEE model, on the other hand, almost always results in underestimation. The error between calculated and measured TOT accumulated over the entire 2017 is 53.3% higher for the IEEE model as compared to the Susa *et al.* model, therefore the rest of the analysis related to HST in this paper is performed using the Susa *et al.* model.

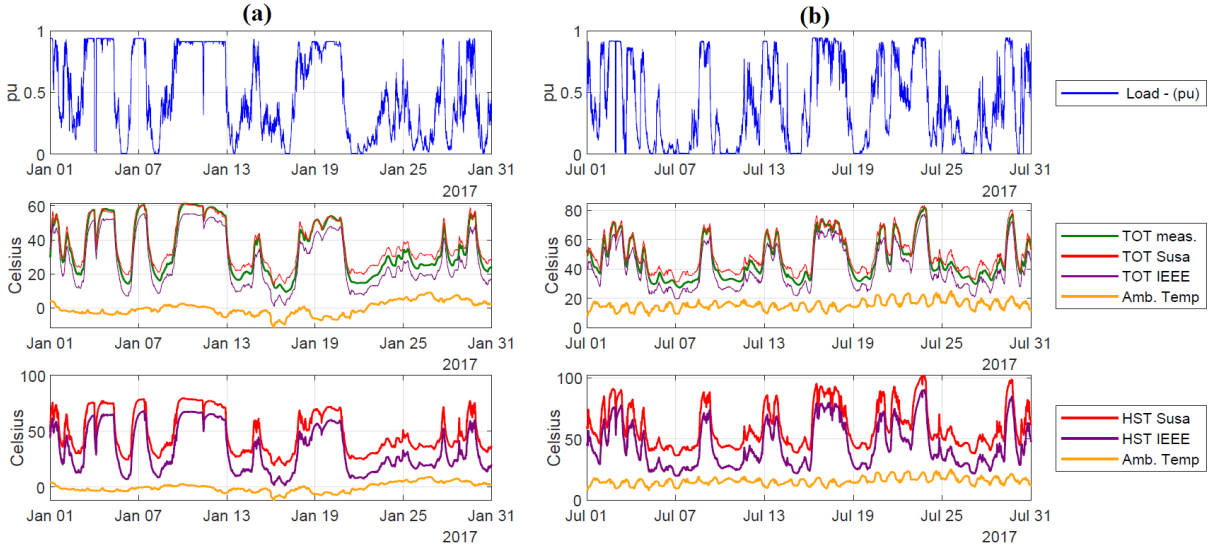

Figure 4. (a): Validation results for January–2017. (b): Validation results for July-2017
Top: Transformer load variation; Middle: Temperatures including Ambient, measured TOT and calculated TOT;
Bottom: Temperatures including Ambient, Calculated HST (IEEE and Susa)

4. THERMAL AGING AND LIMITS FOR ANHOLT EXPORT TRANSFORMERS

Unlike power transformers in the transmission system, windfarm export system transformers are responsible for the transmission of generated wind energy only. Therefore, the intermittent nature of the wind plays a huge role in the utilization of the test transformer. Hence, in order to assess the impact of wind generation patterns on thermal aging of transformer paper insulation in one year, the actual loading and ambient condition history of the 140 MVA windfarm transformers for the year 2017 with 1-minute sampling rate are used.

The degradation mechanism of cellulose, which is the principal component of transformer winding insulation, depends principally on three agents: water, oxygen and heat [5]. But since heat is dependent on transformer loading, while the transformer oil preservation system is responsible for both the insulation water and oxygen content, only the heat-dependent aging of the paper insulation is studied in this paper. This is further complemented by the fact that the studied transformer had been in operation for a relatively small time (<5 years), which is the case for most offshore windfarm transformers with maximum 25 years operation limit. This results in comparatively high insulation tensile strength retention by the end of transformer operation life. Moreover, the oxygen and water content are found to be insignificant for the test transformer.

Dynamic loading of a transformer beyond its rated capacity results in thermal stress which is maximum at the HST location, typically close to the paper insulation at the top winding region. For the reasons explained above, instead of using the Degree of Polymerization (DP), the accelerated aging of paper due to HST thermal stress is directly evaluated to assess the transformer insulation's loss-of-life *(LOL)* using (9) for thermally upgraded paper which is based on Arrhenius reaction rate theory [5] [6].

$$LOL(t) = \int_{t_0}^{t} e^{\left(\frac{15000}{110+273} - \frac{15000}{\vartheta_{hst}(\tau)+273}\right)} d\tau \tag{9}$$

The cumulative loss-of-life (LOL) for the period between t_0 and t represents the aging of paper insulation only, which is the predominant aging phenomenon for transformers that have been in the field for less than 20 years [18]. Other phenomena including residual moisture content in oil/paper, degradation products etc. and the respective aging impacts are not addressed for the test transformer.

The TOT and HST limits specified in international loading guides IEEE C57.91 [5] and IEC 60076-6 [6] for large power transformers are summarized in Table III for different dynamic loading periods. The maximum continuous HST limit of 110 ºC recommended by transformer manufacturers for thermally upgraded paper is hardly ever reached because of protection designs, favorable ambient conditions and conservative operation philosophies. The analysis in this paper limits the HST to 140 ºC, as the dielectric strength of the transformer insulation is at severe risk at temperatures greater than 140 ºC because of acceleration in chemical reactions in oil and formation of gas bubbles [6]. It must be noted that this limit can reduce significantly with increase in the moisture content, but for reasons explained above these impacts are not investigated further in this paper.

TABLE III - THERMAL LIMITS FOR LARGE POWER TRANSFORMERS [5] [6]

	Normal Cyclic Loading	**Emergency Loading** (long-term)	**Emergency Loading** (<30 min)
HST	120 ºC	140 ºC	160/180 ºC
TOT	105 ºC	115 ºC	115/110 ºC

Referring to Fig. 5, the test transformer at Anholt windfarm is found to be statically loaded below its rated capacity throughout 2017 resulting in maximum HST of less than 100 ºC. Consequently, the thermal loss-of-life of the test transformer's paper insulation is approximately 25 days in 2017 which is considerably less than the design *LOL* of 365 days, as shown in Fig. 6.

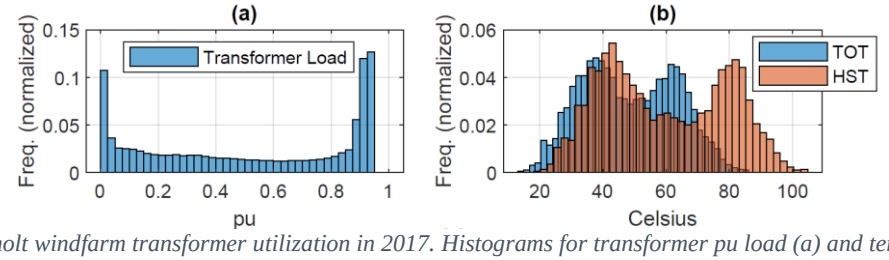

Figure 5 Anholt windfarm transformer utilization in 2017. Histograms for transformer pu load (a) and temperatures (b)

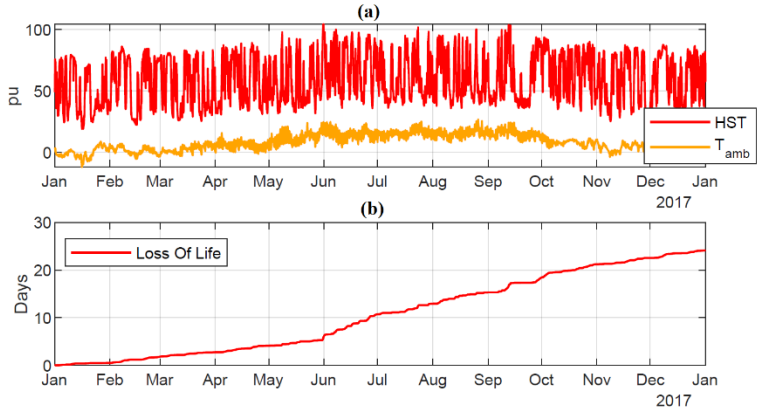

Figure 6. Anholt windfarm transformer utilization in 2017. (a) Ambient Temp. and Calculated HST. (b) Thermal loss-of-life of paper insulation

5. INCREASE IN WIND ENERGY GENERATION FOR OPTIMAL TRANSFORMER UTILIZATION

The discussion so far has established that, thermally, the unutilized potential of windfarm transformers is significant. Therefore, the test case assesses the thermal development of the Anholt windfarm export transformer for increased wind energy generation and evaluates the thermal loss-of-life *(LOL)* for transformer paper insulation in 1 year using the methodology explained in the previous section. The wind energy generation is increased by upscaling the actual instantaneous load of the test transformer for the entire period of 2017. The upscaling factor *'W'* is varied over the range of 1.0 to 1.6 pu with actual instantaneous wind generation in 2017 at Anholt as base. Consequently, two different situations with similar repercussions are emulated. Firstly, in case of long-term transformer contingency (i.e. losing one of the three transformers for a period of 1 year), it is important to assess whether the remaining two transformers can take up the additional 0.5 pu load for short term without resulting in permanent damage to the transformer insulation due to accelerated thermal aging. This is however assessed with the assumptions that the remaining export system components (incl. bus couplers, bus bars, instrument transformers etc.) are dimensioned for n-1 contingency case to bear this additional load and the water and oxygen contamination of the insulation is controlled. Secondly, the assessment of thermal lifetime utilization of the test windfarm transformer for this additional load resembles the situation of offshore windfarm expansion, which can provide insights into transformer dimensioning for OWPP applications.

These impacts are assessed by calculating two critical parameters for the test transformers. The first parameter is the cumulative loss-of-life (LOL) for transformer paper insulation at the end of the year, based on (9). Secondly, the probability of violating the Normal Cyclic and long-term Emergency loading limits of Table III for HST is evaluated by calculating the probability of two possibilities: how frequently the HST limit of 140 ^{o}C is crossed and for how long the limits are continuously sustained (i.e. whether the time limits for cyclic and long-term emergency HST limits are violated). The short-term emergency limits are not considered in this paper because of adverse effects of HST>140 ^{o}C. The calculated probability is represented by the expression *'1 - prob(HST_{max})'*, whose values ranges between 0 and 1, where 1 suggests that the limits are never violated throughout the year and 0 represents the contrary.

The transformer loads and calculated HST for the test transformer are provided in Fig. 7 for different upscaling factors for 3 days in Summer 2017. Referring to Fig. 8(a), it is shown that for the given assumptions, the transformer paper insulation lifetime is optimally utilized without violating the thermal limits of Table III for the upscaling factor *W* of up to 1.52 pu. The thermal aging of paper insulation increases drastically beyond this point because HST starts violating the thermal limits (including bubbling temperature) more frequently and for longer periods resulting in *'1 - prob(HST_{max})'* value of less than 1. This is also visible in Fig. 8(b) where HST never crosses the 140 ^{o}C limit for W = 1.5 pu. The thermal loss-of-life for the test transformer's insulation is extremely close to designed *LOL* of 365 days in 2017 for *W* between 1.5 and 1.52 pu, as shown in Fig. 8(c). Therefore, it is demonstrated that the test transformer could have taken up the additional 0.5 pu load throughout 2017 in case of

contingency of one of the export transformers. Based on this discussion it can be deduced that, thermally, the export transformers for Anholt windfarm can fulfill the *n-1* contingency requirements for long periods and can comfortably allow further wind energy integration in the existing export system.

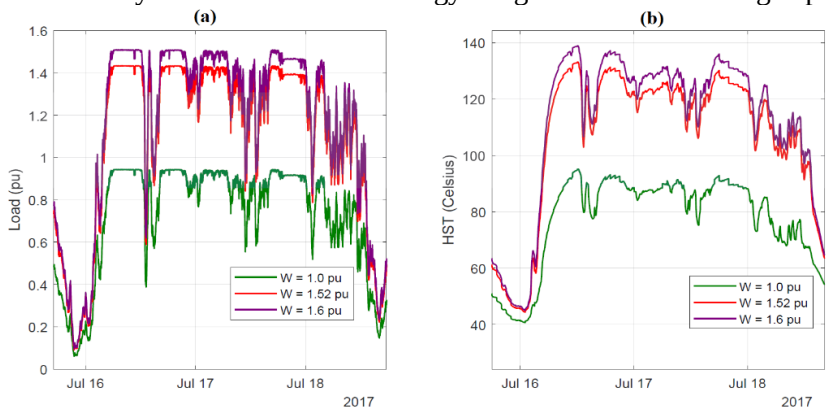

Figure 7. (a) Transformer load (b) Calculated HST for different upscaling factors 'W' for 3 days in Summer 2017

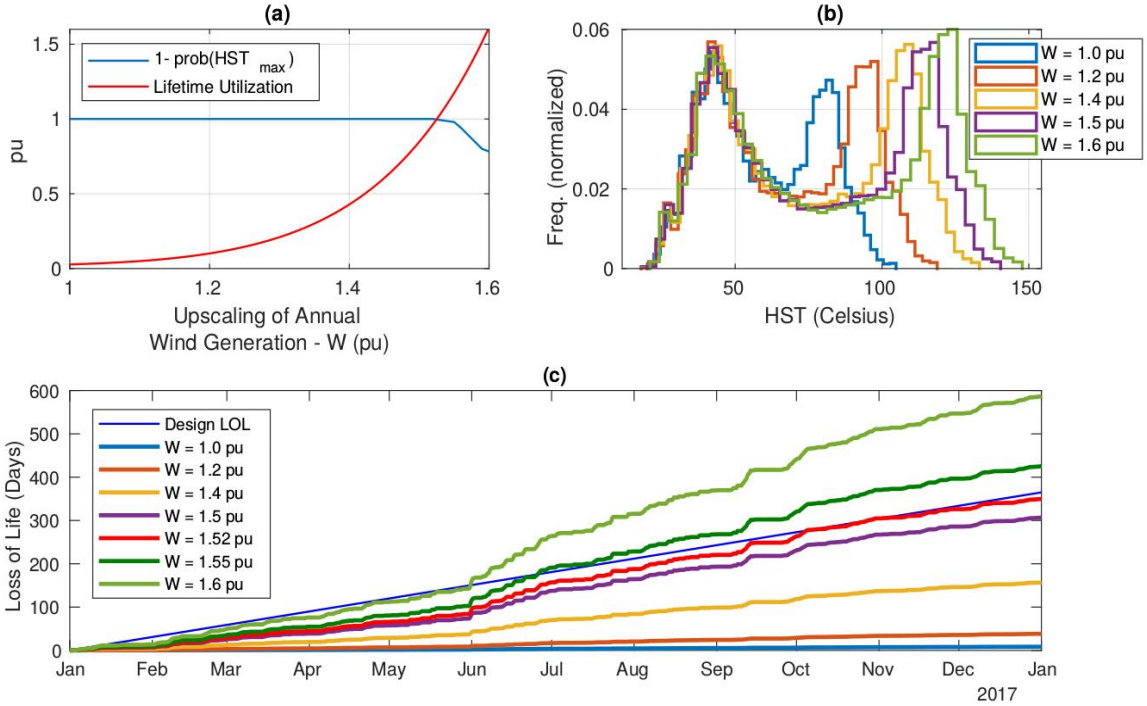

Figure 8. (a): Impact of Wind Generation Increase on Test Transformer. (b): Test Transformer's Year-Round HST Distribution for Increased Wind Generation. (c): Thermal Lifetime Utilization of Test Transformer for Increased Wind Generation. 'W' represents the upscaling factor of wind generation in pu with actual generation in 2017 as base.

6. CONCLUSIONS

The investigation has shown that the intermittent nature of the wind plays a considerable role in thermal utilization of offshore windfarm export transformers, which results in a significant unutilized potential. The thermal utilization is addressed using the loss-of-life of paper insulation due to hot-spot temperature only. This mechanism is known to be the dominant aging phenomena during early-years of transformer operation with functional oil preservation system. The analysis concludes that the intermittent nature of the wind has to be taken into account for transformer design and dimensioning for offshore windfarm applications. It is also shown using the case study of the Danish Anholt offshore windfarm that transformers can potentially be offshore transmission bottlenecks during contingency, but these bottlenecks can be resolved by prolonged dynamic rating operation beyond the transformer's nameplate rating. This characteristic can also facilitate further wind energy integration in the existing export system for offshore windfarms.

7. ACKNOWLEDGEMENTS

Authors would like to thank Sebastian Bille Sørensen and Jacob Kruse from Energinet.dk for the efforts during the case study. The support of Energinet.dk is acknowledged for technical collaborations, along with Innovation Fund Denmark and Ørsted Offshore Wind A/S for project sponsorship. The OPTIMUM framework project collaboration between DTU, Energinet.dk and Ørsted oversees this work.

BIBLIOGRAPHY

[1] 'Denmark's Energy and Climate Outlook 2017' *Danish Energy Agency*, March 2017

[2] W. Winter, K. Elkington 'Pushing the Limits: Europe's New Grid: Innovative Tools to Combat Trans-mission Bottlenecks & Reduced Inertia', *IEEE Power Energy Magazine*, Vol 13, Dec 2014, pp 60-74

[3] T. Gradnik1, A. Polajner, 'The role of direct hot-spot temperature measurements and dynamic thermal models in the determination of power transformers dynamic thermal rating' *CIGRE 2018, Paris, A2-104*

[4] T. Laneryd, A. Gustafsson, B. Samuelsson, Y. Jiao, 'Selecting the right level of complexity for thermal modelling of transformer windings' *CIGRE 2018, 24-29 August, Paris, A2-105*

[5] "IEEE guide for loading mineral-oil-immersed transformers and step voltage regulators - redline," *IEEE Std. C57.91-2011 (Rev. of IEEE C57.91-1995)* - Redline, pp. 1–172, Mar 2011.

[6] IEC, "IEC 60076-7:2005 power transformers - part 7: Loading guide for oil-immersed power transformers," vol. 60076, no. 7, 2005.

[7] D. Susa, M. Lehtonen, and H. Nordman, "Dynamic thermal modeling of power transformers," *IEEE Transactions on Power Delivery*, vol. 20, no. 1, pp.197–204, Jan. 2005.

[8] D.Susa, M. Lehtonen 'Dynamic Thermal Modeling of Power Transformers: Further Development—Part I' *IEEE transactions on power delivery*, vol. 21, no. 4, October 2006, pp 1971 - 1980

[9] N. Viafora, K. Morozovska, S. H. Kazmi and J. Holbøll, "Day-ahead Dispatch Optimization with Dynamic Thermal Rating of Transformers and Overhead Lines," *EPSR Special Issue: Increasing transmission capacity of overhead lines to improve RES integration*, Elsevier, 2018

[10] 'Anholt Offshore Wind Farm - Denmark's largest offshore windfarm' by PensionDenmark, PKA and Ørsted, 2013 (https://stateofgreen.com/files/download/5199)

[11] J. Rossenlind,, "Lifetime modeling and management of transformers," *PhD Dissertation 2013 at KTH*

[12] M. Djamali, S. Tenbohlen, 'Hundred years of experience in the dynamic thermal modelling of power transformers,' *IET Generation Transmission. Distribution.*, 2017, Vol. 11 Iss. 11, pp. 2731-2739

[13] Lapworth, J., Picher, P., Channet, J., et al.: 'Transformer thermal modelling'. *Technical report, Cigre Working Group A2.38*, 2016

[14] F. Bachinger, P. Hamberger, 'Measurement of thermal behavior of an ester-filled power transformer at ultralow temperatures' *CIGRE 2018, 24-29 August, Paris, A2-111*

[15] G. Swift, T. S. Molinski,, "A fundamental approach to transformer thermal modeling. Part I: Theory and equivalent circuit," *IEEE Trans. Power Del.*, vol. 16, no. 2, pp. 171–175, Apr.2001.

[16] H. Nordman, N. Rafsback, D. Susa, "Temperature responses to step changes in the load current of power transformers," *IEEE Trans. Power Del.*, vol. 18, no. 4, pp. 1110–1117, Oct. 2003

[17] L. W. Pierce, "An investigation of the thermal performance of an oil filled transformer winding," *IEEE Trans. Power Del*, vol. 7, no. 3, pp. 1347–1358, Jul. 1992

[18] P. Sen, S. Pansuwan, Overloading and loss-of-life assessment guidelines of oil-cooled transformers, in:*Rural Electric Power Conference*, 2001, IEEE, 2001, pp. 0411-0415

[Pub. C4]

N. Viafora, S. H. H. Kazmi, T. H. Olesen, T. S. Sørensen and J. Holbøll, **"Load Dispatch optimization using Dynamic Rating and Optimal Lifetime Utilization of Transformers,"** *IEEE PES PowerTech*, Milan, Italy, July 2019.

The published version of the paper is attached and also available at https://ieeexplore.ieee.org/document/8811002

Load Dispatch Optimization using Dynamic Rating and Optimal Lifetime Utilization of Transformers

Nicola Viafora* and Joachim Holbøll
Dept. of Electrical Engineering
Technical University of Denmark, DTU
Kgs. Lyngby, Denmark
*nicovia@elektro.dtu.dk

Syed Hamza H. Kazmi †, Thomas H. Olesen and Troels S. Sørensen
Ørsted Offshore Wind A/S,
Gentofte, Denmark
†syeka@orsted.dk

***Abstract*—Power transformers are critical power system components that are generally loaded conservatively, resulting in marginal utilization of their designed lifetime. Dynamic Transformer Rating (DTR) increases the utilization of this asset by limiting its Hot Spot Temperature (HST) rather than the *per unit* load, thereby increasing available network capacity. However, residual lifetime would still be unutilized according to current dimensioning criteria and state-of-the-art lifetime aging models. This paper proposes a novel methodology for DTR, where both thermal and aging dynamics are accounted for in a multi-period DCOPF formulation. Power losses are accounted for by means of an iterative approach that preserves convexity of the optimization problem. The proposed methodology leads to an optimal lifetime utilization of transformers and favours the integration of wind power generation. This novel DTR approach can be beneficial for applications with limited asset lifetime like offshore windfarms or for postponing grid reinforcements for short period of time.**

***Index Terms*—DCOPF, dynamic transformer rating, lifetime model, losses, wind power integration**

I. Introduction

The integration of renewable-based energy sources, with particular regard to wind power generation, can be hindered by limitations in the thermal overload capability of the existing network. Power transformers in transmission and distribution systems are critical components that may constitute a bottleneck as they are conservatively operated. Dynamic Transformer Rating (DTR) can help resolve these bottlenecks by allowing the transformers to be loaded beyond their nameplate rating according to the actual thermal state [1].

Loading guides [2] and [3] allow large power transformers to be dynamically rated up to the Hot Spot Temperature (HST) of 160 °C. However, the traditional operation philosophy and protection design prevent transformers from being operated beyond HST of 110 °C, which is rarely reached because of favorable ambient conditions. Consequently, transformers are distinctly underutilized and the remaining lifetime by the end of designed period (usually 35-40 years) is significant. This can heavily influence the business case for applications like offshore windfarms, which are traditionally designed to operate for 25 years only. Moreover, optimal transformer utilization can help increase the economic turnover and decrease the Cost of Energy (CoE) for such applications.

Unlike offshore windfarms, transmission and distribution utilities may keep old transformers in operation with increased care and condition-based maintenance. In this case, the increased network capacity provided by DTR can help to defer investments for transmission system operators, which are facing a large and rapid growth of renewable energy sources.

This paper builds upon a recent work in [4], where transformer loadability is directly accounted for in a multi-period DC - Optimal Power Flow (DCOPF) algorithm. The novelty of the proposed DTR approach consists in assessing the remaining transformer lifetime using [2] and [3], based on historical load and ambient conditions. Based on this assessment, the solution of the DCOPF considers not only transformer thermal dynamics, but aging rate and cumulative lifetime utilization as well. This loading approach results in a controlled accelerated aging but without breaching the designed lifetime limit. As a result, the transformer is used more effectively compared to common loadability practices as well as other DTR approaches suggested in [5] and [6].

The IEEE RTS 24-bus network with additional wind generation [7] is used as a test system based on actual weather, load and generation data from the Danish system. The presented case study demonstrates the relevance of the method as a means to improve the utilization of low-cost wind energy while accounting for power losses in the transmission system. The proposed methodology could also be incorporated in more detailed cost-benefit analysis and grid expansion planning studies due to its ability to account for transformers' degradation under variable conditions.

The remainder of the paper is organized as follows. The DTR models from [2] are discussed in Section II. Section III elaborates the thermal aging phenomena in transformer and presents the novel DTR approach. The optimization problem for day-ahead dispatch is formulated in Section IV. The case study is presented in Section V, while the results are discussed in Section VI. Section VII concludes the paper.

II. Dynamic Transformer Rating Model

Dynamic loading of transformers can be performed by determining two critical temperatures: Top-Oil Temperature (TOT) and Hot-Spot Temperature (HST). This estimation is performed by using the ANSI/IEEE Clause 7 model [2],

978-1-5386-4722-6/19/$31.00 ©2019 IEEE

because of the well-established popularity in the industry and mathematical suitability as compared to other models [3] [8].

These temperatures are calculated using the non-linear differential equations (1) - (2) which require further simplification to prevent non-convexity of the optimization problem [2].

$$\tau_0 \frac{d\vartheta_{\text{top}}}{dt} + \vartheta_{\text{top}} = \vartheta_{\text{amb}} + \vartheta_{\text{or}} \left(\frac{I_{\text{trf}}^2 R + 1}{R + 1} \right)^{\nu} \tag{1}$$

$$\tau_h \frac{d\vartheta_{\text{hst}}}{dt} + \vartheta_{\text{hst}} = \vartheta_{\text{top}} + \vartheta_{\text{hr}} I_{\text{trf}}^{2\mu} \tag{2}$$

where τ_0 and τ_h are the thermal time constants for oil and winding respectively which are expressed in hours; ϑ_{amb} is the ambient temperature in °C; ϑ_{top} and ϑ_{hst} represent top-oil and hot-spot temperatures respectively in °C; I_{trf} is the transformer load current in p.u. with rated load current as base; R is ratio of load losses to no-load losses at rated load; ϑ_{or} in °C is the top-oil rise over ambient temperature ϑ_{amb} at rated load, while ϑ_{hr} in °C is the rated HST rise over TOT for rated load. The empirically derived exponents ν and μ represent the impact of transformer cooling mode (ONAN, OFAF etc.) on the change in thermal resistance and oil viscosity. The constants have different values for different cooling modes, which are provided in [2].

In order to keep the optimization problem convex, some simplifications are made to the TOT and HST models of (1) and (2). Firstly, the selected transformer is assumed to operate continuously at *Oil-Directed-Air-Forced (ODAF)* mode, allowing both the constants ν and μ to be set to 1, as in the linearized model in [9]. Secondly, hot-spot temperature is modelled in terms of its steady state value, since hourly values are used in the optimization problem. Therefore it is assumed that short term thermal transients would be extinguished within one hour due to the small thermal time constant, as verified by authors of [4]. As opposed to oil time constant τ_0, which is in the range of 60 to 90 minutes, winding time constant τ_h is approximately 7-8 minutes. Resulting top-oil and hot-spot temperature dynamics are modelled by means of linearized IEEE thermal models shown in (3) and (4), respectively.

$$\vartheta_{\text{top}_t} = K_1 I_{\text{trf}_t}^2 + K_2 \vartheta_{\text{amb}_t} + K_3 \vartheta_{\text{top}_{t-1}} + K_4 \tag{3}$$

$$\vartheta_{\text{hst}_t} = \vartheta_{\text{top}_t} + \vartheta_{\text{hr}} I_{\text{trf}_t}^2 \tag{4}$$

Top-oil temperature depends on the squared *per unit* load I_{trf}^2, ambient temperature ϑ_{amb} and value of top-oil temperature reached in the previous time step. This latter term is responsible of coupling top-oil temperature values in time thus reflecting the importance of considering recent loading history for transformers. Lastly, Coefficients K are constants that solely depend on transformer construction.

III. Optimal Lifetime Evaluation of Transformers

A. Thermal Aging of Transformers

The limit for thermal capacity of a transformer is based on the maximum allowable stress on relevant materials. These limits are effectively explored and defined in [2] and [3]. The thermal limits for power transformers greater than 100 MVA rating are provided in Table I for different types of dynamic loading beyond nameplate rating. However, the continuous HST limit for designed transformer lifetime is 110 °C for thermally upgraded paper. This temperature ceiling is scarcely ever reached because of over-dimensioning, protection philosophies and favorable ambient conditions. The thermal stress is known to be maximum at HST location. The heat transfer from HST serves as catalyst for chemical reactions, which accelerates the aging of insulation paper [1]. The Arrhenius reaction rate theory has been adapted in [2] to calculate the transformer loss of life. The relative aging rate for a transformer, also called aging acceleration factor Λ, with thermally upgraded insulation paper is given by (5), while the transformer loss of life is given by (6)

TABLE I
Temperature limits for transformers [2] [3]

	Normal Cyclic Load	**Emergency Load** (long-term)	**Emergency Load** (<30 min)
Hot Spot Temp.	120 °C	140 °C	160 / 180 °C
Top Oil Temp.	105 °C	115 °C	115 / 110 °C

$$\Lambda(t) = e^{\left(\frac{15000}{110+273} - \frac{15000}{\vartheta_{\text{hst}}(t)+273} \right)} \tag{5}$$

$$\lambda(t) = \int_{t_0}^{t} \Lambda(\tau)\, d\tau \tag{6}$$

where Λ is unit-less and represents the aging acceleration factor for reference HST of 110 °C for thermally upgraded insulation paper; $\vartheta_{\text{hst}}(t)$ is the actual hot spot temperature in °C at time *t*; $\lambda(t)$ represents the cumulative loss-of-life for time period from t_0 up to t and in this paper it is expressed in years. Hence the lifetime utilization of transformer is directly dependent on HST. It must be mentioned that the factor Λ represents the thermal aging of paper insulation only and the impacts of residual moisture content in paper and oil along with other aging phenomena on transformer lifetime are not assessed in this paper.

B. Dynamic Rating and Improved Lifetime Utilization

Static Transformer Rating (STR) limits continuous load current to 1 pu for power transformers and cyclic load current to 1.3 pu [2]- [3]. In contrast to this approach, DTR allows the transformer to be loaded based on HST instead of the rated capacity and thereby prevents this temperature from violating the limits of Table I [5] - [6]. The methodology for DTR used in this paper additionally evaluates the consumed lifetime λ of a transformer and it sets the loadability accordingly.

Referring to Fig. 1, it is assumed that until time t_0 the transformer has continuously operated at HST of 98 °C. The relative aging rate Λ is 0.282, which is represented by the slope of black line in the figure. Consequently, the transformer loss-of-life at this point would be $\lambda_A = 0.282\ t_0$. The difference

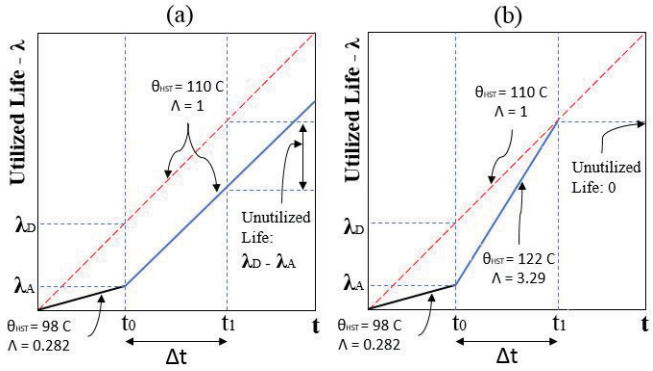

Fig. 1. Methodology for optimal transformer utilization. (a) Fixed HST limit of 110 C. (b) Utilized lifetime (λ) dependent HST limit ($\vartheta_{\text{hst,max}}$ = 140 C)

between designed loss-of-life λ_D for HST of 110 °C and actual λ would continue to increase, if the transformer would keep this loading strategy. DTR can prevent this difference from increasing further by loading the transformer in a way that keeps the HST closer to the design limit of 110 °C, as shown in Fig. 1a. But even with this approach, the residual transformer lifetime by the end of design life would be significant.Therefore, the transformer loading strategy proposed in this paper is meant to maximize component's utilization by considering not only temperature dynamics, but aging rate as well. Fig. 1b illustrates the underlying concept of Enhanced Dynamic Transformer Rating (DTR$^+$).For the period between t_0 and t_1, the limiting factor consists in the designed loss-of-life λ_D, i.e. the red dashed line, rather than the maximum slope associated with HST of 110. As a result, the upper temperature limit is increased to 122°C and the transformer could be loaded even more, thus decresing the unitilized lifetime.

IV. Problem Formulation

In this section the multi-period DCOPF is formulated, where transformer thermal and aging dynamics are directly accounted for along with transmission system losses. The proposed contribution is based on piece-wise linearized transformer aging functions that are incorporated into a DCOPF problem. The same approach could be embedded equally in a ACOPF framework for a more detailed approach.

A. Base DCOPF with quadratic losses

In the considered system the sets of buses, branches, conventional generators and windfarms are indicated with $\mathcal{N}$, $\mathcal{L}$, $\mathcal{G}$ and $\mathcal{W}$, respectively. While the transformers subsets with STR, DTR and DTR$^+$ are identified with $\mathcal{L}_{\text{STR}}$, $\mathcal{L}_{\text{DTR}}$ and $\mathcal{L}_{\text{DTR}^+}$.

This study adopts a DC approximation of the full AC power flow equations. The active power flow on each branch is modelled by means of the Power Transfer Distribution Factor matrix $\boldsymbol{M}$. The matrix $\boldsymbol{M} \in \mathbb{R}^{|\mathcal{L}|\times|\mathcal{N}|}$ expresses the sensitivities of the power flow on each line with respect to the nodal power injections, where the $|\cdot|$ operator indicates the cardinality of the set. The power flow f_ℓ on branch ℓ can then be expressed as $f_\ell = \boldsymbol{M}_\ell \boldsymbol{P}^{\text{inj}}$, where $\boldsymbol{M}_\ell$ is the ℓ-th row of matrix $\boldsymbol{M}$ and $\boldsymbol{P}^{\text{inj}}$ represents a column vector of *per unit* power injection at each bus in the system.

Branch power losses $\boldsymbol{L}$ that are dissipated on transmission lines and transformers are expressed in terms of additional load demand $\boldsymbol{L}^{\text{bus}}$ at each bus. Losses that occur on branch ℓ are equally divided between sending and receiving bus by means of a loss allocation matrix $\boldsymbol{Y} \in \mathbb{R}^{|\mathcal{N}|\times|\mathcal{L}|}$ whose (n,ℓ) component is defined in (7).

$$Y(n,\ell) = \begin{cases} 0.5 & \text{if line } \ell \text{ is connected to bus } n \\ 0 & \text{otherwise} \end{cases} \tag{7}$$

The nodal power injection at bus n can then be written as

$$P_n^{\text{inj}} = P_g + P_w - \left(P_n - P_n^{\text{sh}} + L_n^{\text{bus}}\right) \tag{8}$$

where P_g and P_w represent thermal and wind power generation; P_n and P_n^{sh} represent net load demand and load shedding; L_n^{bus} expresses nodal power losses where $L_n^{\text{bus}} = \boldsymbol{Y}_n \boldsymbol{L}$ and $\boldsymbol{Y}_n$ is the n-th row of the loss allocation matrix.

In order to consider quadratic power losses in the DCOPF while preserving its convexity, an iterative approach has been implemented. This method is inspired by existing algorithms in the literature that account for power losses by means of quadratic inequality constraints [10]. However, as discussed in [11], these approaches may introduce additional fictitious losses in the presence of negative locational marginal prices due to congestions in the transmission system. Therefore, the iterative approach adopted in this study introduces an upper bound for power losses which is lowered accordingly at each iteration, should the losses be overestimated. The main steps are:

1) Set the upper bound for power losses to the value corresponding at the maximum power flow and set a tolerance δ for the convergence.
$$L_{(1)}^{\max} = R\, f^{\max^2} \tag{9}$$
2) Solve DCOPF (12) and obtain resulting power flows $f_{(k)}$ and power losses $L_{(k)}$ for the k-th iteration.
3) Compute the difference between estimated losses and actual losses for the resulting power flows.
$$\Delta L_{(k)} = L_{(k)} - R f_{(k)}^2 \tag{10}$$
If $\Delta L_{(k)} \leq \delta$ a solution is found, otherwise proceed to next step.
4) Update the upper bound for power losses with the losses corresponding to the power flows at step k, plus a small margin ε. Then return to step 2.
$$L_{(k+1)}^{\max} = R f_{(k)}^2 + \varepsilon \tag{11}$$

This iterative approach allows to solve the DCOPF with a quadratic representation of power losses while still preserving the original convexity, which guarantees uniqueness of the solution. This is achieved by gradually reducing the size of the feasible region for branch losses.

The optimization problem in (12) is the base multi-period DCOPF for a generic iteration (k), where losses are accounted

for. The objective is to find the optimal 24-hours day-ahead energy dispatch, which minimizes total generation cost over the period $\mathcal{T}$, where all constraints have to hold $\forall t \in \mathcal{T}$. The base lossy-DCOPF is formulated in a compact form in (12) and it is solved in the matlab-based modeling system CVX [12] using a Mosek academic license.

$$\min_{\Xi} \quad \sum_{t\in\mathcal{T}} \left(\sum_{g\in\mathcal{G}} c_g P_{g,t} + \sum_{w\in\mathcal{W}} c_w P_{w,t} + \sum_{n\in\mathcal{N}} c^{\text{sh}} P^{\text{sh}}_{n,t} \right) \tag{12a}$$

s.t.

$$\sum_{g\in\mathcal{G}} P_{g,t} + \sum_{w\in\mathcal{W}} P_{w,t} - \sum_{n\in\mathcal{N}} (P_{n,t} - P^{\text{sh}}_{n,t} + L^{\text{bus}}_{n,t}) = 0, \tag{12b}$$

$$P^{\min}_g \le P_{g,t} \le P^{\max}_g \qquad \forall g \in \mathcal{G}, \tag{12c}$$

$$-\Delta P^{\max}_g \le P_{g,t} - P_{g,t-1} \le \Delta P^{\max}_g \qquad \forall g \in \mathcal{G}, \tag{12d}$$

$$-f^{\max} \le f_{\ell,t} \le f^{\max} \qquad \forall \ell \in \mathcal{L}, \tag{12e}$$

$$R f^2_{\ell,t} \le L_{\ell,t} \le L^{\max}_{(k)} \qquad \forall \ell \in \mathcal{L}, \tag{12f}$$

$$0 \le P_{w,t} \le P^{\text{av}}_w \qquad \forall w \in \mathcal{W}, \tag{12g}$$

$$0 \le P^{\text{sh}}_{n,t} \le P_n \qquad \forall n \in \mathcal{N} \tag{12h}$$

where $\Xi = [P_{g,t}, P^{\text{sh}}_{n,t}, P_{w,t}, L_{\ell,t}]$ is the set of decision variables that for each time step *t* represent scheduled generator's output $P_{g,t}$, shed load $P^{\text{sh}}_{n,t}$ and dispatched wind power $P_{w,t}$ for every generator, bus and wind farm, respectively. Branch power losses $L_{\ell,t}$ are modelled by means of an auxiliary decision variable in conjunction with quadratic and linear inequality constraints.

The objective function in (12a) consists of three terms: the cost of dispatching conventional generators in the system over period $\mathcal{T}$ considering linear generation cost functions; a small, negligible cost for dispatching wind power in order to improve convergence of the algorithm; the additional cost of preemptive corrective actions such as load shedding. Constraint (12b) enforces system day-ahead power balance for each hour in the considered time period. Constraints (12c) and (12d) impose operational limits on conventional generators in terms of their power outputs and ramping capabilities, whereas branch power flow are limited by constraints (12e). Branch power losses are bounded by constraints (12f). The lower bound consists in their correct quadratic representation, whereas the upper one is necessary to avoid the introduction of fictitious losses. This term is the sole to be iteratively reduced whenever power losses do not lie close enough to the lower boundary in terms of the chosen tolerance δ. Lastly, constraints (12g) and (12h) impose physical limitations on the availability of wind power generation at each bus and the amount of load that can be shed, respectively. Available nodal wind power injections P^{av}_w is modelled as in [4], where time series of wind speed at several locations in the Danish power system are converted to wind power generation time series by means of a multi-turbine wind power curve fitted on historical data. Decision variable P_w in the optimization problem selects the available amount to be dispatched depending on the load demand or the presence of congestions in the grid.

B. Additional constraints for STR

In order to express the loading of the transformer on branch ℓ, the power flow f_ℓ is scaled accordingly with the ratio of base system *per unit* power S^{base} to the nameplate rating of the transformer S^{trf}_ℓ. This scaling factor allows to show the loading I_{trf_ℓ} defined in (13) relatively to the size of the transformer.

$$I_{\text{trf}_{\ell,t}} = f_{\ell,t} \frac{S^{\text{base}}}{S^{\text{trf}}_\ell} \tag{13}$$

The subset $\mathcal{L}_{\text{STR}}$ of transformers that are statically rated can then be represented in the base DCOPF (12) by introducing additional constraints (14) that limit the power flow on the corresponding branch ℓ for all considered time periods.

$$-1 \le I_{\text{trf}_{\ell,t}} \le 1, \qquad \forall \ell \in \mathcal{L}_{\text{STR}}, \quad \forall t \in \mathcal{T} \tag{14}$$

C. Additional constraints for DTR

The loading of transformers that are dynamically rated is limited by operating hot-spot and top-oil temperatures rather than *per unit* load. Top-oil and hot-spot temperature variations are bounded by predefined values that ensure transformers are used within their thermal capabilities, according to state-of-the-art loading guidelines. As discussed in [4], ϑ_{top} and ϑ_{hst} are modelled by means of quadratic inequality constraints which keep the resulting optimization problem a convex one. The extensive form of such values is provided in expressions (3) and (4) in Section II.

$$\vartheta_{\text{top}_{\ell,t}} \le \vartheta^{\max}_{\text{top}} \qquad \forall \ell \in \mathcal{L}_{\text{DTR}}, \quad \forall t \in \mathcal{T} \tag{15}$$

$$\vartheta_{\text{hst}_{\ell,t}} \le \vartheta^{\max}_{\text{hst}} \qquad \forall \ell \in \mathcal{L}_{\text{DTR}}, \quad \forall t \in \mathcal{T} \tag{16}$$

Adding (15) and (16) to the base DCOPF formulation in (12) will consider the effect of having transformers dynamically rated during the 24-hours dispatch period.

D. Additional constraints for DTR+

The third loading strategy proposed in this paper takes into account not only temperature dynamics, but also transformer aging rate. This aspect is likely to play a role only in the long term, but it provides indication of how the transformers loading could be affected by cumulative lifetime consumption during continued high temperature operation. In order to do so, the exponential aging acceleration factor Λ defined in Section III is included in the base DCOPF (12) by means of a set of linear inequality constraints that form a convex piece-wise linear approximation. Coefficients m_i and q_i in (17) are the slope and intercept values of the *i*-th tangent line that forms the approximation of Λ.

$$\Delta\lambda_t = \max_i \{m_i \vartheta_{\text{hst}_t} + q_i\} \approx \Lambda_t \tag{17}$$

The expression in (17) relates the transformer hot-spot operating temperature ϑ_{hst_t} to the corresponding incremental lifetime utilization $\Delta\lambda_t$. The cumulative lifetime utilization λ_t is then evaluated in a discrete form in (18)

$$\lambda_t = \lambda_{t-1} + \Delta\lambda_t \tag{18}$$

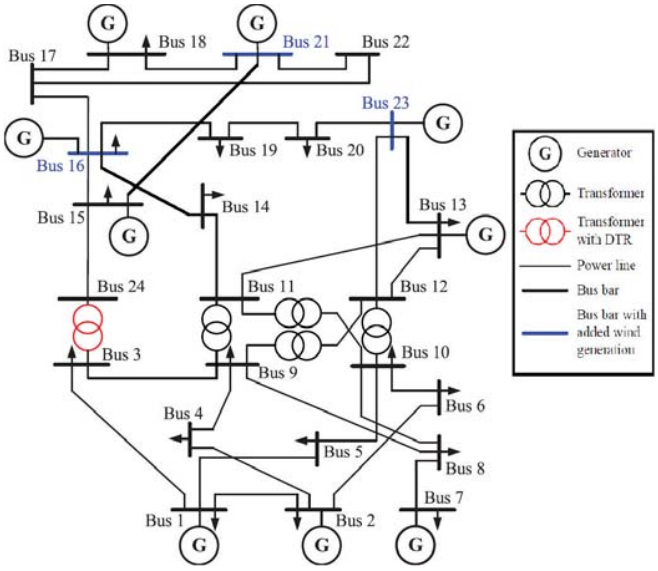

Fig. 2. Modified IEEE RTS 24-bus system [7]

As the transformer is dynamically rated considering lifetime consumption as well, constraints (15) and (16) are added to the base DCOPF (12) together with (19), where λ_0 represents the initial lifetime of the component, α the desired maximum aging rate which in this study has been assumed 1 and t is the time counter during the simulation.

$$\lambda_{\ell,t} \leq \lambda_0 + \alpha t \qquad \forall \ell \in \mathcal{L}_{\text{DTR}^+}, \quad \forall t \in \mathcal{T} \qquad (19)$$

Ultimately, this approach allows to set a higher temperature limit on transformer operation as long as the designed lifetime consumption limit is not reached. Once the upper boundary of lifetime utilization is met, the binding constraint will switch from hot-spot temperature to used cumulative lifetime, thus limiting the operation of the component accordingly.

V. Case Study

The IEEE RTS 24-bus network with additional wind generation from [7] has been adopted in this study with some modifications. Referring to Fig. 2, wind generation is concentrated at Bus 16, 21 and 23, whereas different nameplate ratings are considered for the transformer located between bus 3 and 24, namely 150, 175 and 200 MVA. The data used to model transformer thermal dynamics is provided in [8].

The multi-period DCOPF problem of Section IV is solved in a moving window of 24 hours for the 3-year period between 2014 and 2016. Different test cases compare the system and transformer performance for STR, DTR with $\vartheta_{\text{hst}}^{\max}$ at 110 °C and DTR$^+$ with $\vartheta_{\text{hst}}^{\max}$ at 140 °C combined with optimal lifetime utilization. The assumptions for the DTR$^+$ test case are quite conservative. The transformer is assumed to be in operation for 3 years with DTR resulting in cumulative loss-of-life of 1.5 years, which is cautiously chosen based on operational experience of large transformers.

Historical daily load profiles from the Danish power system have been scaled accordingly with respect to the peak demand in [7]. Total load demand is then increased by 25 percent during the central hours of each day in order to account for future network changes and to enhance the need for DTR in the given system. Lastly, historical time series of ambient temperature from the same system have been used in the thermal rating algorithm for transformers. This allows to take the weather correlation between wind speed and ambient temperature into account. Such a correlation will be reflected between the available wind power generation and the loadability of transformers.

VI. Results and Discussion

The analysis starts from considering the overall impact of the tested loading strategies on the cumulative lifetime utilization of a 175 MVA transformer, shown in the left part of Fig. 3. It stands out as the STR approach practically does not cause any significant aging over the entire 3-years period, in agreement with conservative common loading practices. As opposed to STR, DTR$^+$ pushes the utilization of the component to the designed limit in less than 1 year. Once the maximum aging rate is met, the component will keep using the available designed lifetime at disposal, according to the proposed loading strategy presented in this paper.

The resulting aging profiles can be motivated by considering a three-day period in Fig. 4, where transformer loading and corresponding hot-spot temperatures are shown. As long as the transformer load is limited in terms of its *per unit* nameplate rating, the associated hot-spot temperature remains well below the allowed operational limits due to favourable weather conditions and dimensioning criteria. The resulting low HST profile coupled with the exponential aging acceleration factor shown in the right part of Fig. 3 will yield a close-to-zero aging rate for STR. However, in this condition the transformer branch constitutes a bottleneck in the grid, thus causing increased dispatch costs for the system.

Moving the transformer limiting factor from the *per unit* load to the hot-spot temperature by means of DTR allows to significantly increase the power flow. This would help releasing grid congestions and dispatching more wind power generation from the buses where it is located, at a cost of

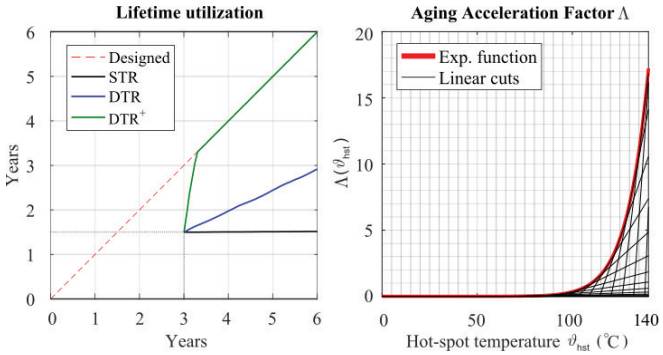

Fig. 3. Cumulative lifetime utilization over the 3-years period for different loading strategies (left). Exponential aging acceleration factor and fitted linear approximations (right).

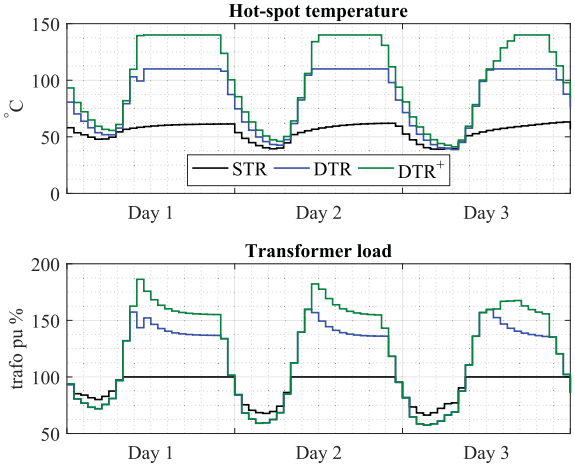

Fig. 4. Transformer hot-spot temperature (above) and transformer load (below). Focus on three days for STR, DTR and DTR+

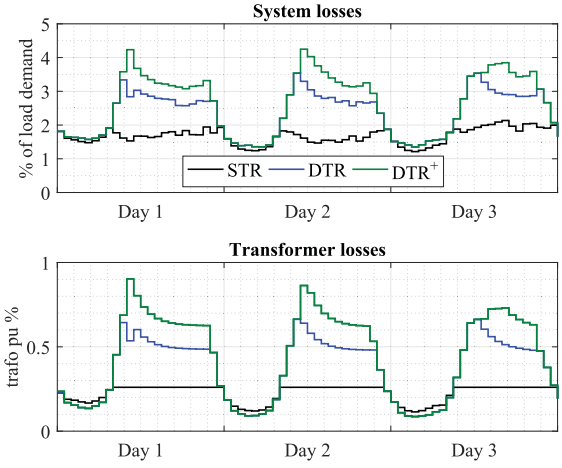

Fig. 5. Total system losses (above) and transformer losses (below). Focus on three days for STR, DTR and DTR+

increasing the lifetime utilization of the component. This mechanism is further enhanced by considering DTR+, which allows the transformer hot spot temperature to be set even higher, as long as the aging rate does not reach the predefined limit, as shown in Fig. 3. Once the maximum aging rate is reached, the constraint on lifetime utilization will prevent the hot-spot temperature to reach the maximum value, thus resulting in a lowered loading capability.

The operation beyond nameplate rating causes additional power losses, not only in the component that is being dynamically rated, but in the remainder of the system as well. This aspect can be seen in Fig. 5, where transformer and system losses are shown for the same 3-days period. Relieving grid congestions by means of DTR or DTR+ will result in increased power flows across the grid, which will in turn cause additional system losses. Despite increasing system losses, the solution of the multi-period DCOPF suggests that there would still be economic benefits from the increased power flow in the grid, as summarized in Table II, where losses are taken into account.

TABLE II
COST REDUCTION AND LIFETIME USE AFTER 1 YEAR COMPARED TO STR

Transformer Size (MVA)	Cost Reduction (%)		Used Lifetime (%)	
	DTR	DTR+	DTR	DTR+
150	-10.1	-11.5	+41.5	+166
175	-8.1	-8.8	+31.1	+166
200	-6.4	-7.1	+24.2	+166

VII. CONCLUSION

This paper proposes a novel approach for optimal transformer lifetime utilization. This approach incorporates both thermal and aging dynamics into a convex optimization problem based on a multi-period DCOPF, while accounting for quadratic power losses in the system. The proposed algorithm maximizes the transformer utilization ensuring that neither thermal nor aging rate limits are violated during operation. The results suggest that the proposed DTR algorithm reduces the cost of load dispatch and yields a substantial increase in network capacity. It is also observed that accounting for the temperature-dependent aging rate can allow a better utilization of the transformer designed lifetime. This aspect is likely to improve the business case for applications with limited asset lifetime like offshore windfarms. It could also be beneficial for TSO which have to face rapid growth of renewable-based generation and postpone the required grid reinforcements.

REFERENCES

[1] J. Rossenlind, "Lifetime modeling and management of transformers," Ph.D. dissertation, KTH, Electromagnetic Eng., Stockholm, 2013.
[2] "IEEE guide for loading mineral-oil-immersed transformers and step-voltage regulators - redline," *IEEE Std C57.91-2011 (Revision of IEEE Std C57.91-1995) - Redline*, pp. 1–172, Mar 2011.
[3] IEC, "IEC 60076-7:2005 power transformers - part 7: Loading guide for oil-immersed power transformers," vol. 60076, no. 7, 2005.
[4] N. Viafora, K. Morozovska *et al*, "Day-ahead dispatch optimization with dynamic thermal rating of transformers and overhead lines," *Electric Power Systems Research*, vol. 171, pp. 194–208, 2019.
[5] M. Humayun, M. Degefa, A. Safdarian, and M. Lehtonen, "Utilization improvement of transformers using demand response," *IEEE transactions on power delivery*, vol. 30, no. 1, pp. 202–210, Feb 2015.
[6] T. Bajracharya, G. Koltunowicz *et al*, "Optimization of transformer loading based on hot-spot temperature using a predictive health model," in *Int. Conf. on Condition Monitoring and Diagnosis*, Sept 2010, pp. 914–917.
[7] C. Ordoudis, P. Pinson, J. Morales González, and M. Zugno, *An Updated Version of the IEEE RTS 24-Bus System for Electricity Market and Power System Operation Studies*. Technical University of Denmark, 2016.
[8] D. Susa, M. Lehtonen, and H. Nordman, "Dynamic thermal modelling of power transformers," *IEEE Trans. on Power Del.*, vol. 20, no. 1, pp. 197–204, 2005.
[9] L. Jauregui-Rivera and D. J. Tylavsky, "Acceptability of four transformer top-oil thermal models—part i: Defining metrics," *IEEE Transactions on Power Delivery*, vol. 23, no. 2, pp. 860–865, April 2008.
[10] R. A. Jabr, "Modeling network losses using quadratic cones," *IEEE Transactions on Power Systems*, vol. 20, no. 1, pp. 505–506, Feb 2005.
[11] O. W. Akinbode and K. W. Hedman, "Fictitious losses in the dcopf with a piecewise linear approximation of losses," in *IEEE PES GM*, July 2013, pp. 1–5.
[12] M. Grant and S. Boyd, "CVX: Matlab software for disciplined convex programming, version 2.1," http://cvxr.com/cvx, Mar. 2014.

[Pub. C5]

S. H. H.Kazmi, T. H. Olesen, T. S. Sørensen and J. Holbøll, **"Machine Learning based Temperature Forecast of Offshore Windfarm Export Cables"**, *B1-109 CIGRE*, Paris, France, Aug 2020.

The published version of the paper is attached.

CIGRE SESSION 48

B1-109

Paris 2020

Machine Learning Based Temperature Forecast for Offshore Windfarm Export Cables

S. H. H. KAZMI*, B. CORDES*, J. HOLBØLL†, T. H. OLESEN*, T. S. SØRENSEN*
*Ørsted Offshore A/S, †Technical University of Denmark
Denmark

SUMMARY

Export cables are considered to be the most critical component of the offshore windfarm electrical export system because they contribute significantly to the capital expenditures, which limits the possibility of improving their redundancy. As a result, offshore windfarm export cables are crucial for system availability and monitoring of these cables is extremely important. Fibre-optics based Distributed Temperature Sensing (DTS) equipment are commonly used for real-time monitoring of these cables providing temporal evolution of the temperature variations along the cable route with good precision. However, for optimal wind energy dispatch using dynamic rating and for other applications, the load and ambient conditions dependent variations of the cable temperature need to be forecasted in advance.

In this paper, supervised Machine Learning (ML) is explored to perform the thermal prediction. ML-based forecast algorithms are found to supersede the commonly used methods based on Finite Element and Thermoelectric Equivalent (TEE) modelling because they require minimal information regarding the cable construction and commissioning, and also because these methods allow the DTS data to be handled more intelligently. The verification process for the algorithms is performed for different sections of the offshore windfarm cables which tend to behave as thermal bottlenecks under different conditions for two offshore windfarm cables: 258 MW Burbo Bank Extension (BB2) in UK and 407 MW Horns Reef 3 (HR3) in Denmark. The qualification of test models applicable for different metrics is ensured by testing a range of grey and black box models for all the test cases. The performance of the tested method is evaluated by considering the following parameters: accuracy, flexibility of application, simplicity and physical interpretability. The models tested in this paper perform temperature forecast with a high degree of accuracy. However, the models that do not use cable load and ambient conditions as input are suitable for short-term prediction only. Whereas for long-term prediction, models have to be trained for all the available inputs for significant periods of time. Complex black-box test models are found to be prone to overfitting, which can be improved by using simple approximations and employing grey-box modelling features.

KEYWORDS

Real-time condition monitoring, Thermal forecast, Offshore Windfarms, HV Subsea Cables, HV Underground Cables, J-tubes, Machine Learning, Artificial Neural Networks, Distributed Temperature Sensing (DTS)

syeka@orsted.dk

1. Introduction

Offshore Wind Power Plants (OWPPs) are usually connected to the onshore grid using one or more export cables. These cables supposedly account for the largest contribution to the capital expenditures of the offshore windfarm electrical export systems. Consequently, export cables are considered to be the most critical component of the OWPP export system not only because of their monetary value and their importance to ensure system availability, but also because they are often the primary bottleneck in the system [1].

For hotspot identification and localization, real-time condition monitoring of OWPP export cables is often performed using Distributed Temperature Sensing (DTS) equipment [2]. Such an equipment can provide temporal evolution of the cable temperature across the different cable sections, with high degree of accuracy and can be used for hot spot detection along the route of the cable. These hotspots or thermal bottlenecks are caused by variation of thermal parameters along the sea bed or by change of ambient temperatures [3]. Moreover, the installation conditions in the different cable sections can also result in inherent thermal bottlenecks [4].

In order to perform dynamic rating of cables for optimized wind energy transmission and to employ advanced condition monitoring techniques, the variation of cable temperature for different loading conditions needs to be forecasted in advance. Up until now, cable conductor temperature estimation and forecast is performed either by using finite element methods or by Thermoelectric Equivalent (TEE) models. Both these techniques require extensive knowledge about the cable design and the layout conditions, which are not always available. As a result, certain approximations are made that can lead to inaccuracies. Moreover, such techniques tend to ignore the change in dynamic behaviour of the cable surroundings over the years and consequently useful information is lost. Such information can allow windfarm developers and operators to improve commissioning practices, resolve thermal bottlenecks and upgrade cable monitoring procedures for both the future and existing windfarm projects.

This paper explores Machine Learning (ML) as a tool to perform the High Voltage (HV) cable's thermal forecast for varying load and ambient conditions. The methods presented in this paper would allow the DTS data to be handled more intelligently and can help resolve the problems mentioned earlier. The paper is structed as follows: Chapter 2 provides the rationale behind using ML-based algorithms for cable temperature forecasts for OWPPs. Chapter 3 presents the two OWPP export cables to be used as test cases, followed by Chapter 4 which presents the methodology for the chosen ML-based algorithms for both short-term and long-term thermal predictions. Finally, the performance of these models is compared for different cable sections in Chapter 5, which is accompanied with possible improvements in the future.

2. Machine Learning – Essential for DTS-based Export Cable Monitoring for Offshore Windfarms

The continuous loadability of the cable in real time can be calculated by using tools like Real Time Thermal Rating (RTTR), which collect the cable load and DTS temperature in real time and can be parameterized for different cable types [4]. These tools can also determine the overloadability of the cables in the near future based on their present state. However, the long submarine and underground cables used in the OWPP export systems exhibit inherent patterns and trends that are either difficult to interpret physically or are hardly visible even to the trained eye. Therefore, accurate scrutiny of the thermal development of these cables over time would require detailed analysis of the entire cable route, if machine learning is not used. The rationale behind this statement is explained further in the points that follow.

2.1 Debottlenecking and Sectionalisation of Offshore Windfarm Export Cables

The offshore windfarm export cables have inherent thermal bottlenecks which not only depend upon the variation in operating conditions like intermittent wind energy production, ambient temperature variation, sand wave movement along the sea-bed, sedimentation in the offshore section etc. [3], but are also highly influenced by the installation and commissioning practices [5]. Based on the thermal behaviour and without any specific thermal obstacles, the entire OWPP export cable can be sectionalized into five segments: Onshore (buried in duct), Horizontal Directional Drilling (HDD), Offshore (subsea, directly buried), Cable Protection System (CPS) and J-tube, as identified in Figure 1. The difference in construction and commissioning conditions of these sections influence the temperature gradient and thermal time constants, as shown in Figure 2. Similarly, by using machine learning, locations that exhibit thermal behaviour both coherent and incoherent to their neighbouring sections can be clustered (for example, unburied segments in the offshore cable section), thereby allowing further sectionalisation as per the user's needs.

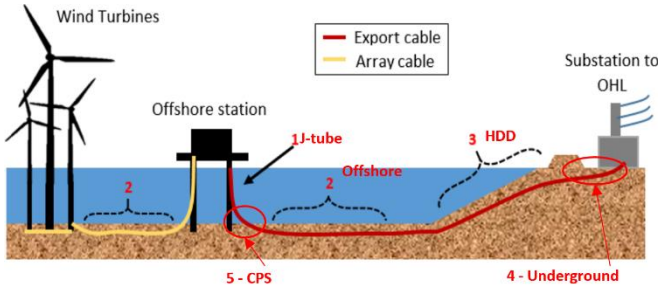

Figure 1. Layout of the OWPP export cable. 5 inherent sections are identified: Jtube, CPS, Offshore, HDD, Onshore.

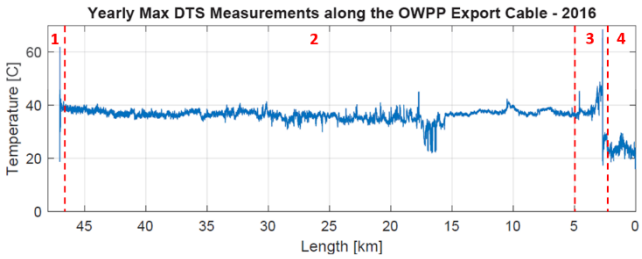

Figure 2. Maximum measured temperatures in year 2016 along the entire cable length with respect to the onshore substation for an offshore windfarm in UK. Temperature peaks at sections 1 (J-tube) and 3 (HDD). Sections 2 (Offshore) and 4 (Underground) are stably cold, except some incoherence in the 15-18 km region.

2.2 Big Data

The DTS equipment on long OWPP export cables generate extremely large data sets that can only be analysed computationally to reveal patterns, trends and associations that would otherwise be overlooked. Also, the impact of seasonal variation on wind production and ambient conditions requires analysis of long-term data. Figure 3 gives an impression of the amount of data that would have to be dealt with for a typical offshore section of the export cables. The 1.26 Million data points needed to represent 35 days of activity would be difficult to utilize for operators without appropriate data handling or machine learning tools.

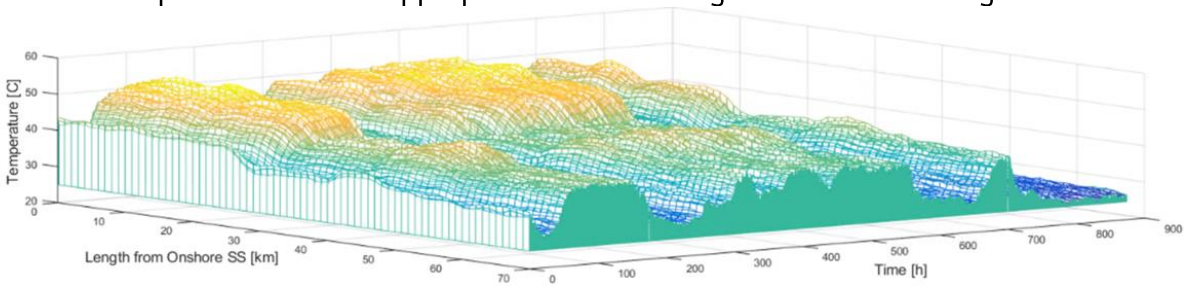

Figure 3. DTS-based cable temperature variation over 35 days for the offshore section of a windfarm export cable. The pattern in this figure is based on 1.26 Million data points

3. Test Cases for Verification of Models

In order to evaluate the performance of the chosen Machine Learning (ML) thermal forecast models for offshore windfarm cables, two test cases have been examined: 258 MW Burbo Bank Extension (BB2) which is 25 km off the west coast of UK and 407 MW Horns Reef 3 (HR3) in the North Sea, 25-40 km off the Danish peninsula Jutland coast. The export cables for the two test cases are similar in design and layout which is convenient for the comparison.

For BB2, 220kV export cables with aggregate length of approximately 35.6km are utilized over different sections identified in the previous chapter. These sections not only use cables with different dimensions (718-1080 A, 1000-1200 sq.mm) but the cable designs differ as well (3-core for subsea and 3x1-core for land). The 35.1 km long export cable for HR3 is installed in an area with great seabed mobility but it exhibits properties similar to BB2 in terms of layout and dimensions [4]. From each of these wind farms, export cable aggregate load (current) and DTS measurements along the cable for 27.5 days with 30-minutes sampling rate are used for analysis. In Table 1, start and end points for four cable sections of the two test cases are provided. The fact that J-tube and HDD constitute the shortest sections is confirmed. The sampled test points for all sections which are used to train and test the ML algorithms are also provided in Table 1.

Table 1. Start and End points for different cable sections for BB2 and HR3 test cases. Test points for each section are also mentioned. All the values are in metres.

Section	BB2			HR3		
	Start	End	Test Point	Start	End	Test Point
Onshore	0	9948	5000	0	2450	1250
HDD	9950	10616	10300	2450	2590	2520
Offshore	10618	35080	20000	2590	35580	22000
J-tube	35082	35112	35098	35580	35644	35620

4. Methodology

In this section, the development of statistical and Machine Learning (ML) based models is described for temperature forecast of DTS temperatures. The models that can be used to perform such tasks can be classified into 3 categories: white-box, gray-box and black-box models. This classification is based upon the amount of physical insight required to construct the model. The Thermo-Electric Equivalent (TEE) models of [6, 7] can be classified as white-box models because all the physical parameters and the underlying principles are available or approximated. On the opposite side of the spectrum, physical insights are not required to build the black-box models and election of the models to be tested is performed by considering the models with good track records for similar problems. Whereas, grey-box models combine the properties of the other two.

In order to comply with the guidelines of system identification in [8, 9] for qualification of test models applicable for different metrics, a range of grey and black box models have been tested in this paper for all the test cases. Each of the tested models has its strengths and weaknesses which are evaluated by considering the following parameters: accuracy of prediction, flexibility of application, simplicity of development and physical interpretability. The latest parameter is critical for test system characterization and is also crucial for this application especially when one needs to use these models in cooperation with or to improve the existing white box models. The prediction accuracy is assessed by calculating the Normalized Mean Squared Error (NMSE) in (2).

$$MSE = \frac{1}{N}\left\| y_{ref}(t) - y_{pred}(t) \right\|^2 \tag{1}$$

$$NMSE = 100\left(1 - \frac{MSE}{\sigma^2}\right) = 100\left(1 - \frac{\left\| y_{ref}(t) - y_{pred}(t) \right\|^2}{\left\| y_{ref}(t) - y_{mean}(t) \right\|^2}\right) \tag{2}$$

Where, y_{ref} and y_{pred} represent the actual and the predicted DTS temperature values respectively, while y_{mean} represents the mean value for N observations. The Mean Squared Error (MSE) is an effective metric for evaluation of model fitting, as large errors are penalized equivalently. However, NMSE offers two distinct advantages over MSE: the normalization over the system variance (σ^2) accounts for the inherent variation of the dataset. Secondly, the physical interpretation is rather simple which makes it convenient to compare models. In terms of percentage, NMSE of 100 means a perfect fit, while 0 represents the case for $y_{pred} = y_{mean}$. Hence any model with NMSE (%) in interval [0 100] would perform better than simply using the mean value [10].

Considering the applicability of the tested models, they are further classified into 2 categories: short-term prediction models and long-term prediction models. This section briefly explains the mechanism of the chosen models. For detailed description of the respective models, the referred literature can be reviewed.

4.1 Short-term Prediction Models (Regression-based)

Predicting the cable DTS temperature over a short time span (up to 12 hours for 30-minute sampling rate) can be performed using regression-based models. The formulation of the models used in this paper predict the DTS temperature without using known independent variables (current, ambient temperature). The impact of seasonal variation on ambient conditions and wind energy production does not need to be accounted for either, therefore one-step or multi-step predictions can easily be performed using Least Square estimators [11]. All of these models are black-box models as no physical interpretation is performed.

4.1.1 General Linear Model (GLM)

General Linear Model (GLM) can have a number of formulations depending on the available inputs and the required applications. The following model is based on the simplest form of linear regression:

$$y(t) = a_0 + a_1\, t + e(t) \tag{3}$$

Where t is time, y is the response variable (DTS temperature in this case), a_0 and a_1 are the parameters, e is white noise which is assumed to be based on a set of Independent and Identically Distributed (IID) random variables. Although GLM is not used on data in this paper because of its ineffectiveness for this application, it is still necessary to mention this in order to comprehend the models that follow.

4.1.2 Exponential Smoothing Model

In contrast to the general linear model, where each observation contributes equally to the predictions, the exponential smoothing allows for weighting of each observation. As a result, the most recent observations are weighed more than the observations in the past. The simple exponential smoothing (also called first order exponential smoothing) sequence [11] is given by (4) in discrete form.

$$\hat{y}_N = (1 - \lambda)\, y_{N-1} + \lambda\, \hat{y}_{N-1} \tag{4}$$

Where λ $(0<\lambda<1)$ is the forgetting factor (weight for the previous estimate) and $1\text{-}\lambda$ is the smoothing constant (weight for the latest available observation). y is the observed DTS temperature, N represents the number of observations which increases by 1 after each step. $\hat{y}$ is the predicted DTS temperature for each step and its influence diminishes over time depending on the chosen forgetting factor. Since this is a locally constant mean model, it can reliably perform one-step prediction only. The l-step prediction given by (5) suggests that any future forecast will be the last one-step estimate if further DTS temperature observations are not available:

$$\hat{y}_{N+l\,|\,N} = \hat{y}_{N\,|\,N} \tag{5}$$

Since the horizon of prediction is one step, the forgetting factor λ of 0.2 is used which allows the highest weight [smoothing factor of 0.8] to be allotted to the most recent application. The high smoothing factor gives a quick response to changes in the mean value of the process.

4.1.3 Local Linear Trend Model

This method combines the properties of GLM and exponential smoothing by forgetting the old observations in an exponential manner. Equation (3) for GLM can be rewritten in discrete form:

$$y_{N+j} = a_0 + a_1\, j + \ e_{N+j} \tag{6}$$

$$y_{N+j} = u^T(j)\ a\ + \ e_{N+j} \tag{7}$$

Where $u^T[j] = [1\ \ j]^T$, $a = [a_0\ a_1]$, j represents the number of discrete time steps, N represents the total number of observations and e is white noise. The l-step prediction is given by

$$\hat{y}_{N+l\,|\,N} = u^T(l)\ \hat{a}_N \tag{8}$$

The first step in this process is to estimate the parameters a, which can be found by minimizing the Sum of weighted squared errors $S[a; N]$ for a given forgetting factor λ.

$$\hat{a}_N\ =\ \arg min_a\, S(a;N) \tag{9}$$

$$S(a;N) = \sum_{j=0}^{N-1} \lambda^j \left[y_{N-j} - \mathrm{u}^T(-\mathrm{j})a\right]^2, \quad 0 < \ \lambda < 1 \tag{10}$$

In order to obtain the best fit with minimum error, optimization of the forgetting factor needs to be performed based on (11) and (12) which is a recurring process in association with (10). The results of this optimization are provided in Figure 4 for the test case of BB2 J-tube, which gives the optimal fit for λ = 0.67. Consequently, the reduction in weight of observations further from the most recent observation for BB2 J-tube's optimal model is also provided in Figure 4.

$$\hat{\lambda} =\ \arg min_\lambda\, S(\lambda;N) \tag{11}$$

$$S(\lambda;N) = \sum_{t=1}^{N} \left[y_t - y_{t\,|\,t-1}(\lambda)\right]^2 \tag{12}$$

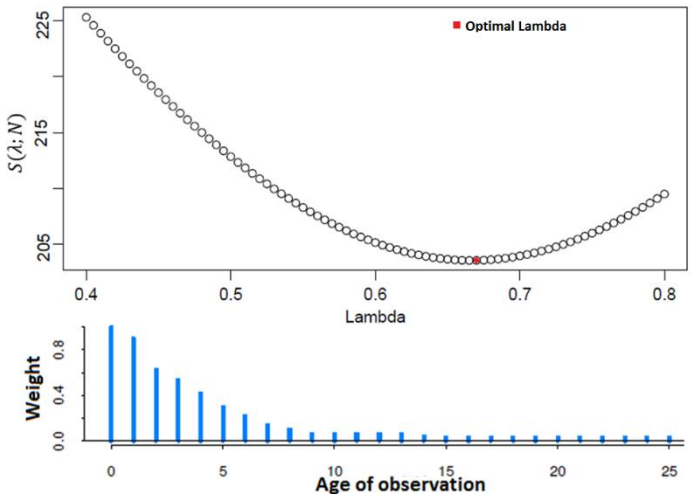

Figure 4. Top: Optimization of forgetting factor (λ) for local linear trend model for BB2 J-tube. Bottom: Exponential reduction in weights of observations BB2 J-tube [0 means latest observation, 25 is the oldest in the given window]

4.2 Long-term Prediction Models

The commonly used 60-40 principle is used for the long-term prediction models. This principle allows the 60 percent of the available data to be used for training of the ML models, while the rest is used for validation. Hence for both the test cases with 27.5 days of available data, the long-term prediction models are first allowed to train on current and DTS measurements of the first 16.5 days for all the sections, as shown in Figure 5. The trained models are then used to predict the DTS measurements for the remaining 11 days by providing the load current as model input. Therefore, each long-term prediction model is trained and tested four times for each test case because each cable section is expected to behave differently. This is visible in Figure 5 because for similar load current variation, the temperature gradient and thermal time constants are different for each section. The temperature seems to vary more frequently for J-tube as compared to other sections. Onshore and HDD are found to have largest thermal time constants.

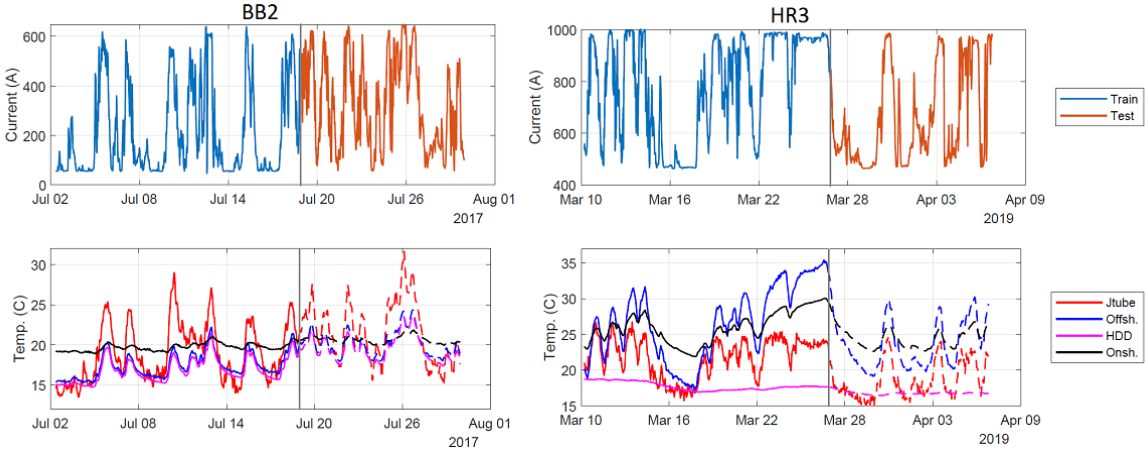

Figure 5. Top: Current, Bottom: DTS measurements. The first 16.5 days represent the training data (used to train the models) and the remaining 11 days are test data (only the current is provided to the models and temperature is calculated) Solid lines represent signals visible to the models and dashed ones need to be predicted. Dashed signals are to be used for the assessment of models' performances.

4.2.1 Process Model

This model acquires its name from its common utilization in the process control applications (e.g. PID tuning). This gray-box model is close to the TEE models of [6, 7] as it interprets the physical aspects of the problem by duplicating the heat-dissipation phenomena in HV cables using first-order differential equations. The transfer function of (13) represents a simple model with limited number of parameters which makes it less prone to overfitting.

$$G(s) = \frac{K}{1 + s\,T_{p1}}\, e^{-s\,T_d} \tag{13}$$

where K is the gain, T_{p1} represents the main time constant of the system and T_d is the delay or dead-time between input and output. This formulation of the process model cannot handle disturbances that may arrive due to changes in weather and other ambient conditions. Similarly, the long-term trends are also difficult to model. Therefore, heat loss from the cable (conductor, armour and screen) are considered dominant for defining the DTS temperature.

The parameters obtained from fitting the process model for training data sets for BB2 and HR3 are provided in Table 2. The parameters seem to be in agreement for different sections, which substantiates the underlying physical principles of each section. One hypothesis is that the time constant for onshore section is significantly larger because the fibre-optic is not lined inside the cable and the temperature of the cable duct is being monitored instead.

Table 2. Parameters for trained Process Model for different cable sections of BB2 and HR3 test cases

Parameters	BB2				HR3			
	Onshore	HDD	Offshore	J-tube	Onshore	HDD	Offshore	J-tube
K [C/A²] ($\times 10^{-5}$)	1.47	2.62	2.55	4.24	1.19	2.98	2.27	4.05
τ_{p1} [h]	36.93	14.37	11.49	7.11	25.91	12.60	11.58	3.37
τ_d [h]	0.00	0.00	0.00	0.73	0.00	2.57	0.00	0.91

4.2.2 ARX Model

The ARX model [Auto-Regressive eXogenous or Auto-Regressive model with eXtra variable] has previously been used in [12] as a simplistic replacement to TEE models of [6, 7]. The underlying assumption of the model is that the system can be represented by a random process, where the value depends on a linear combination of previously predicted values, a stochastic term and a series of known inputs.

The ARX is a typical linear black box model used in system identification [8]. The model predicts output based on previously predicted values and inputs with time lags. The model is based on the following equation:

$$\hat{y}(t) = a_1\,\hat{y}(t-1) + \cdots a_n\,\hat{y}(t-n) + b_0\,u(t) + b_1\,u(t-1) + \cdots b_m\,u(t-m) + e(t) \qquad (14)$$

where $\hat{y}$[t] is the predicted output representing the DTS temperature in this case, $u(t)$ is the input representing cable current, while $e(t)$ is a sequence of random variables [white noise]. The weights a and b are the parameters to be fitted for the training dataset and the model order n x m is to be chosen in advance by testing various combinations in a reasonable range and selecting the model orders which gives an acceptable error with the lowest possible order. The ARX implementation in the MATLAB System Identification toolbox [13], handles this automatically. Order n = 10 and m = 8 are used for the test cases.

4.2.3 Artificial Neural Network [ANN] Model

The models discussed so far are linear in nature, but in order to capture the behaviour of cable thermal development and to account for multiple factors affecting the process, the flexibility of these models need to be increased. The ANN model uses the same exact inputs as the ARX model. However, instead of using a weighted linear combination, the variables pass through a neural network with non-linear combination of the input variables to produce the prediction. Such models have previously been used for widescale applications, but the utilization of ANN in [14] is relevant to the goal of this paper.

The fundamental principle of a simple neural network is illustrated in Figure 6 [15]. At each vertex of the hidden layers, illustrated as blue circles, a non-linear activation function is applied to the input. The popular ReLU activation function [16] has been used in this case. The neural network can be made more complicated, by for instance adding more hidden layers. For a more detailed introduction to neural networks see [16, 17].

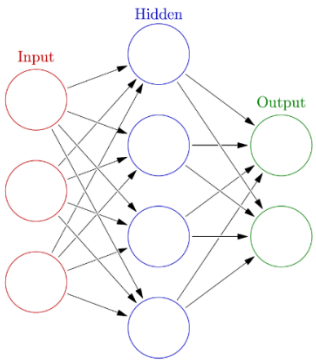

Figure 6. Simple artificial neural network [ANN] consisting of a single hidden layer [15]

For this system, a feed-forward neural network with two hidden layers is used, with 5 neurons in the first layer and 20 neurons in the second layer. The size and number of hidden layers have been chosen as a compromise between computation time and sufficient model complexity. The non-linearity in the neural network model suggests that fewer assumptions are made about the system, which in turn means that more data is required to train the model. But this makes the ANN prone to over-fitting [10].

5. Results and Discussion

In this section, the DTS temperature forecast results are provided for all the tested models. The results for the selected short-term prediction models (Exponential Smoothing and Local Linear Trend) are plotted together. Whereas for the long-term prediction case, only the models that result in best and worst fit for each section are presented.

Since the models had to be repeatedly trained and parametrized for each cable section, the results are also provided separately for each cable section for both the test cases of BB2 and HR3. First and foremost, the results for J-tube section are provided in Figure 7, followed by the offshore cable section in Figure 8. Afterwards, the DTS temperature forecast results for HDD and onshore are presented in Figures 9 and 10 respectively. This is followed by evaluation of the short-term and long-term prediction models' performances based on the criteria defined in Chapter 4.

In each of these figures, the short-term prediction models perform 24-step predictions for the 30-minutes DTS samples. Therefore, the real-time DTS measurements (blue) are used to perform forecast of the temperature (black and red) 12 hours into the future. Hence the prediction for July 08 (15:00) will be based on all the available DTS measurements until July 08 (03:00). The process continues for the entire period as more and more observations become available over time. All of these lines are plotted together to assess the models' performance compared to actual measurements. The long-term prediction models are simpler to understand because the first 16.5 days are simply used for training, and rest of the period represent the predicted temperatures.

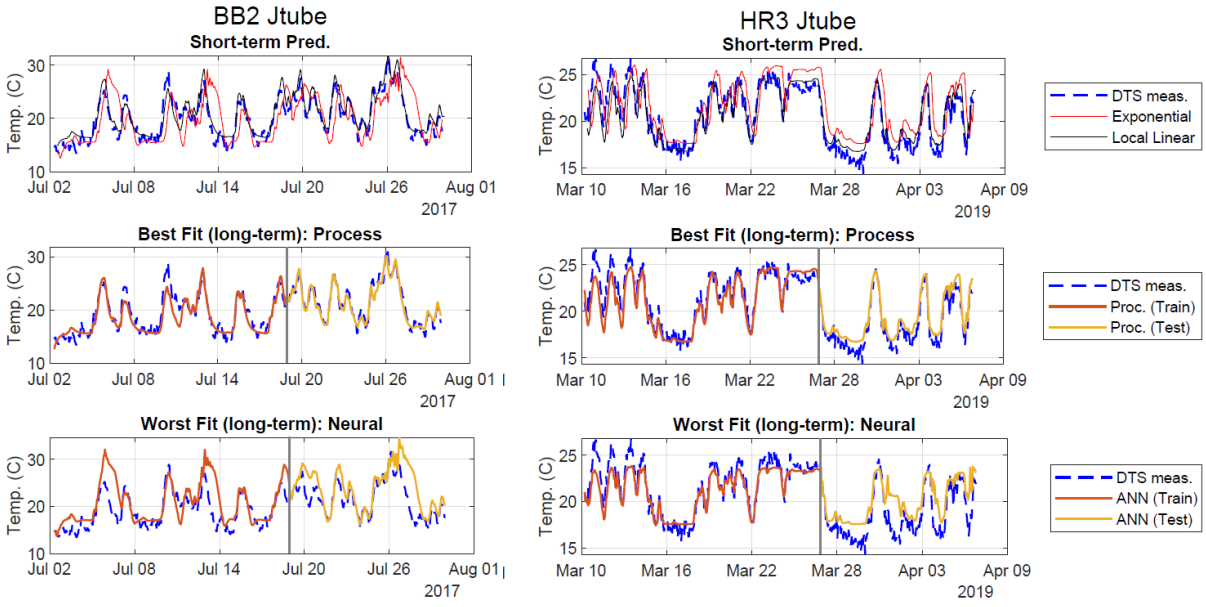

Figure 7. Machine Learning based DTS temperature forecast results for J-tube section of BB2 and HR3 test cases. Top: Short-term prediction models. Middle: Long-term prediction model with best fit for J-tube section (Process). Bottom: Long-term prediction model with worst fit for J-tube section (ANN). Training and test periods are separated by a grey line.

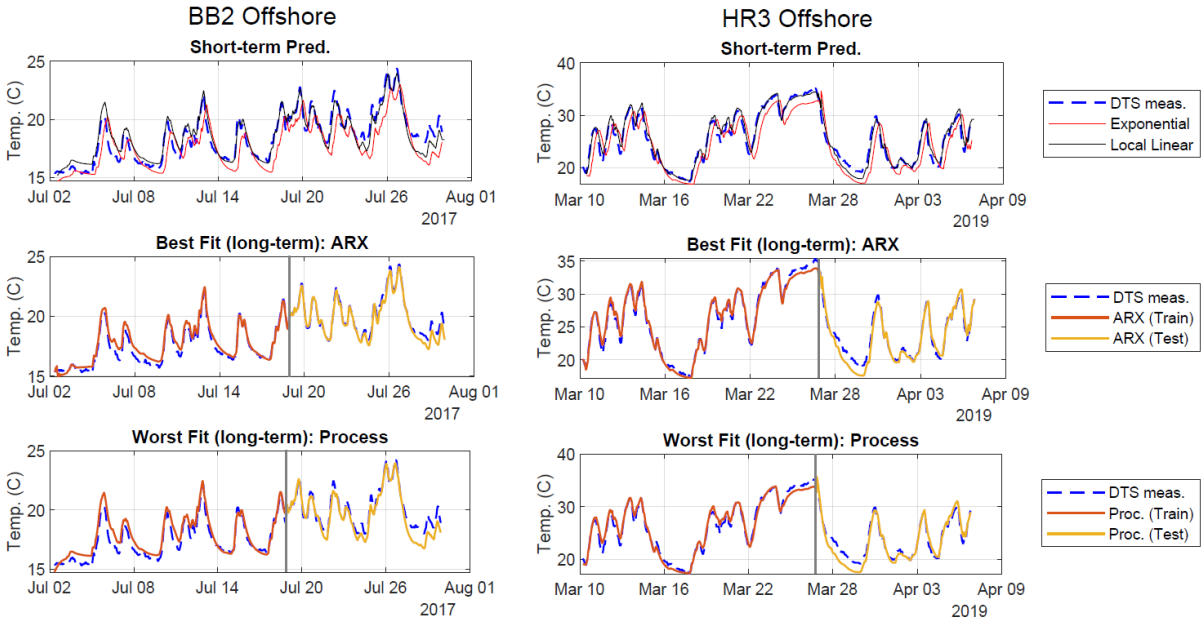

Figure 8. Machine Learning based DTS temp. forecast results for offshore section of BB2 and HR3 test cases. Top: Short-term prediction models. Middle: Long-term prediction model with best fit for offshore section (ARX). Bottom: Long-term prediction model with worst fit for offshore section (Process). Training and test periods are separated by a grey line.

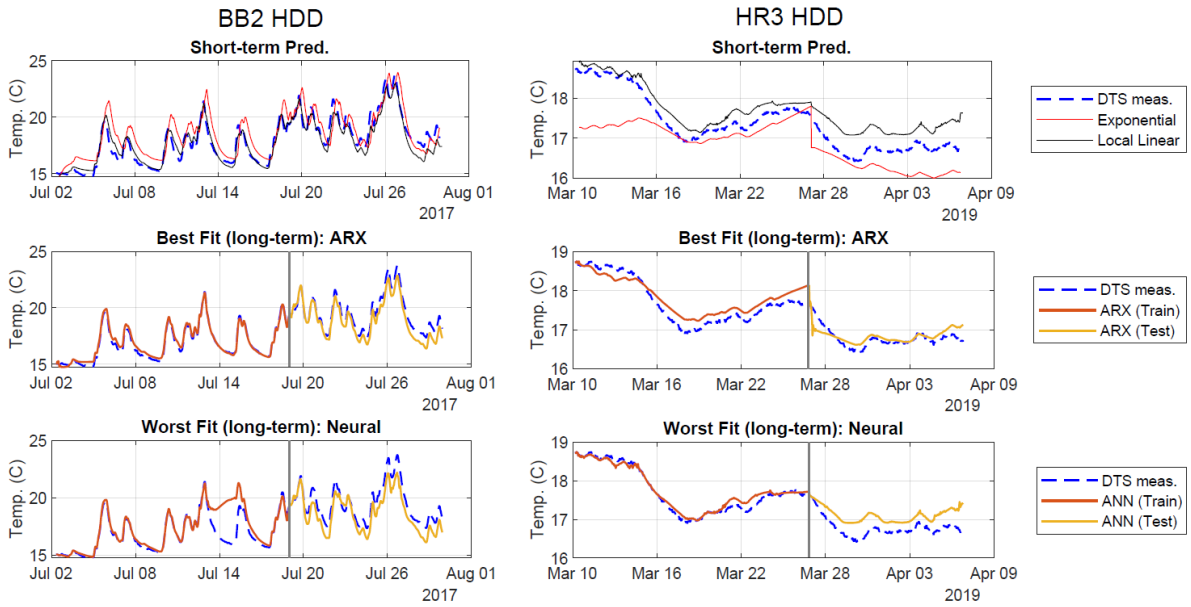

Figure 9. Machine Learning based DTS temperature forecast results for HDD section of BB2 and HR3 test cases. Top: Short-term prediction models. Middle: Long-term prediction model with best fit for HDD section (ARX). Bottom: Long-term prediction model with worst fit for HDD section (ANN). Training and test periods are separated by a grey line.

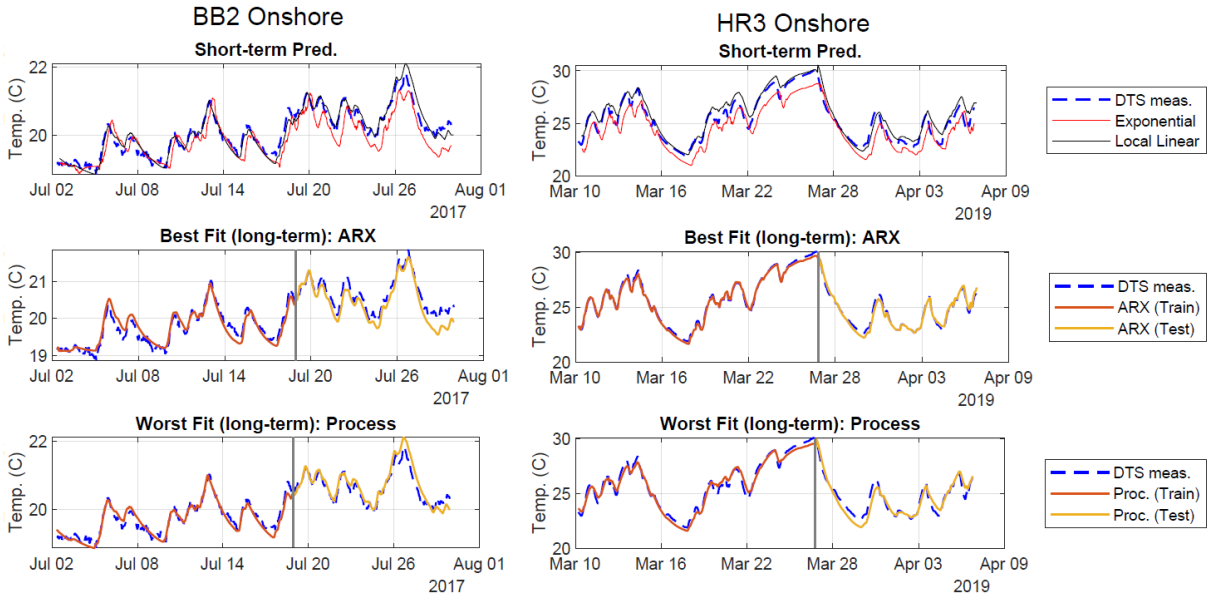

Figure 10. Machine Learning based DTS temp. forecast results for onshore section of BB2 and HR3 test cases. Top: Short-term prediction models. Middle: Long-term prediction model with best fit for onshore (ARX). Bottom: Long-term prediction model with worst fit (Process). Training and test periods are separated by a grey line.

5.1 Evaluation of Short-term Prediction Models

For regression-based short-term prediction models, exponential smoothing and local linear trend are chosen over the general linear model described in Chapter 4.1. Both the models do not use cable load as input and perform single or multi step prediction based on historical DTS measurements only. Although both the models are not constant mean models and the latest observations/estimates are given the highest weight, they are still found to be slower to react to temperature changes. Local linear trend model is found to outperform exponential smoothing model for most cases not only because the forgetting (or smoothing) factor λ has been optimized to give the best fit, but also because unlike exponential smoothing, it employs piece-wise linearization. However, these models are only suitable for short-term (up to 12 hours) and can further be improved by accounting for the variation in cable load or by performing multi-step prediction mechanisms.

5.2 Evaluation of Long-term Prediction Models

The three models chosen for this analysis are fundamentally different from each other. Although all of these models use both the real-time cable load and historic DTS measurements as inputs, they do not treat them in the same manner. The process model tends to interpret the physics behind the cable heat dissipation, whereas the ARX model works statistically but solves the problem linearly [18]. The ANN model on the other hand, while using the same set of inputs, brings non-linearity into account which can lead to over-fitting if not treated methodologically.

In Table 3, the goodness-of-fit for all the tested long-term prediction models is provided for each cable section of the two test cases, which is based on the Normalized Mean Squared Error (NMSE) of the training and test periods, as defined in Chapter 4. The closer the NMSE for the test period is to 100, the better the model performs. It must be noted that comparison of goodness-of-fit for the test period with the training period is performed to compare the consistency of the model only, because higher NMSE for the training period doesn't necessarily stipulate better performance because the models can have the tendency to overfit the data. Therefore, the models are assessed solely on their performance during the test periods.

Based on the figures in Table 3, the ARX model is often found to perform best for both the test cases and for most of the cable sections. The only exception is observed for the J-tube section which finds the best fit using the process model. This is particularly interesting because the dynamic thermal variation of cables in the J-tube section is more rapid as compared to other sections [5], which enhances the influence of cable load on temperature. The process model can be made to perform even better by employing differential equations of higher-order for the base model, such that these equations closely follow the TEE model structures of [6, 7]. Finally, the structure of the chosen ANN model results in performance limitations which results from data overfitting (higher accuracy during train period as compared to test period) can be improved by either increasing the number of layers (thereby increasing the model complexity and may cause further overfitting) or by allowing the model to train over longer timeframe. On the other hand, the overall process for evaluation of long-term prediction models can be improved by using cross validation.

Table 3. Goodness-of-fit for all the tested long-term prediction models based on NMSE from (2). 100 means perfect fit and 0 means model is not appropriate. The performance during training and test periods for all the cable sections in the BB2 and HR3 test cases are provided.

Long-term Prediction Models		BB2				HR3			
		Onshore	HDD	Offshore	J-tube	Onshore	HDD	Offshore	J-tube
Process	Train	70.46	75.03	60.33	58.74	83.49	16.29	84.05	62.10
	Test	57.63	52.42	57.77	74.23	63.97	16.67	65.58	67.20
ARX	Train	67.56	84.04	72.13	58.38	91.29	61.02	88.26	63.70
	Test	45.44	58.78	75.28	73.18	82.62	47.84	73.42	65.54
ANN	Train	66.17	26.70	79.10	50.94	92.67	82.78	87.82	61.42
	Test	28.55	39.35	39.91	44.01	76.13	46.74	67.72	22.61

5.3 Discussion on Application of Machine Learning Based Prediction Models

In section 2, the necessity of using machine learning for handling of and improving practicability of DTS data was discussed. Since the tested prediction models are found to be appropriate for both long-term and short-term forecast, the possible applications of such a tool in the offshore industry should be highlighted as well.

For both the offshore windfarm developers and system operators, thermal optimization of HV export cables for different energy production and ambient condition scenarios is necessary for optimal wind energy transfer based on real-time dynamic rating of cables. Such an optimization can be performed more efficiently by using these ML-based methods as compared to the existing techniques. The long-term prediction models take longer to train and require at least a few days of load and DTS data before the predictions become intelligible and usable. Whereas, the short-term models can be up and running in real-time owing to their simplicity and reduced accuracy. In this domain, the operators and system designers can also use these models for thermal assessment of cables during contingency situations.

Offshore windfarms require periodic monitoring of the offshore export cable route through physical surveys to check for cable exposure. The expensive vessels and tools required to carry out such surveys can ramp up the costs to several million Euros. The cable sections exposed to the sea water are known to exhibit different thermal behaviour as compared to the properly buried ones. By using ML-based algorithms of this study, the alteration of surroundings over time of the export cable offshore section due to sediment movement etc. can be detected automatically, which can reduce and even annul the need for periodic physical surveys. Similarly, the unique thermal performance of cable sections that behave as

thermal bottlenecks (J-tube, HDD etc.) is easily detected by the tools discussed in this paper. The thermal design and interpretation of these sections can consequently be improved.

6. Conclusion

Application of machine learning for temperature forecast has proven to be efficient in this study. Among other applications, these tools can be used for thermal optimization of the export cables, which is crucial for optimal transmission of wind energy from offshore windfarms. The real-time temperature of the OWPP export cable across the entire cable length can be obtained using the fibre-optics based DTS equipment, which can improve the temperature forecast models necessary for dynamic rating. But in order to resolve the challenges introduced by the amount of data generated by DTS and also to deal with the complex heat dissipation phenomena of different cable sections, supervised machine learning based models have been tested and promising results have been obtained. 27.5 days of continuous DTS data from export cables of two offshore windfarms Burbo Bank Extension and Horns Reef has been used for testing. The inherent sectionalisation of these cables in terms of thermal performance is utilized by assessing the performance of the chosen models for J-tubes, HDD, undersea and underground cable sections. The tested models are classified as grey-box (with methodological physical interpretation of the heat dissipation) and black-box (requiring no physical insights at all).

For short-term prediction, models that do not require cable load and ambient information as inputs are used. The exponential smoothing model, although simpler to design, is found to be outperformed by the local linear trend model for short term forecast because it combines the piecewise linearization of GLM and employs exponentially decreasing weights from the latest to the oldest observations. Whereas for long-term prediction, different models are found to perform better for different sections. ARX performs best for all the sections except the J-tube, while the process model seems to adapt best for this section. This is primarily because the heat dissipation phenomena are complicated in J-tubes and longer training data would be required for tuning of the ARX model. Similarly, artificial neural networks over fit the training data because of the non-linearity that these models introduce but they are also expected to perform better with the increase in training periods. The process model can further be improved by adapting the structure of the trained transfer function to match the physical process of each section, especially HDD and Onshore.

7. Acknowledgements

The support of Innovation Fund Denmark, which is sponsoring this project is highly appreciated. The OPTIMUM framework project collaboration between DTU, Energinet.dk and Ørsted oversees this work. Authors would also like to thank Joachim Niemann-Larsen from Energinet.dk for his efforts in connection with the case study

BIBLIOGRAPHY

[1] J. S. González, M. B. Payán and J. R. Santos, "Optimum design of transmissions systems for offshore wind farms including decision making under risk," Renewable Energy, vol. 59, pp. 115 - 127, 2013.

[2] Working Group SC B1.45 CIGRE, 'Thermal monitoring of cable circuits and grid operators' use of dynamic rating systems' (Technical Brochure 756, Feb 2019)

[3] T. Hughes, T. Henstock, J. Pilgrim, J. Dix, T. Gernon and C. Thompson, "Effect of Sediment Properties on the Thermal Performance of Submarine HV Cables," IEEE Transactions on Power Delivery, vol. 30, no. 3, pp. 2443-2450, 2015.

[4] Working Group SC B1.40 CIGRE, 'Offshore Generation Cable Connections' (Technical Brochure 610, Feb 2015)

[5] R. D. Chippendale, J. A. Pilgrim, K. F. Goddard, P. Cangy, 'Analytical Thermal Rating Method for Cables Installed in J-Tubes', IEEE Transactions on Power Delivery, Vol 32, Issue 4, pp 1721 - 1729, Aug 2017

[6] IEC 60287-1-1 ed 2.0, "Electric cables - Calculation of the current rating - Part 1-1: Current rating equations (100 % load factor) and calculation of losses - General," 2006.

[7] IEC 60287-2-1 ed 2.0, "Electric cables - Calculation of the current rating - Part 2-1: Calculation of Thermal Resistance," 2006

[8] Ljung L. System Identification - Theory for the User. Prentice-hall, Inc., 1999.

[9] Lennart Ljung. System identification and simple process models. Linköping University. Electronic Press, 2003.

[10] Gavin C Cawley and Nicola LC Talbot. On over-fitting in model selection and subsequent selection bias in performance evaluation. Journal of Machine Learning Research, pp: 2079–2107, 2010.

[11] Henrik Madsen, 'Time Series Analysis', Chapter 3 Regression-based Models, Chapman & Hall, CRC, 2008.

[12] J. Fulcher, D. Martin, O. Krause, 'Developing Simplified Thermal Models for 11 kV Underground Cables in Australia', IEEE PES Asia-Pacific Power and Energy Engineering Conference, Brisbane Australia, Nov 2015.

[13] Inc. The MathWorks. MATLAB and System Identification Toolbox Release 2019b. Natick, Massachusetts, United States, 2019.

[14] K. Zhang, A. Guliani, G. Memik, 'Machine Learning-Based Temperature Prediction for Runtime Thermal Management Across System Components', IEEE Transactions on Parallel and Distributed Systems, Vol 29, Issue 2, July 2017

[15] T. Herlau, M. N. Schmidt and M. Mørup, 'Neural Networks - Introduction to Machine Learning and Data Mining', Technical University of Denmark, pp 185-202, Jan 2018

[16] Christopher M Bishop et al. Neural networks for pattern recognition. Oxford university press, 1995.

[17] Aurélien Géron 'Hands-on machine learning with Scikit-Learn and TensorFlow: concepts, tools, and techniques to build intelligent systems' O'Reilly Media Inc., 2017.

[18] M. Hezri, F.I Rahiman, M. N. Taib, 'Performance of multi-step-ahead-prediction ARX for steam temperature in a self-refilling distillation essential oil extraction system', International Conference on Control, Automation and Systems, Seoul, Korea, Oct 2007

[Pub. C6]

S. H. H.Kazmi, T. H. Olesen, T. S. Sørensen and J. Holbøll, **"Thermal Analysis and Debottlenecking of HVAC Export Cables for Offshore Windfarms"**, Accepted (awaiting presentation), *3rd CIGRE South East European Regional Council Conference*, Vienna, Austria, Nov 2021.

The accepted version of the paper is attached.

16 – 19 JUNE 2020
3rd SEERC Conference Vienna 2020
Cooperation • Sustainability • Future

South East European Regional Council

CIGRE South East European Regional Council
Conference 2020 in Vienna, Austria

Cross Border Cooperation + Innovation & New Technologies

Thermal Analysis and Debottlenecking of HVAC Export Cables for Offshore Windfarms

S. H. H. Kazmi[×], R. Østerø[×], J. Holbøll[†], T. H. Olesen[×], T. S. Sørensen[×]
[×]Ørsted Offshore A/S, [†]Technical University of Denmark
Denmark
syeka@orsted.dk

SUMMARY

The HV export cables connecting offshore windfarms to the grid are optimally rated to reduce the overall windfarm CAPEX without resulting in revenue loss due to energy curtailment. The substantial costs combined with the influence on energy availability requires extensive thermal evaluation of these cables. The analysis in this paper reveals that the offshore windfarm cables can be divided into onshore (underground), landfall, offshore (subsea) and J-tube sections based on their unique thermal behaviour. Current practices suggest that the export cables can be dynamically rated during the design phase based on long-term historical wind data and during the operation phase based on real-time measurements from Distributed Temperature Sensing (DTS) equipment. The utilization of long-term DTS data from a specific windfarm export cable in UK reveals that the J-tube and landfall sections are the major thermal bottlenecks along with the cable joints/transition-points at onshore and offshore. Landfall is found to comprise of the most thermally strenuous environment due to large burial depths. While J-tube is influenced significantly by the ambient conditions in its air-section, thereby making it most prone to be affected by the local weather. Whereas, the thermal instability of the lengthy offshore section comes from the diffusion of thermal properties of surrounding material due to seabed geology and variation of cable burial depth over time due to seabed movement and sedimentation. Onshore cable section is found to be thermally stable and free from hotspots not only because of the difference in cable design and utilization of ducts for installation but also because the fibre optic cable for DTS is not embedded inside the cable. The temperature offset therefore needs to be established for the land and submarine cables respectively in order to obtain a more accurate account of the conductor temperature. In conclusion, employment of modern techniques combined with thermal analysis of each section can improve the existing design and operation practices.

KEYWORDS

Distributed Temperature Sensing (DTS), Offshore Windfarms, HV Underground Cables, HV Subsea Cable, Real-time Condition Monitoring, Thermal Bottlenecks, J-tubes, Cable Hotspots.

S. Hamza H. Kazmi – Young CIGRE Member (Denmark)

1. Introduction

The cost of energy from Offshore Wind Power Plants (OWPPs) has decreased by more than 60% over the last decade. The export cables that are used to connect OWPPs to the grid on land are known to be the primary contributor to the CAPEX of the electrical export system. As a consequence, the ratings of these export cables are statistically optimized to reduce the cost of energy even further [1] [2]. Therefore, the export cables are not only critical for ensuring energy availability but also to optimize the system's capital and operation expenditures. Thermal monitoring of cables in real-time is possible using fibre-optics based Distributed Temperature Sensing (DTS) equipment. This equipment allows the system operators to assess the variation of cable temperature over time along the entire cable route with an acceptable degree of accuracy. Such an equipment can be used for extensive thermal analysis of the inherent bottlenecks in the export cable system.

In this paper, debottlenecking of the OWPP export cable is performed by identifying cable sections which are not only influenced by the variation in operating conditions (energy production, ambient temperatures, sea-bed movement, sedimentation etc.) but are also highly dependent on the installation and commissioning practices. These sections include onshore (buried in duct), Horizontal Directional Drilling (HDD) for landfall, offshore (subsea, directly buried), Cable Protection System (CPS) and J-tube. The export cable for a specific offshore windfarm in UK is used as test case. Moreover, the entire cable route of the analysed test case is examined and a comprehensive portrayal of the thermal development across the cable's length is provided for two different years to evaluate the impact of varying ambient conditions and wind energy production. Moreover, the necessity and methodology of employing dynamic rating for export cables during design and operation is also discussed.

2. Offshore Windfarm Design and Cable Layout

The OWPP export system based on HVAC technology consists of two or more substations: an offshore one close to the wind turbines in the sea and an onshore one on land which serves as an interface to the transmission network, as shown in Figure 1. The HV components that constitute this system include HV/MV cables, power transformers, shunt reactors, HV filters, gas insulated switchgears and compensators (incl. STATCOM, FACTS, SVC etc.). The HVAC solution is suitable for offshore windfarms up to 70 km from the shore; the distance can further be increased by using intermediate HVAC reactors in the export system. There are usually multiple parallel circuits to improve the system reliability and availability. One such setup with two export cable circuits is presented in Figure 1 (bottom). A choice is made by the system designers to either use multiple circuits with lower transmission voltage or single circuit with high voltage, each solution differing significantly in CAPEX and OPEX.

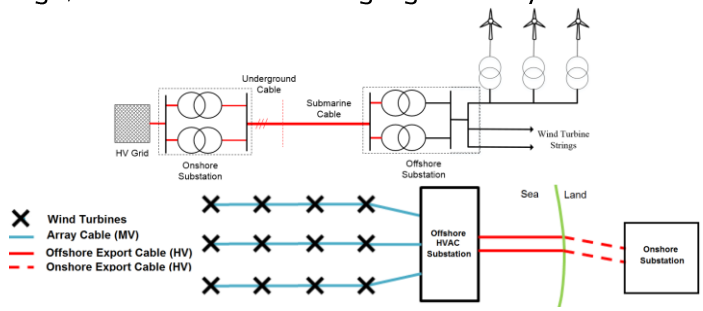

Figure 1. Top: Simplified layout of HVAC-based OWPP export system [3], Bottom: Two HVAC export cables layout

The typical layout of export cables for OWPP transmission system based on HVAC technology is provided in Figure 2. One 3-core subsea cable per circuit is shallow buried directly in the sea bed. At the offshore substation end, the fibre-optics embedded HV cable passes through the Cable protection System (CPS) which protects it from mechanical stress during installation while maintaining an appropriate bending radius during operation. The cable also goes through the J-tube section before entering the offshore platform hang-off where the cable armour is terminated. At the other end, the 3-core cable goes through a Horizontal Directional Drilling (HDD) pipe before transitioning to an underground cable connecting to the onshore substation. For underground transmission, single-core cables in ducts are commonly used, which requires the presence of transition joints between HDD and the onshore sections. Further details regarding each section of the export cable are provided in Section 4.

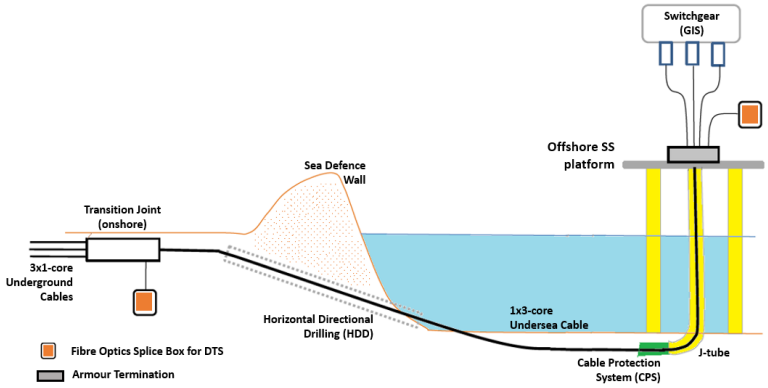

Figure 2. Overview of main components/sections for the HVAC-based export cable system for OWPPs

As a result of the high costs of long HVAC cables, offshore windfarms are usually overplanted, which allows the continuous transmission capacity of export cables to be less than the windfarm size. This practice is appropriate for OWPP design because of a number of reasons. The intermittent nature of wind energy production accompanied with the large thermal inertia of cables (particularly for deeply buried sections) which slows down the cable heating up process suggests that the cable doesn't heat up to its maximum temperature limit because high wind energy production periods do not sustain for long enough. This is demonstrated in Figure 3 for a windfarm site in UK over the period of 15 years, where Moving Average (MA) method with 7-day MA window is used to identify the intermittency of wind speed and windfarm production. This technique imitates the slow thermal development phenomena in cables and it can be seen that even though the instantaneous wind production is 100% quite often, it does not sustain long enough for the red line to ever touch the 100% mark. Moreover, the improved cooling of exposed cable sections during high wind periods and unavailability of some wind turbines at any given time further facilitates this process.

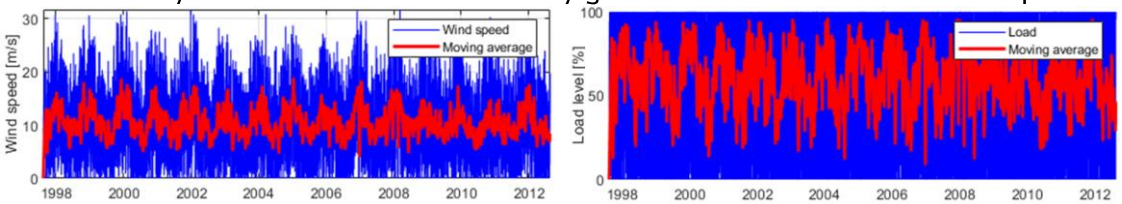

Figure 3. Feasibility assessment of production and cable design for an offshore windfarm site in UK. Left: Instantaneous and 7-day averaged windspeeds for 15 years. Right: Instantaneous and 7-day averaged energy production for 15 years. The difference b/w red and blue lines exhibits intermittency of wind generation.

3. Design and Operation of OWPP Export Cables Based on Dynamic Rating

The discussion so far suggests that the utilization of steady state ratings from IEC 60287 [4] [5] would result in a conservative export cable design. Dynamic rating of HV components including overhead lines and transformers for renewable integration is addressed extensively in the literature [6], but the additional complexity of modelling the thermal properties of cable surroundings under different installation conditions makes the task more challenging.

Dynamic rating of OWPP export cables can be performed at two stages, each of which addresses two different sets of problems. At first, the cable rating is optimized for the windfarm lifetime during the design stage. Statistics combined with long-term data processing facilitates this process. The methodology published in [7] uses probabilistic lifetime utilization of cables embedded in an optimization problem for optimal sizing of these cables during the design phase. In contrast to this technique, methods described in [1] and [8] use mathematical manipulation of the wind energy production. The approach in [1], for e.g., uses a step-load profile which represents the worst-case load for different sections of the OWPP export cables based on the historic windspeeds spanning over long periods (>15 years) for the investigated windfarm site. This methodology ensures that the designed cable doesn't violate the thermal limits set by the manufacturer unless exposed to load higher than worst-case conditions. These worst-case load conditions follow an identical pattern for different windfarm sites on the west and east coasts of UK, which can be observed in Figure 4 (left). The figure shows that due to the intermittent nature of the wind, the windfarm can sustainably produce at its rated capacity for a limited time (usually up to five days) and the production levels drop if the time span of the continuous observation period is increased. On the right of Figure 4, the step load profiles for offshore, HDD and onshore sections of the export cable for a windfarm in UK are provided along with its worst-case load condition. This methodology is also available in appendix of [2]. This can further be improved by employing modern machine learning based methods for forecast of short-term and long-term energy yields from offshore windfarms [9] [10].

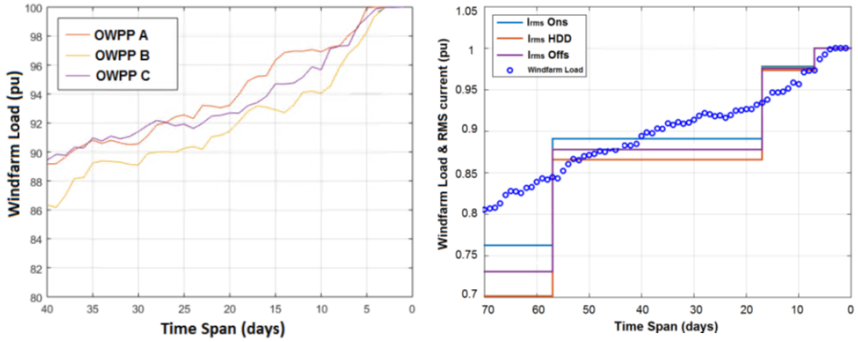

Figure 4. Left: Worst case load profiles for three different offshore windfarms in UK. Right: Step-load profile for different cable sections and worst-case load condition (blue circle) for a windfarm in UK. The graphs are based on the methodology of step-load profile based dynamic rating calculation for OWPP export cable design [1]

The export cables designed dynamically using the method mentioned above can still require real-time dynamic loading during the operation stage in contingency conditions, when one of the parallel cables from Figure 1 is not available. In this situation, wind energy transmission can be maximized using real-time temperature measurements from DTS. This information combined with prebuilt thermal models for the cable design and its surroundings allow

operators to load the cables dynamically during the contingency period. However, the extensive differences in installation conditions of the prevailing cable sections create hurdles. The next chapter tries to identify these sections and elaborates the relevant challenges.

4. Analysis of Prominent Sections for Offshore Windfarm Export Cables

In section 2, it was revealed that from the design and commissioning point of view, export cables can be sectionalized into onshore (underground), HDD, offshore (subsea), CPS and J-tube sections. In this chapter, individual thermal analysis of these sections (except CPS) is performed for the test case of a windfarm in UK.

The temperature measurements from DTS can be used to identify and localize the hotspots (and thermal bottlenecks) in the export cable system. The temporal evolution of the cable temperature distribution along the cable route over long periods, as shown in Figure 5 for the test windfarm, can be examined to avoid misidentification of these bottlenecks. From Figure 5, it can be deduced that there are regions (or pinch points) along the cable route that exhibit uniform thermal behaviour over time and are always warmer than their neighbouring sections. While it is possible to have inherent 'pinch-points' in OWPP cable circuits for all periods, it is also common for the thermal bottlenecks to move from one section to another because of change in seasons, tidal movement etc. The increase in rating of J-tube cable section from summer to winter is the most common example of this behaviour.

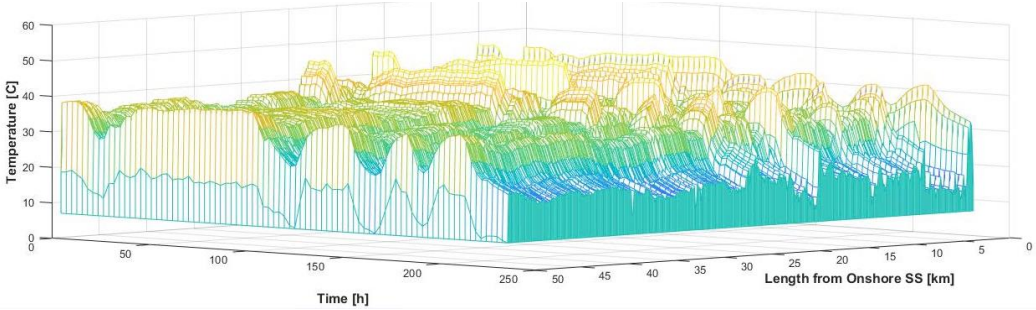

Figure 5. DTS-based cable temperature variation over eight days along the entire length with respect to the onshore substation for the test windfarm. The thermal behavior is consistent along the route.

4.1 Offshore Section:

The directly buried, 3-core, armoured, subsea cables usually constitute the largest section for OWPP export cables in terms of length. The burial depth of this section can ideally vary between 1 and 3 metres below the seabed surface, depending on a range of reasons (ease of burial, threat of anchor impact etc.) [2]. Over time, the burial depth can change significantly due to sedimentation and seabed movement because of phenomena like scouring, migrating sand waves, storms etc. This can cause the thermal behaviour of localized offshore sub-sections to change with time, which may result in development of new thermal bottlenecks.

On the other hand, the thermal resistivity and heat capacity of the seabed greatly influence the temperature variation for these cables. The composition of the materials surrounding the offshore cable can generally vary along its route, as shown in Figure 6 for an OWPP along with the instantaneous cable DTS measurement. In Figure 6, the change in cable temperature is notable to the trained eye for subsections with different thermal properties. The thermal resistivity of soft mud (clay) can range between *0.56-2.5 m·K/W* and has the tendency to be

significantly higher than that of gravel [*0.33-0.55 m·K/W*], which can explain the sudden drop in temperature around the *28-km* mark. On the other hand, heat capacity (dependent on material porosity) is fairly similar for both. Therefore, it can be concluded that seabed material composition influences the rating of offshore cable section significantly [11].

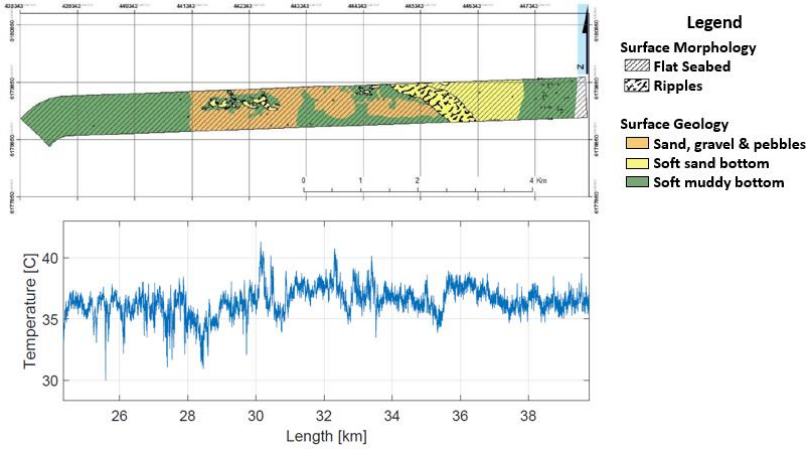

Figure 6. Top: Seabed geology of the offshore cable section for an offshore windfarm. Bottom: Cable temperature distribution (based on DTS measurements) for the same windfarm at an instant in time.

4.2 J-tube Section:

The cable that rises from the sea to the offshore platform needs additional protection from waves and tides. Using J-tubes for this transition is one of the solutions commonly used in the OWPP industry. The general layout of J-tubes is illustrated in Figure 7, along with the instantaneous DTS measurements for the export cable's J-tube section for the test windfarm. The three main subsections of the J-tube highlighted in the layout are: water, air and armour termination (hang-off). The air subsection is exposed to solar heating during the day, which when combined with the poor thermal dissipation properties of the surrounding air and the influence of air ambient temperature makes this subsection one of the main thermal bottlenecks for export cables. This, however, is found to be less problematic during night time and during winter season. The longitudinal heat flow between the water and air subsections results in cable temperature gradient near the boundary. The temperature reaches a plateau as the longitudinal heat flow diminishes and starts to decrease as the cable approaches the air and hang-off boundary [12]. The empirical method of [13] and analytical method of [14] have been extensively used for thermal analysis of HV cables in J-tubes, but the analytical inclusion of longitudinal heat flow in the method proposed in [12] makes it more accurate.

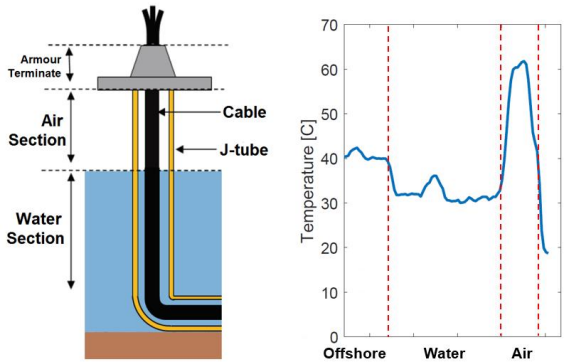

Figure 7. Left: Typical J-tube layout [12]. Right: Temp. distribution in subsections of the test windfarm J-tube.

4.3 Onshore and HDD Sections:

In comparison with the directly buried offshore cables, the onshore cables are laid in a much stable environment. As shown in Figure 8, the DTS measurements are significantly lower and relatively stable for the onshore section, the reasons for which are touched upon in Section 5. As the 3-core offshore cable reaches land, it passes through the landfall section (commonly HDD) before being connected to 3 x 1-core cables at the onshore transition joint.

Besides having significant burial depth compared to the subsea cable, the HDD section is known to have the most thermally strenuous environment as compared to the remaining sections which makes it the most critical thermal bottleneck in the export cable system [15]. The situation is worsened during summer due to ambient temperatures higher than offshore and also because of drying of the local soil due to possible migration of moisture. However, there are methods of resolving these thermal pinch points which includes filling up the HDD pipes with material with superior thermal properties like bentonite and utilization of cables with larger conductor cross-section etc. Consequently, the cable temperature for HDD is significantly reduced but it remains to be the thermal bottleneck as compared to its surrounding section, which can be seen in Figure 8.

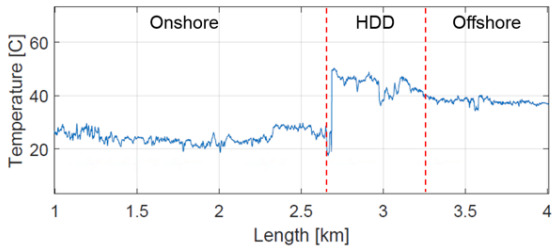

Figure 8. Temperature distribution in different sections for the test windfarm at an instant in 2014.

5. Temporal Variation of Thermal Properties for Export Cables

Based on the discussion so far, it can be deduced that although there are sections in the OWPP export cable system that constitute inherent thermal bottlenecks, the instantaneous temperature that each cable section (and subsection) heats up to depends on a number of factors including local ambient temperature, sustained cable load and variation of thermal properties of cable surroundings. To illustrate this further, the maximum annual temperature measurements along the entire cable route for the test windfarm is provided in Figure 9, two years apart for 2014 and 2016. Throughout 2016, maximum wind energy production did not sustain long enough for the cable temperature to rise as high as it did in 2014. This was further facilitated by colder ambient temperatures which were 2.6 °C less on average for 2016 compared to 2014.

As already identified in Section 4, it is observed in Figure 9, that the maximum DTS measurements for 3 single-core cables for the onshore section are less than the temperature of the 3-core submarine cable in the offshore section for both the years. This difference appears because of different cable designs and also because for the onshore section, the optical fiber cable is placed in a duct and outside the individual pipes containing the 3 phase conductor cables, while the single 3-core cable in the offshore section is embedded with the optical fibre. The temperature offset therefore needs to be established for the land and submarine cables respectively in order to obtain a more accurate account of the conductor

temperature. It is further reinstated in Figure 9 (bottom) that the cable temperature in the offshore section (7-46.8 km) is highly dependent on the burial depth of the cable with respect to the sea-bed and also on the type of material surrounding the cable in the back-filled region.

There are two distinct temperature peaks: one due to the onshore transition joint between HDD and onshore, while the other in the air section of J-tube for both the years. Further analysis reveals that J-tube's air section exhibits max temperature during summer (when production is not maximum) in contrast to other sections which are hottest during sustained high load conditions. This proves the fact that J-tube section is influenced by ambient conditions more than other sections. There is another interesting observation around the 16-km mark, where the higher rating cable of HDD is connected to the offshore cable of smaller cross-section. The temperature cable variation for the offshore section is significantly larger beyond this point as compared to the relatively stable distribution before.

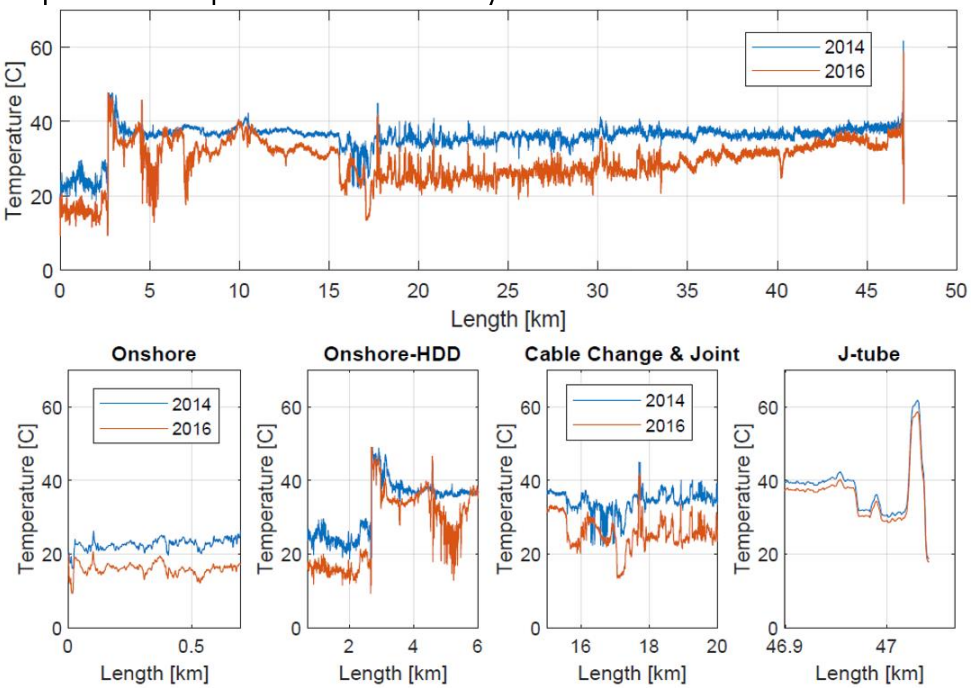

Figure 9. Top: Maximum measured temperatures in years 2014 and 2016 along the entire length for the test windfarm export cable. Bottom: Closer look of different sections of interest.

6. Discussion on Existing Monitoring Practices and Future Design Challenges

In section 2 and 3, it was identified that long-term historical wind generation data of around 12-15 years is usually used for site assessment and windfarm cable design. Such an approach allows to account for any aberrations that can lead to wind energy curtailment if dynamic rating is used for cable design due to overheating of the cable. During the operation phase, the only method to prevent cable overheating is to monitor its temperature in real-time. The utilization of numerical thermal models for cables has widely been used for this purpose until recently. The parametrization of these models is arduous and requires explicit information about the cable design and its surroundings, which includes temporal progression of soil thermal resistivity, ambient temperature for ground and seabed, solar radiation (for J-tubes) and other thermal issues identified in section 4. Consequently, these thermal models must be validated periodically using the DTS measurements.

The influence of variation of the identified parameters on the accuracy of numerical models' temperature predictions results in operators turning to DTS instead. Even though the DTS suppliers affirm high accuracy with exemplary spatial resolution for their equipment, it is inadequate to rely completely on the DTS measurements for curtailment of wind energy because of the significant economic impact on the business case of offshore windfarms. Besides the issues related to calibration and reliability of measurements, there are some inherent risks with the technology which primarily include uncertainty of fibre location in the cable core, particularly in the case of 3-core undersea cables where fibre core is lined inside the export cable core. However, these risks can be mitigated by reducing the influence of human intervention and by relying more upon the computationally intensive but adaptable machine-learning algorithms because of their ability to identify underlying principles that are not always visible even to the trained human eye [16].

For the offshore section, the foremost challenge in the variation of cable burial depth over time. This is ensured by pushing windfarm developers to perform periodic surveys of the cable route which are expensive. The frequency of these surveys is high in the initial years but can typically be reduced with time. Adequate analysis of thermal properties in combination with thermal models and long-term DTS measurements can reduce the frequency of these surveys considerably.

7. Conclusion

The debottlenecking of offshore windfarm export cables has successfully shown that there is a need to address the different design concepts and commissioning practices for dynamic rating-based cable operation and design. The five identified cable sections including onshore (underground), landfall (HDD), offshore (subsea), cable protection system and J-tube have their unique thermal behaviour. This behaviour needs to be accounted for, in order to prevent revenue loss due to wind energy curtailment during sustained high production periods, particularly for cables that are optimally rated using dynamic loading to reduce overall windfarm capital expenses. By using real-time cable temperature measurements from Distributed Temperature Sensing (DTS) equipment, the operators can control cable load and optimize wind energy transmission in case of contingency. Similar DTS data has been used in this paper for one of the export cables from a specific test windfarm in UK. The useful insights about each cable section obtained from evaluation of long-term DTS measurements of the export cable are generally applicable to all offshore cable installations.

Subsea cables in the offshore section and underground cables in the onshore one are not found to be thermally limiting as compared to the HDD and J-tube sections. Even though the variation of thermal properties of the material surrounding the cable in offshore section due to change in seabed geology and cable burial depth along the directly buried undersea cable results in irregular fluctuations in cable temperature, the maximum temperature is still acceptable. Whereas, for the J-tube and HDD, there are sudden peaks in the DTS readings localized to certain regions in each section which can limit the cable load particularly during dynamic load conditions. The temperature peaks of J-tube are particularly housed by air filled subsection because of its exposure to solar heating during the day and the poor thermal dissipation properties of air as compared to sea water. Whereas, the increased depth of burial is the main reason for cable hotspots in the HDD section. For both these sections, the

situation is worst during summer due to higher ambient temperatures and solar radiation. Therefore, both these sections can have seasonal bottlenecks which disappear in winter, particularly J-tube. The risks involved with thermal estimation using DTS measurements and numerical models can, however, be resolved by using modern data manipulation techniques.

8. Acknowledgements

The support of Innovation Fund Denmark, which is sponsoring this project is highly appreciated. The OPTIMUM framework project collaboration between DTU, Energinet.dk and Ørsted oversees this work.

BIBLIOGRAPHY

[1] T. Kvarts, I. Arana, R. Olsen and P. Mortensen, “Systematic Description of Dynamic Load for Offshore Wind Farms. Method and Experience”, B1-303, CIGRE 2016.
[2] Working Group B1.40, “Offshore Generation Cable Connections”, CIGRE Technical Brochure 610, Feb 2015.
[3] S. H. H. Kazmi, J. Holbøll, T. H. Olesen, T. S. Sørensen, “Dynamic Thermoelectric Modelling of Oil-filled Power Transformers for Optimization of Offshore Windfarm Export Systems”, CIGRE Symposium, Aalborg, June 2019.
[4] IEC 60287-1-1 ed 2.0, "Electric cables - Calculation of the current rating - Part 1-1: Current rating equations (100 % load factor) and calculation of losses - General," 2006.
[5] IEC 60287-2-1 ed 2.0, "Electric cables - Calculation of the current rating - Part 2-1: Calculation of Thermal Resistance," 2006
[6] N. Viafora, K. Morozovska, S. H. H. Kazmi, J. Holbøll, “Day-ahead dispatch optimization with dynamic thermal rating of transformers and overhead lines”, Electric Power Systems Research 171, 2019, pp 194–208 (https://doi.org/10.1016/j.epsr.2019.02.026)
[7] Pérez-Rúa, J-A., Das, K., & Cutululis, N. A. “Optimum sizing of offshore wind farm export cables. International Journal of Electrical Power and Energy Systems”, 2019, pp 982-990.
[8] S. Catmull, R. D. Chippendale, J. A. Pilgrim, H. G and P. Cangy, “Cyclic Load Profiles for Offshore Wind Farm Cable Rating,” *IEEE Transactions on Power Delivery,* 2015.
[9] J. W. Taylor, P. E. McSharry and R. Buizza, “Wind Power Density Forecasting Using Ensemble Predictions and Time Series Models,” IEEE Transactions on Energy Conversion, vol. 24, no. 3, pp. 775-782, 2009
[10] M. C. Mabel and E. Fernandez, “Estimation of Energy Yield from Wind Farms Using Artificial Neural Networks,” IEEE Transactions on Energy Conversion, pp. 459-464, 2009
[11] T. Hughes, T. Henstock, J. Pilgrim, J. Dix, T. Gernon and C. Thompson, “Thermal Ratings of Submarine HV Cables Informed by Environmental Considerations,” 9th International Conference on Insulated Power Cables, 2015
[12] R. D. Chippendale, J. A. Pilgrim & P. Cangy, ‘Analytical Thermal Rating Method for Cables Installed in J-Tubes’, IEEE Transactions on Power Delivery vol. 32, Issue 4, Aug 2017
[13] M. Coates, “Rating cables in J tubes (88-0108),” ERA technology, 1988
[14] R. A. Black and W. Hartlein, “Ampacity of electric power cables in vertical protective rises,” IEEE transaction on power apparatus and systems, vol. 102, no. 6, 1983
[15] T. Worzyk, Submarine Power cables, Springer, 2009.
[16] S. H. H. Kazmi, B. Cordes, J. Holbøll, T. H. Olesen, T. S. Sørensen, “Machine Learning Based Temperature Forecast for Offshore Windfarm Export Cables”, CIGRE, Paris, 2020

[Pub. C7]

S. H. H. Kazmi, T. H. Olesen, T. S. Sørensen and J. Holbøll, **"Machine Learning based Dynamic Thermal Modelling of Offshore Wind Turbine Transformers"**, Accepted (awaiting presentation), *41st CIGRE Symposium*, Ljubljana, Slovenia, Jun 2021.

The accepted version of the paper is attached.

Machine Learning based Dynamic Thermal Modelling of Offshore Wind Turbine Transformers

S. H. H. Kazmi [1], T. H. Olesen [1], T. Laneryd [2], T. S. Sørensen [1], J. Holbøll[3]
[1] Ørsted Offshore Wind A/S, Gentofte, Denmark
syeka@orsted.dk
[2] Hitachi ABB Power Grids Research, Västerås, Sweden
[3] Technical University of Denmark, Lyngby, Denmark

Abstract – Oil-filled power transformers are critical for nominal operation of Offshore Windfarms (OWFs), as these transformers are employed not only in the transmission system, but also in each Wind Turbine Generator (WTG). With the advent of large-scale OWFs comprising of more than 100 WTG transformers, effective thermal condition monitoring of these transformers has become a challenge. In this paper, a number of physical, semi-physical and non-physical empirical thermal models based on data analytics and Machine Learning (ML) are developed that are fit for dynamic thermal estimation of WTG transformers. Unlike conventional computational fluid dynamics and white box Thermo Electric Equivalent (TEE) models, the statistical approach to thermodynamic modeling of transformers is found to be less complex to design as it requires minimal system information and more flexibility. The physical insights based ML models (grey-box) are closer to conventional TEE models proposed by IEEE and prominent publications, but the remaining models can be built from scratch based on available data as they require little to no physical operational or design knowledge (black-box). The data driven ML models are trained and tested for a number of test cases in this paper. Firstly, controlled heat run tests performed on a 630 kVA lab transformer under dynamic load conditions are used to validate these models. But due to limitation of training data, the grey-box models which rely heavily on available system information and correct parameterization are found to underperform compared to white-box TEE and black-box neural network models. Afterwards, the available thermal and load monitoring data from ten actual offshore WTG transformers (6.8 – 7.2 MVA) located in the nacelle is used for durations up to 2 years. This long-term data is found to be sufficient for proper training of all the developed ML models. As a result, the physics-based ML models that use linear differential equation functions are found to be more consistent compared to the non-linear black-box models as the latter models have the tendency to overfit the data. This consistency remains even when the models are trained on one of the available WTG transformers and the trained models are later tested on completely different WTG transformers. Hence, it is shown that the application of data analytics and machine learning has a huge potential in widescale condition monitoring of transformers with similar constructional features, particularly for WTG transformers in large-scale offshore windfarms.

Keywords: Dynamic thermal rating, Transformers, Wind turbine generators, Offshore windfarms, Hot spot temperature, Top oil temperature, Machine learning, Data analytics, Artificial neural network, Ordinary differential equations, Auto regression, State space models.

1 INTRODUCTION

Thermal estimation of high voltage components is crucial for sustainable design and operation of transmission and distribution systems. Oil-filled HV components like transformers and reactors are particularly influenced by load-dependent heating. Therefore, approximation of two quantities is of great importance: the measurable Top Oil Temperature (TOT) and the critical Hot Spot Temperature (HST), along with their variation with load and ambient conditions [1]. Oil-filled power transformers are crucial for the design and operation of Offshore Windfarms (OWFs), as each Wind Turbine Generator (WTG) includes a transformer.

Accurate estimates of these transformer temperatures require detailed knowledge of geometry and loss distribution, and the nonlinear nature of fluid flow will tend to amplify any uncertainty in the parameters. Modelling techniques such as computational fluid dynamics and thermal hydraulic networks are widely used for steady state thermal assessment [2]. For dynamic, load-dependent thermal estimation, Thermo-Electric Equivalent (TEE) models are typically used, which require transformer construction information that is often unavailable and could potentially change over operation time. In this paper, it is shown that Machine Learning (ML) based dynamic thermal estimation of oil-filled components can resolve these challenges.

Four flexible, adaptable, computationally efficient, self-learning models with completely different structures and formulations are developed and tested for dynamic thermal estimation of WTG transformers. The complexity of dynamic ML-based models for time series data, as described in [3] [4] is resolved using system identification principles of [5]. Some of the developed models utilize the available physical insights based on the principles explained in [6], while the computational stress of non-linearities are resolved using the suggestions of [7]. The models are validated for a 630 kVA lab transformer and 10 WTGs transformers rated between 6.8 and 7.2 MVA.

2 DATA DRIVEN THERMAL MODELING OF WTG TRANSFORMERS

This section provides detailed explanation behind the rationale for using Machine Learning (ML) based dynamic thermal models for WTG transformers, along with their methodological descriptions.

2.1. MOTIVATION AND POTENTIAL

Over the years, the size of offshore windfarm projects has increased dramatically. The typical layout of large OWFs with >100 WTGs, as shown in Fig. 1, determines the extent of operational and monitoring challenges for developers and operators. Furthermore, transformers in each OWF WTG generate large amounts of monitoring data that is difficult to manipulate and analyze with conventional methods. Therefore, in order to fully utilize the information hidden behind the thermal measurements of transformers to identify potential maintenance activities to be performed on these transformers, intelligent algorithms should be developed that are computationally efficient, have the ability to handle large bandwidth of data and can generate reliable results. The ML algorithms proposed in this paper can perform these tasks effectively.

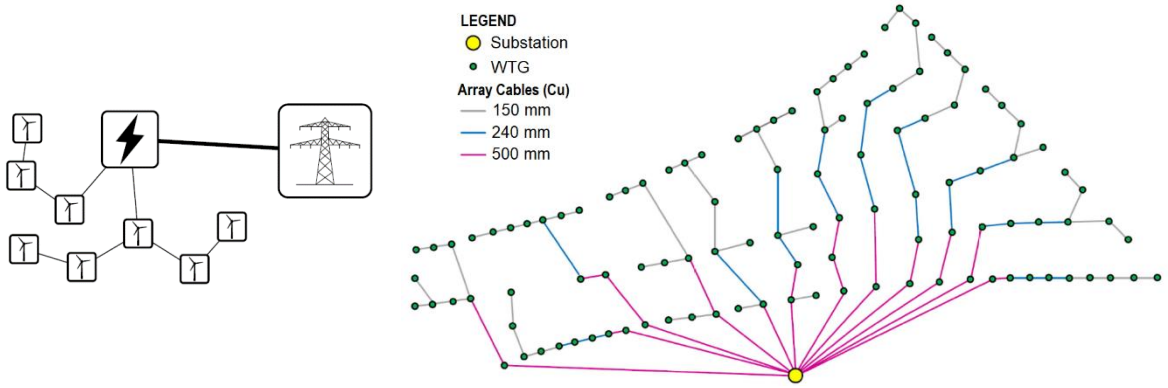

Figure 1. Left: Illustration of transmission system overview for offshore windfarms. Anholt Offshore collection system layout showing 111 WTGs connected within asymmetrical offshore 33 kV electrical infrastructure [8]

2.2. METHODOLOGY OF DESIGN

The data-analytics based ML models presented in this paper undergo two phases for thermal estimation of power transformers. These phases are highlighted in Fig. 2 as Training and Testing, while the overall mechanism is also defined in the figure. During the Training phase, three different sets of inputs are made available to the relevant ML-based model:

- The 'predetermined parameters' are a collection of constants that are predefined during the development of the model. Since data-analytics based models offer exceeding flexibility of design, these parameters allow the designer to determine the problem structure, model order and the relevant functions in advance. Understandably so, this step requires extensive information about the model framework to ensure efficient design.
- The set of 'training inputs' are measured time-variant variables that should supposedly be available to the models at all times. For dynamic thermal modeling of transformers, load current (I_t) and ambient temperature (${\vartheta_t}^{amb}$) are used as training inputs in this paper.
- The last set of inputs, called 'training measurements', consist of the signals that are to be predicted by the ML-based model. For thermal estimation of transformers, the top-oil (${\vartheta_t}^{tot}$) and hot-spot (${\vartheta_t}^{hst}$) temperatures are to be predicted.

The relevant model uses these predetermined parameters and the considerably long duration of time-variant inputs to train itself. By the end of the training phase, the parameters that define the thermal characteristics of the transformers, termed as 'estimated parameters' in Fig. 2, are determined. Once the ML-based models are trained and the characteristic estimated parameters are defined, the Testing phase commences. This phase uses the time variant test inputs I_t and ${\vartheta_t}^{amb}$ to predict the temporal variation of the critical transformer temperatures ${\vartheta_t}^{tot}$ and ${\vartheta_t}^{hst}$. It should be mentioned that the HST is not readily measured in WTG transformers, therefore TOT will be used for predictions and benchmarking of the developed models for offshore turbine transformers in this paper.

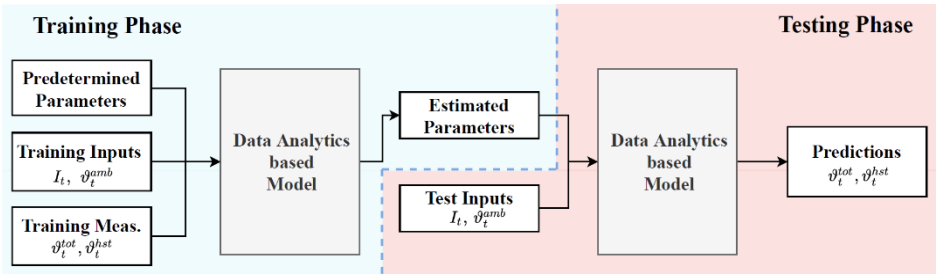

Figure 2. Process followed during training and testing phase for ML-based dynamic thermal estimation models for WTG transformers.

In order to benchmark the models formulated for this paper with regards to their prediction accuracy and to constitute the training convention, Normalized Mean Square Error (NMSE) is used. The calculation of Mean Squared Error (MSE) and NMSE are provided in (1) and (2) respectively, where ${y_t}^{ref}$ and ${y_t}^{pred}$ represent the measured and predicted values of the temperature at time *t* and μ represents the average. By normalizing MSE by variance σ^2, NMSE offers a unique advantage for generality of application [9]. Furthermore, as the NMSE in (2) ranges between negative infinity and 100, where 100 corresponds to a perfect fit and 0 represents the equivalency to a general mean model, it provides easier interpretability of results. This is true because the performance of the models with NMSE in the range of 0 to 100 is better than constant mean models [10]. Besides the utilization of prediction accuracy, the models formulated in this paper are also compared based on their design simplicity and application flexibility.

$$MSE = \frac{1}{N}\left\| {y_t}^{ref} - {y_t}^{pred} \right\|^2 \tag{1}$$

$$NMSE = 100\left(1 - \frac{MSE}{\sigma^2}\right) = 100\left(1 - \frac{\left\| {y_t}^{ref} - {y_t}^{pred} \right\|^2}{\left\| {y_t}^{ref} - \mu \right\|^2}\right) \tag{2}$$

2.3. CLASSIFICATION OF ML MODELS

In this paper, empirical models for dynamic thermal estimation are preferred because the experiential and statistical character of the empirical models, when combined with their increased computational efficiency, higher

adaptability and design simplicity make them ideal for application of data analytics and machine learning [9]. Referring to Fig. 3, the models identified in this paper are briefly classified in to three shades of grey, depending on the model's requirement of physical information about the system and how these required insights blend with the empirical observations.

The white-box models have conventionally been proposed in the literature as Thermo Electric Equivalent (TEE) models. These linear and non-linear differential equations-based models not only require extensive knowledge about the system design and its thermodynamic behavior, but the estimation of physical parameters and the set of underlying equations is made in advance and cannot be changed during estimation. In this paper IEEE Clause 7 model from IEEE 57.91 [1] and the Susa model from [11] are used as white-box TEE models because of their proven applicability for dynamically loaded WTG transformers [12].

On the other hand, the black-box models require minimal system information which make them ideal for applications where physical insights are either unavailable or too complicated to design, as demonstrated for similar applications in [4, 13]. Finally, the grey-box models combine the features of the remaining two, as these models use limited system insights to design the problem structure and can efficiently be used for application where the system parameters tend to change over time. Consequently, the system designer can define the problem structure based on known information, while the unknown parameters are determined using data-analytics [5]. Black-box and grey-box models along with their sub-groups are briefly explained in Table 1, but the readers are directed towards publications [14] and [15] for detailed information regarding problems' structural formulations and parameter estimation.

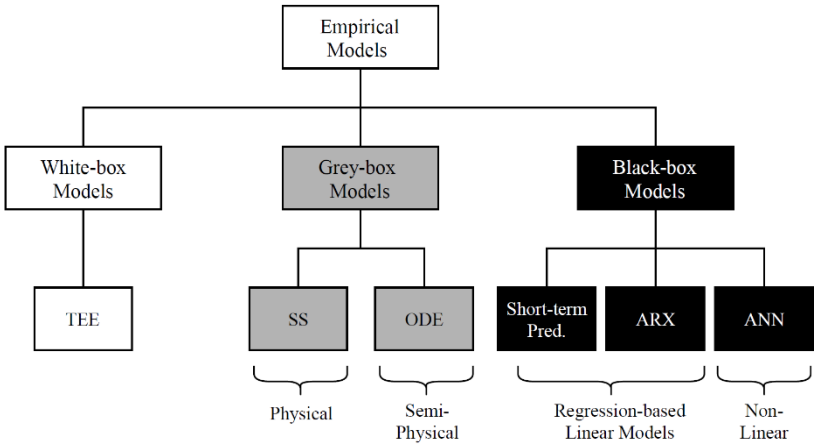

Figure 3 Empirical thermal estimation models classification with focus on grey-box and black-box machine learning models

Table 1. Classification of the proposed machine learning models and their description

Name	Type	Description
ODE	Grey-box	The Ordinary Differential Equation (ODE) model is a continuous-time, semi-physical model, for which first-order linear differential structure is used in this paper. Model coefficients can be tuned to accurately assess the temperature rise and thermal time constants for transformers. [16].
ARX	Black-box (Trend-based)	The statistical linear regression based Auto Regressive eXogenous (ARX) model uses a linear combination of previously predicted & measured values of critical transformer temperatures along with a stochastic term (noise) and a series of known inputs (load) [3]. The model order is predefined, while the coefficients are trained to fit the training data.
ANN	Black-box	The classical Artificial Neural Network (ANN) model uses non-linear weighing of input signals [4]. The order of the model, number of layers, sub-layers and neurons have been chosen to optimize the complexity, solution time & accuracy.
SS	Grey-box	The State Space (SS) model based on a set of first-order differential eqs. defines the system using state variables and is linear in nature [17]. This model is physics-based and similar in operation to the process model. The higher the amount of available system information, the better the structure of these models can be constructed.

3 LAB TRANSFORMER SETUP AND RESULTS

As mentioned earlier, WTG transformers in offshore windfarms do not have provisions to measure HST, which leaves only TOT for validation purposes. Therefore, the performance of data-driven ML-based models proposed in this paper are compared with the conventional white-box TEE models by using a test transformer setup in the DTU HV PowerLab, as specified in Table 2 The cooling mechanism of the test transformer (former distribution transformer manufactured in 1990), along with the electrical/mechanical design and the dynamic load applied during the controlled heat-run tests indicate that the results are easily scalable to offshore WTG transformers.

Table 2. Specifications for 630 kVA Test transformer in DTU HV Power Lab

Parameter	Value
Rating	630 kVA
Voltage	0.4/10 kV ± 5%
Vector Group	Dyn11
Percentage Impedance	5 %
Frequency	50 Hz
Oil Weight	460 kg
Winding Time Constant	6 min
Rated No-load/Full-load Losses	586/5064 W
Cooling Mode	ONAN

For the test transformer setup in Fig. 4(a), by removing the active part of Fig. 4(b) after oil drainage, temperature sensors were placed in the right locations. Referring to Fig. 4(c), a total of 6 Type-K thermocouple temperature sensors (T1-T6) were placed for TOT measurements such that two sensors were used for either side of each phase winding. On the other hand, 7 sensors (H1-H7) located close to the top region of the windings were used for tracking HST variation over time. As per experience and manufacturer's recommendations, a significant number of these sensors were placed on the middle phase. After initial investigations, sensors T2 and H3, shown in Fig. 4(d) and 4(e), were found to provide accurate TOT and HST measurements respectively. The ambient temperature of surroundings was measured using the mathematical average of a number of Type-K sensors placed around and on the surface of the lab transformer. The relevance of the test setup for intermittently loaded WTG transformers in offshore windfarms with dynamic rating is ensured by subjecting the lab transformer to two different dynamic load profiles, one below the rated capacity and the other up to 1.4 pu of the lab transformer rating.

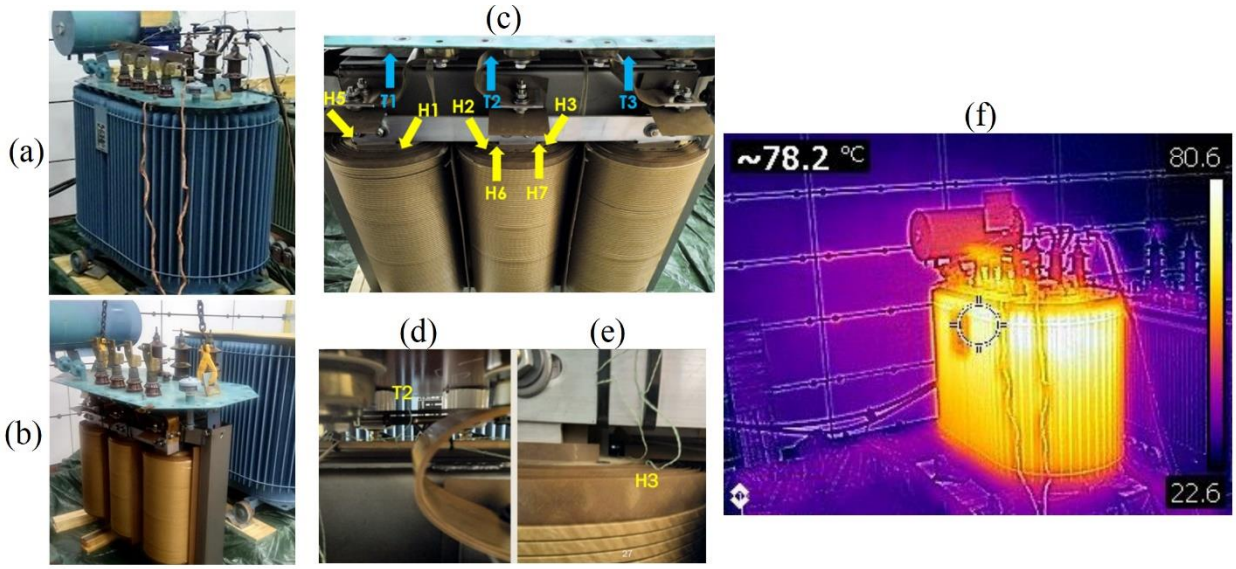

Figure 4. (a) Energization setup for the lab test transformer (LV side). (b) Transformer's active part ready for sensor placement. (c) Location of TOT sensors T1-T3 (T4-T6 on the opposite sides) and HST sensors H1-H7 (except H4). (d) (e) Zoomed-in view of T2 and H3 sensors chosen for thermal validation. (f) Infrared thermal image of the test transformer for sustained overload (1.4 pu) at 2.5-hour mark

The two load profiles and the resulting measurements for TOT (sensor T2) and HST (sensor H3) are provided in Fig. 5 Furthermore, the calculated temperature using the conventional white-box TEE models (Susa and IEEE) and the data-analytics ML-based models explained earlier are also provided in the figure. The performance is

found to be consistent for both the test load profiles, as white-box models outperform the ML-based models consistently, with the Susa model offering the highest accuracy. It is important to mention that the abundance of design and operational information available for the lab transformer allowed the white-box TEE models to be developed with high level of technical details, which contributed to the increased accuracy of their predictions.

The ML-based models presented in this paper are trained over the entire dataset. Contrary to expectations, the physics-based grey-box models (ODE and SS) return below-par results, as these models fail to accurately predict the lab transformer's TOT and HST for the two load profiles. On the other hand, linear black-box ARX model offers acceptable accuracy, while the non-linear ANN model provides the best-fit. The lack of data due to relatively shorter heat-run tests is found to be the problem for these results. In contrast to the remaining models, the inherent degree-of-freedom offered by the highly non-linear ANN model allows accurate replication of the measured temperatures, but this can lead to data overfitting and the results needs to be reviewed for untrained datasets and should be cross-validated before definite conclusions are made. One important point to note is the measured temperature in the thermal image of Fig. 4(f) at the 2.5 hour mark for the high load case is around 80.6 ºC, which corresponds to the TOT measured at the same time in Fig. 5(c) and also indicates consistent concentration of high temperature in the top region of the transformer.

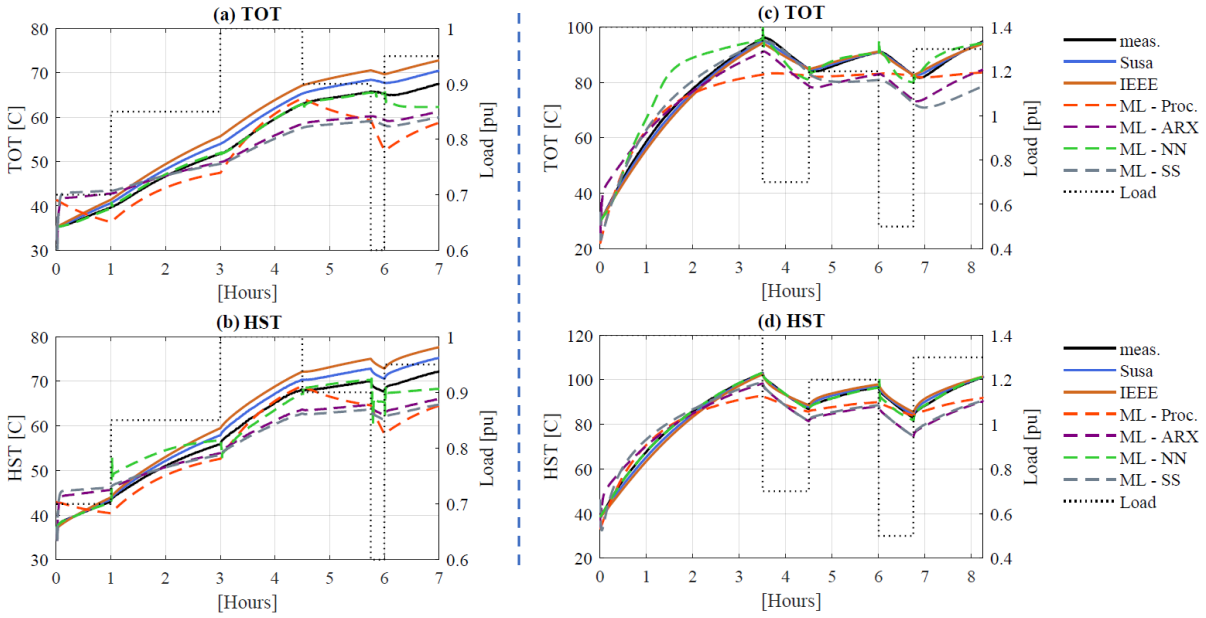

Figure 5. Comparison of calculated TOT and HST using TEE models from Susa [11], IEEE [1] and ML models (Table 1) with the measured values for the 630 kVA lab transformer. (a)-(b): load ≤ 1pu. (c)-(d): load > 1pu.

4 TEST CASE WTG TRANSFORMERS IN OFFSHORE WINDFARMS

In order to validate the four ML-based models proposed in this paper for wind turbine transformers in OWFs, ten different WTG transformers of similar rating (6.7 – 7.2 MVA) and same construction/installation characteristics (electrical/mechanical design, cooling modes, manufacturer, located in WTG Nacelle etc.) are used. These WTG transformers are spread across four offshore windfarm sites in UK and Denmark, while 10-minute sampled measurement data of up to 3 years is used for training and tested purposes. This data includes inputs which are readily available during both the training and test phase (incl. load and ambient nacelle temperature), while the TOT measurements are only used in training the models and then benchmarking the results by comparing the calculated temperatures with the measured ones.

5 VALIDATION RESULTS AND POSSIBLE APPLICATIONS

In this section, the validation results of the proposed ML-based models for dynamic thermal estimation of test case WTG transformers are provided. Furthermore, the possibilities of applying these modeling techniques for self-monitoring of the test WTG transformers (train and test on the same transformer) and for cross-monitoring of these transformers (train on one transformer and test on remaining) are also presented.

5.1. TRAIN AND TEST ON THE SAME WTG TRANSFORMER

In this approach, the ML-based models are trained and tested separately for each of the test WTG transformers. Hence, in total 10 models are trained for each of the four ML-based models (ODE, ARX, ANN and SS), thereby resulting in a total of 40 individually trained models. By using the 60-40 principle, 60% of the available 3-year (730 days) TOT measurements, load data and ambient temperature measurements are used for training the models, while the rest are used for predicting the TOT for validation purposes. In Fig. 6 and 7, the validation results of the four ML-based models are provided for two different WTGs for a short duration at the border of training and test intervals. The dark-orange line represents the predicted TOT measurements during the training phase, while the light-orange line represents the predictions for the test phase. It can be seen that for all the tested models except ANN, the prediction performance during the training and testing periods are generally similar. In contrast to the observations for lab transformers, the availability of long-term data from WTG transformers ensures that physics-based ML models (ODE and SS) perform considerably better, while the ANN model is found to overfit the data due to its highly non-linear nature.

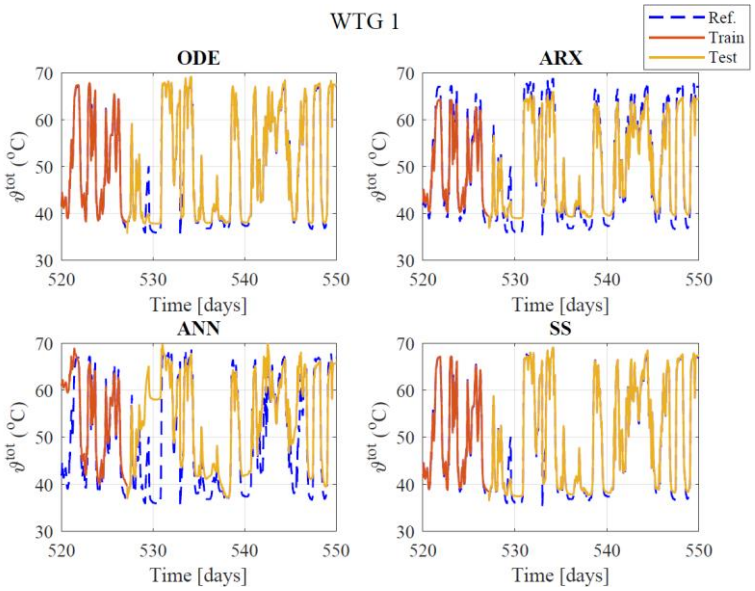

Figure 6. Results for WTG 1 transformer when the ML models are trained and tested on its own measured TOT data. 2 years of data is used in total, but the results are presented for a 30-day window for elaboration purpose.

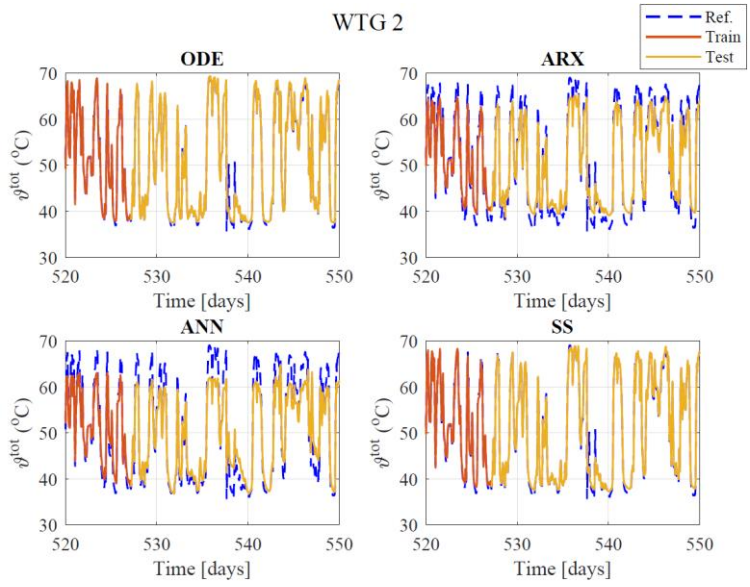

Figure 7. Results for WTG 2 transformer when the ML models are trained and tested on its own measured TOT data. 2 years of data is used in total, but the results are presented for a 30-day window for elaboration purpose.

Furthermore, the four ML-based models proposed in this paper are benchmarked using the NMSE results. These results are summarized in Fig. 8 using boxplots for the ten WTG test transformers which visualize the calculated TOT's distribution and its skewness, along with the median values. It can be deduced that both the physics-based

models consistently result in highest accuracy (NMSE close to 100%), while the ANN models perform the worst. ARX models result in acceptable results which can further be improved by increasing the model order. For comparison, NMSE for Susa and IEEE models are found to lie in the range of 89-95% and 83-91% respectively. The unique consistency of physics-based ML models makes them fit for dynamic thermal estimation of WTG transformers, if considerable training data is available.

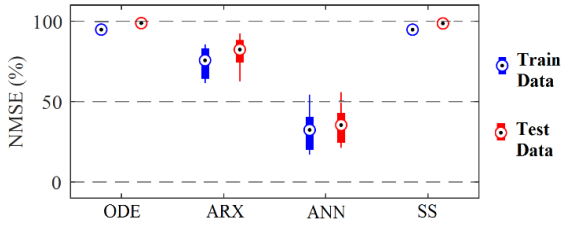

Figure 8 Comparison of NMSE (%) results for the 4 developed ML model types using boxplots, when the models are trained and tested on the same WTG transformer (all 10 WTGs are trained and tested individually).

5.2. TRAIN AND TEST ON DIFFERENT WTG TRANSFORMERS

As further large-scale offshore windfarms are built farther from the shore, the number of WTGs in an OWF rise considerably. Some of the latest OWF projects are found to employ up to 200 WTGs. Since each WTG has a power transformer, effective thermal monitoring and condition-based maintenance of these transformers can lead to significant challenges for the system operators. Therefore, in this section, another approach has been proposed to assess the potential of cross-application of the developed models.

The rationale behind this approach is to use the common thermodynamic design of WTG transformers that the data-analytics ML-based models can familiarize with by training over a limited set of sampled transformers. Hence, for this analysis, the developed ML-based models are trained for each of the 10 test WTG transformers separately. Afterwards, the trained models for each WTG transformer is tested on the 9 remaining test transformers. In total, a total of 90 tests are carried out for each model type. The results for one of these experiments are summarized in Fig. 9, where the four ML-based models are first trained on the complete 2-year data set of a certain WTG transformer and then tested on three different WTG transformers. It can be seen that all the developed models, with the exception of ANN model, predict the transformer TOT with acceptable accuracy under dynamic load conditions even though these models have not been trained on the respective test transformer. This is further demonstrated using the NMSE boxplots in Fig. 10, where ODE and SS models consistently predict the thermal development for training and testing on different WTG transformers. On the other hand, the developed framework for ANN model is not found to be fit for this application. Hence, it can be concluded that by using physics-based grey-box models, one can stipulate the thermal development of a large population of WTG transformers by training these models for a limited number of these transformers. The potential to employ these techniques for wide-scale monitoring of offshore windfarm transformers has been demonstrated in this section.

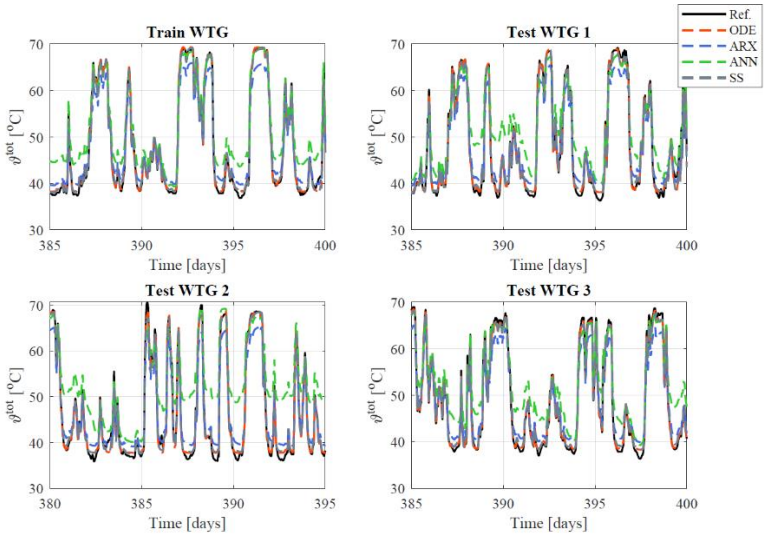

Figure 9. Results of thermal estimation of WTG transformers when the ML models are trained for TOT measurements of one transformer and then tested on the data for three different WTG transformers of same characteristics. 2 years of data is used in total, but the results are presented for a 30-day window.

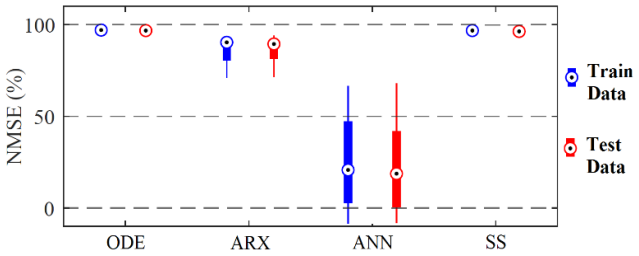

Fig. 10. Comparison of NMSE (%) results for the 4 developed ML model types using boxplots, when the models are trained on one transformer and tested on the remaining 9 WTG transformers (repeated for all transformers).

6 CONCLUSION

In this paper, it has been shown that application of Machine Learning (ML) and data analytics can provide significant value for effective thermal monitoring of Wind Turbine Generator (WTG) transformers in large-scale Offshore Windfarms (OWFs). The paper has presented a number of grey-box (physical/semi-physical) and black-box (non-physical regression-based) models that are considerably different to design compared to the conventional Thermo Electric Equivalent (TEE) models. The proximity of grey-box models to physical insights of the transformer tank make them suitable to detect anomalies that are related to thermodynamic behavior of the transformer, while the flexibility and adaptability of black-box models allow the user to mold the models as per their individual needs. The widescale validation tests carried out on long-term monitoring data from ten different WTG transformers and controlled heat run tests on a lab transformer has shown that the performance of grey-box models is dependent on the amount of available data. Similarly, these models are found to be applicable in cases where thermal monitoring is performed on a limited set of WTG transformers, while the operators needs to determine the condition of all the transformers. Hence, the analysis has revealed that under the circumstances of limited design information and large-scale data production, data-driven ML models (particularly grey-box models) can facilitate and significantly improve the dynamic thermal estimation process for WTG transformers.

REFERENCES

[1] IEEE guide for loading mineral-oil-immersed transformers and step-voltage regulators - redline, IEEE Std C57.91-2011 - Redline (2011) 1-172

[2] C. COTAS *et. al.* 'Development of a dynamic thermal hydraulic network model for core-type power transformers windings', CIGRE, Paris, 2018

[3] Henrik Madsen. Time Series Analysis. Chapman & Hall CRC, New York, USA, 2008.

[4] Christopher M Bishop. Neural Networks for Pattern Recognition. Oxford University Press, UK, 1995.

[5] Lennart Ljung. System Identification and Simple Process Models. Linkoping University, Linkoping, Sweden, 2013.

[6] K Zhang, A. Guliani & G. Memik. Machine learning-based temperature prediction for runtime thermal management across system components. IEEE Transactions on Parallel and Distributed Systems, 29(2):2079–2107, July 2017.

[7] M. Raissi, P. Perdikaris, and G. E. Karniadakis. Hidden physics models: Machine learning of nonlinear partial differential equations. Journal of Computational Physics, 357(1):125 to 141, Nov 2018

[8] L. H. Kocewiak, O. Holmstrøm, K. H. Jensen 'Resonance damping in array cable systems by wind turbine active filtering in large offshore wind power plants' IET Renewable Power Generation Vol. 11 Issue 7, Jan 2017

[9] Geron and Aurelien. Hands-on machine learning with Scikit-Learn and TensorFlow: concepts, tools, and techniques to build intelligent systems. O Reilly Media Inc, Massachusetts, United States, 2017.

[10] Gavin C Cawley and Nicola LC Talbot. On over-fitting in model selection and subsequent selection bias in performance evaluation. Journal of Machine Learning Research, pages 2079–2107, Nov 2010

[11] D. Susa, M. Lehtonen, Dynamic thermal modeling of power transformers: further development-part I, IEEE Transactions on Power Delivery 21 (4) (2006) 1961-1970

[12] S. H. H.Kazmi, T. H. Olesen, T. S. Sørensen and J. Holbøll, "Dynamic Thermoelectric Modelling of Oil-filled Power Transformers for Optimization of Offshore Windfarm Export Systems", CIGRE Symposium, Aalborg, Denmark, June 2019.

[13] M Raissi, P. Perdikaris, and G. E. Karniadakisa. Physics-informed neural networks: A deep learning framework for solving forward and inverse problems involving nonlinear partial differential equations. Elsevier Journal of Computational Physics, 378(2):686 to 707, Feb 2019.

[14] S. H. H.Kazmi, T. H. Olesen, T. S. Sørensen and J. Holbøll, "Machine Learning based Temperature Forecast of Offshore Windfarm Export Cables", B1-109 CIGRE, Paris, France, Aug 2020.

[15] S. H. H. Kazmi. (2021). Dynamic Rating based Design and Operation of Offshore Windfarm Export System. DTU Elektro, Centre of Electric Power and Energy, PhD Dissertation (submitted Jan 2021)

[16] M. Raissi, P. Perdikaris, and G. E. Karniadakis. Machine learning of linear differential equations using gaussian processes. Journal of Computational Physics, 348(1):683 to 693, Nov 2017.

[17] M. Raissi, P. Perdikaris, and G. E. Karniadakis. Inferring solutions of differential equations using noisy multi-fidelity data. Journal of Computational Physics, 335(1):736 to 746, July 2017.

Department of Electrical Engineering
Center for Electric Power and Energy (CEE)
Technical University of Denmark
Elektrovej, Building 325
DK-2800 Kgs. Lyngby
Denmark

www.elektro.dtu.dk/cee
Tel: (+45) 45 25 35 00
Fax: (+45) 45 88 61 11
E-mail: cee@elektro.dtu.dk